Distribution Agreement

In presenting this thesis or dissertation as a partial fulfillment of the requirements for an advanced degree from Emory University, I hereby grant to Emory University and its agents the non-exclusive license to archive, make accessible, and display my thesis or dissertation in whole or in part in all forms of media, now or hereafter known, including display on the world wide web. I understand that I may select some access restrictions as part of the online submission of this thesis or dissertation. I retain all ownership rights to the copyright of the thesis or dissertation. I also retain the right to use in future works (such as articles or books) all or part of this thesis or dissertation.

Signature:

Michelle Johnson _____

Date

Deciphering how N-terminal phosphorylation alters
fused in sarcoma (FUS) function:
Implications for FTD/ALS pathogenesis

By

Michelle Johnson
Doctor of Philosophy

Graduate Division of Biological and Biomedical Sciences
Neuroscience

_____

Thomas Kukar, Ph.D.
Advisor

_____

Ellen Hess, Ph.D.
Committee Member

_____

Nicholas Seyfried, Ph.D.
Committee Member

_____

Anita Corbett, Ph.D.
Committee Member

_____

Gary Bassell, Ph.D.
Committee Member

Accepted:

_____

Lisa A. Tedesco, Ph.D.
Dean of the James T. Laney School of Graduate Studies

_____

Date

Deciphering how N-terminal phosphorylation alters fused in sarcoma (FUS) function: Implications for FTD/ALS pathogenesis

By

Michelle Johnson
B.A., Oberlin College, 2015

Advisor: Thomas Kukar, Ph.D.

An abstract of a dissertation submitted to the Faculty of the James T. Laney School of Graduate Studies of Emory University in partial fulfillment of the requirements for the degree of Doctor of Philosophy in Neuroscience
2021

Abstract

Deciphering how N-terminal phosphorylation alters
fused in sarcoma (FUS) function:
Implications for FTD/ALS pathogenesis

By Michelle Johnson

Fused in sarcoma (FUS) is an RNA/DNA binding protein that shuttles between the nucleus and cytoplasm to accomplish its various cellular functions. Genetic and nongenetic factors can trigger FUS to accumulate into toxic cytoplasmic aggregates. These aggregates occur in ~1% of amyotrophic lateral sclerosis (ALS) cases and ~10% of frontotemporal dementia (FTD) cases. While over 70 mutations in *FUS* are cause either FTD or ALS pathology, most cases with FUS pathology are not caused by genetic mutation. Identifying triggers of FUS aggregation independent of *FUS* genetic mutations is imperative to understanding FUS pathology. Certain post-translational modifications (PTMs) can shift a proteins cellular localization. Phosphorylation is the most common PTM used to regulate protein function in the cell. FUS can be phosphorylated at multiple N- and C-terminal residues. Specifically, our lab discovered that double strand DNA breaks (DSBs) induces DNA-PK to phosphorylate FUS at 12 N-terminal residues. Phosphorylated FUS then accumulates into cytoplasmic punctate. Nonetheless, it remains unclear 1) what mechanism mediates phosphorylated FUS to accumulate in the cytoplasm and 2) whether accumulation of phosphorylated FUS affects cellular function. Therefore, the goal of this dissertation was to investigate the role of N-terminal phosphorylation in shaping FUS function. In this dissertation, we established that mouse-derived cells do not phosphorylate or re-localize FUS following calicheamicin γ1 (CLM) induced DSBs. This finding suggests that mouse cells may not be a good model of DSB induced FUS pathology. Next, we performed proximity labeling via ascorbate peroxidase 2 (APEX2) paired with mass spectrometry to investigate whether phosphorylation shifts the FUS interactome and protein function. We found that expression of a mimetic of N-terminal phosphorylation, phosphomimetic FUS, shifted the FUS proteome towards regulating mRNA translation and metabolism. Overall, these studies indicate that phosphorylation of FUS is a primate specific response that may be an important regulator of FUS function and pathology.

Deciphering how N-terminal phosphorylation alters fused in sarcoma (FUS) function: Implications for FTD/ALS pathogenesis

By

Michelle Johnson
B.A., Oberlin College, 2015

Advisor: Thomas Kukar, Ph.D.

An dissertation submitted to the Faculty of the James T. Laney School of Graduate Studies of Emory University in partial fulfillment of the requirements for the degree of Doctor of Philosophy in Neuroscience
2021

Acknowledgements

This dissertation would not have been possible without the support of so many people.

I would first like to thank my advisor, Dr. Thomas Kukar. I appreciate everything you have done for me during these past four years. I would not be the scientist I am without your support, dedication, and willingness to listen to my crazy ideas. You showed me how to go above and beyond. Thank you for taking a chance on me.

I would next like to thank all of my lab members, both past and present. Our lab was my greatest support system, and I will miss our blue walls, hanging lanterns, and chats about how bad (and overpriced) the coffee at a certain campus coffee shop is.

Thank you to my committee (Dr. Seyfried, Dr. Hess, Dr. Corbett, and Dr. Bassell) for your thoughtful discussions and continued support. You all taught me how to question my assumptions and this is a skill I will use for the rest of my career.

Lastly, thank you to all of my friends and family (especially the ones who helped edit this document). I am so fortunate to have so much support in my life.

Table of contents

List of Figures and Tables

Chapter 1: Introduction

1.1 Overview

Frontotemporal dementia (FTD) and amyotrophic lateral sclerosis (ALS) are two neurodegenerative diseases that share many genetic and neuropathological markers. One such marker is the abnormal aggregation of the protein fused in sarcoma (FUS) into cytoplasmic inclusions in neurons and glia. FUS is a multifunctional RNA/DNA binding protein that shuttles between the nucleus and cytoplasm. The toxic accumulation of FUS in the cytoplasm is thought to occur when shuttling is impaired through genetic mutation or other mechanisms.

Over 70 genetic mutations have been linked to FUS pathology. Even so, most cases of FTD/ALS are not caused by genetic mutation. Therefore, investigating nongenetic causes of cytoplasmic FUS accumulation is imperative to building an understanding of FUS mediated pathology. Outside of genetic mutations, environmental stressors that cause DNA damage can trigger FUS pathology. Our lab was the first to discover that double strand DNA breaks (DSBs) trigger phosphorylation of FUS at N-terminal residues. Following this event, phosphorylated FUS accumulates in the cytoplasm. Nonetheless, it remains unclear what role this mechanism could play in FUS pathology**. Therefore, the overarching question of this dissertation was to investigate what role N-terminal phosphorylation plays in shaping FUS function**.

In this chapter, I provide an overview of the clinical and neuropathological characteristics of FTD and ALS followed by evidence that FTD and ALS exist on a disease spectrum. I then discuss the homeostatic functions of FUS and how disruption can result in FTD/ALS pathology. Finally, I conclude the chapter with a list of goals for the dissertation.

1.2 Frontotemporal Dementia (FTD)

1.2.1 A brief history of FTD

In 1892 Arnold Pick described a patient who exhibited aphasia, left temporal lobe atrophy, and presenile dementia (Pick, 1892). Following Pick's observation, silver staining of the patient's brain tissue revealed abnormally ballooned neuronal cells filled with cytoplasmic aggregates termed inclusions (Alzheimer, 1911). It was A. Gans in 1923 who first used the term "Pick's Atrophy" to describe these unique cases of dementia with atrophy of the frontal and temporal lobes (Gans, 1923). An understanding of disease pathogenesis would begin when K. Onari and H. Spatz showed that the characteristic neuronal inclusions were connected to the cortical atrophy. This led them to redesignate these cases "Pick's Disease" (Olney et al., 2017; Thibodeau and Miller, 2013). Finally, in 1994 Pick's Disease was re-classified under the umbrella term frontotemporal dementia (FTD) (1994). Though pathological inclusions had been connected to FTD since 1911, dysfunction of the integral RNA/DNA binding protein FUS would not be linked to FTD until 2009 (Neumann et al., 2009a).

1.2.2 Epidemiology of FTD

FTD is now classified as a heterogenous group of clinical disorders characterized by progressive deficits in language, executive function, and/or behavior (Bang et al., 2015; Mann and Snowden, 2017). Although FTD was originally thought to be a rare form of dementia, it is now appreciated to be a common and devasting neurodegenerative disease. The prevalence of FTD ranges widely depending on measurement used and the origin of the analyzed population. Specifically, FTD cases can vary between 0.01 to 4.61 cases per 1000 people in the general population (Hogan et al., 2016; Thibodeau and Miller, 2013). It is currently unclear what factors account for

this large range, but it likely includes non-genetic factors (this topic will be further elaborated in **section 1.5.5**). When the analysis is restricted to people age 65 or younger, the prevalence range narrows to 0.07 to 0.3 FTD cases per 1000 people (Hogan et al., 2016). This narrowing of the range likely reflects the consistently higher occurrence of FTD in this age group. Incidence, or the rate of occurrence of new cases of disease, is estimated to be between 0 and 0.33 cases per 1000 for the general population and between 0 and 0.06 cases per 1000 for persons 65 years and younger (Hogan et al., 2016). By the field's current understanding, FTD is the second most common form of early onset dementia and carries a lifetime risk of 1 in 742 (Coyle-Gilchrist et al., 2016; Erkkinen et al., 2018). A recent metanalysis found that individuals with FTD generally have a disease duration ranging from 2.5-8.2 years after symptom onset (Kansal et al., 2016). As such, FTD remains a relatively common and devasting disease for those it affects.

While early studies reported that men are more affected than women by FTD, subsequent studies have found no sex difference (Hodges et al., 2003; Hogan et al., 2016; Mercy et al., 2008; Ratnavalli et al., 2002). It should be noted that most past epidemiology studies of FTD have been heavily bias toward Caucasian subjects. Consequently, sex differences may exist in populations not currently studied (Onyike and Diehl-Schmid, 2013). Medical professionals and researchers should take this into account when working with non-Caucasian populations.

1.2.3 Clinical subtypes of FTD

FTD is subdivided into two clinical subtypes based on symptom presentation: behavioral variant frontotemporal dementia (bvFTD) and primary progressive aphasia (PPA) (Bang et al., 2015; Mackenzie et al., 2009; Olney et al., 2017). As the disease

progresses, the symptoms of the two subtypes can converge as patients develop global cognitive impairments and motor deficits (Bang et al., 2015).

bvFTD accounts for ~80% of FTD cases and is most common subtype of FTD (Hogan et al., 2016). It is primarily characterized by behavioral symptoms including personality changes, behavioral disinhibition, impulsivity, apathy, inertia, loss of empathy or sympathy, and compulsive or ritualistic behavior (Bang et al., 2015; Young et al., 2018). Even though bvFTD has a wide breath of potential symptoms, most patients exhibit some degree of apathy (O'Connor et al., 2017).

The primary symptom of PPA is language impairment with progressive worsening of language production, object naming, syntax and word comprehension (Bang et al., 2015; Gorno-Tempini et al., 2004). PPA can be further subdivided into semantic variant (svPPA), non-fluent variant (nvPPA), and logopenic variant (lvPPA) depending on the core features of the patient's dysfunction (Gorno-Tempini et al., 2004). Interestingly, while patients with PPA tend to progress more slowly toward severe disease stages than bvFTD, mean survival is shorter for PPA than bvFTD (Kansal et al., 2016; Mioshi et al., 2010). The reason for this discrepancy is currently unknown.

It should be noted that a large minority (estimated to be 33%) of PPA patients have pathology more consistent with Alzheimer's disease than FTD (Knibb et al., 2006). While FTD and AD are closely linked neurodegenerative diseases, the scope of this dissertation will focus on pathology related to frontotemporal lobar degeneration (as discussed in the **section 1.2.4**). Furthermore, in addition to the two subtypes of FTD discussed above, there are three additional clinical disorders that exist within the FTD spectrum that I will enclose under the broad category of FTD. These disorders result in either a motor neuron disease or parkinsonism. These are corticobasal degeneration,

progressive supranuclear palsy, and FTD with motor neuron disease (Woollacott and Rohrer, 2016).

1.2.4 Neuropathology of frontotemporal lobar degeneration (FTLD)

Frontotemporal lobar degeneration (FTLD) is the term used to describe the pathology that commonly underlies FTD (Mackenzie et al., 2009; Younes and Miller, 2020). FTLD arises from progressive neuronal loss, gliosis and microvascular changes in both frontal and temporal lobes (Bang et al., 2015; Kril and Halliday, 2011). The hallmark of FTLD is atrophy of frontal and temporal regions coupled with a general sparing of posterior cortical areas (Rohrer, 2012). Interestingly, the clinical subtypes discussed above show unique patterns of atrophy that can be detected by neuroimaging. For example, patients with bvFTD have more gray matter atrophy in frontal lobes, the anterior cingulate and the insula, areas typically associated with personality. In contrast, patients with PPA have predominately left side atrophy in areas typically associated with language production and comprehension. In svPPA, atrophy in anterioinferior temporal lobe and temporal gyrus is prominent. In nvPPA, the inferior-frontal regions and the insular cortex are major sites of atrophy (Bruun et al., 2019).

FTLD can be subdivided into proteinopathies based on the neuropathology of the cytoplasmic inclusions found in degenerating neurons (and to a lesser extent, glia) (Van Mossevelde et al., 2018). These subtypes are named after the major immunoreactive protein component of the cytoplasmic inclusions. These proteins are the RNA/DNA binding protein TAR DNA-binding protein 43 (TDP-43), the microtubule associated protein tau, and the FET family of proteins (FTLD-TDP, FTLD-Tau, and FTLD-FET, respectively) (Arai et al., 2006; Buée and Delacourte, 1999; Neumann et al., 2007; Neumann et al., 2009a; Neumann et al., 2006; Urwin et al., 2010). Lastly, an estimated

30%-60% of inclusions will also stain positive for ubiquitin, a major protein marker of degradation (Josephs et al., 2004; Shi et al., 2005).

The three proteinopathies can be distinguished further based on the structure of the associated neuropathological inclusions. ~50% of FTLD-Tau cases exhibit inclusions consistent with the classical rounded neuronal intracytoplasmic inclusions (NCI) termed Pick bodies first described by Alzheimer (Shi et al., 2005). In contrast, FTLD-TDP cases will exhibit some combination of NCI and dystrophic neurites (Mann and Snowden, 2017). Lastly, FTLD-FET cases exhibit NCIs that are immunoreactive for all three members of the FET family of proteins, TATA-box binding protein associated factor 15 (TAF15), Ewing's sarcoma (EWS), and FUS (Andersson et al., 2008; Neumann et al., 2011; Urwin et al., 2010).

FTLD-FET cases can further be broken down into three subtypes: Neuronal Intermediated Filament Inclusion Body Disease (NIFID), Basophilic Inclusion Body Disease (BIBD), and atypical FTLD-U (Mackenzie et al., 2008; Mann and Snowden, 2017; Munoz et al., 2009). Although these subtypes are currently grouped together as FTLD-FET, there are neuropathological differences that suggest they may be caused by distinct disease processes.

In brief, NIFID is characterized by positive FUS immunoreactivity in small round or oval compact NCIs in a variety of brain regions (cortex, hippocamps, striatum, etc.) (Cairns et al., 2004; Neumann et al., 2009b). BIBD is characterized by strong positive FUS immunoreactivity in round compact NCIs that are found in fewer brain regions than NIFID and consistent positive staining for ubiquitin (Mackenzie et al., 2011; Munoz et al., 2009). Lastly, atypical FTLD-U has the most restrictive positive FUS immunoreactive staining (mostly in the frontal cortex) and is characterized by neuronal

intranuclear inclusions (NII), uniform/round/oval shape NCI and glial cytoplasmic inclusions (Mackenzie et al., 2011; Neumann et al., 2009b).

1.2.4 Current treatments for FTD

Currently, there are no disease modifying treatments approved by the Food and Drug Administration (FDA) for FTD patients. Some symptoms can be managed with physical, occupational, and speech therapy. Clinicians often prescribe off-label use of certain medications to treat symptoms such as depression or anxiety (i.e. selective serotonin reuptake inhibitors, antipsychotics, cholinesterase inhibitors, N-methyl-D-aspartic acid (NMDA) receptor antagonists) (Tsai and Boxer, 2014; Younes and Miller, 2020). However, none of these interventions address the pathogenic mechanisms that cause neurodegeneration in FTD. Therefore, continued research is necessary to dissect why neuropathology arises in FTD subtypes in order to understand how it may be prevented.

1.3 Amyotrophic Lateral Sclerosis (ALS)

1.3.1 A brief history of ALS

ALS is a motor neuron disease that was first described in 1862 by Lockhart Clarke and Charles Bland Radcliffe who wrote of “a case of paralysis and muscular atrophy with disease of the nervous centres” coupled with “degeneration of the lateral columns in the spinal cord and atrophy of the anterior roots of the spinal cord and bulbar motor nerves” (Magnussen and Glass, 2017; Radcliffe and Clarke, 1862). Twelve years later, Jean-Martin Charcot coined the term “la sclérose amyotrophique”, or amyotrophic lateral sclerosis (ALS). ALS was the first description of a disease that involved both upper and lower motor neurons. This was a seminal finding as many researchers

believed pathology in both neuronal groups was impossible (Charcot, 1874; Turner et al., 2010). It should be noted that another researcher F. Aran described a similar muscular disease he termed progressive muscular atrophy that affected only lower motor neurons and some contemporary researchers have suggested that these patients may have had ALS (Al-Chalabi and Hardiman, 2013; Aran, 1850).

ALS was formally recognized under the umbrella term of motor neuron disease (MND) in 1962 along with progressive muscular atrophy and progressive bulbar palsy as diseases of upper neurons, lower neurons and mixed populations (Brain, 1956; Brain, 1962; Turner et al., 2010). While the first instance of heritable ALS was recognized in 1880 by Sir William Osler, the first mutation would not be mapped until 1993 (Rosen et al., 1993; Siddique and Ajroud-Driss, 2011). From there, it would take another decade for a mutation in *FUS* to be linked to ALS (Kwiatkowski et al., 2009; Vance et al., 2009b).

1.3.2 Epidemiology of ALS

A recent metanalysis estimated the worldwide incidence of ALS to be 1.68 per 100,000 individuals with evident heterogeneity between different countries (1.89 per 100,000 people in North Europe, 0.83 per 100,000 people in East Asia) (Marin et al., 2017). Furthermore, prevalence is estimated to be between 4.1 and 8.4 per 100,000 people (Longinetti et al., 2019). These rates may be increasing. One study estimated a 36% rise in incidence over a 25-year period and another estimated global prevalence to increase by 69% between 2015 and 2040 (Arthur et al., 2016; Leighton et al., 2019). It remains unclear whether ALS is becoming more common as these increases may be due to better diagnostic techniques coupled with an aging population (Marin et al., 2017).

Unlike FTD, sex differences of ALS have been consistently reported. On average, men are diagnosed 1.7x more often than women (McCombe and Henderson, 2010). Overall, the median age of onset is between 51 and 66 years of age, with men exhibiting an earlier age of onset than women (Longinetti et al., 2019; McCombe and Henderson, 2010). European countries tend to exhibit a later age of onset than Asian countries suggesting that some interplay of genetic and environmental factors may affect disease onset (Longinetti et al., 2019). Unlike the heterogeneity in disease onset, the median survival for most patients is between 20 and 48 months (Chiò et al., 2009a). Interestingly, ~5-10% of patients survive for greater than 10 years after symptom onset but the root cause of this enhanced survival is unknown. It has been suggested that men with symptom onset before 40 years of age tend to exhibit longer survival times but, overall, gender does not play a role in patient outcomes (Chiò et al., 2009a).

As with FTD, it should be noted that epidemiological studies of ALS usually contain data from populations of either European or Asian descent (Marin et al., 2017). Therefore, incidence and prevalence rates may be different for populations of non-Caucasian/Asian descent.

1.3.3 Clinical presentation of ALS

ALS is the most common clinical presentation of MND (Foster and Salajegheh, 2019). Approximately 70% of ALS patients will present with unilateral and focal limb weakness (~40% in lower limbs and ~30% in upper limbs) (Chiò et al., 2002). Owing to the heterogenous nature of ALS, the clinical presentation often varies from patient to patient but tends to fall into two general categories: limb-onset with a combination of upper and lower motor dysfunction (~75% of patients) or bulbar-onset with speech and swallowing dysfunction followed by limb dysfunction later in disease (~25-35% of

patients) (Kiernan et al., 2011; Traynor et al., 2000). Upper motor neuron involvement tends to present as limb spasticity, weakness, and brisk deep tendon reflexes. Lower motor neuron involvement tends to present with fasciculations, wasting and weakness (Kiernan et al., 2011). Furthermore, while it does not matter where disease symptoms originate (either upper or lower motor neurons), the disease must be progressive for patients to qualify for an ALS diagnosis (Brooks et al., 2000).

1.3.5 Neuropathology of ALS

No gross structural changes are observed in the gray matter of post-mortem brains from ALS patients. More sophisticated imaging methods such as voxel-based magnetic resonance imaging (MRI) morphometry have revealed that ALS patients display some level of global brain atrophy compared to aged-matched controls. Furthermore, they will generally have decreased volume in motor regions such as the right-hemisphere primary motor cortex. In contrast, white matter in the corticospinal tract may be increased, possibly due to alterations in oligodendrocyte myelin production although this may be age-dependent (Kassubek et al., 2005). Another study with slightly older participants showed slightly more brain atrophy. Patients exhibited bilateral decreased gray matter in premotor areas followed by frontal, temporal, and parietal lobes volume loss and reduced white matter volume in the right interior frontal gyrus (Senda et al., 2011). Lastly, ALS patients who have exhibited dementia show atrophy of the frontal and temporal lobes in line with the anatomical changes typically seen in FTD patients.

Gross morphological changes in the spinal cord tend to be more pronounced than in the brain. A recent longitudinal study of 158 patients was able to quantify the amount of cervical spinal cord atrophy and found a reduction from 63.8mm^2 to 60.8mm^2 with

the amount of atrophy worsening overtime. Furthermore, the study found that atrophy was worse for patients who exhibited a limb-onset rather than bulbar-onset (Wimmer et al., 2020). Post-mortem examination of the spinal cord typically reveals significant neuronal and myelinated axon loss in the lateral and anterior columns along with an overall decrease in the size of the anterior horn of the spinal cord. Lastly, there is a decrease in number and size in all motor neurons of the anterior horn. Other common features observed in the spinal cord include vacuolization, spongiosis, and massive astrogliosis due to the widespread neuronal loss (Boillée et al., 2006; Saberi et al., 2015). A recent study reported that long-term ALS patients (+10 after symptom onset) tend to exhibit less motor neuron degeneration and a lower density of microglia in the corticospinal tract and the anterior horn of the spinal cord (Spencer et al., 2020). These findings may suggest that a patient's prognosis is dependent on the rate of neuronal degeneration and glial activity.

Like FTD, ALS can be subdivided into three main neuropathological designations based on the proteins found in the cytoplasmic inclusions. Inclusions containing the protein superoxide dismutase 1 (SOD1) became the first identified neuropathological subtype outside of general ubiquitin aggregation (Kato et al., 2000; Saberi et al., 2015). It is now recognized that SOD1 positive inclusions account for ~2% of ALS cases (ALS-SOD1) (Ling et al., 2013). Next, in 2006 TDP-43 was identified as a major protein component of the ubiquitin positive inclusions, making it a new subtype (ALS-TDP) (Arai et al., 2006; Neumann et al., 2006). Over 90% of ALS cases are positive for both TDP-43 and ubiquitin, making it the most common neuropathology in ALS (Ling et al., 2013). The last protein to be identified as a major component of pathogenic inclusions in ALS was FUS (Kwiatkowski et al., 2009; Vance et al., 2009a). FUS is found in TDP-43

negative, ubiquitin positive inclusions in ~1% of ALS cases (Ling et al., 2013). It was these similarities in protein pathology between ALS and FTD that provided strong evidence that ALS and FTD may be linked (Abramzon et al., 2020; Mackenzie and Neumann, 2017).

1.3.4 Current treatments for ALS

The FDA has approved two different pharmacological medications for the treatment of ALS. The first to be approved was Riluzole (2-amino-6-(trifluoromethoxy)benzothiazole, RP 54274) in 1995. Riluzole is thought to slow the progression of disease in younger patients by inhibiting the release of the excitatory neurotransmitter glutamate (Bensimon et al., 1994; Martin et al., 1993; Miller et al., 2012). Following this, an easier to administer liquid form of Riuzole, Tiglutik, was approved in 2018. The second drug to be approved was Edaravone (3-methyl-1-phenyl-2-pyrazolin-5-one), which acts as an antioxidant, a free radical scavenger, and generally reduces oxidative stress (Cruz, 2018). The exact mechanisms of action for both Riluzole and Endaravone are currently unknown. Even so, there is evidence that both drugs provide a modest benefit: Riluzole slows disease progression by an estimated 3 months and Endaravone increases patient functioning on the standardized ALS-functional rating scale (Chen, 2020; Cruz, 2018).

Clinicians may prescribe other medications to treat some of the associated symptoms of ALS: depression, muscle cramps, constipation, uncontrolled laughing or crying. Additional therapies such as physical therapy, speech therapy, diet changes, and breathing support can all help better the quality of life for patients (Chen, 2020). Nonetheless, just like FTD, no treatments currently exist that directly target the protein neuropathology associated with ALS.

1.4 Evidence of FTD/ALS spectrum

1.4.1 The overlapping clinical profiles of FTD and ALS

For the past 20 years, pathological and genetic similarities between FTD and ALS have led researchers to suggest that FTD and ALS may exist on the same disease spectrum with the "pure" cases of FTD and ALS representing two extremes (Abramzon et al., 2020; Burrell et al., 2011; Chiò et al., 2019; Mackenzie and Neumann, 2017). It is now estimated that up to 30% of ALS patients develop cognitive impairments similar to FTD, and, conversely, 30% of FTD patients develop some level of motor dysfunction during the course of their disease (Burrell et al., 2011; Lomen-Hoerth et al., 2003). A further 50% of ALS patients will develop some level of cognitive impairment even if it does not reach diagnostic criteria for FTD (Lomen-Hoerth et al., 2003; Neary et al., 2000; Ringholz et al., 2005).

The level of cognitive impairment between patients with bulbar-onset ALS vs limb-onset ALS does not seem to differ but patients with bulbar-onset ALS are more likely to develop behavioral symptoms. Overall ALS patients have been reported to exhibit apathy, disinhibition and executive dysfunction, all symptoms consistent with bvFTD (Grossman et al., 2007; Lillo et al., 2010; Ringholz et al., 2005). While there is evidence that ALS patients can exhibit deficits in verbal fluency, these deficits are thought to originate from higher-order processing dysfunction and not impairment in primary linguistic abilities as observed in PPA (Abrahams et al., 2000). Taken together, ALS patients tend to develop symptoms more in line with bvFTD than PPA.

Of the large subset of ALS and FTD patients that exhibit some degree of symptom overlap, 12.5% of patients with FTD reach full diagnostic criteria for motor neuron disease (termed FTD-MND) (Burrell et al., 2016). FTD-MND patients provide a good

opportunity to study how FTD and ALS may overlap. Patients with FTD-MND can present with either cognitive or motor symptoms (Ahmed et al., 2020). These patients usually exhibit a faster disease progression and worse prognosis than “pure” FTD patients, suggesting FTD-MND causes more severe pathology (Hodges et al., 2003). A large percentage of FTD-MND patients will clinically exhibit behavioral changes and language dysfunction (>80% and >90%, respectively). However, it should be noted that the severity of behavioral changes and language dysfunction in FTD-MND patients is less extreme than “pure” cases of bvFTD and PPA (Long et al., 2021).

1.4.2 The overlapping neuropathology of FTLD and ALS

We can use the neuropathology of FTD-MND cases to examine the overlap of FTD and ALS. Even though most FTD-MND patients will have TDP-43 pathology, FTD-MND patients with FUS pathology will typically experience an earlier onset of symptoms. They often have little to no family history and exhibit primary symptoms consistent with bvFTD such as repetitive behaviors and social withdrawal (Bradfield et al., 2017; Burrell et al., 2016; Gowell et al., 2021; Lee et al., 2012; Snowden et al., 2011). Like FTD, all FTD-MND patients exhibit signs of frontal and anterior temporal atrophy, with the more severe cases showing more bilateral atrophy than controls. Moderate to severe FTD-MND cases will also show degeneration of various tracts including the bilateral corticospinal tract, a feature common in ALS (Long et al., 2021). This pathological evidence lends critical support to the theory that FTD and ALS exist on a disease spectrum (**Figure 1.1**).

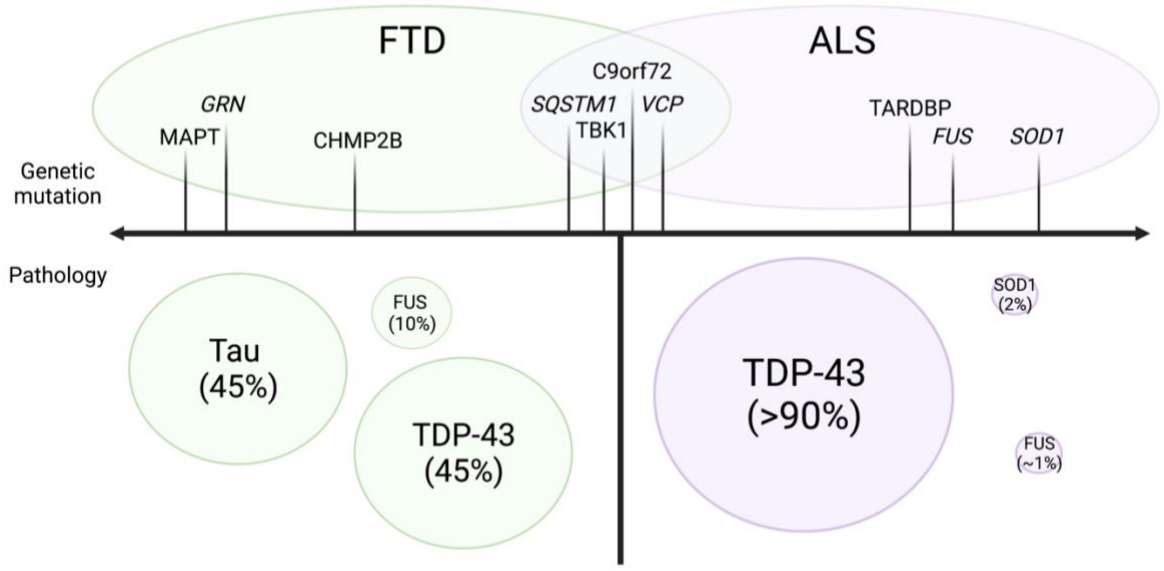

Figure 1.1 The FTD/ALS Spectrum

A graphical representative of the FTD/ALS disease spectrum. The FTD/ALS spectrum is defined by two factors: (1) Various genetic mutations can result in FTD or ALS. Of these commonly mutated genes, a subset will only result in FTD (green circle), a subset will only in ALS (purple circle) and a subset can cause either FTD or ALS (overlap). (2) FTLD/ALS are defined by the pathological inclusions found in post-mortem tissue. This pathology spectrum is shown on the bottom. The protein pathology associated with FTD (Tau, TDP-43, and FUS) is represented by green circles. The protein pathology associated with ALS (TDP-43, SOD1, and FUS) is represented by purple circles. Size of the circle corresponds to percentage of cases that are immunoreactive for the listed protein. Created with BioRender.com

1.4.3 The genetic interplay of FTD and ALS

FTD is a highly heritable disorder, with up to 40% of cases showing some level of family history (Moore et al., 2020; Rohrer et al., 2009a). This clear heritability of FTD suggests a strong role for genetics in disease onset and these cases are termed familial FTD (fFTD). Heritability differs across clinical FTD subtypes with bvFTD showing the strongest genetic association (Rohrer et al., 2009a). The majority of heritable FTD cases are caused by autosomal dominant mutations in three genes: progranulin (*GRN*), microtubule-associated protein tau (*MAPT*) and chromosome 9 open reading frame 72 (*C9orf72*). Repeat expansions in *C9orf72* were first discovered in 2011 and are the most common genetic cause of FTLD worldwide, accounting for ~25%-40% of fFTD cases (DeJesus-Hernandez et al., 2011; Moore et al., 2020; Renton et al., 2011; Tang et al., 2020b). Mutations in *GRN* and *MAPT* account for ~30% and 20% of fFTD cases, respectively (Moore et al., 2020; Olszewska et al., 2016). Autosomal dominant mutations in *VCP, CHMP2B, TARDBP, FUS, SQSTM1, TBK1,* and other genes account for the remaining ~10% of fFTD cases and <5% of all FTD cases (Greaves and Rohrer, 2019; Olszewska et al., 2016).

In contrast to FTD, familial ALS (fALS) accounts for only ~5-10% of total ALS cases. This suggests that ALS pathogenesis is less dependent on genetics than FTD (Abramzon et al., 2020; Ling et al., 2013). Mutations in *SOD1* were the first to be identified to cause ALS (Rosen et al., 1993). Since 1993, almost 200 *SOD1* mutations have been discovered to cause ALS. These variants account for ~2% of ALS cases (Kim et al., 2020). Outside of *SOD1*, mutations in over 50 genes account for an estimated 40-55% of fALS cases (Mejzini et al., 2019). The most commonly occurring genetic variations are in the following genes (in order of frequency): *C9orf72*, *SOD1*, *TARDBP*

and *FUS*. Like FTD, repeat expansions in C9orf72 account for ~34% of familial cases (DeJesus-Hernandez et al., 2011; Renton et al., 2011). Additionally, mutations in *TARDBP*, which codes for TDP-43, account for 4% of fALS (Kim et al., 2020; Neumann et al., 2006).

The role of *FUS* mutations in disease pathogenesis differs in FTD and ALS. Causative mutations in *FUS* that lead to pure FTD are very rare, with FTD symptoms usually developing after a primary diagnosis of MND (Blair et al., 2010; Broustal et al., 2010; Ticozzi et al., 2009). Only four mutations (M254V, P106L, P125P, and Q179H) in *FUS* have been linked to FTD without MND to date (Huey et al., 2012; Van Langenhove et al., 2010). Unlike FTD, over 50 causative *FUS* mutations have been identified to cause ALS (Kim et al., 2020). These mutations account for ~4% of fALS and cause an accumulation of FUS into cytoplasmic inclusions in neurons and glia (Kwiatkowski et al., 2009; Vance et al., 2009a). Causative *FUS* mutations tend to associate with an early onset of disease suggesting FUS dysfunction causes severe cellular toxicity. Due to the presence of *FUS* mutations in familial and sporadic FTD/ALS, understanding how FUS dysfunction occurs could allow for treatments that slow down disease progression (Gromicho et al., 2017; Hübers et al., 2015; Zou et al.). Refer to **Table 1.1** for a full list of identified genetic mutations in *FUS*.

1.4.4 FUS on the spectrum of FTD and ALS

A question has continuously plagued the FTLD-FET field: why do *FUS* mutations account for so few FTD cases but FUS pathology is seen in 10% of post-mortem FTD brains (**Figure 1.1**)? Past studies have used ALS-linked *FUS* mutations as proxies for FTLD-FET linked pathology. The problem with this paradigm is that by using a genetic model of FUS mislocalization, studies have been unable to study what factors may

trigger FUS mislocalization and accumulation independent of genetic factors. Furthermore, while FTLD-FET and ALS-FUS pathology overlaps, FUS inclusions in ALS are not immunoreactive for proteins commonly seen in FTLD-FET inclusions including the FET proteins (EWS and TAF-15), various heterogenous nuclear ribonucleoproteins (hnRNPs), and transportin-1 (TNPO1) (Gami-Patel et al., 2016; Neumann et al., 2011; Neumann et al., 2012) Nongenetic triggers of pathology, which are discussed in more detail in **section 1.5.5**, may hold the key to understanding how FUS dysfunction first arises and whether early triggers of dysfunction can be targeted to prevent neuronal death.

1.5 FUS-mediated pathology

1.5.1 Identification of FUS as a ubiquitously expressed, multifunctional protein

FUS, also known as translocated in liposarcoma (TLS), was originally identified in 1993 as a novel protein that replaced its RNA binding domain with the DNA-binding and leucine zipper dimerization domain of the transcriptional repressor, C/EBP Homologous Protein (CHOP;GADD153), creating a fusion protein that promoted the development of human myxoid liposarcoma (Aman et al., 1992; Crozat et al., 1993; Rabbitts et al., 1993). Following this, the same low-complexity domain of FUS was also found fused to the transcriptional activator, erythroblast transformation-specific related gene (ERG), in a human myeloid leukemia tumor (Prasad et al., 1994). As a novel protein at the time, the homeostatic functions of FUS were unknown. Early reports speculated that FUS was an RNA-binding protein due to the dual presence of a glycine-rich region and the RNA binding RGG domains that had been similarly mapped in other RNA binding proteins (Crozat et al., 1993). FUS binding to RNA was confirmed *in vitro*

when it was shown that FUS complexes with pre-mRNAs and other RNA binding proteins in conditions that promote splicing (Calvio et al., 1995). The full cDNA and amino acid sequence for FUS was eventually mapped, which revealed a structure where the N-terminal region contains a low-complexity SYGQ-domain paired with multiple RNA binding domains (RGG domains) in the C-terminus (Aman et al., 1996). Subsequent mapping of the gene through improved sequencing has led to current consensus on the protein domains in FUS shown in **Figure 1.2**.

While many were investigating the role of FUS fusion proteins in tumor formation, the normal functions of the full length FUS protein remained unknown. Zinszner et al. was the first to show *in vivo* that FUS rapidly shuttles between the nucleus and cytoplasm of the cell and can interact with RNA in both cellular compartments (Zinszner et al., 1997). FUS functions continued to add up as FUS was also linked to 1) modulating the granulocyte-colony stimulating factor receptor expression, 2) acting as a transcriptional modulator for various steroid receptors, 3) modulating the binding of a transcription factor, Spi-1/PU.1, to DNA, and 4) acting as a splicing factor (Hallier et al., 1998; Perrotti et al., 1998; Powers et al., 1998). In addition to its RNA and protein binding, FUS was further confirmed as a DNA binding protein that promotes the formation of D-loops, an essential process in DSB DNA repair, leading FUS to be re-classified as a RNA/DNA binding protein (Baechtold et al., 1999).

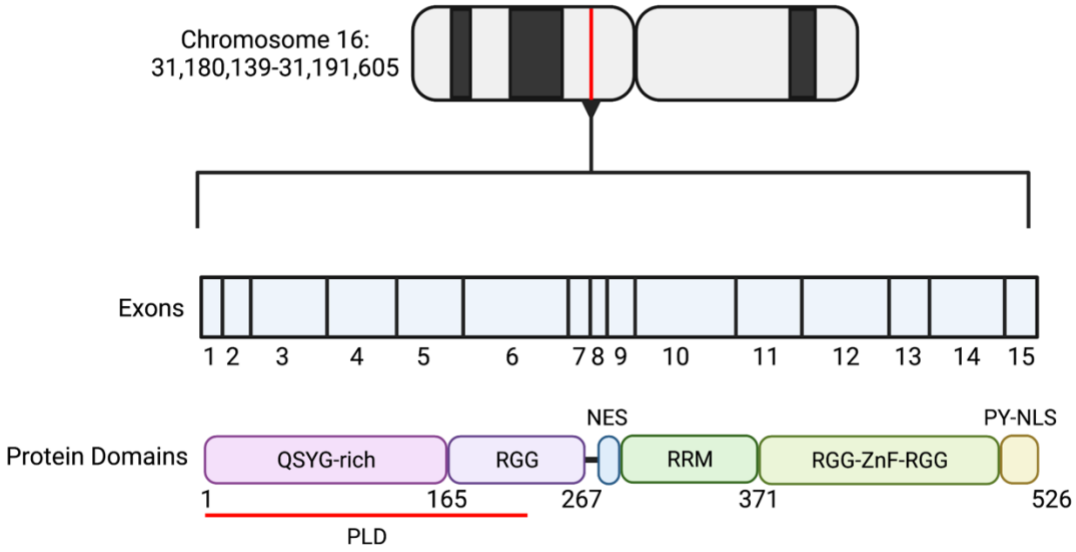

Figure 1.2 The genomic location and protein structure of FUS

The FUS gene is located on chromosome 16. The major transcript contains 15 exons that translate to a 75kDa protein. The FUS protein contains multiple domains and can be broken down into two major parts: an N-terminal low complexity region and a C-terminal RNA binding region. Specifically, it is comprised of a low complexity (LC) QSYG-rich domain and an RGG-rich domain. These two domains together compose the prion-like domain (PLD). Next, FUS contains a predicted nuclear export sequence (NES). The functionality of the NES has not been confirmed. Following this are the RNA binding domains, RNA recognition motif (RRM) and an RGG-Zinc Finger-RGG (RGG-ZnF-RGG) domain. Lastly, the protein contains a modified PY-nuclear localization sequence (PY-NLS). Created with BioRender.com

Knockout (KO) studies in mice were the gold standard for exploring *in vivo* homeostatic protein function for decades. Two different groups attempted to KO FUS in various mouse lines. Hicks et al. created an insertion mutation in exon 12 of FUS, leading to complete loss of wildtype protein production in inbred C57 BL/6 mice (Hicks et al., 2000). Mice homozygous for the insertion (Hicks-FUS$^{-/-}$) failed to suckle and died within 16 hours of birth. While histology revealed no gross anatomical anomalies, Hicks-FUS$^{-/-}$ mice had reduced white blood count, decreased B cell activation, and various chromosomal abnormalities including chromosome breakage, centromeric fusion, and extrachromosomal elements suggesting general genomic instability (Hicks et al., 2000). Around the same time, Kuroda et al. created an insertion mutation in exon 8 leading to loss of intact FUS protein in both the outbred CD1 mouse line and the inbred 129svev mouse line (Kuroda-FUS$^{-/-}$) (Kuroda et al., 2000). Unlike Hicks-FUS$^{-/-}$ mice, Kuroda-FUS$^{-/-}$ mice survived into adulthood, albeit slightly smaller in size than their wildtype littermates. Survival of these mice allowed further study of mouse development in the absence of FUS protein. Outbred Kuroda-FUS$^{-/-}$ mice were developmentally normal. In contrast, when FUS was KO'd in the inbred 129svev mouse line, survival was greatly impaired unless the animals were housed in a pathogen-free facility, suggesting immune dysfunctions similar to what was observed in the Hicks-FUS$^{-/-}$ mice. Furthermore, male inbred Kuroda-FUS$^{-/-}$ mice had reduced fertility and increased sensitivity to ionizing irradiation, a marker for dysfunctional DNA repair processes. Altogether, these reports provided the first evidence that FUS is an essential protein for immune system development and DNA repair.

The next eight years of FUS research focused on the role of FUS in spliceosome assembly and transcription (Meissner et al., 2003; Uranishi et al., 2001). First, various

groups determined preferential RNA and DNA sequences for FUS (Lerga et al., 2001; Takahama et al., 2009; Takahama et al., 2008). It was also during this time that Husai et al. first linked FUS to a neuronal function by identifying it as a binding partner to an excitatory NMDA neuronal receptor (Husi et al., 2000). Fujii et al. further expanded upon this finding by showing *in vivo* that FUS localized to the post-synaptic density of hippocampal dendrites in a mGluR5-dependent manner. It was also reported that loss of FUS led to decreased spine number and maturity, possibly due to changes in FUS-mediated shuttling of transcripts essential to dendrite structure (e.g. the transcript for the actin-stabilizing protein, Nd1-L) (Fujii et al., 2005; Fujii and Takumi, 2005). Along with this, FUS was also linked to two other proteins that are important for neuronal function: FMRP and HTT. Specifically, isoform 4 mRNA of FUS was found to be a target of the RNA binding protein, fragile X mental retardation protein (FMRP), whose loss leads to the development of fragile X syndrome (Chen et al., 2003). FUS was also identified as a co-aggregating protein with huntingtin (HTT), the protein responsible for Huntington's disease pathology, both *in vitro* and *in vivo* (Doi et al., 2008).

Finally, in 2009 and 2011 FUS was identified as a major component protein of the cytoplasmic protein inclusions in ALS and FTD, respectively (Kwiatkowski et al., 2009; Neumann et al., 2009a; Neumann et al., 2009b; Vance et al., 2009a). These discoveries fueled a new resurgence of FUS research, expanding the knowledge of FUS exponentially and proving that FUS is essential for both nuclear and cytoplasmic functions.

1.5.2 Current understanding of the FUS gene and protein structure

The *FUS* gene is ~11,467 bp long, located on chromosome 16, and contains 15 exons that translate to 13 transcripts that can be alternatively spliced into three protein

isoforms (https://www.ncbi.nlm.nih.gov/gene/2521) (Brunet et al., 2021). While a recent report shows some compelling data suggesting that *FUS* codes for two independent proteins, with both forms meditating toxicity, this finding has yet to be recapitulated (Brunet et al., 2021). Therefore, I will focus my summary on the traditional single FUS protein. Of the three isoforms, the most abundant is isoform 1 which codes for a 526-amino acid/75 kDa multi-domain protein (**Figure 1.2**). Expression of the FUS protein is a tightly regulated process. Overexpression of exogenous human FUS can trigger a decrease in endogenous FUS (Mitchell et al., 2012; Zhou et al., 2013). This compensatory mechanism is most likely the result of FUS autoregulation, where it has been shown that the FUS protein binds to the 7th exon of its own pre-mRNAs leading to a splice variant of FUS that is quickly targeted for nonsense mediated decay (NMD) (Zhou et al., 2013).

FUS is a member of the ubiquitously expressed FET family of proteins (composed of FUS, EWS and TAF15) (Andersson et al., 2008). Like all members of the FET family, FUS contains a low-complexity (LC) N-terminal domain and multiple C-terminal RNA binding domains (Svetoni et al., 2016). Although historically the N-terminus was viewed as a transcriptional activation domain, involved in binding DNA, while the C-terminus was viewed as the RNA binding domain, containing multiple RNA binding motifs (RNA-recognition motif (RRM) and a RGG-Zn-RGG domain) recent studies have mapped novel functions to the N-terminus (Crozat et al., 1993; Matsumoto et al., 2018; Patel et al., 2015; Prasad et al., 1994; Yang et al., 2014). It is now understood that the N-terminus is primarily composed of a prion-like domain (PLD) (the QSYG-rich domain and a portion of the RGG-rich region). Considered a subset of the broader category of LC domains, a PLD is a common feature of RNA binding proteins (RBP), as these

domains mediate the liquid-phase separation of RBPs that allows the sequestration of various proteins and RNAs into a transient membrane-less compartment in the cell (Hennig et al., 2015). The most important feature of this domain is that it allows for the *reversible* aggregation of proteins and RNA (Patel et al., 2015). From this, FUS can assemble and dissemble into multiple ribonucleoprotein (RNP) granules, including cytoplasmic stress granules and nuclear paraspeckles (Bosco et al., 2010; Hennig et al., 2015; Kato et al., 2012; Molliex et al., 2015; Sama et al., 2013).

Because PLD domains are disordered, the three-dimensional structure of these regions have been difficult to map. In 2017, Murray et al. was the first to characterize the structure of the PLD showing that it forms a 57-amino acid long "structured" fibril core. While this core resembles the characteristic (and pathogenic) amyloid fibrils seen in Alzheimer's disease (described in more detail in **section 4.4**), the amyloid core in FUS lacks the necessary hydrophobic sidechains. The absence of these sidechains is thought to give the PLD its propensity to disassemble and allows FUS to mediate *reversible* phase separation (Luo et al., 2018; Murray et al., 2017). Following this original report, Luo et al. further divided the 57-amino acid fibril core into two separate segments that form amyloid fibrils that have a structure directly mediated by temperature and phosphorylation state of the protein, again suggesting that there is a *reversible* nature to the structure of the domain (Luo et al., 2018).

There is some evidence that regions of the FUS amyloid core are more prone to aggregate when they exist as peptides outside of the full-length FUS protein but future studies will need to study this in the context of the full length protein before we can begin to understand how these different amyloid regions contribute to aggregation (Ding et al., 2020). It should now be noted that phase separation of FUS is a complex

process and is mediated by multiple factors including protein-protein interactions, interaction of the arginine rich C-terminal domain with the tyrosine rich N-terminal domain through pi-pi cation interactions, and RNA binding. Disruption of any of these interactions can trigger formation of stable FUS RNP granules that are toxic to the cell (Bogaert et al., 2018; Hofweber et al., 2018a; Maharana et al., 2018; Qamar et al., 2018). To prevent toxicity, the cell must tightly regulate these interactions to ensure dynamic phase separation of FUS RNP granules. Besides mediating phase separation, there is evidence that the RGG domain in the PLD may robustly bind RNA, albeit to a lower extent compared to the C-terminus (Ozdilek et al., 2017; Schwartz et al., 2013). Whether this property of the PLD domain effects protein function remains to be determined.

Outside of the N-terminal RGG domain, the C-terminus is littered with multiple domains capable of binding multiple types of RNA sequences (Schwartz et al., 2013; Wang et al., 2015). These domains are the RNA recognition motif (RRM) and RGG-ZnF-RGG domain (**Figure 1.2**). Even though earlier reports debated the RNA binding abilities of the RRM, it is now recognized that both the RRM and the RGG-ZnF-RGG domains bind RNA and DNA (Liu et al., 2013; Schwartz et al., 2013). In line with this, the mechanism that the C-terminus of FUS uses to bind RNA has been recently elucidated. Specifically, the ZnF domain binds to GGU regions of RNA and the RRM domain binds to the classical RNA stem loop. From here the RGG domains act as a magnet, increasing the affinity of FUS binding to RNA (Loughlin et al., 2019). Through these features, FUS is able to bind RNA and DNA within multiple cellular compartments.

Finally, FUS contains a non-classical proline-tyrosine nuclear localization sequence (PY-NLS) (located at the C-terminus) and a predicted nuclear export sequence

(NES) that mediate its movement between the nuclear and cytoplasmic compartments. The mechanism of FUS nuclear import is well documented. It is through the PY-NLS that transportin-1/2 (TNPO), a nuclear import receptor, binds FUS and traffics the protein from the cytoplasm into the nucleus in a GTP-dependent manner (Dormann et al., 2010; Güttinger et al., 2004; Niu et al., 2012). Interestingly, the PY-NLS may also play an indirect role in FUS phase separation as loss of TNPO1 binding to FUS leads to enhanced aggregation (Hofweber et al., 2018b; Yoshizawa et al., 2018). Unlike nuclear import, it remains unknown whether FUS participates in active nuclear export mediated through the NES. There is evidence that the NES is nonfunctional and that a majority of FUS export is mediated through passive diffusion through the nuclear pore (Ederle et al., 2018). This could be possible as large proteins up to 230 kDa have been shown to cross the nuclear pore within minutes to hours (Timney et al., 2016). Even so, it has been suggested that a post-translational modification (PTM) in FUS could "activate" the NES, allowing exportin proteins to shuttle FUS into the cytoplasm, but more work will need to be done to examine this possibility (Kırlı et al., 2015). For now, the functionality of the NES is disputed.

1.5.3 Homeostatic FUS functions

FUS is an abundant, widely-expressed protein found in most cells that was traditionally thought to localizes primarily to the nucleus (Svetoni et al., 2017). Even so, FUS is still relatively abundant in the cytoplasm with a subpopulation specifically localizing to the dendritic spines of neurons (Deng et al., 2014b; Fujii et al., 2005). Owing to its relative abundance in both the nucleus and the cytoplasm, FUS function can be broken down by cellular compartment. It should be noted that there is interplay between its functions in both compartments. As such, these functions should not be

considered separate entities as they do influence each other even though this discussion will categorize each function based on compartment.

1.5.3.1 Nuclear functions

FUS performs and regulates multiple processes in the nucleus of the cell. First, FUS associates with transcriptionally active chromatin through its PLD in an RNA-dependent manner. From here, FUS specifically accumulates at transcriptional start sites. This association impedes the necessary phosphorylation of the C-terminal domain of RNA Polymerase II, the major polymerase responsible for synthesizing pre-mRNA transcripts, mediating the transcription for ~20% of cellular genes. Interestingly, many of these transcripts are related to mitochondrial function, mRNA splicing, mRNA processing and mRNA metabolism suggesting a role for FUS in mediating these functions (Kwon et al., 2013; Schwartz et al., 2012; Tan et al., 2012; Zhou et al., 2014). Second, FUS mediates the alternative splicing of ~300 pre-mRNAs *in vivo*, possibly through repressing exon recognition (Lagier-Tourenne et al., 2012). Third, FUS is involved in the formation of paraspeckles, nuclear bodies involved in sequestering transcripts during cellular stress events, by complexing with the major constituents, NEAT1 and NONO, through its PLD (Shelkovnikova et al., 2014). Lastly, as introduced in **section 1.5.1**, FUS expression is integral to DNA repair. However, to understand the impact FUS has on DNA repair mechanisms, we must first understand DNA damage.

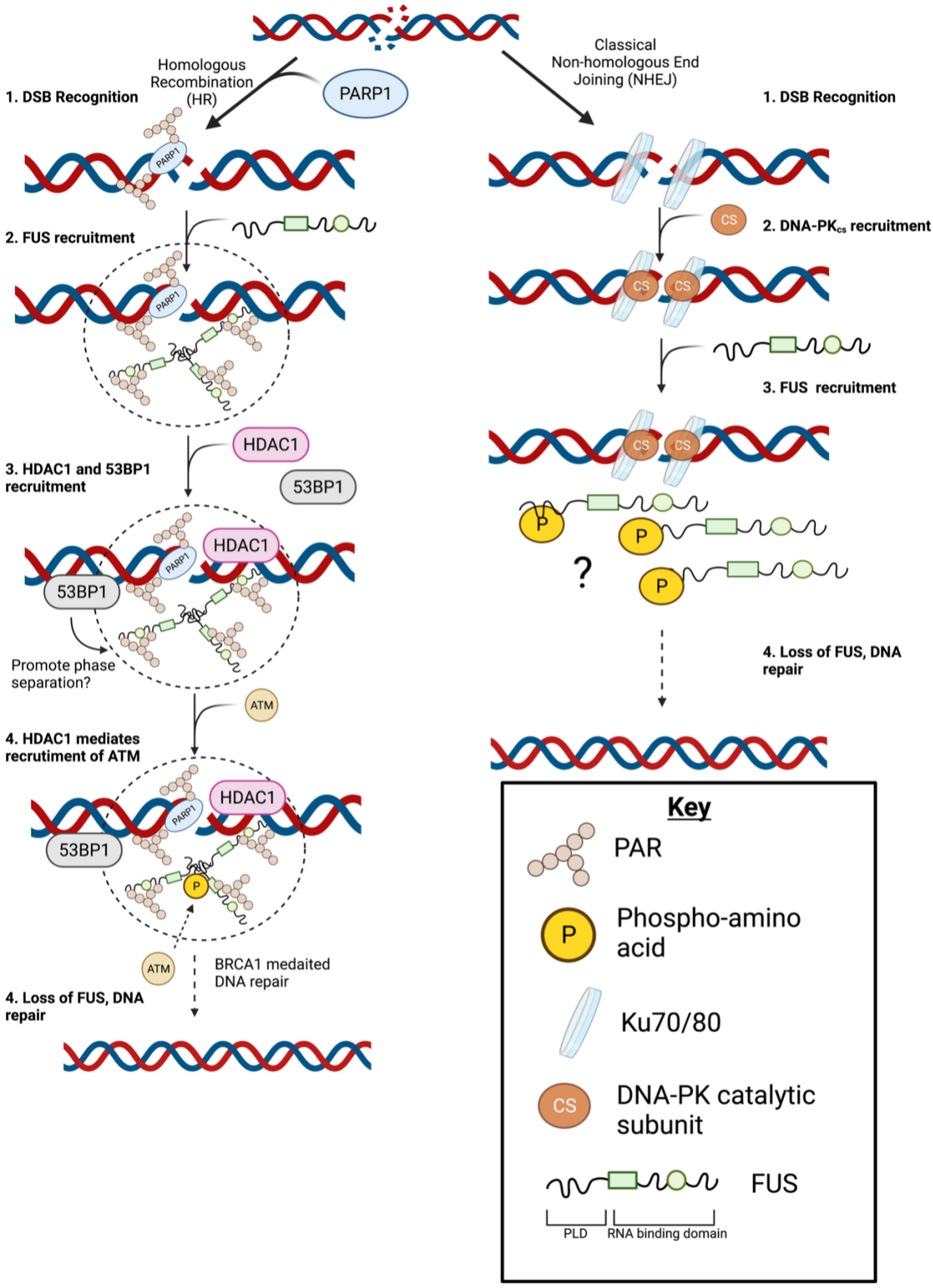
Homologous Recombination (HR)
PARP1
1. DSB Recognition
2. FUS recruitment
3. HDAC1 and 53BP1 recruitment
HDAC1
53BP1
Promote phase separation?
4. HDAC1 mediates recrutiment of ATM
ATM
BRCA1 medaited DNA repair
4. Loss of FUS, DNA repair
Classical Non-homologous End Joining (NHEJ)
1. DSB Recognition
CS
2. DNA-PKcs recruitment
3. FUS recruitment
P
?
4. Loss of FUS, DNA repair
Key
PAR
Phospho-amino acid
Ku70/80
DNA-PK catalytic subunit
FUS
PLD
RNA binding domain

Figure 1.3 FUS in DSB repair

FUS recruitment to sites of DNA damage is integral to supporting homologous recombination (HR) and non-homologous end joining (NHEJ). On the left is HR: (1) PARP1 acts as a DNA damage sensor and is recruited early to the DSB site. PARP1 begins polyADP-ribosylation (PARylation) modification of target proteins. (2) PARylation recruits FUS to DSB. FUS triggers phase separation, creating a compartment of damaged DNA and DNA repair proteins. (3) Downstream DNA repair proteins such as HDAC1 and 53BP1 are recruited to the DSB. 53BP1 may assist in phase separation. (4) ATM is recruited, possibly by HDAC1, and phosphorylates FUS. (5) FUS dissociates and DNA is repaired in a BRAC1-dependent process. On the right is classical NHEJ: (1) Ku70/80 acts as a DNA damage sensor and is recruited to the DSB site. (2) Ku70/80 recruits DNA-PK catalytic subunit (cs) (3) FUS is recruited to DSB site. (4) DNA-PK$_{cs}$ phosphorylates FUS. FUS dissociates from the DNA. Downstream process allows DNA repair. Created with BioRender.com

1.5.3.1.2 DNA damage and repair

DNA can be damaged by endogenous (e.g. replication errors and reactive oxygen species mediated damage) and exogenous sources (i.e. UV exposure, ionizing radiation, and carcinogenic chemicals) (Chatterjee and Walker, 2017). These events result in different classes of DNA damage: DNA lesions, single base damage, bulky lesions, base mismatch, intrastrand crosslinks, translesion synthesis, single strand DNA breaks (SSBs), and double strand breaks (DSBs) (Chatterjee and Walker, 2017). FUS has a weak affinity for double strand DNA in general. However, it is specifically recruited to sites of SSBs and DSBs to participate in one of three mechanisms: base excision repair (BER) for SSBs and homologous recombination (HR) and non-homologous end-joining (NHEJ) for DSBs (**Figure 1.3 for HR and classical NHEJ, Figure 4.1 for modified atypical NHEJ**) (Mastrocola et al., 2013; Rulten et al., 2013; Sama et al., 2014; Singatulina et al., 2019; Sukhanova et al., 2020; Wang et al., 2015). Many of the methods used to study FUS mediated DNA repair produce a mixture of base lesions, SSBs and DSBs. Therefore, this discussion will highlight the method that was used to induce DNA damage as a proxy for the type of damage.

HR and NHEJ are complex repair processes dependent on sequential recruitment of various proteins to the site of DNA damage. Two enzymes in the phosphoinositide 3-kinase related kinase (PIKK) family, ataxia-telangiectasia mutated (ATM) and DNA-dependent protein kinase catalytic subunit (DNA-PK_{cs}), are responsible for recruiting additional proteins to sites of DSB for HR and NHEJ, respectively. FUS is a known target of both kinases (**Figure 1.3**) (Deng et al., 2014b; Gardiner et al., 2008). FUS expression is required for efficient DNA repair. Inhibiting FUS recruitment to sites of DNA damage following UVA micro-irradiation results in

diminished HR and NHEJ (Mastrocola et al., 2013; Muster et al., 2017; Wang et al., 2013). Furthermore, FUS regulates the mRNA for 60% of the genes involved in both pathways (Zhou et al., 2014). Taken together, these data support early observations that FUS KO leads to chromosomal instability and dysfunctional DNA repair (**section 1.5.1**).

What role does FUS recruitment play in DNA repair? FUS recruitment is facilitated by the essential upstream enzyme poly(ADP-Ribose) polymerase (PARP1). UVA micro-irradiation causes PARP1 to induce PARylation or the synthesis of PAR chains which attach to various proteins surrounding the site of DNA damage. These PAR chains recruit FUS to the sites of DNA damage in a poly(ADP-ribose) glycohydrolase (PARG)-dependent manner (Muster et al., 2017; Rulten et al., 2013; Sukhanova et al., 2020). Following recruitment, integral downstream proteins including HDAC1, γH2AX, 53BP1, and p-ChK2 depend on FUS to facilitate their own recruitment (Gong et al., 2017; Wang et al., 2013). Taken together, FUS recruitment is an early and essential component of HR and NHEJ.

What role could FUS be having in DNA repair outside of recruitment? Recently, a report provided evidence that FUS induces the formation of a compartment of FUS, the PAR polymers, other RNA binding proteins with low-complexity domains and the damaged DNA through phase separation. This compartmentalization may be important for DNA repair initiation as it allows for more contact with damaged DNA and repair proteins, potentially leading to more efficient DNA repair (Levone et al., 2021; Singatulina et al., 2019). Even so, many aspects of FUS-mediated DNA repair remain unclear: Does FUS play an active role in recruiting the downstream enzymes? Is FUS required for the actual repair of DNA or does it only serve to recruit proteins to the

repair site? Is FUS preferentially used in HR or NHEJ? And specifically, what role does PIKK mediated phosphorylation of FUS play in DNA repair? Future studies should focus on how FUS phase separation mediates downstream protein recruitment to understand the role FUS is directly playing in DNA repair.

1.5.3.2 Cytoplasmic functions

In the cytoplasm, FUS mediates various functions related to mRNA trafficking, metabolism, translation, and suppression. Overall, FUS is estimated to have ~5,500 mRNA targets of which >700 transcripts are targeted specifically in the cytoplasm (Colombrita et al., 2012; Lagier-Tourenne et al., 2012). These targets tend to be involved in processes related to FUS function including regulation of transcription, RNA processing, and cellular response to stress (Colombrita et al., 2012). Once bound to these transcripts, FUS can traffic a subset of mRNA transcripts to distal cellular locations such as the dendrite to mediate local translation (Shiihashi et al., 2017). FUS expression can also act as a negative regulator of translation by ensuring efficient ribosomal stalling in a mTOR-dependent manner (Kamelgarn et al., 2018; Sévigny et al., 2020). Lastly, FUS expression mediates mRNA metabolism through associating with transcript that are targets of nonsense mediated decay (Ho et al., 2021).

One of the most important functions of FUS in the cell occurs during a stress event. During times of cellular stress, cytoplasmic FUS enters stress granules (SG), which are membrane-less organelles that reduce stress-related damage by sequestering proteins and mRNA to silence translation, thereby minimizing energy use during a stress event (Baron et al., 2013; Lenzi et al., 2015; Mahboubi et al., 2013; Shelkovnikova et al., 2013). Various stressful events can promote the formation of SG including heat

stock, osmotic stress, and oxidative stress (Lenzi et al., 2015; Sama et al., 2013). FUS directly associates with multiple major stress granule components, including G3BP1 and TIA1 (Baron et al., 2013; Markmiller et al., 2018). Known SG markers such as PABP1 and eIF4G, have also been shown to co-localize with insoluble inclusions in FTLD-FUS patients (Dormann et al., 2010). This, along with other lines of evidence, has led to a general model of FUS pathology where cells that have undergone multiple stress events begin to create stable granules that are less dynamic and, eventually, fail to dissemble. As these SGs become less dynamic, FUS and other proteins begin to aggregate leading to the characteristic insoluble inclusions seen in ALS and FTLD (Dormann and Haass, 2011; Patel et al., 2015). The propensity of FUS to form these aggregates is dependent on both genetic and nongenetic factors.

1.5.4 Role of genetic mutations in FUS-mediated ALS/FTD pathology

Causative *FUS* mutations have been linked to disrupting almost every aspect of homeostatic FUS function. Most FUS mutations will impair the binding of FUS to its nuclear export protein, TNPO1. This results in a buildup of cytoplasmic FUS that eventually accumulates into insoluble inclusions (Dormann et al., 2010; Matsumoto et al., 2018; Niu et al., 2012). Outside of the creation of inclusions, evidence suggests that ALS-linked mutations also cause FUS to develop toxic gain-of-functions (López-Erauskin et al., 2018; Scekic-Zahirovic et al., 2016; Shiihashi et al., 2016). In the nucleus, ALS-linked mutations (R521G and R495X) disrupt FUS binding to active chromatin, suggesting mutant cells express altered RNA Pol II activation patterns and, subsequently, altered transcription patterns (De Santis et al., 2017; Yang et al., 2014). Splicing is also affected by ALS-linked mutations, trapping essential minor spliceosome proteins U11 and U12 into cytoplasmic aggregates and altering the splicing of U11/12-

target minor introns (Reber et al., 2016). In line with this, ALS-linked *FUS* mutations shift the global transcriptome, enriching for mRNAs related to cell adhesion and nervous system development (De Santis et al., 2017). Furthermore, ALS-linked mutations disrupt FUS recruitment to sites of DNA damage (Naumann et al., 2018). Lastly, ALS-linked mutations disrupt FUS autoregulation leading to increased FUS protein levels (Humphrey et al., 2020; Zhou et al., 2013). All these changes to cellular function eventually cause the cell to accumulate DNA damage in the nucleus.

In the cytoplasm, ALS-linked mutations generally shift the cellular proteome, upregulating proteins related to catabolic processes and downregulating proteins related to neuron development (Baron et al., 2019; Boehringer et al., 2017; Garone et al., 2020; Kamelgarn et al., 2016). Expression of ALS-linked mutant FUS also alters translation and mRNA catabolism (Kamelgarn et al., 2018). Most importantly, expression of ALS-linked mutant FUS is linked to increased recruitment of FUS into stress granules, altered stress granule homeostasis, and, eventually, a diminished capacity for stress granule disassembly (Baron et al., 2013; Lenzi et al., 2015; Lo Bello et al., 2017; Patel et al., 2015; Shelkovnikova et al., 2013).

FUS dysfunction can also affect neuronal function. Genetic deletion of the FUS PY-NLS causes widespread dysfunction, decreasing neuronal firing, dendrite spine number, and disrupts mRNA transport in neurons (Shiihashi et al., 2017). Furthermore, neurons expressing ALS-linked mutant FUS have decreased mobility of key organelles needed at distal cellular sites including the mitochondria and lysosomes, suggesting FUS mutations can instigate general trafficking and autophagy dysfunction (Naumann et al., 2018). But, as stated above, most FUS pathology is not caused by genetic mutation. Therefore, we must explore alternative modulators of FUS function.

1.5.5 Role of nongenetic factors in FUS mediated ALS/FTS pathology

Protein function is mediated not only by its amino acid sequence but also by the enzymatic modifications that can occur on various amino acids after translation. Termed post-translational modifications (PTMs), these nongenetic mediators of FUS dysfunction may hold the key to understanding what triggers disease pathogenesis. Past reports have linked various PTMs to FUS dysfunction including changes in methylation and phosphorylation status (Bowden and Dormann, 2016; Darovic et al., 2015; Dormann et al., 2012; Higelin et al., 2016; Sama et al., 2013; Scaramuzzino et al., 2013; Singatulina et al., 2019; Verbeeck et al., 2012).

Changes in arginine methylation of FUS has the strongest evidence for its involvement in FUS pathology (**Figure 1.3**). Specifically, arginine methylation in the RGG3 domain by PRMT1 is thought to disrupt TNPO1 binding to FUS leading to increased cytoplasmic localization. In parallel, unmethylated and monomethylated forms of FUS show increased binding affinity for TPNO1 suggesting that modifying methylation state may reduce FUS pathology (Dormann et al., 2012; Scaramuzzino et al., 2013; Suárez-Calvet et al., 2016; Tradewell et al., 2012). No causative mutations for FTLD have been found in the methyltransferase proteins (PRMT1, PRMT3, and PRMT8) responsible for regulating FUS methylation state suggesting these disease processes exist outside of genetic mutation (Ravenscroft et al., 2013). However, while there is evidence that post-mortem tissue from ALS patients contain a dimethylated (or hypermethylated) form of FUS, post-mortem tissue from FTLD patient inclusions contains a monomethylated (or hypomethylated) form of FUS, suggesting divergent disease processes may be responsible for FUS aggregation in ALS and FTLD (Dormann et al., 2012; Suárez-Calvet et al., 2016). In line with this, there is now strong evidence

that hypomethylation of FUS at these C-terminal arginine residues promotes the formation of stable β sheets that result in solid and undynamic RNP granules that resemble toxic inclusions (Hofweber et al., 2018a; Qamar et al., 2018). As such, the methylation model of FUS pathology currently suggested by Hofweber et al. postulates that ALS-FUS patients express a hypermethylated form of FUS that has a low binding affinity for its nuclear import protein/chaperone, TNPO1. Without contact from its chaperone, FUS begins to accumulate into less dynamic RNP granules and form insoluble inclusions leading to pathology. In contrast, FTLD-FUS patient cells lose TNPO1 activity through some undetermined mechanism and FUS begins to aggregate in the cytoplasm. Overtime, the loss of the TNPO1/FUS interaction triggers some unknown compensatory mechanism that promotes hypomethylation of FUS to try to increase TNPO1/FUS affinity. Unfortunately, un/monomethylated FUS has a higher propensity to form stable RNP granules leading to the formation of the characteristic FUS inclusions. This may explain why FTLD-FUS and not ALS-FUS inclusions are immunoreactive for TNPO1 as the un/monomethylated form of FUS can still bind the activity-depleted TNPO1 and sequester it into the cytoplasmic inclusions (Hofweber et al., 2018a; Troakes et al., 2013). However, this model does not address how TNPO1 activity loss initially occurs. Could another modification be responsible for dysregulating FUS/TNPO1?

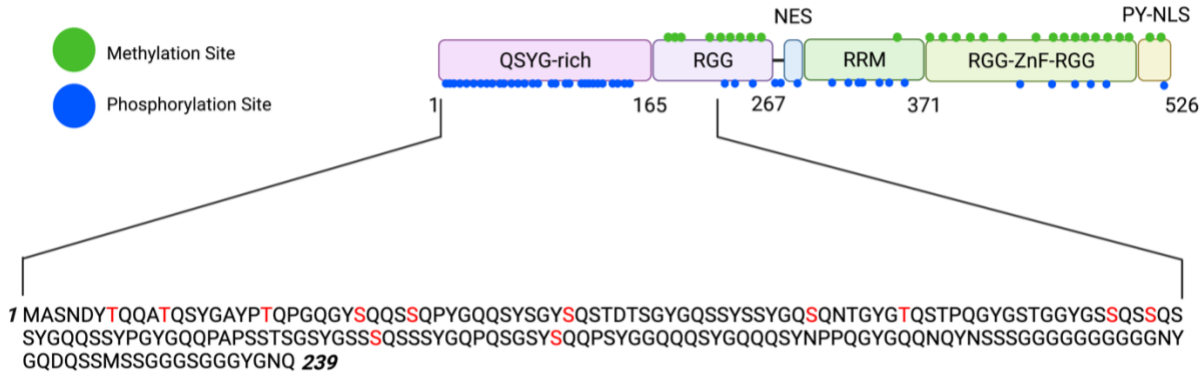

Figure 1.4 Methylation and phosphorylation sites of FUS

Graphical representation of the methylation and phosphorylation sites with FUS domain structure. Methylation sites are represented by green circle, phosphorylation sites are represented by blue circle (Rhoads et al., 2018b). Methylation sites tend to group near C-terminus, phosphorylation sites tend to group near N-terminus. Amino acid sequence for the prion-like domain (PRL) is highlighted. S/T_Q sites phosphorylated by DNA dependent protein kinase catalytic subunit (DNA-PK$_{cs}$) are highlighted in red. Created with BioRender.com

PTM's can have synergistic effects on proteins. It may be possible that some environmental factor triggers novel/different PTM's on FUS that initiates dysfunction. One potential PTM is phosphorylation, which has also been linked to increased cytoplasmic localization of FUS. Phosphorylation is the covalent addition of a phosphate group to a serine, threonine, or a tyrosine residue. It is the most common reversible PTM, thought to work as a biological switch that allows the cell to turn various cellular processes (signaling pathways, metabolism, receptor activity) on and off (Virág et al., 2020). Like other proteins of a similar size, FUS can be phosphorylated at multiple N- and C-terminal residues by multiple kinases (Owen et al., 2020; Rhoads et al., 2018b). The first biologically relevant phosphorylation site to be described in FUS was S256 when it was shown that phosphorylation at this site mediates its proteasome-dependent degradation (Perrotti et al., 2000). Following this report, FUS was also shown to be phosphorylated at S42 by the PIKK enzyme, ATM (Gardiner et al., 2008). Still, it was not until the next decade when two reports showed that phosphorylation could shift FUS cellular localization. The first, Darovic et al., showed that phosphorylation at Y526 located in the PY-NLS leads to decreased affinity between FUS and TNPO1 (Darovic et al., 2015). However, our lab was the first to show that a biologically relevant trigger, DSB, triggers DNA-PK$_{cs}$ to phosphorylate FUS at N-terminal residues in the PLD (Deng et al., 2014b). Our original report predicted that DNA-PK$_{cs}$ phosphorylated FUS at 12 S/T_Q residues. These sites were all confirmed in subsequent publications by other groups (Deng et al., 2014b; Monahan et al., 2017; Murray et al., 2017) (**Figure 1.3**). Subsequently, our lab then showed that this new species of phosphorylated FUS then accumulates in the cytoplasm along with the FET protein, TAF-15, and TNPO1 (Deng et al., 2014b). While there was some early disagreement in the literature about FUS

localization following DSB, the observation that phosphorylated FUS accumulates in the cytoplasm following DSB has now been recapitulated by other groups (Bennetzen et al., 2018; Monahan et al., 2017; Naumann et al., 2018; Rhoads et al., 2018a; Singatulina et al., 2019).

So, how might DNA damage play a role in FUS mediated pathology? There are multiple reports that FTLD-FUS and ALS-FUS patients have increased p-H2AX, a marker of DNA damage that can be activated by DNA-PK$_{cs}$ and ATM (Deng et al., 2014b; Naumann et al., 2018; Wang et al., 2013). There is also evidence that DSB directly trigger the formation of cytoplasmic FUS inclusions signifying that DNA damage may be an upstream process of FUS inclusion formation (Deng et al., 2014b; Naumann et al., 2018). Lastly, inhibition of PARP1, the protein responsible for recruiting FUS to sites of DSB, can indirectly trigger cytoplasmic FUS aggregation (**section 1.5.3.1.2**) (Naumann et al., 2018). Thus, DSB induced N-terminal FUS phosphorylation may represent a new mechanism through which FUS dysfunction is triggered.

1.6 Summary and goals of dissertation

The evidence overwhelmingly indicates that FTLD/ALS-mediated FUS pathology is triggered by FUS cytoplasmic accumulation. Understanding the primary triggers of FUS accumulation in the cytoplasm will be integral to determining what aspects of FUS biology may be possible targets to prevent pathology. DNA damage is a common marker of FTLD/ALS pathology. As such, the discovery that DSB mediates N-terminal phosphorylation FUS provides the first mechanism for how a biologically relevant environmental stress may cause FUS pathology. Unfortunately, phosphorylated FUS accumulates in the cytoplasm, it still remains unclear whether N-terminal

phosphorylation affects cellular function. As discussed above, FUS is involved in multiple cellular functions and phosphorylation is a known mediator of protein function. Therefore, N-terminal phosphorylation may change multiple cellular functions at once. **Thus, the overall goal of this dissertation is to determine whether N-terminal phosphorylation shifts FUS function.**

In line with this goal, I explored the effect of N-terminal phosphorylation at 12 key residues in FUS. In **Chapter 2**, I report that mouse cells do not phosphorylate FUS following DSB possibly due to impaired DNA-PK activation. In **Chapter 3**, I focused my studies on a human-derived model of FUS function to investigate whether DSB-mediated phosphorylation of FUS alters function by shifting the FUS protein-protein interaction network. I provide compelling evidence that N-terminal phosphorylation leads to meaningful shifts in the FUS proteome towards a translational active state. Finally, in **Chapter 4**, I summarize the significance of these findings and provide a description of possible future studies.

Clinical pres.	DNA change (cDNA)	Protein change	Reference(s)
ALS	c.6C > T	p.Ala2Ala*	(Belzil et al., 2011)
ALS	c.52C>T	p.Pro18Ser	(Belzil et al., 2011)
ALS	c.147C>A	p.Gly49Gly*	(Zou et al., 2012)
ALS	c.(170_172del), c.170_172del	p.Ser57del	(Belzil et al., 2009)
ALS	c.198T>C	p.Tyr66Tyr*	(Lai et al., 2011)
ALS	c.269C > T	p.Tyr91Tyr*	(Belzil et al., 2011)
ALS	c.287_291delinsAT	p.Ser96del	(Yan et al., 2010)
ALS	c.291C>T	p.Tyr97Tyr*	(Zou et al., 2012)
ALS	c.344G>A	p.Ser115Asn	(van Blitterswijk et al., 2012)
ALS	c.430_447del	p.Gly144_Tyr149del	(Belzil et al., 2011; Brown et al., 2012)
ALS	c.453C>T	p.Pro151Pro*	(Zou et al., 2012)
ALS	c.467G>A	p.Gly156Glu*	(Ticozzi et al., 2009)
ALS	c.515delGAGGTGGAGGTG	p.Gly 171_174del	(Corrado et al., 2010)
ALS	c.521_523+3del	p.Gly174_Gly175del	(Kwiatkowski et al., 2009; Yan et al., 2010)
ALS	c.521_523+3delGAGGTG	p.Gly174del	(Brown et al., 2012; Hewitt et al., 2010)
ALS	c.insGAGGTG523	p.insGG	(Kwiatkowski et al., 2009)
ALS	c.delGAGGTG523	p.delGG	(Kwiatkowski et al., 2009)
ALS	c.559G>A	p.Gly187Ser	(Rademakers et al., 2010)
ALS	c.571G>A	p.Gly191Ser	(Corrado et al., 2010)
ALS	c.616G>A	p.Gly206Ser	(Yan et al., 2010)
ALS	c.646C>T	p.Arg216Cys	(Corrado et al., 2010)
ALS	c.648C>T	p.Arg216Arg*	(Zou et al., 2012)
ALS	c.661_663delAGT	p.Ser211del	(Lattante et al., 2012)
ALS	c.666_667insGGC	p.G222_G223insG	(Belzil et al., 2011)

Clinical pres.	DNA change (cDNA)	Protein change	Reference(s)
ALS	c.667-678delGGCGGCGGCGGC	G223-G226del	(Yan et al., 2010)
ALS	c.674G>T	p.Gly225Val	(Corrado et al., 2010)
ALS	c.676_684del	p.228_230delGGG	(Kwon et al., 2012)
ALS	c.679_681delGGC	p.Gly 223del	(Corrado et al., 2010)
ALS	c.679_684delGGCGGC	p.Gly 223_Gly224del	(Corrado et al., 2010)
ALS	c.680_691delGGCGGCGGTGGT	p.Gly 227_Gly230del	(Corrado et al., 2010)
ALS	c.681_684delGGC	p.230delG	(Kwon et al., 2012)
ALS	c.682_687delGGCGGT	p.Gly 228_Gly229del	(Corrado et al., 2010)
ALS	c.684C > T	p.G228G	(Belzil et al., 2011)
ALS	c.688G>T	p.Gly230Cys	(Corrado et al., 2010)
ALS	c.700C>T	p.Arg234Cys	(Corrado et al., 2010)
ALS	c.701G>T	p.Arg234Leu	(Ticozzi et al., 2009)
ALS	c.730C>T	p.Arg244Cys	(Kwiatkowski et al., 2009)
ALS	c.1173C > A	p.Pro391Pro*	(Belzil et al., 2011)
ALS	c.1196G>T	p.Gly399Val	(Kwon et al., 2012)
ALS	c.1204_1232delinsGGAGGTGGAGG	p.Ser402_Pro411delinsGlyGlyGlyGly	(DeJesus-Hernandez et al., 2010)
ALS	c.1317T>C	p.Ser439Ser*	(Brown et al., 2012)
ALS	c.1385C>T	p.Ser462Phe	(Groen et al., 2010)
ALS	c.1392G>T	p.Met464Ile	(Nagayama et al., 2012)
ALS	c.1395_1541+1del	p.Gly466ValfsX14	(DeJesus-Hernandez et al., 2010)

Clinical pres.	DNA change (cDNA)	Protein change	Reference(s)
ALS	c.1449-1488delCTACCGGGGCCGCGGCGGGGACCGTGGAGGCTTCCGAGGG	p.Tyr485AfsX514	(Yan et al., 2010)
ALS	c.1459C>T	p.Arg487Cys	(van Blitterswijk et al., 2012)
ALS	c.1464C > T	p.Gly488Gly*	(Belzil et al., 2011; Zou et al., 2012)
ALS	c.1483C>T	p.Arg495X	(Kim et al., 2015; Kwon et al., 2012; van Blitterswijk et al., 2012; Yan et al., 2010)
ALS	c.1483delC	p.Arg495GlufsX527	(Yan et al., 2010)
ALS	c.1485delA	p.Gly497AlafsX527	(Yan et al., 2010)
ALS	c.1506dupA	p.Arg502fsX15	(Belzil et al., 2011)
ALS	c.1507_1508delAG	p.Gly503TrpfsX12	(Kwon et al., 2012)
ALS	c.1509_1510del	p.Gly504TrpfsX12	(Kim et al., 2015; Kwon et al., 2012; Zou et al., 2012)
ALS	c.1156C > A	p.Arg386Arg*	(Belzil et al., 2011)
ALS	c.1520G>A	p.Gly507Asp	(Corrado et al., 2010; Hewitt et al., 2010; Lai et al., 2011)
ALS	c.1527insTGGC	p.Lys510TrpfsX517	(Yan et al., 2010)
ALS	c.1528A>G	p.Lys510Glu	(Suzuki et al., 2010; Syriani et al., 2011)
ALS	c.1537T>C	p.Ser513Pro	(Suzuki et al., 2010)
ALS	c.1540A>G	p.Arg514Gly	(Vance et al., 2009a)
ALS	c.1542G>T	p.Arg514Ser	(Kwiatkowski et al., 2009; Robertson et al., 2011; Suzuki et al., 2010)

Clinical pres.	DNA change (cDNA)	Protein change	Reference(s)
ALS	c.1542G>C	p.Arg514Ser	(Chiò et al., 2009b; Kwiatkowski et al., 2009; Millecamps et al., 2010; Robertson et al., 2011)
ALS	c.1543G>T	p.Gly515Cys	(Kwiatkowski et al., 2009)
ALS	c.1547A>T	p.Glu516Val	(Robertson et al., 2011)
ALS	c.1549C>G	p.His517Asp	(Tsai et al., 2011)
ALS	c.1550A>C	p.His517Pro	(Suzuki et al., 2010)
ALS	c.1551C>G	p.His517Gln	(Kwiatkowski et al., 2009)
ALS	c.1552A>G	p.Arg518Gly	(Lai et al., 2011)
ALS	c.1553G>A	p.Arg518Lys	(Kwiatkowski et al., 2009)
ALS	c.1554_1557del	p.Gln519IlefsX9	(Bäumer et al., 2010)
ALS	c.1555C>T	p.Gln519X	(Belzil et al., 2011)
ALS	c.1561C>T	p.Arg521Cys	(Belzil et al., 2009; Blair et al., 2010; Chiò et al., 2011; Corrado et al., 2010; Groen et al., 2010; Kwiatkowski et al., 2009; Lai et al., 2011; Millecamps et al., 2010; Rademakers et al., 2010; Suzuki et al., 2010; Ticozzi et al., 2009; Vance et al., 2009a; Yan et al., 2010)

Clinical pres.	DNA change (cDNA)	Protein change	Reference(s)
ALS	c.1561C>G	p.Arg521Gly	(Brown et al., 2012; Kwiatkowski et al., 2009; Sproviero et al., 2012; Ticozzi et al., 2009)
ALS	c.1561C>A	p.Arg521Ser	(Millecamps et al., 2010)
ALS	c.1562G>A	p.Arg521His	(Belzil et al., 2009; Blair et al., 2010; Broustal et al., 2010; Groen et al., 2010; Kwiatkowski et al., 2009; Lai et al., 2011; Millecamps et al., 2010; van Blitterswijk et al., 2012; Van Langenhove et al., 2010; Vance et al., 2009a; Yan et al., 2010; Zou et al., 2012)
ALS	c.1562G>T	p.Arg521Leu	(Lattante et al., 2012; Millecamps et al., 2010; Yan et al., 2010; Zou et al., 2012)
ALS	c.1564A>G	p.Arg522Gly	(Kwiatkowski et al., 2009)
ALS	c.1566G>A	p.Arg522Arg*	(Ticozzi et al., 2009)
ALS	c.1570A>T	p.Arg524Trp	(Hewitt et al., 2010)
ALS	c.1571G>C	p.Arg524Thr	(Kwiatkowski et al., 2009)
ALS	c.1572G>C	p.Arg524Ser	(Kwiatkowski et al., 2009; Yan et al., 2010)

Clinical pres.	DNA change (cDNA)	Protein change	Reference(s)
ALS	c.1574C>T	p.Pro525Leu	(Bäumer et al., 2010; Brown et al., 2012; Chiò et al., 2009b; Kwiatkowski et al., 2009; Mochizuki et al., 2012; Yan et al., 2010)
ALS	c.1575G>T	p.Pro525Pro*	(Lai et al., 2011)
ALS	c.1581del	p.X527TyrextX1	(Kwon et al., 2012)
FTD and/or ALS	c.4180–4185 delGAGGTG	Gly174-Gly175 del GG	(Huey et al., 2012)
FTD and/or ALS	c.1566G > A	p.Arg522Arg*	(Broustal et al., 2010)
FTD	c.22508384>T	p.Pro106Leu	(Huey et al., 2012)
FTD	???	p.Pro125Pro*	(Huey et al., 2012)
FTD	???	p.Gln179His	(Huey et al., 2012)
FTD	c.760A>G	p.Met254Val	(Van Langenhove et al., 2010)

(*) synonymous mutation; Clinical pres. (Clinical presentation)

Table 1.1 Genetic Variations in *FUS* linked to ALS and FTD

Chapter 2: Divergent FUS phosphorylation in primate and mouse cells following double-strand DNA damage

Adapted from: Johnson MA, Deng Q, Taylor G, McEachin ZT, Chan AWS, Root J, Bassell GJ, Kukar T. Divergent FUS phosphorylation in primate and mouse cells following double-strand DNA damage. *Neurobiol Dis*. 2020 Sep 17:105085. doi: 10.1016/j.nbd.2020.105085.

2.1 Abstract

Fused in sarcoma (FUS) is an RNA/DNA protein involved in multiple nuclear and cytoplasmic functions including transcription, splicing, mRNA trafficking, and stress granule formation. To accomplish these many functions, FUS must shuttle between cellular compartments in a highly regulated manner. When shuttling is disrupted, FUS abnormally accumulates into cytoplasmic inclusions that can be toxic. Disrupted shuttling of FUS into the nucleus is a hallmark of ~10% of frontotemporal lobar degeneration (FTLD) cases, the neuropathology that underlies frontotemporal dementia (FTD). Multiple pathways are known to disrupt nuclear/cytoplasmic shuttling of FUS. In earlier work, we discovered that double-strand DNA breaks (DSBs) trigger DNA-dependent protein kinase (DNA-PK) to phosphorylate FUS (p-FUS) at N-terminal residues leading to the cytoplasmic accumulation of FUS. Therefore, DNA damage may contribute to the development of FTLD pathology with FUS inclusions. In the present study, we examined how DSBs effect FUS phosphorylation in various primate and mouse cellular models. All cell lines derived from human and non-human primates exhibit N-terminal FUS phosphorylation following calicheamicin γ1 (CLM) induced DSBs. In contrast, we were unable to detect FUS phosphorylation in mouse-derived primary neurons or immortalized cell lines regardless of CLM treatment, duration, or concentration. Despite DNA damage induced by CLM treatment, we find that mouse cells do not phosphorylate FUS, likely due to reduced levels and activity of DNA-PK compared to human cells. Taken together, our work reveals that mouse-derived cellular models regulate FUS in an anomalous manner compared to primate cells. This raises the possibility that mouse models may not fully recapitulate the pathogenic cascades that lead to FTLD with FUS pathology.

2.2 Introduction

Frontotemporal dementia (FTD) is the most common form of dementia in people under the age of 60 and the third most common form of dementia in the United States overall (Boxer et al., 2020; Hodges et al., 2003; Knopman and Roberts, 2011; Vieira et al., 2013) Although a heterogeneous disorder, FTD symptoms typically include progressive deficits in behavior, executive function, and/or language (Bang et al., 2015). The neuropathology underlying FTD is called frontotemporal lobar degeneration (FTLD). FTLD is defined by neurodegeneration, gliosis and microvascular changes within the frontal and/or anterior temporal brain cortices (Bahia et al., 2013; Mackenzie et al., 2009, 2010). FTLD is further subdivided into groups based on the major protein found in neuronal and glial inclusions. The four subgroups of FTLD are defined by the abnormal accumulation of the following proteins: 1) tau, 2) TAR DNA-binding protein 43 (TDP-43), 3) the FET (FUS, EWS, TAF-15) proteins, or 4) ubiquitin/proteasome system proteins (FTLD-tau, FTLD-TDP, FTLD-FET, and FTLD-UPS, respectively) (Neumann and Mackenzie, 2019). While the majority of FTLD cases have tau or TDP-43 pathology (36–50% and ~50%, respectively), a significant proportion of FTLD cases have inclusions containing the FET proteins (~10%) (Neumann et al., 2009).

The FET family of proteins includes fused in sarcoma (FUS), Ewing's sarcoma (EWS), and TATA binding protein-associated factor 15 (TAF-15) (Andersson et al., 2008). FUS, EWS, and TAF-15 are ubiquitously expressed, multi-functional RNA/DNA binding proteins (Deng et al., 2014a). FUS was the first FET protein linked to FTD (Kwiatkowski et al., 2009; Neumann et al., 2009a; Vance et al., 2009a). Like the other FET proteins, FUS contains three characteristic domains: a low complexity SYGQ domain, a 3-glycine/arginine rich RGG domains, and a zinc finger domain (Andersson

et al., 2008; Svetoni et al., 2016). FUS utilizes these domains to facilitate multiple cellular functions in both the cytoplasm and nucleus including DNA transcription, RNA translation, mRNA splicing, stress granule formation, and DNA repair (De Santis et al., 2017; Fujii et al., 2005; Kamelgarn et al., 2016; Sama et al., 2014; Schwartz et al., 2012; Shelkovnikova et al., 2013; Tan et al., 2012; Yang et al., 2014; Zinszner et al., 1997). Given this diverse set of functions, FUS must shuttle rapidly between the nucleus and cytoplasm of the cell. However, in FTLD-FET, disrupted nuclear/cytoplasmic shuttling causes FUS to accumulate into insoluble cytoplasmic inclusions. Multiple studies have shown that FUS-positive cytoplasmic inclusions can trigger a toxic gain-of-function that leads to cell death in a concentration dependent manner (Deng et al., 2014b; Mitchell et al., 2012; Scekic-Zahirovic et al., 2016). In other words, the more FUS that accumulates in the cytoplasm, the greater the toxicity.

Pathogenic FUS mutations almost invariably cause ALS (Renton et al., 2014). FTD caused by a FUS mutation is extremely rare or leads to a combined FTD-ALS presentation (Broustal et al., 2010; Rohrer et al., 2009a; Snowden et al., 2011). For that reason, FTLD-FET pathogenesis is thought to primarily occur independent of genetic factors, and may instead be the result of broader impairments in the transport or function of these RNA-binding proteins (Darovic et al., 2015; Deng et al., 2014a; Dormann et al., 2012; Gami-Patel et al., 2016; Niu et al., 2012; Ravenscroft et al., 2013). In line with this idea, various non-genetic models of FUS transport deficits have been described including changes in methylation status, loss of transportin-1/FUS interaction, cellular stress events, and phosphorylation (Bowden and Dormann, 2016; Darovic et al., 2015; Dormann et al., 2012; Higelin et al., 2016; Sama et al., 2013; Scaramuzzino et al., 2013; Singatulina et al., 2019; Verbeeck et al., 2012). Previous

studies from our lab and others have shown that double-stranded DNA damage induces phosphorylation of N-terminal residues in FUS (Deng et al., 2014b; Monahan et al., 2017; Rhoads et al., 2018a). Following this event, we have shown that p-FUS begins to accumulate in the cytoplasm of the cell (Deng et al., 2014b). Evidence suggests that DNA damage is a common hallmark of FUS protein pathology (Deng et al., 2014b; Higelin et al., 2016; Naumann et al., 2018). Therefore, DNA damage induced N-terminal phosphorylation may be a critical pathological event leading to FUS cytoplasmic accumulation and toxicity.

Here, we aimed to study FUS phosphorylation in mouse primary cellular models because they are a tractable and scalable model that have been used to study neurodegeneration in other contexts. Surprisingly, we were unable to detect FUS phosphorylation following calicheamicin-γ1 (CLM) induced double-strand DNA damage in primary mouse neurons. Further, we found that mouse-derived immortalized cell lines show no detectable phosphorylation of FUS or cytoplasmic accumulation in response to CLM treatment. Our data suggests that decreased expression and activity of the DNA-dependent protein kinase (DNA-PK) in mouse cells compared to human cells may underlie the species-specific difference we observed. These data indicate that there are fundamental differences in DNA damage and repair pathways between rodents and primates.

2.3 Materials and Methods

2.3.1 Cell culture

2.3.1.1 Primary Mouse Neurons. All animal experiments were reviewed and approved by the Institutional Animal Care and Use Committees at Emory in accordance with the National Institutes of Health Guide for the Care and Use of Laboratory

Animals. Mouse primary cortical neurons were isolated and cultured according to a previously described procedure (Sala et al., 2000). In brief, mouse primary cortical neurons were isolated from E18 C57BL/6 mouse brain cortices, plated on 12-well plates and cultured in neurobasal medium (Giboco) containing 2% B27 (GIBCO). Neurons were used 7-14 days after plating. The cultures were maintained at 37°C in a 5% CO_2 incubator. The culture medium was changed with the same solution 24 hours after plating and then half-changed once every week.

2.3.1.2 Nonhuman primate induced pluripotent stem cells (iPSCs), neural progenitor cells, and differentiated cells. Wild type non-human primate iPSCs, neural progenitor cells (NPC), differentiated neurons were generated and cultured as published (Carter et al., 2014; Cho et al., 2019a; Cho et al., 2019b). In brief, iPSCs were dissociated from MEF feeder layers and were cultured in MEF-conditioned ES cell medium without bFGF (R&D). After 7 days, ES cell medium was replaced with derivation medium. After another 7 days, neurospheres were plated on P/L-coated cell culture dishes and expanded in neural proliferation medium. After 7-10 days, neural rosettes were manually picked and seeded onto fresh cell culture dishes in differentiation medium. Cells were finally differentiated with the supplement of SHH and FGF and ascorbic acid.

2.3.1.3 Human-derived iPSC Maintenance and motor neuron differentiation. A control iPS cell line was maintained on Matrigel coated dishes and fed every day with mTesR1 medium (Stem Cell Technologies). Cells were passaged every 5-7 days using ReLesR passaging reagent. For differentiation to motor neurons, iPSC colonies were treated with 10 μM ROCK inhibitor, Y-27632 (Stem Cell Technologies), for ~1 hour before being dissociated to single cells using Accutase (Stem Cell

Technologies) for ~8 minutes. Cells were resuspended in motor neuron differentiation medium (1:1 Advanced DMEM-F12/Neurobasal, 1× N2, 1× B27, 0.2 % penicillin/streptomycin (Pen/Strep), 1× Glutamax, 110 μM β-mercaptoethanol) and seeded in 10 cm Ultra-Low Attachment dishes (Corning) in order to form embryoid bodies. Cells were maintained as embryoid bodies throughout the differentiation procedure and were fed every 2 days. The differentiation medium contained 3 μM CHIR99021 (Stem Cell Technologies), 10 μM SB431542 (Stem Cell Technologies), 10 μM DMH1, and 10 μM Y-27632. On Day 2, 1 μM Retinoic Acid (Sigma) and 500 nM Smoothened Agonist (Millipore) were added to the differentiation medium. CHIR99021 was removed from the medium on Day 6 and SB and DMH1 were removed from the medium on Day 10. Subsequently, on Day 14, 10 ng/mL BDNF (Peprotech) and 10 ng/mL GDNF (Peprotech), and 10 μM DAPT (Tocris) were added. On day 20, embryoid bodies were disassociated to single cells using papain/DNase (Worthington Bio) and plated on polyornithine/laminin coated cell culture plates.

2.3.1.4 Human neurons. Human neurons were purchased from ScienCell and cultured according to manufacturer recommendations (ScienCell, #1520).

2.3.1.5 Immortalized Cell Lines. Human neuroglioma cells (H4; ATCC) were cultured in Opti-MEM medium plus 5% fetal bovine serum (FBS) and 1% Pen/Strep. Human embryonic kidney cells (HEK293T; ATCC) and mouse embryonic fibroblasts (MEF; kindly provided by Dr. Bob Farese) were cultured in DMEM medium plus 10% FBS and 1% Pen/Strep (Gibco). Human SH-SY5Y cells (SH-SY5Y; ATCC) and mouse Neuro2A (N2A; ATCC) cells were cultured in MEM medium plus 1% Pen/Strep and either 15% FBS and 10% FBS, respectively. All cultures were maintained at 37˚C with 5% CO_2.

2.3.2 Drug Treatments

Calicheamicin $\gamma 1$ (CLM) was obtained from Pfizer. Staurosporine was purchased from Cell Signaling Technologies (CST; #9953). Calyculin A (Cal A) was purchased from Cell Signaling Technology (CST; #9902). All drugs were resuspended in DMSO and aliquoted and stored at either -20˚C or -80˚C until use. Cells were plated into 60mm dishes and dosed 72 hours later at between 70-85% confluency.

2.3.3 Cell Transfection

Mouse and human GFP-FUS plasmids were obtained from Dr. Keith W. Caldecott. HEK293T and N2A cells were plated into 6-well plate and allowed to grow overnight. The next day, cells were transfected with 2.5 ug of mouse GFP-FUS or human GFP-FUS DNA using the TransIT®-LT1 Transfection Reagent (Mirus; MIR2300) Cells were allowed to express plasmids for 24 hours before treatment.

2.3.4 Western blotting

Cell lysis and western blotting was performed as previously described with minor modifications (Holler et al., 2017). In brief, cells were lysed on ice in either RIPA Buffer (50mM tris pH=8.0, 150mM NaCl, 0.1% SDS, 1% trition-x-100, 0.5% sodium deoxycholate) or cytoplasmic lysis buffer (50mM tris pH=8.0, 150mM NaCl, 0.5% trition-x-100) with 1% protein/phosphatase inhibitor (ThermoFisher; 78442). The RIPA lysate was sonicated and centrifuged for 15 min at 14,000 rpm at 4°C. The cytoplasmic lysate was vortexed and centrifuged for 15 minutes at 14,000 rpm at 4˚C. The supernatant was saved as the detergent soluble protein fraction. Protein concentration were measured in the detergent soluble protein fraction by BCA assay (Pierce). Next, cell lysates were analyzed for relative protein expression using SDS/PAGE followed by two-channel infrared quantitative western blots as described previously (Deng et al., 2014b).

The samples were denatured in 1× Lammeli loading buffer with 5% tris(2-carboxyethyl)phosphine (TCEP) at 70°C for 15 min. Equal amounts of protein were loaded into either 4-20% or 12% PROTEAN TGX Precast Gels (Bio-Rad). After transferring to 0.2 μm nitrocellulose membranes, blots were stained with Revert 700 (LI-COR; 926-11010) to measure total protein for normalization, captured at 700nm on an Odyssey Fc Imaging System (LI-COR), then destained following the manufacture's protocol. Protein blots were then blocked in Odyssey or Intercept blocking buffer in TBS (LI-COR; 927-500000 or 927-60001, respectively) for 1 h at room temperature and incubated with primary antibodies (diluted in 1:1 blocking buffer and TBS plus 0.2% Tween 20) overnight at 4°C. Membranes were washed three times for five minutes in TBST and then incubated with the appropriate secondary antibody (10% blocking buffer diluted in TBS plus 0.1% Tween 20 (TBST)) for 60 minutes at room temperature. Membranes were then washed three times with TBST for five minutes and visualized using the Odyssey Fc Imaging System (LI-COR). The following primary antibodies were used: FUS (1:1000; Santa Cruz; sc47711), FUS (1:2000; Bethyl Laboratories; A300-302A), phospho-ATR/ATM Substrate Motif [(pS/pT) QG] (1:1000; Cell Signaling Technologies; 6966), H2AX (1:1000; Millipore; AB10022), p-H2AX (1:1000; Millipore; 05-636), GAPDH (1:10,000; Cell Signaling Technologies; 2118), Mouse Specific cleaved PARP (1:1000; Cell Signaling Technologies; 9544), tubulin (1:20,000; Epitomics), total DNA-PK (1:500; ThermoFisher; PA5-86134), and p-DNA-PK (S2056) (1:1000; Abcam; ab18192). p-FUS (Ser30) antibody was kindly provided by Dr. Frank Shewmaker (Rhoads et al., 2018a).The following secondary antibodies were used: Donkey anti-mouse IgG Alexa Fluor Plus 680 (1:10,000; ThermoFisher; A32788) and Donkey anti-rabbit IgG Alexa Fluor Plus 800 (1:10,000; ThermoFisher; A32808).

2.3.5 Immunofluorescence

Following CLM treatment, cells were washed three times at room temperature with DPBS and fixed in 4% paraformaldehyde for 15 min. After washing, cells were permeabilized in -20˚C 100% methanol for 5 minutes. Cells were then washed three times in DPBS and blocked in 3% BSA for 1 hour at room temperature. After blocking, cells were incubated overnight at 4˚C in primary antibody diluted in blocking buffer. The next day cells were washed three times with DPBS and incubated in goat anti-rabbit 488 secondary antibody (1:400; ThermoFisher; A-21206). Following incubation, cells were washed three times in DPBS and mounted onto glass slides using Prolong Gold with DAPI (ThermoFisher; P36935). The following primary antibodies were used: total DNA-PK (1:200; ThermoFisher; PA5-86134), and p-DNA-PK (S2056) (1:200; Abcam; ab18192).

2.3.6 Image Analysis

Following the above staining protocol, images were collected on a Leica DMi8 THUNDER Inverted Fluorescence Microscope with a DFC7000 T camera (Leica). Quantified images were collected at 20x (HC PL FLUOTAR L 20x/0.4 Dry); representative images were collected at 63x (HC PL APO 63x/1.400.60 Oil). For quantified images, images were collected at four randomized points/condition for all three replicates. Microscope settings including gain, exposure time, and LED intensity were identical between cell lines. All images for both cell lines were collected during the same day. Images were processed in the open source software, Fiji (Schindelin et al., 2012; Schneider et al., 2012). In brief, all images were background subtracted using the rolling ball macro, followed by application of a gaussian blur of 2 sigma, and automatic thresholding using the Otsu dark method. Average signal intensity of goat anti-rabbit

488 secondary antibody (termed “Total DNA-PK”) was determined by applying a threshold mask to determine the boundaries of the GFP signal in each object (i.e. cell). The mean 488 signal of each object was then calculated. The average signal within the nucleus (termed “Nuclear DNA-PK”) was determined by creating a threshold mask based on the boundaries of the DAPI signal. This mask was then applied to the companion 488 image and the mean 488 signal within this was then calculated. The mean signal intensity of each replicate was then averaged together to determine average signal intensity. The mean signal intensity from an average of 527 cells were used per condition per replicate.

2.3.7 Statistical Analysis

All statistical analysis was performed using GraphPad Prism 8 (San Diego, CA). Effect of treatment and cell line was determined using a two-way ANOVA with Tukey’s post-hoc test (**Figures 2.3, 2.4 and 2.6E-H**). Effect of cell line was determined using an unpaired two-tailed t-test (**Figures 2.6I-L**). Significance was reached at $p<0.05$. Significance is designated as $p<0.05$ (*), $p\leq0.0021$ (**), $p\leq0.0002$ (***), $p\leq0.0001$ (****). All quantified blots were normalized to total protein (**Appendix A Supplementary Figure 4**).

2.4 Results

FUS can be phosphorylated in cell culture following different drug treatments (Deng et al., 2014b; Monahan et al., 2017; Rhoads et al., 2018a). In particular, our lab discovered that the DNA-dependent protein kinase (DNA-PK) phosphorylates FUS in human-derived neurons and immortalized cell lines following double-strand DNA breaks (DSBs) induced by CLM (Deng et al., 2014b). However, the role of FUS phosphorylation in disease pathogenesis is unclear. Given this, we aimed to use primary

mouse neurons as an in vitro model to investigate the function and disease mechanisms associated with FUS phosphorylation. Towards this aim, we first cultured primary cortical neurons from E18 C57BL/6 mice for 14 days then treated cultured neurons with increasing doses of CLM (1 to 1000 nM). Intriguingly, regardless of CLM concentration or length of treatment, we did not observe an increase in the molecular weight of FUS, an indication of FUS phosphorylation, in primary mouse neurons treated with CLM (**Figure 2.1A**). Although we did not observe the appearance of p-FUS, we did detect phosphorylation of H2AX (p-H2AX), a marker of DNA damage, confirming CLM treatment caused DNA damage in mouse neurons (Podhorecka et al., 2010). In contrast, treatment of a human H4 neuroglioma cell line with CLM resulted in robust phosphorylation of FUS and H2AX (**Figure 2.1A**). CLM treatment in mouse cells did lead to the production of multiple smaller fragments of FUS, which may indicate proteolytic cleavage, at the highest concentrations (100 and 1000 nM) and longest treatment times in primary mouse neurons (**Figure 2.1A**, indicated by *). Interestingly, no smaller fragments of FUS were detected in multiple immortalized cell lines (HEK293T, SH-SY5Y or N2A) following CLM treatment, suggesting this cleavage may be unique to primary neuronal cells and should be examined in future studies (**Appendix A Supplemental Figure 1**). These data demonstrate that while CLM treatment causes DNA damage in mouse immortalized cells, it does not lead to phosphorylation of mouse FUS.

Because our previously published work exclusively utilized human-derived immortalized cell lines and primary neurons, we wondered whether CLM induced phosphorylation of FUS only occurred in human cells or if other primate cells exhibited the response. To investigate this, we asked if FUS phosphorylation occurred after CLM

treatment in other primary cell lines derived from primates. First, we treated neural progenitor cells (NPCs) derived from the rhesus macaque monkey with CLM. We observed a robust increase in p-FUS at 10 and 20 nM CLM in monkey NPCs (**Figure 2.1B**). Neurons derived from monkey NPCs also phosphorylated FUS in response to CLM treatment (**Figure 2.1C**). Lastly, we treated human iPSC-derived motor neurons (**Figure 2.1D**) and primary human neurons (**Figure 2.1E**) with increasing doses of CLM and saw a similar dose-dependent increase in p-FUS and p-H2AX signal. These data suggest that FUS phosphorylation following DSBs is a conserved phenomenon for multiple stages of primate neural development and does not occur in mouse-derived cells.

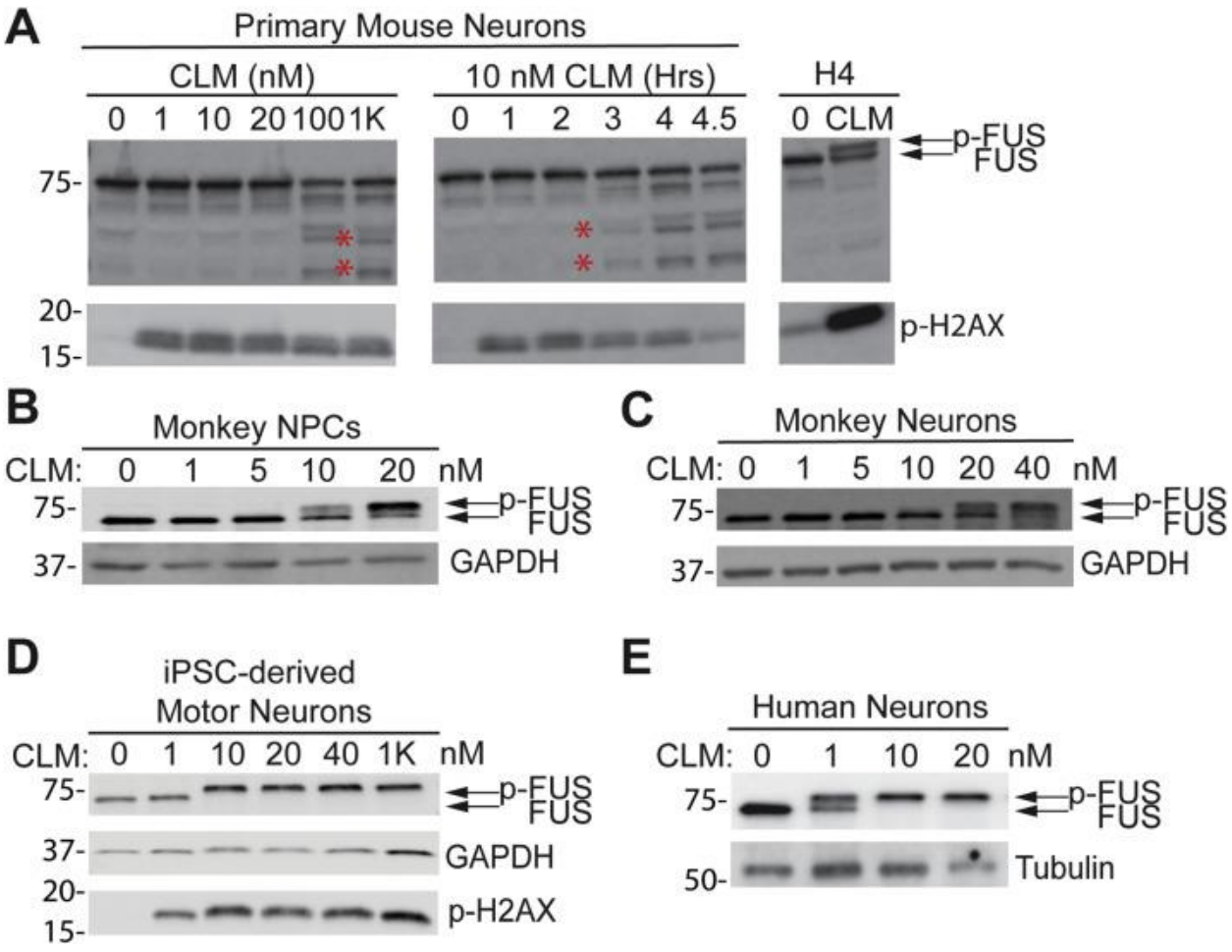

Figure 2.1 Calicheamicin ɣ-1 (CLM) treatment induces FUS phosphorylation in human and non-human primate neurons, but not primary mouse neurons

(A) Primary mouse neurons were treated either with increasing doses of CLM (nM) for 2 h (left) or with 10 nM CLM for increasing times (0 to 4.5 h) (right). In comparison, human H4 neuroglioma cells were treated with either DMSO (vehicle) or 10 nM CLM for 3 h. RIPA extracted whole cell lysates were analyzed by immunoblotting using indicated cellular markers. A positive p-H2AX signal indicates the occurrence of double strand DNA damage in mouse and human cells. (*) indicates potential FUS cleavage products following CLM treatment. In contrast, all human and non-human

primate (monkey) derived neuronal models display the characteristic dose dependent phosphorylation of FUS following CLM treatment. (B) Nonhuman primate neural progenitor cells (NPCs) and (C) non-human primate primary neurons were treated with DMSO (vehicle) or CLM at indicated CLM concentrations (nM) for 2 h. (D) Wild-type iPSC-derived motor neuron and (E) primary human neurons were treated with DMSO or CLM at indicated concentrations (nM) for 2 h. Wild-type iPSC-derived motor neurons show clear p-H2AX activation following CLM treatment. RIPA extracted whole cell lysates (B-E) were analyzed by immunoblotting using indicated antibodies: FUS, p-H2AX, GAPDH, tubulin. Refer to methods section for catalog numbers of the specific antibodies used. GAPDH and Tubulin are used as loading controls to verify equal protein loading. Position of molecular weight markers (kDa) labeled on left side of each immunoblot.

Previously we demonstrated that multiple human-derived immortalized cell lines can robustly phosphorylate FUS following CLM treatment (Deng et al., 2014b). Upon observing that primary murine cells did not phosphorylate FUS after CLM treatment, we asked if mouse-derived immortalized cell lines were able to phosphorylate FUS in response to CLM treatment. Unlike primary cells, immortalized cell lines are clonal, uniform, and can be grown indefinitely. As such, they offer a useful model for understanding cell-specific gene and protein dynamics (Kovalevich and Langford, 2013; Lendahl and McKay, 1990; Lin et al., 2014b). We compared FUS phosphorylation following CLM treatment in HEK293T cells, a widely utilized human embryonic kidney cell line, to an immortalized mouse embryonic fibroblast (MEF) cell line. HEK293T cells showed a robust dose-dependent increase in FUS phosphorylation following CLM treatment indicated by a shift in molecular weight and co-immunoreactivity with a phospho-ATR/ATM Substrate Motif antibody, which detects the (pS/pT)QG motif that is phosphorylated by DNA-PK, ATR, and ATM (three closely related phosphoinositide 3-kinases) following DNA damage, as previously described (Blackford and Jackson, 2017; Deng et al., 2014b) (**Figure 2.2A**). Alongside the appearance of the characteristic p-FUS top band, we observed a dose-dependent increase in p-H2AX signal, confirming that CLM treatment caused DNA damage (**Figure 2.2A**). In contrast, MEF cells exhibited no detectable FUS phosphorylation at any dose of CLM, despite having a robust p-H2AX signal (**Figure 2.2B**). To determine if increased time may be necessary, we treated HEK293T and MEF cells in parallel with 10 nM CLM for 0.5 to 4 h and again found no detectable FUS phosphorylation signal in MEF cells (**Figure 2.2B**). These data strongly suggest that MEF cells do not phosphorylate FUS following CLM induced double-strand DNA damage.

Given that FTD is a neurodegenerative disease, we examined the effect of CLM treatment on neuroblastoma cell lines, which have been used extensively as neuronal cell models of neurodegeneration (Xicoy et al., 2017). We observed a similar divergent response to CLM treatment in human SH-SY5Y neuroblastoma cells compared to mouse Neuro2A (N2A) neuroblastoma cells. SH-SY5Y cells showed a dose (**Figure 2.2C**) and time (**Figure 2.2D**) dependent phosphorylation of FUS following CLM treatment, similar to what we observed in other human-derived cell lines. In contrast, we did not detect any appreciable phosphorylation of FUS in the mouse-derived N2A cells in any condition tested (**Figure 2.2C, D**). Regardless of species, both human and mouse cell lines showed clear activation of p-H2AX response (**Figure 2.2C, D**). Importantly, only human-derived HEK293T and SH-SY5Y cells had robust (pS/pT) QG immunoreactive bands following CLM treatment, suggesting there are differences in DNA damage response pathways in human versus mouse cells.

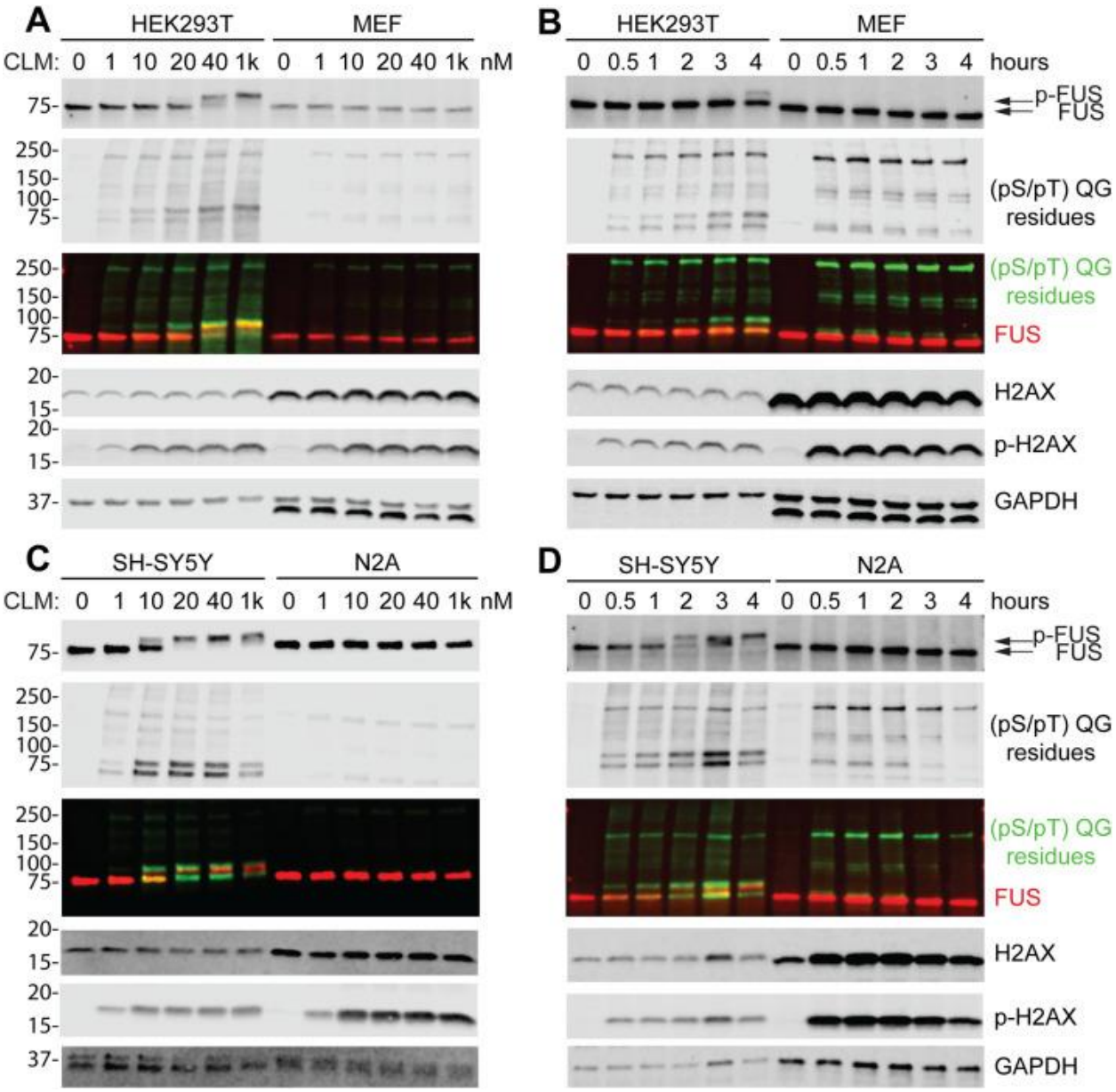

Figure 2.2 FUS is phosphorylated following CLM treatment in immortalized cell lines or human origin but not mouse

In human embryonic kidney (HEK293T) cells there is a (A) dose and (B) time dependent increase in phosphorylated FUS in response to CLM treatment. In contrast, phosphorylated FUS is undetectable in MEF cells at all tested doses and times. HEK293T and mouse embryonic fibroblasts (MEF) were treated with increasing

concentrations (nM) of CLM for 2 h (A) or 10 nM CLM for 0 to 4 h (B). Similar to HEK293T cells, SH-SY5Y, a human neuroblastoma cell lines, displays a (C) dose and (D) time dependent increase in phosphorylated FUS following CLM treatment. In contrast, the appearance of phosphorylated FUS after CLM treatment is undetectable in Neuro2A (N2A) cells, a mouse neuroblastoma cell line. SH-SY5Y and N2A cells were treated with increasing concentrations of CLM for 2 h (C) or 20 nM CLM for 0–4 h (D). All control cells (0) were treated with the vehicle, DMSO, for either 2 (A, C) or 4 (B, D) hours. RIPA extracted whole cell lysates were analyzed with indicated antibodies: FUS, (pS/pT) QG residues, H2AX, p-H2AX, and GAPDH. p-H2AX activation, a marker of double strand DNA damage, occurs in all cells treated with CLM regardless of species. GAPDH is used as a loading control.

Next, we quantified the difference in phosphorylation response following CLM treatment between the human-derived SH-SY5Y cells and mouse-derived N2A cells (**Figure 2.3A**). Given that the (pS/pT) QG residue antibody is not specific to only DNA-PK based phosphorylation, we also utilized a p-FUS antibody that specifically detects FUS phosphorylated at serine 30, one of the residues on FUS phosphorylated by DNA-PK following CLM treatment (Monahan et al., 2017; Murray et al., 2017; Rhoads et al., 2018a) (**Figure 2.3C, G**). Additionally, we measured the amount of FUS present in the higher molecular weight band as in Deng et al. (Deng et al., 2014b) (**Figure 2.3B, F**). Using these two methods, we found that SH-SY5Y cells show a reproducible, dose-dependent and significant increase in both the total amount of p-FUS signal (**Figure 2.3B**) and amount of p-FUS (Ser30) signal present (**Figure 2.3C**). In agreement with our original results (**Figure 2.2**), N2A cells showed no detectable p-FUS signal (**Figure 2.3B, C**). Previously, we reported that p-FUS accumulates in the cytoplasm of cells following CLM induced DSB (Deng et al., 2014b). Therefore, we tested if cytoplasmic FUS increased in N2A cells following CLM treatment (**Figure 2.3D**). SH-SY5Y cells showed a significant increase in the total amount of FUS (**Figure 2.3E**) and p-FUS (**Figure 2.3F–G**) localized to the cytoplasmic fraction. In contrast, there was not a significant increase in FUS (**Figure 2.3E**) or p-FUS (**Figure 2.3F–G**) in the cytoplasm of mouse N2A cells following CLM treatment. Our data suggests that FUS is not phosphorylated, nor increased in the cytoplasm of mouse cells, following CLM induced DSB. In light of these findings, we aimed to determine why mouse cells did not phosphorylate FUS following CLM treatment.

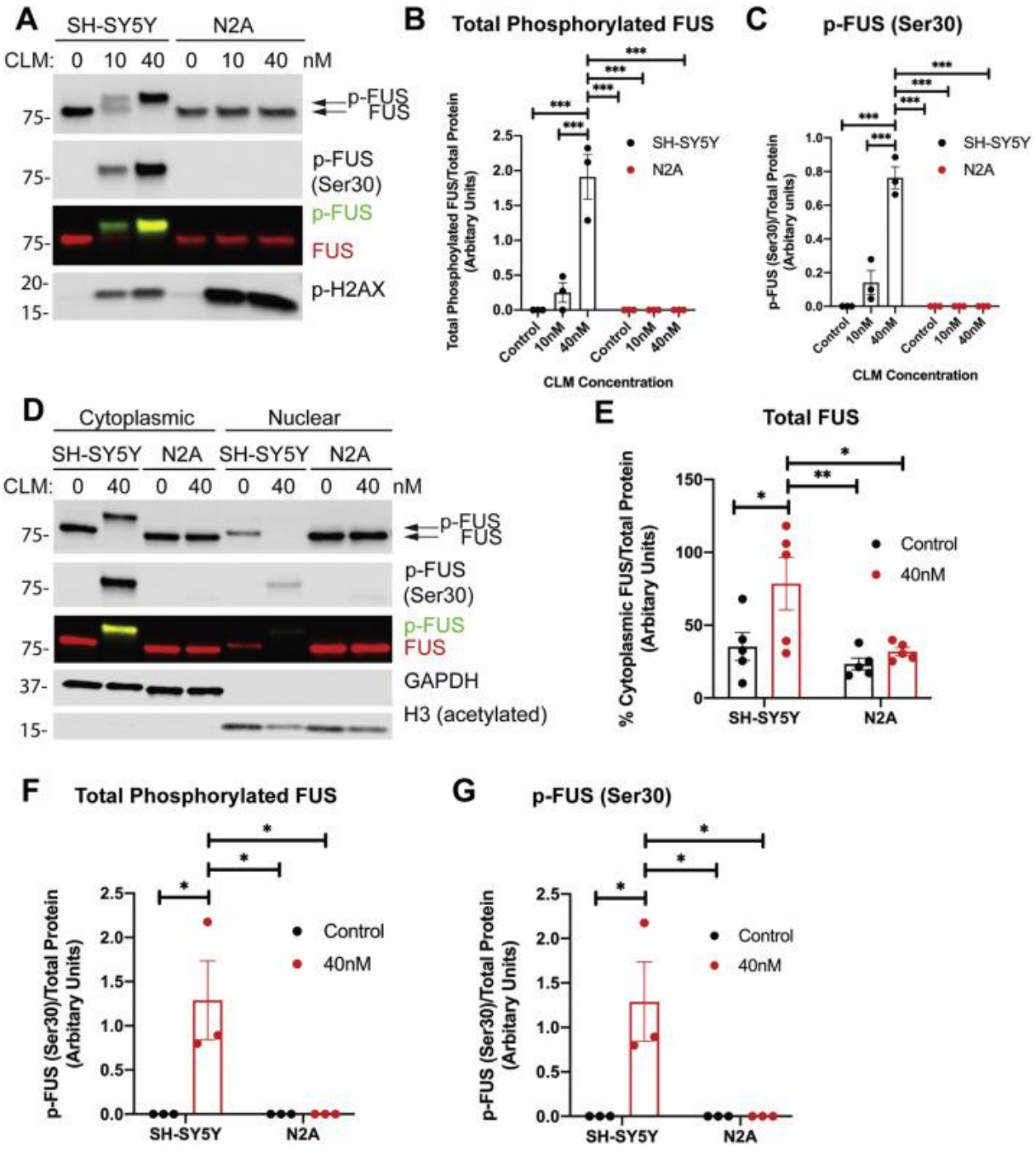

Figure 2.3 FUS is not phosphorylated or re-localized to the cytoplasm in mouse cells following CLM treatment

Human derived SH-SY5Y cells and mouse derived N2A cells were directly compared by western blot. (A) SH-SY5Y and N2A cells were treated with increasing doses of CLM

for 2 h. Following treatment, RIPA extracted whole cell lysate was analyzed using the following antibodies: FUS, p-FUS (Ser30), and p-H2AX. (B) Quantification of (A) for phosphorylation of FUS (top band) at different concentrations of CLM were normalized to total protein. (C) Quantification of (A) for phosphorylation of FUS at residue Ser30 at different concentrations of CLM were normalized to total protein. Error bars indicate mean ± SEM (n = 3). (D) SH-SY5Y and N2A cells were treated with increasing doses of CLM for 2 h. Cytoplasmic and nuclear fractions were collected and analyzed by western blot using the following antibodies: FUS, p-FUS (Ser30), GAPDH and H3. GAPDH and H3 were used as markers for cytoplasmic and nuclear fractions, respectively. (E) Quantification of (D) for the percentage of FUS found within the cytoplasmic fraction was normalized to total protein. (F) Quantification of (D) showing phosphorylation of FUS (top band) at different concentrations of CLM was normalized to total protein. (G) Quantification of (D) for phosphorylation of FUS at residue Ser30 at different concentrations of CLM was normalized to total protein. Error bars indicate mean ± SEM (n = 5). All control cells (0) received DMSO for 2 h.

First, we asked if mouse cells were capable of phosphorylating FUS under conditions that broadly increase protein phosphorylation. To do this, we treated cells with Calyculin A (Cal A), an inhibitor of the serine/threonine phosphatases PP1 and PP2A, which increases the appearance of the phosphorylated species of FUS (Deng et al., 2014b; Ishihara et al., 1989). Given the wide breath of targets for PP1 and PP2A and the ~50 residues spread throughout the primary amino acid sequence of FUS that can be phosphorylated, the phosphorylated species of FUS triggered by Cal A may not be same as the phosphorylated FUS caused by DNA damage mechanisms (Rhoads et al., 2018a). Therefore, we aimed to confirm whether mouse FUS could be phosphorylated independently of DNA damage response pathways. Increasing doses of Cal A in mouse N2A cells caused the appearance of a slightly higher molecular weight FUS band, which could be due to phosphorylation (**Figure 2.4A**). However, there was little to no overlap between the p-FUS band and signal from the (pS/pT)QG antibody suggesting Cal A treatment may lead to FUS phosphorylation at non-DNA-PK target residues. Therefore, we tested whether phosphorylation of the DNA-PK target residue Ser30 could be detected following Cal A treatment (**Figure 2.4B**). SH-SY5Y showed a significant increase in p-FUS signal following Cal A treatment ($p = 0.0491$; **Figure 2.4C**). Although we were able to detect a faint p-FUS (Ser30) band in both SH-SY5Y and N2A cells following Cal A treatment, the N2A treated cells did not have a significantly different p-FUS signal compared to controls ($p = 0.3439$; **Figure 2.4C**). These data suggests that although FUS can be phosphorylated in mouse cells, this response is not robust following Cal A treatment and the overall extent of phosphorylation appears much lower than in primate-derived cell lines (**Appendix A Supplemental Figure 2C**). Next, we asked if staurosporine, a broad kinase inhibitor, inducer of apoptosis, and

an activator of DNA-PK, could induce p-FUS in mouse cells (Chakravarthy et al., 1999; Karaman et al., 2008). We focused on staurosporine because it was the original chemical we first used to discover FUS phosphorylation and a known inducer p-H2AX (Deng et al., 2014b; Solier and Pommier, 2009). Treatment of mouse N2A cells with 1 μM staurosporine for up to four hours did not cause phosphorylation of FUS (**Figure 2.4D**). However, staurosporine did induce apoptosis and DNA damage at this dose as confirmed by the appearance of cleaved Poly (ADP-ribose) polymerase (PARP) and an increase in p-H2AX signal (**Figure 2.4D**). In contrast, treatment of SH-SY5Y cells with 1 or 2 μM staurosporine induced reliable FUS phosphorylation detected by a band shift (**Appendix A Supplemental Figure 2A**) and p-FUS (Ser30) signal (**Figure 2.4E**). This difference was quantified showing that p-FUS (Ser30) was significantly higher in SH-SY5Y following staurosporine treatment compared to controls ($p = 0.0145$) or N2A cells (**Figure 2.4G**).

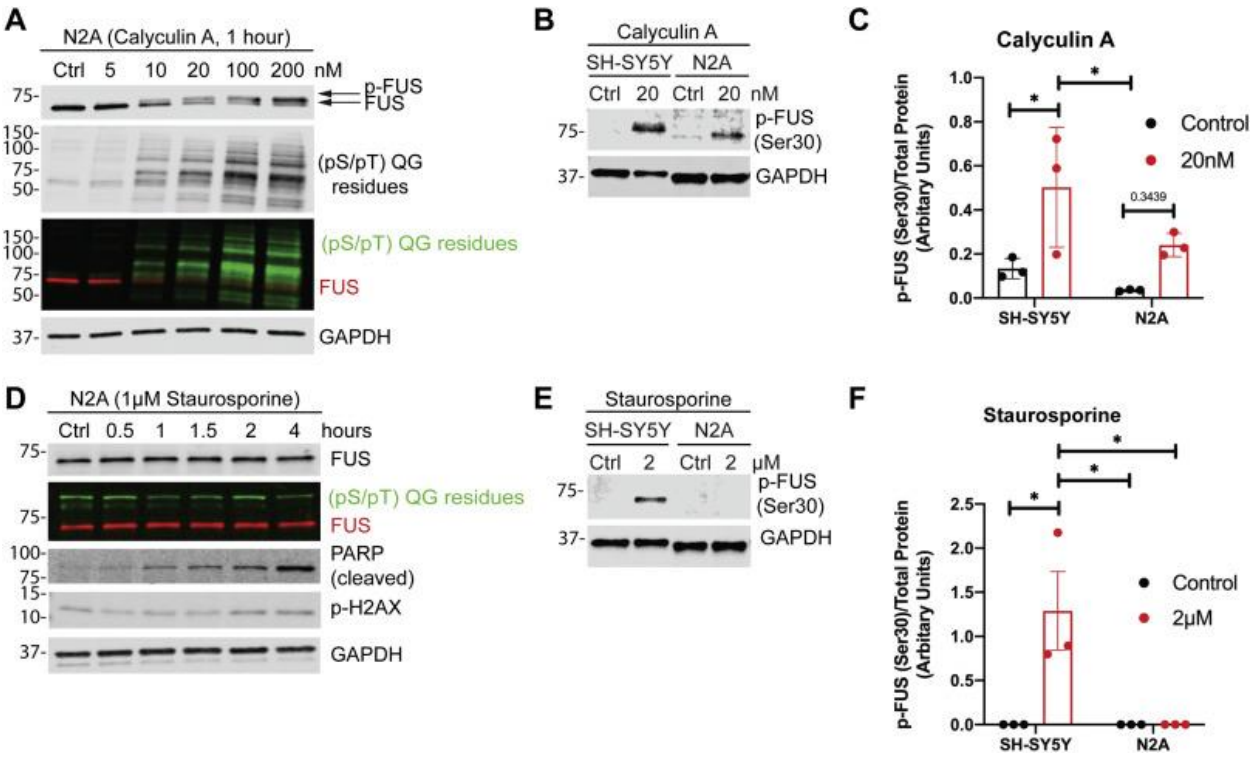

Figure 2.4 Neither calyculin A or staruosporine induces robust phosphorylation of mouse FUS

Calyculin A, an inhibitor of protein phosphatases PP1 and PP2A, causes a minor dose dependent increase in phosphorylated FUS (p-FUS) in mouse-derived cells. (A) Neuro2A (N2A) cells were treated with either the vehicle, DMSO (0), or increasing doses of Calyculin A for 1 h. RIPA extracted whole cells lysates were analyzed with indicated antibodies: FUS, p-Ser/Thr, and GAPDH. (A) N2A and SH-SY5Y cells were treated with 20 nM Cal A for 15 min. (C) Samples shown in (B) were quantified and normalized to total protein. Error bars indicate mean ± SEM (n = 3). All control cells (0) received DMSO for 15 min. (D) N2A cells were treated with staurosporine, a nonselective inhibitor of protein kinases that causes double strand DNA damage and cell apoptosis, showed no indication of FUS phosphorylation response. PARP-1 cleavage is an indicator apoptosis and a known consequence of staurosporine

treatment acts as a positive control for staurosporine treatment. RIPA extracted whole cell lysates were analyzed with indicated antibodies: FUS, p-Ser/Thr, mouse specific-PARP (cleaved) p-H2AX, and GAPDH. (E) N2A and SH-SY5Y cells were treated with 1 μM Staurosporine for 1.5 h. Cellular fractionation was performed to extract cytoplasmic proteins and detect p-FUS by western blotting. (F) Samples shown in (D) were quantified. Error bars indicate mean ± SEM (n = 3). All control cells (0) received DMSO for 1.5 h.

Taken together, these data suggest that while mouse cells are capable of phosphorylating FUS, DSBs may not cause robust phosphorylation of FUS. Therefore, we conclude that the DNA damage response triggered by double-strand breaks does not initiate FUS phosphorylation in mouse-derived cells.

Since mouse cells did not phosphorylate FUS following either CLM or staurosporine induced DNA-damage, we reasoned that either 1) mouse cells lack the required signaling cascade to activate DNA-PK or 2) mouse FUS does not contain the correct amino acid residues to be phosphorylated after DNA damage. While FUS can be phosphorylated at many sites, double-strand DNA damage induces phosphorylation at 12 specific serine or threonine residues spread throughout the N-terminus of the protein (Gardiner et al., 2008; Monahan et al., 2017). This N-terminal region, deemed the low-complexity domain, contains a SYGQ-rich and a glycine-rich domain. Human and mouse FUS are very similar and share ~95% amino acid identity over the entire protein (**Figure 2.5A**). However, there are 26 amino acid differences and 25 of those exist in the low complexity domain of the N-terminus of the protein (**Figure 2.5A**). Therefore, we asked if the inability of mouse cells to phosphorylate FUS following CLM treatment could be due to these sequence differences. We tested this by expressing GFP-tagged mouse FUS (GFP-mFUS) in human HEK293T cells and GFP-tagged human FUS (GFP-hFUS) in mouse N2A cells. Then, we treated cells with CLM to induce FUS phosphorylation. In HEK293T cells, both endogenous human FUS and exogenously expressed GFP-mFUS were phosphorylated (**Figure 2.5B**). FUS phosphorylation was confirmed by an increase in molecular weight and the appearance of a p-FUS signal using the antibody specific to FUS phosphorylated at Ser30, a residue that is present in both human and mouse FUS.

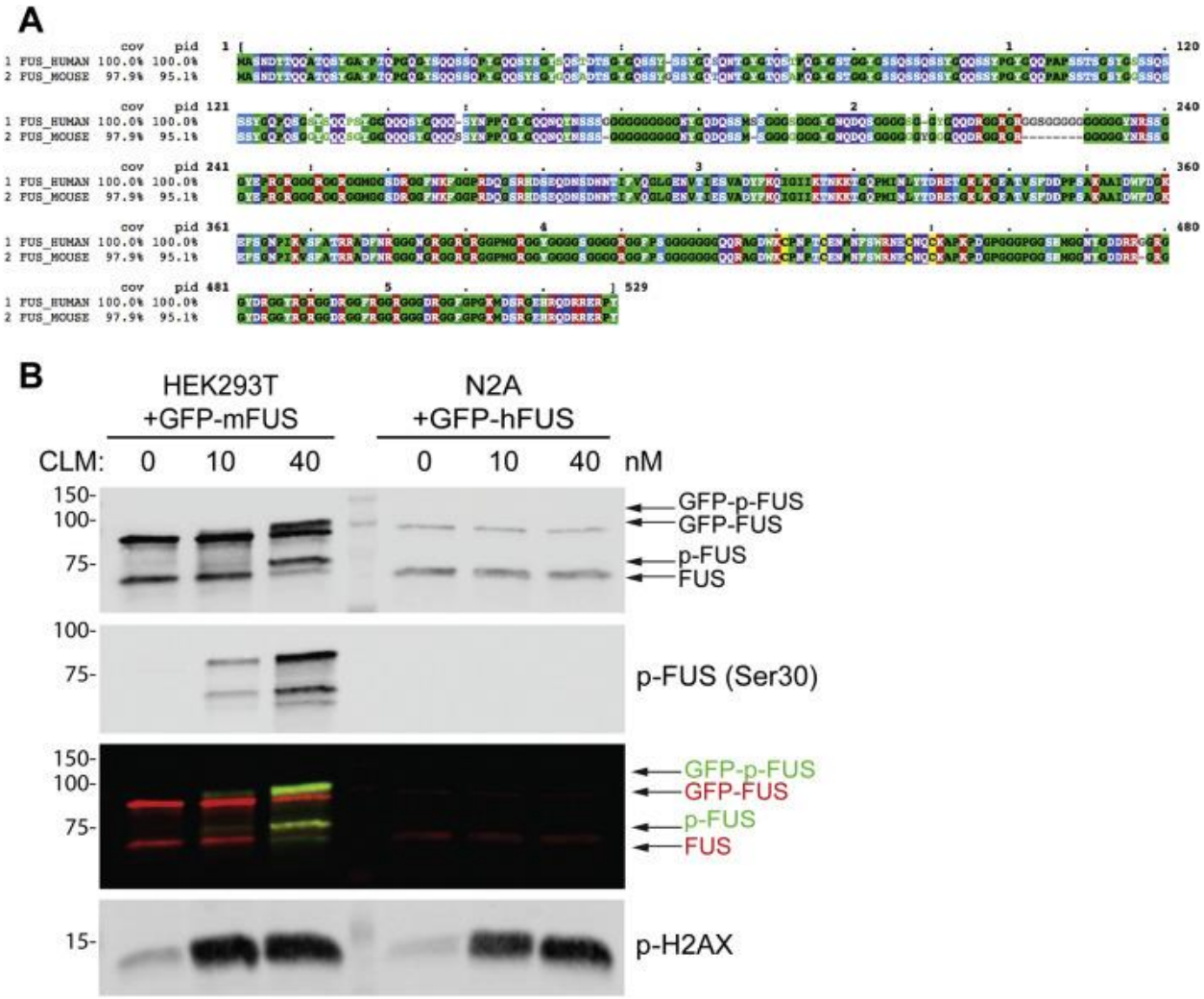

Figure 2.5 Mouse FUS can be phosphorylated in human cells following CLM treatment

We tested if mouse FUS can be phosphorylated in human cells following CLM treatment. Human and mouse FUS share ~95% sequence identity. (A) Graphical representation of amino acid sequence alignment for human (FUS_H) and mouse (FUS_M) FUS. Different colors indicate amino acid physical properties. Graphical representation was generated using Cluster Omega (Sievers et al., 2011). (B) GFP-tagged mouse FUS was transfected into HEK293T cells while GFP-tagged human FUS was transfected into N2A cells. GFP-tagged mouse FUS is phosphorylated when expressed in human cells treated with calicheamicin γ-1 (CLM). 24 h post transfection

cells were treated with varying concentrations of CLM for 2 h and the whole cell lysate was harvested and analyzed with indicated antibodies: FUS, p-FUS (Ser 30), and p-H2AX. All control (0) cells received DMSO for 2 h.

In contrast, we did not detect phosphorylation of endogenous mouse FUS or exogenous GFP-hFUS in N2A cells (**Figure 5B**). These data reveal that while mouse FUS can be robustly phosphorylated in human cells, mouse cells do not phosphorylate human FUS, suggesting the pathways necessary to phosphorylate FUS following DNA damage in mouse cells are not present, or as active, compared to primate cells.

Given that mouse FUS can be modestly phosphorylated, we next asked whether some aspect of the pathway leading to FUS phosphorylation is different between human and mouse cells. We focused on DNA-PK because DNA-PK phosphorylates FUS following CLM induced double-strand DNA damage (Deng et al., 2014b). Moreover, previous reports suggest that the concentration of DNA-PK is lower in mouse cells compared to human cells (Finnie et al., 1995; Lees-Miller et al., 1992). Therefore, we first aimed to determine if N2A cells have a lower concentration of total DNA-PK compared to SH-SY5Y cells. We used a DNA-PK antibody that can detect both human and mouse DNA-PK species (**Appendix A Supplemental Figure 3**). Immunoblotting of cell lysates revealed that while SH-SY5Y and N2A cells express similar levels of FUS protein, SH-SY5Y cells express much higher levels of total DNA-PK compared to N2A cells (**Figure 2.6A**). Treatment of either cell line with CLM did not change the total levels of DNA-PK (**Figure 2.6A**). We next asked if mouse DNA-PK was properly activated following CLM treatment. DNA-PK's catalytic activity is dependent on phosphorylation of residue S2056 in humans, S2053 in mice, making phosphorylation of S2056/3 a widely used marker of DNA-PK activity (Chan et al., 2002; Chen et al., 2005; Jiang et al., 2019; Merkle et al., 2002). It should be noted that the antibody used to detect phosphorylated DNA-PK has been validated to cross-react with the mouse S2053 site by immunofluorescence allowing us to use the same antibody

in our comparison (Roch et al., 2019). Treatment of SH-SY5Y cells with CLM at 10 and 40 nM caused activation of DNA-PK, as detected by the appearance of phosphorylated DNA-PK (p-DNA-PK at S2056/3). In contrast, we did not detect phosphorylation of DNA-PK or FUS in N2A cells via immunoblot at any dose of CLM tested (**Figure 2.6B**).

Next, we used immunofluorescence to examine the subcellular localization of DNA-PK in SH-SY5Y and N2A cells using a total DNA-PK antibody that recognizes both mouse and human DNA-PK. The overall fluorescent intensity for DNA-PK was significantly higher in SH-SY5Y compared to N2A cells, confirming our western blot results (**Figure 2.6C, E**). Intriguingly, the DNA-PK signal appeared more diffuse throughout the cytoplasm and the nucleus of N2A cells, while DNA-PK immunoreactivity in SH-SY5Y cells was more predominant in the nucleus (**Figure 2.6C**). Quantification of immunofluorescence confirmed the presence of significantly more DNA-PK in the nucleus of SH-SY5Y compared to N2A regardless of treatment (**Figure 2.6F**). Furthermore, CLM treatment for either SH-SY5Y or N2A cells did not change the cellular localization of DNA-PK (**Figure 2.6F**). In line with this, the proportion of DNA-PK signal remained unchanged (around ~1) between control and treatment for both SH-SY5Y and N2A cells when examining the whole cell (**Figure 2.6I**) and nucleus (**Figure 2.6J**).

We next asked if DNA-PK was activated following CLM treatment in mouse and human cells. We treated SH-SY5Y and N2A cells with CLM (20 nM) and measured the amount of phosphorylated DNA-PK S2056 (p-DNA-PK) signal. In untreated control cells, p-DNA-PK staining in both N2A and SH-SY5Y cells was weak and diffuse throughout the nucleus and cytoplasm (**Figure 2.6D**). As expected, SH-SY5Y cells had robust DNA-PK activation following CLM treatment, as measured by phosphorylation of

the S2056 (S2053 for N2A cells) residue on DNA-PK (**Figure 2.6D, G**). Unexpectedly, N2A cells exhibited an increase in p-DNA-PK whole cell signal (**Figure 2.6G**) and nuclear signal (**Figure 2.6H**) following CLM treatment. However, the proportion of p-DNA-PK signal was significantly higher in SH-SY5Y compared to N2A for both the whole cell ($p = 0.0442$; **Figure 2.6K**) and the nucleus ($p = 0.0389$; **Figure 2.6L**). Overall, this data suggests that while mouse cells are capable of activating DNA-PK in response to CLM, the amount of p-DNA-PK available is significantly lower in mouse cells compared to human cells. Taken together, these data support the idea that CLM treatment of mouse cells does not lead to FUS phosphorylation due to differences in the DNA-PK mediated DNA damage and repair response in mice versus human cells.

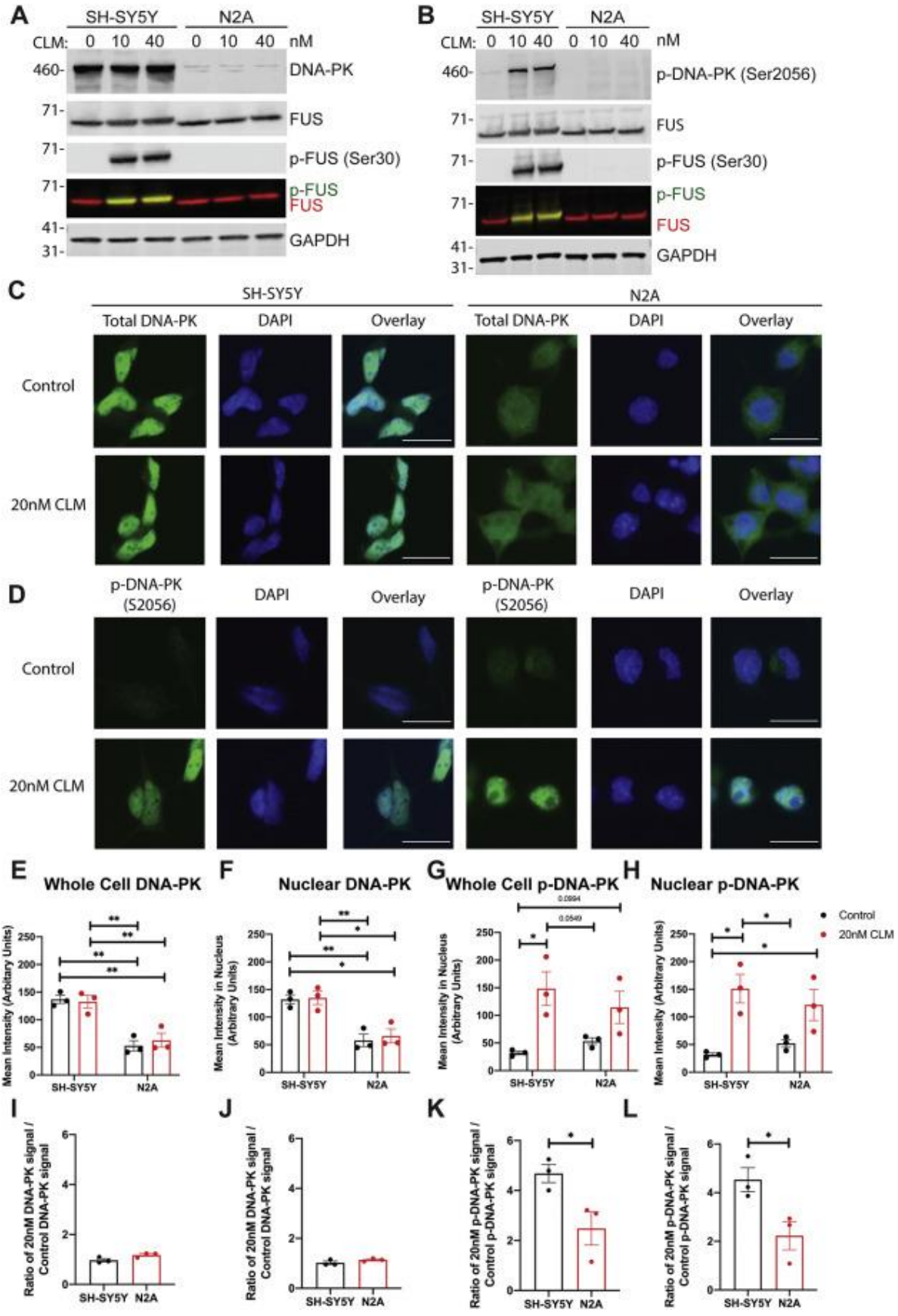
A
SH-SY5Y
N2A
CLM: 0 10 40 0 10 40 nM
460-
DNA-PK
71-
FUS
71-
p-FUS (Ser30)
71-
p-FUS
FUS
41-
31-
GAPDH
B
SH-SY5Y
N2A
CLM: 0 10 40 0 10 40 nM
460-
p-DNA-PK (Ser2056)
71-
FUS
71-
p-FUS (Ser30)
71-
p-FUS
FUS
41-
31-
GAPDH
C
SH-SY5Y
N2A
Total DNA-PK
DAPI
Overlay
Control
20nM CLM
D
p-DNA-PK (S2056)
DAPI
Overlay
Control
20nM CLM
E
Whole Cell DNA-PK
Mean Intensity (Arbitary Units)
SH-SY5Y
N2A
F
Nuclear DNA-PK
Mean Intensity in Nucleus (Arbitrary Units)
SH-SY5Y
N2A
G
Whole Cell p-DNA-PK
Mean Intensity in Nucleus (Arbitrary Units)
SH-SY5Y
N2A
H
Nuclear p-DNA-PK
Mean Intensity (Arbitrary Units)
Control
20nM CLM
SH-SY5Y
N2A
I
Ratio of 20nM DNA-PK signal / Control DNA-PK signal
SH-SY5Y N2A
J
Ratio of 20nM DNA-PK signal / Control DNA-PK signal
SH-SY5Y N2A
K
Ratio of 20nM p-DNA-PK signal / Control p-DNA-PK signal
SH-SY5Y N2A
L
Ratio of 20nM p-DNA-PK signal / Control p-DNA-PK signal
SH-SY5Y N2A

Figure 2.6 Compared to human cells, mouse cells have deceased levels of DNA-PJ and activation following double strand DNA breaks induced by CLM treatment

SH-SY5Y cells show a distinct increase in activated DNA-PK whereas N2A cells lack a significant DNA-PK response following CLM treatment by western blot. SH-SY5Y and N2A cells were treated with increasing concentrations of CLM for 2 h. Following treatment, RIPA extracted whole cell lysates were analyzed for (A) total and (B) activated DNA-PK signal using the following antibodies: DNA-PK, p-DNA-PK, FUS, p-FUS (Ser30), and GAPDH. (C/D) N2A cells have lower total and activated DNA-PK following CLM as compared to SH-SY5Y cells by immunofluorescence. SH-SY5Y and N2A cells were treated with DMSO (control) or CLM (20 nM CLM) for 2 h and stained for (C) total and (D) activated DNA-PK. Nuclei were counter-stained with DAPI. Four images with an average of 527 cells each were used for quantification per replicate (n = 3). Total and activated DNA-PK signal was quantified for both the (E/G) whole cell and (F/H) nucleus. SH-SY5Y cells show robust (E/F) total and (G/H) activated DNA-PK (p-DNA-PK, S2056) signal following CLM while N2A cell signal remains modest in presence of CLM. (I/J/K/L)The ratio of the signal from treated (20 nM CLM) to the signal from untreated (control) cells was calculated for each graph. Error bars on graphs indicate mean ± SEM.

2.5 Discussion

Our previous work found that both primary and immortalized human cells robustly phosphorylate FUS in response to DSBs and that this response is mediated by DNA-PK activation. Furthermore, we found that CLM treatment in particular is a potent and useful chemical trigger of FUS phosphorylation (Deng et al., 2014b). Previously, we and others have shown that CLM-induced FUS phosphorylation can be detected through 1) a band shift, or more precisely, an increase in the apparent molecular weight of FUS migrating on a SDS/PAGE gel due to phosphorylation and 2) overlap of the higher-molecular weight FUS with a phospho ATM/ATR substrate motif antibody that specifically detects (pS/pT) QG phosphorylation, the preferred phosphorylation site of DNA-PK (Deng et al., 2014b; Kim et al., 1999; Rhoads et al., 2018a). In this current work, we utilized both detection methods and found that neither primary nor immortalized mouse-derived cells phosphorylate FUS following CLM treatment. Although we were unable to detect a band shift, or overlap in FUS signal with the p-S/p-T antibody in mouse derived cells, we did see the appearance of p-H2AX, a crucial regulator of the DSB response and a known target of DNA-PK, verifying that CLM treatment was adequate to induce DNA damage and repair processes (An et al., 2010).

CLM is not the only known chemical that induces FUS phosphorylation. Our previous work showed that treatment of human cells with Cal A and staurosporine caused FUS phosphorylation. Cal A is an potent inhibitor of the PP1 and PP2A protein phosphatases and Cal A treatment is known to cause an increase in global protein phosphorylation by blocking de-phosphorylation (Chartier et al., 1991). Surprisingly though, Cal A only induced a modest amount of FUS phosphorylation in mouse cells suggesting mouse cells achieve less FUS phosphorylation than human cells. At the

protein sequence level, mice and human FUS are nearly identical and contain almost all the same phosphorylation target residues. Therefore, future studies should explore whether this difference in basal phosphorylation is due to 1) differences in mouse PP1 and PP2A protein phosphatase activity and 2) whether other the post-translational modifications such as acetylation or ubiquitination are also different between mouse and human FUS.

Staurosporine is a cell permeable broad protein kinase inhibitor previously shown to activate DNA-PK (Chakravarthy et al., 1999). Treatment with staurosporine did not cause FUS phosphorylation or the appearance of p-H2AX in mouse cells. Interestingly, human cells treated with staurosporine show robust p-H2AX activation (**Appendix A Figure. 2B**). Histone H2AX is a substrate of the phosphoinositide 3-kinase-related protein kinases, DNA-PK, ATM, and ATR, which phosphorylate H2AX at residue Ser139 in response to DSBs (An et al., 2010; Podhorecka et al., 2010). p-H2AX is thought to act as a docking site that recruits repair factors to the site of repair (Podhorecka et al., 2010). In line with this, evidence suggests that reduced phosphorylation of H2AX leads to improper DSB repair and genomic instability (Celeste et al., 2003; Revet et al., 2011). As such, the lack of p-H2AX and p-FUS activation suggests that mouse cells have a divergent response to staurosporine induced DNA-PK activation. Taken together, our data demonstrate that mouse cells exhibit divergent FUS phosphorylation when compared to human cells.

Next, we investigated why mouse cells exhibit this divergent response to DSB. As stated, CLM is a potent inducer of DSBs (Dedon et al., 1993; Elmroth et al., 2003). DSBs are repaired in mammalian cells through either homologous recombination or non-homologous end-joining (NHEJ) (Bohgaki et al., 2010). DNA-PK is thought to be both a

sensor and a transducer of DNA-damage and autophosphorylation of DNA-PK at S2056 (S2053 for mice) after DNA-damage is required for efficient NHEJ (Chan et al., 2002; Chen et al., 2005; Jiang et al., 2019; Merkle et al., 2002). Furthermore, activation of DNA-PK leads to the recruitment and phosphorylation of other DNA-repair proteins (Burma and Chen, 2004). Therefore, improper activation of DNA-PK would inhibit the DNA damage response. We showed that mouse cells do not phosphorylated FUS in response to two DNA-PK activators, CLM and staurosporine. Furthermore, our data show that mouse FUS can be phosphorylated when expressed in human cells, suggesting the issue lies in the response of mouse cells to DNA damage and not mouse FUS itself. Together, these data suggests that the divergent response is due to mouse DNA-PK not being properly activated.

Previously, it has been reported that DNA-PK activity is much lower in mouse than in human tissue (Finnie et al., 1995; Lees-Miller et al., 1992). We recapitulated this finding and found that DNA-PK expression is much lower in mouse cells compared to human cells. Further, CLM treatment causes decreased activation of DNA-PK in mouse cells compared to human cells. Adequate DNA-PK activity and expression is necessary for proper DSB repair (Okayasu et al., 2000). As such, decreased DNA-PK expression in mice would affect DSB repair. DNA-PK expression and activation are not the only differences between mice and human DNA repair. Specifically, it is known that longer-lived species such as humans have higher expression of DNA repair genes and pathways (Chinwalla et al., 2002; MacRae et al., 2015). Additionally, multiple aspects of the DNA damage response and DNA repair pathways are significantly different between human and mouse neurons (Martin and Chang, 2018). As such, extensive prior data

demonstrate that mouse cells do not recapitulate all aspects of DNA damage response and repair pathways that occur in human derived cell models.

Given these reported differences in DNA repair, we show that DNA-PK expression and activation is lower in mouse-derived cells, but the cause is unclear. DNA-PK activation is a complex process where multiple proteins and responses can lead to autophosphorylation and activation of DNA-PK (Burma and Chen, 2004). Our work and others show that mouse DNA-PK is sufficiently activated enough by CLM induced DSBs to cause phosphorylation of H2AX (p-H2AX) (Audebert et al., 2004; Deng et al., 2014b; Podhorecka et al., 2010). In addition, we find a CLM dependent increase in the immunostaining of p-DNA-PK in mouse cells. Both of these lines of evidence suggest DNA-PK is activated to some extent, yet this still does not lead to phosphorylation of FUS. It is possible that activation, or inhibition, of another protein is required to enable DNA-PK mediated phosphorylation of FUS. One possibility is PARP1, a known binding partner of FUS (Mastrocola et al., 2013). Recent work shows that PARP1 directs FUS to sites of DNA damage (Rulten et al., 2013; Singatulina et al., 2019). Therefore, ineffective PARP1 activation or recruitment to sites of DSBs might cause improper trafficking of FUS to these sites preventing the interaction of FUS and DNA-PK. In support of this idea, PARP1 inhibition has been shown to cause increased p-H2AX, a characteristic difference we noticed between mouse and human cells following CLM treatment (Audebert et al., 2004). This suggests PARP1 may not be activated in mouse cells following CLM treatment. Future studies should examine the PARP1-FUS-DNA-PK interaction complex further.

The species-specific difference in FUS phosphorylation we uncovered is also relevant for attempts to model FUS and FET pathology in mice. Broadly speaking,

mouse models have yielded valuable insights into the pathogenesis of FTD and ALS (Ahmed et al., 2017; Van Damme et al., 2017). However, these models also have limitations, and often do not fully recapitulate all aspects of FTD or ALS (Dawson et al., 2018; Perrin, 2014). Most relevant to this work is the lack of a mouse model that recapitulates FTLD with FET pathology. One roadblock to this goal is that the specific genetic or environmental cause of FTLD-FET is still unclear. For example, although FUS is hypomethylated in FTLD-FET inclusions, mutations in protein N-arginine methyltransferase genes are not found in FTLD, leaving the cause unknown (Dormann et al., 2012; Ravenscroft et al., 2013). Recently, additional heterogeneous nuclear ribonucleoproteins (hnRNP P and Q) were found to co-aggregate with FUS, suggesting that wide-spread dysfunction of RNA metabolism contributes to the development of FTLD-FET (Gami-Patel et al., 2016; Gittings et al., 2019; Lagier-Tourenne et al., 2010; Ravenscroft et al., 2013). More research is needed to understand the similarities, differences, and cause(s) of the various FTLD sub-types. As such, our study suggests that the fundamental differences in DNA damage response between mice and humans should be considered in efforts to model FTD pathology, as well as understand pathogenesis.

In summary, we have uncovered a distinct inability of mouse cells to phosphorylate FUS following DNA damage. Even in the presence of DSBs and p-H2AX, mouse cells do not phosphorylate FUS. Our data suggest that decreased levels and activity of DNA-PK are an important factor for why FUS is not phosphorylated in mouse cells following CLM treatment. We cannot rule out that impairments in other components involved in the DNA damage response pathway also contribute to the lack of FUS phosphorylation we observe in multiple mouse cell lines. Future studies should

examine in more detail the differential response of mouse cells to CLM compared to human cells.

2.6 Acknowledgements

We would like to thank the members of the Kukar lab and the Emory Center for Neurodegenerative Disease for useful discussions and suggestions about this work. We also thank Dr. Frank Shewmaker and his lab for generously providing p-FUS specific antibodies.

Chapter 3: Quantitative proteomics reveals that DNA damage-induced N-terminal phosphorylation of fused in sarcoma (FUS) leads to distinct changes in the FUS proteome

Michelle A. Johnson[1,2], Thomas A. Nuckols[1,2], Paola Merino[1,2], Pritha Bagchi[3], Srijita Nandy[1,2], Jessica Root[1,2], Georgia Taylor[1,2], Nicholas T. Seyfired[2,3,4,5], Thomas Kukar[1,2,3*]

Affiliations

[1]Department of Pharmacology and Chemical Biology, [2]Center for Neurodegenerative Disease, [3]Emory Integrated Proteomics Core, [4]Department of Neurology, [5]Department of Biochemistry, Emory University, School of Medicine, Atlanta, GA,

This chapter has been modified from

https://www.biorxiv.org/content/10.1101/2021.06.11.448082v1

3.1 Abstract

Fused in sarcoma (FUS) is an RNA/DNA binding protein that participates in both nuclear and cytoplasmic functions. However, accumulation of FUS in the cytoplasm can lead to the formation of pathologic inclusions related to two neurodegenerative disorders, frontotemporal lobar degeneration (FTLD) and amyotrophic lateral sclerosis (ALS). While most ALS-FUS cases are caused by pathogenic mutations in FUS, most FTLD-FUS cases are not caused by FUS mutations. Therefore, identification of non-genetic mediators of FUS accumulation is crucial to understanding FTLD and ALS pathogenesis. To this end, DNA damage can trigger the DNA dependent protein kinase (DNA-PK) to phosphorylate FUS at N-terminal residues leading to FUS accumulation in the cytoplasm. However, the functional consequences of FUS phosphorylation are unknown. Proximity labeling approaches paired with mass spectrometry (MS) allow identification of a target protein's interactome by labeling its potential interacting partners. In this study, we performed proximity-dependent biotin labeling via ascorbate peroxidase 2 (APEX2) paired with MS to investigate whether phosphorylation shifts the FUS interactome and protein function. We mapped the interactome of wild-type FUS, phosphomimetic FUS (a proxy for phosphorylated FUS), and FUS P525L (a pathogenic mutation that causes ALS). We demonstrate that expression of phosphomimetic FUS shifts the FUS interactome toward more cytoplasmic functions including mediation of mRNA metabolism and translation. Our findings reveal that phosphorylation of FUS may disrupt homeostatic translation and steady state levels of certain mRNA transcripts. These results highlight the importance of phosphorylation as a modulator of FUS interactions and functions with a potential link to disease pathogenesis. Data are available via ProteomeXchange with identifier PXD026578.

3.2 Introduction

Frontotemporal lobar degeneration (FTLD) is a neurodegenerative disease characterized by atrophy of the frontal and temporal lobes. The clinical manifestation of FTLD is frontotemporal dementia (FTD) (Bang et al., 2015). FTD is a heterogenous group of clinical disorders that either results in alterations to behavior and personality or impairments in language comprehension and communication (Bang et al., 2015; Mann and Snowden, 2017). Pathological and genetic similarities between FTD and another neurodegenerative disease, amyotrophic lateral sclerosis (ALS), suggest that FTD and ALS exist on a disease spectrum (Abramzon et al., 2020; Burrell et al., 2011; Chiò et al., 2019; Mackenzie and Neumann, 2017). ALS is a progressive motor neuron disease characterized by degeneration of upper and lower motor neurons (Abramzon et al., 2020; Brown and Al-Chalabi, 2017). While ALS typically targets a different neuronal population compared to FTLD, neurodegeneration in a subset of both diseases has been linked to the abnormal aggregation of the fused in sarcoma (FUS) protein (Ferrari et al., 2011; Ling et al., 2013; Neumann and Mackenzie, 2019; Svetoni et al., 2016).

FUS is a pleiotropic RNA/DNA binding protein involved in gene transcription, DNA-repair pathways, mRNA splicing, mRNA transport, and stress granule assembly (De Santis et al., 2017; Fujii et al., 2005; Kamelgarn et al., 2016; Sama et al., 2013; Schwartz et al., 2012; Shelkovnikova et al., 2013; Svetoni et al., 2016; Tan et al., 2012; Yang et al., 2014; Zinszner et al., 1997). In FTD and ALS, FUS typically aggregates in the cytoplasm of neurons and glia forming toxic inclusions. Cellular dysfunction related to FUS aggregation is thought to be driven by novel gain-of-functions that trigger cellular death (López-Erauskin et al., 2018; Mitchell et al., 2012; Qiu et al., 2014; Scekic-Zahirovic et al., 2016; Sharma et al., 2016; Shiihashi et al., 2016). Understanding how

these gain-of-functions contribute to toxicity will inform our understanding of disease pathogenesis and develop targeted therapies.

Neuronal cytoplasmic inclusions that contain FUS occur in ~10% of FTD cases and ~5% of ALS cases (Bang et al., 2015; Neumann et al., 2011; Nolan et al., 2016). Genetic mutations in *FUS* typically cause ALS and are rarely associated with FTLD (Broustal et al., 2010; Kwiatkowski et al., 2009; Snowden et al., 2011; Vance et al., 2009a). This leaves the proximal cause of FUS pathology in FTLD unknown. One possibility is that FUS pathology is caused by exposure to an environmental toxin or dysregulated post-translational modifications (PTMs), such as phosphorylation or methylation (Bowden and Dormann, 2016; Darovic et al., 2015; Dormann et al., 2012; Higelin et al., 2016; Sama et al., 2013; Scaramuzzino et al., 2013; Singatulina et al., 2019; Verbeeck et al., 2012).

Phosphorylation is the most common reversible PTM that regulates protein function in the cell (Ubersax and Ferrell, 2007). Abnormal or dysregulated protein phosphorylation is a common feature of many neurodegenerative disorders, including FTLD and ALS (de Boer et al., 2020; Tenreiro et al., 2014). FUS can be phosphorylated at multiple N- and C-terminal residues, but the functional consequence of these modifications remain largely unexplored (Darovic et al., 2015; Deng et al., 2014b; Droppelmann et al., 2014; Monahan et al., 2017; Murray et al., 2017). Our lab discovered that phosphorylation of 12 specific N-terminal residues in FUS by the DNA-dependent protein kinase (DNA-PK) causes the cytoplasmic accumulation of phosphorylated FUS (Deng et al., 2014b; Johnson et al., 2020; Singatulina et al., 2019). This cascade is triggered by double strand DNA breaks (DSB). Various studies have found that FTLD and ALS exhibit markers of DNA damage. Given this, the cytoplasmic

re-localization of FUS induced by N-terminal phosphorylation may contribute to pathology in a subset of FTLD and ALS cases (Deng et al., 2014b; Higelin et al., 2016; Rhoads et al., 2018a; Wang et al., 2013). However, it remains unclear how N-terminal phosphorylation alters FUS function. Past studies have utilized both targeted immunoprecipitations and whole cell analysis to map how the toxic ALS-linked FUS mutations (i.e. P525L, R495X) shifts FUS function by examining the whole cellular proteome (Baron et al., 2019; Garone et al., 2020; Kamelgarn et al., 2018). Another study has also mapped the protein-protein interactions of wild-type (WT) and ALS-linked R521G FUS (Kamelgarn et al., 2016). Furthermore, a recent study looked directly at the interactome level changes in purified WT and P525L FUS droplets (Reber et al., 2021). Even so, no study has directly mapped how a PTM FUS variants may shift the protein-protein interactions FUS. Therefore, in the current study we aimed to elucidate how the FUS protein interactome changed in response to phosphorylation at these 12 key N-terminal residues.

We performed proximity-mediated biotin labeling coupled with label-free mass spectrometry to determine whether N-terminal phosphorylation alters the protein binding partners of FUS (Lam et al., 2015). Chemically induced DSBs lead to robust phosphorylation of FUS but are toxic to cells making proteomic analysis challenging (Deng *et al.*, 2014b). To overcome this hurdle, we focused our analysis on a phosphomimetic variant of FUS (FUS PM) that mimics the cytoplasmic localization caused by DSBs (Deng et al., 2014b). We engineered synthetic genes that fused APEX2 to human wild-type FUS (FUS WT), FUS PM, or the ALS-linked mutant P525L (FUS P525L) to enable proximity-dependent biotinylation of potential protein binding partners (Lam et al., 2015). Label-free proteomic analysis revealed that a majority of

FUS PM binding partners bind either FUS WT and/or FUS P525L. Differential expression analysis revealed that the FUS PM interactome was enriched for cytoplasmic proteins involved in “mRNA catabolic process”, “translation initiation”, and “stress granule assembly” over FUS WT. In contrast, the FUS PM interactome was enriched for nuclear proteins involved in functions such as “spliceosome”, “ribonucleoprotein complex biogenesis”, and “covalent chromatin modification” compared to FUS P525L. We found that cells expressing FUS PM exhibited functional alterations in mRNA catabolic processing and translation. Taken together, these data suggest that phosphorylation results in a novel FUS interactome that exists between the pathogenic FUS P525L ALS-linked mutation, and the homeostatic functions of FUS WT. Our analysis is the first comprehensive study of how a disease-relevant post-translational modification in FUS may shift its protein interactome towards a disease state. Findings from these studies will inform how phosphorylation of FUS and an ALS-linked FUS mutation contribute to neurodegeneration.

3.3 Materials and Methods

3.3.1 Plasmid creation

The DNA sequences for the APEX2-FUS variants were designed *in silico* then codon optimized and custom synthesized by GenScript. The amino acid sequence for the engineered APEX2 was taken from Addgene plasmid #212574. The wild-type FUS sequence was taken from NCBI reference sequence RNA-binding protein FUS isoform 1 [Homo sapiens] (NP_004951.1). A Twin-Strep-tag® was added to the N-terminus of the APEX2 sequence. A linker region $(GGGS)_3$ was inserted at the end of APEX2 followed by the FUS sequence. Synthetic APEX2-FUS gene constructs were designed to add a 5’

BamHI restriction digestion site (GGATCC) followed by a Kozak sequence (GCCACC) before the ATG start codon of APEX2, a 3' stop codon (TAG) and an ending with a XhoI restriction digestion site (CTCGAG). Following synthesis, the APEX2-FUS WT fusion protein was inserted into the pcDNA3.1/Hygro(+) vector using a BamHI/XhoI cloning strategy. The APEX2-FUS P525L and APEX2-FUS PM constructs was generated from the donor APEX2-FUS WT construct by express mutagenesis through GenScript.

The GFP tagged FUS variants were designed by adding EGFP to the N-terminus of the previously described FUS variants in Deng et al. (Deng et al., 2014b). In brief, the FUS variants (WT, Ala sub, PM, and delta 15) were synthesized and ligated into pcDNA3.1(+) Hygro by GeneArt (ThermoFisher Scientific). These constructs were then digested at NheI/HindIII sites upstream of the FUS sequence. EGFP was PCR amplified to introduce an NheI restriction site at the 5' end and a HindIII site at the 3' end. The EGFP was then digested and ligated into each construct. The primers used to generate EGFP were: GFP.Nhe.Sense (CACTATAGGGAGACCCAAGCTGGCTAGCgccaccATGGTGAGCAAGGGCGAGGAGCTG) and GFP.Hind.Antisense: (GGGACCAGGCGCTCATGGTGGCAAGCTTCTTGTACAGCTCGTCCATGCCGAG).

The GFP tagged FUS P525L variant was created by site directed mutagenesis on the GFP tagged FUS WT construct using the QuikChange II XL Site-Directed Mutagenesis Kit (Agilent; 200521). The primers used to generate the construct were: P525L_Sense (gacagaagagagaggctctactgactcgagtct)
P525L_Antisense (agactcgagtcagtagagcctctctcttctgtc)

All constructs were verified using DNA sequencing, restriction digests, and/or PCR amplification. The full DNA sequence for each synthesized sequence can be found in Supplemental Table 1

3.3.2 Cell culture

Human embryonic kidney cells (HEK293T, ATCC) were cultured in DMEM medium supplemented with 10% fetal bovine serum (FBS, Atlanta Biological) and 1% Pen/Strep (Gibco). Cells were maintained at 37˚C with 5% CO_2.

3.3.3 Cell transfection and APEX2-mediated biotinylation

HEK293T cells were seeded onto a poly-L-lysine coated 10-cm cell culture grade dish and cultured for 2 days prior to transfection. Cells were transfected at ~60% confluency with 2.5 µg of the appropriate DNA construct using the TransIT-LT1 Transfection Reagent (Mirus; MIR2300) and cultured for an additional 2 days. At ~48 hours post transfection, 500 µM biotinyl tyramide (biotin phenol) (Tocris; #6241) supplemented in DMEM media with 10% FBS/1% Pen/Strep was added to all experimental plates except for the non-transfected control plates. Labeling was initiated after 30 minutes by adding hydrogen peroxide (1 mM final concentration) for 1 minute. The labeling reaction was the quenched aspirating the media from the plate and immediately rinsing three times with the quenching solution: 5 mM trolox ((+/-)-6-Hydroxy-2,5,7,8-tetramethylchromane-2-carboxylic acid, Sigma; 238813), 10 mM sodium L-ascorbate (Sigma; A4034) and 10 mM sodium azide in PBS supplemented with 1x phenylmethylsulfonyl fluoride (PMSF), a serine protease inhibitor. Cells were then incubated on ice in fresh quenching solution four times for 5 minutes each. Following last wash, the quenching solution was aspirated off and 600 µl cold lysis buffer (50 mM Tris, 150 mM NaCl, 0.4% SDS, 0.5% sodium deoxycholate, 1% Triton X-100, 10 mM

sodium azide, 10 mM sodium ascorbate, and 5 mM Trolox) supplemented with 1x Halt protease/phosphatase inhibitor (ThermoFisher; 78446) was added to each plate. Samples were collected with cell scrapers into Protein lo-bind tubes (Eppendorf) and sonicated 2x on ice (25 amplitude: 10 seconds total on ice, 2 seconds on/2 seconds off). Samples were cleared by centrifugation at 16,500xg for 10 minutes at 4˚C and supernatant was collected into fresh protein lo-bind tubes. 540 µl of pre-chilled 50 mM Tris pH=7.4 was added to wash each pellet and samples were spun at 16,500xg for 10 minutes at 4˚C. Supernatant was collected and combined to previous samples and samples were stored at -80˚C. Protein concentration was assayed using RC DC protein assay (Bio-Rad; 5000121).

3.3.4 Streptavidin-based purification of biotinylated targets

For affinity purification, 240 µl of NanoLINK Streptavidin Magnetic Beads (TriLink Biotechnologies; M-1002) were washed 3x in 1x tris buffered saline (TBS) containing 0.1% tween-20. 1.8 mg of total protein was then added onto washed beads and allowed to incubate overnight at 4˚C with mixing. Beads were then collected against a magnetic stand and the supernatant was set aside for future analysis (termed flow-through). Beads were then washed in wash buffer 1 (50 mM Tris, 150 mM NaCl, 0.4% SDS, 0.5% sodium deoxycholate, and 1% Triton X-100) and gently mixed with rotation for 5 minutes at room temperature. Supernatant was discarded. Beads were then washed in wash buffer 2 (2% SDS in 50 mM Tris HCl, pH 7.4) and gently mixed with rotation for 5 minutes at room temperature. Supernatant was discarded. Beads were then washed 2x in wash buffer 1 with rotation for 5 minutes at room temperature. 10% of bead slurry from each sample was set aside for future analysis (termed elution). Remaining beads were then washed 4x in 1x phosphate buffered saline (PBS) and stored at -20˚C.

3.3.5 On-bead digestion and label-free mass spectrometry

8 M urea was added to the beads and the mixture was then treated with 1 mM dithiothreitol (DTT) at room temperature for 30 minutes, followed by 5 mM iodoacetimide (IAA) at room temperature for 30 minutes in the dark. Typically, proteins were digested with 0.5 µg of lysyl endopeptidase (Wako) at room temperature for 4 hours and were further digested overnight with 1 µg trypsin (Promega) at room temperature. Resulting peptides were desalted with HLB column (Waters) and were dried under vacuum.

3.3.6 Mass Spectrometry

The data acquisition by LC-MS/MS was adapted from a published procedure (Seyfried et al., 2017). Derived peptides were resuspended in the loading buffer (0.1% trifluoroacetic acid, TFA). Peptide mixtures were separated on a self-packed C18 (1.9 µm, Dr. Maisch, Germany) fused silica column (50 cm x 75 µm internal diameter (ID); New Objective) attached to an EASY-nLC™ 1200 system and were monitored on a Q-Exactive Plus Hybrid Quadrupole-Orbitrap Mass Spectrometer (ThermoFisher Scientific). Elution was performed over a 106 min gradient at a rate of 300 nL/min (buffer A: 0.1% formic acid in water, buffer B: 0.1 % formic acid in acetonitrile): The gradient started with 1% buffer B and went to 7% in 1 minute, then increased from 7% to 40% in 105 minutes, then to 99% within 5 minutes and finally staying at 99% for 9 minutes. The mass spectrometer cycle was programmed to collect one full MS scan followed by 20 data dependent MS/MS scans. The MS scans (350-1500 m/z range, 3 x 10^6 AGC target, 100 ms maximum ion time) were collected at a resolution of 70,000 at m/z 200 in profile mode. The HCD MS/MS spectra (2 m/z isolation width, 28% collision energy, 1 x 10^5 AGC target, 50 ms maximum ion time) were acquired at a

resolution of 17,500 at m/z 200. Dynamic exclusion was set to exclude previously sequenced precursor ions for 30 seconds within a 10 ppm window. Precursor ions with +1, and +8 or higher charge states were excluded from sequencing.

3.3.7 Proteomic Data Processing

3.3.7.1 Raw Data Processing

Raw files were processed by MaxQuant with default parameters for label-free quantification (Tyanova et al., 2016). MaxQuant employs the proprietary MaxLFQ algorithm for LFQ. Quantification was performed using razor and unique peptides, including those modified by acetylation (protein N-terminal), oxidation (Met) and deamidation (NQ). Spectra were searched against the Human Uniprot database (90,300 target sequences). The resulting data with intensity scores were run through the Significance Analysis of INTeractome (SAINT) software (version 2.5) to identify and remove proteins that were unlikely to be true bait-prey interactions (Choi et al., 2012). This was performed comparing protein intensity values in the negative control condition to the corresponding intensity values in the samples. Proteins with less than 95% probability to be significantly different from the negative control in all samples were removed. The mean intensity values of control were subtracted from each sample intensity value for the remaining proteins.

3.3.7.2 Statistical Analysis

The resulting protein groups information was read in R and analyzed using Proteus to determine differentially expressed proteins between groups (Gierlinski et al., 2018). Label-free quantitation (LFQ) intensities of each sample were $\log_2$ transformed and compared using a linear model with standard errors smoothed by empirical Bayes

estimation, taken from the R package limma, to determine differentially enriched proteins. Nominal p-values were transformed using the Benjamini-Hochberg correction to account for multiple hypothesis testing (Ritchie et al., 2015). Proteins were considered significantly differentially enriched if they had q values less than 0.01 and an absolute value of $\log_2$ fold change greater than 1, or twice as enriched linearly.

Data quality were assessed through distance matrices and through principal component analysis. Volcano plots were custom generated but drew heavily from thematic elements from the R package Enhanced Volcano (Blighe et al., 2020). Pathway overrepresentation analysis was performed using MetaScape with default settings (Zhou et al., 2019). Pathway overrepresentation p-values were adjusted using the Benjamini-Hochberg correction and significant pathways were determined from those with q values less than 0.01. Biologically interesting pathways were selected manually, and the gene sets that constituted those pathways were submitted to ProHitz-viz Dotplot generator to view protein-level enrichment differences for the selected pathways (Knight et al., 2017). In the ProHitz dotplots, the rows were sorted by hierarchical clustering using Canberra distance and Ward's minimum variance method for clustering. The columns were sorted manually. Venn diagrams for overlapping proteins across the conditions were generated using the R packages ggvenn or ggVennDiagram (Gao, 2021; Yan, 2021).

3.3.8 Immunofluorescence

24 hours post-transfection, cells were washed three times at room temperature with DPBS and fixed in 4% paraformaldehyde for 15 min. After washing, cells were permeabilized in 0.5% Trition-X-100 for 10 min. Cells were then washed three times in either 1x DPBS or 1x Tris-buffered saline (TBS) and blocked in 3% BSA for 1 h at room

temperature. After blocking, cells were incubated overnight at 4 °C in primary antibody diluted in blocking buffer. The next day cells were washed three times with DPBS or TBS and incubated in secondary antibody diluted 1:500 or 1:750 in blocking buffer (Cy5 Donkey anti-rabbit, 711-175-152; Cy5 Donkey anti-mouse, 715-175-151; 488 Goat anti-mouse, A-11029). Following incubation, cells were washed three times in DPBS or TBS and mounted onto glass slides using Prolong Gold with DAPI (ThermoFisher; P36935). The following primary antibodies were used: UPF1 (Cell Signaling Technologies; 12040S; 1:2000), MOV10 (Proteintech; 10370-1-AP; 1:1000), VPS35 (Cell Signaling Technologies; 81453S; 1:500), eIF2α (Cell Signaling Technologies; 9722S; 1:500), G3BP1 (Proteintech; 13057-2-AP; 1:2500), PABP1 (Cell Signaling Technologies; 4992S; 1:500), CLTA (Proteintech; 10852-1-AP; 1:500), Twin-Strep-tag® (IBA Lifesciences; 2-1517-001; 1:1000); and Streptavidin 660 Conjugate (ThermoFisher Scientific; S21377; 1:500). Images were collected on a Leica DMi8 THUNDER Inverted Fluorescence Microscope with a DFC7000 T camera (Leica).

3.3.9 Immunoprecipitation

24 hours post-transfection, cells were washed two times on ice with DPBS. Cells were lysed on ice in either a low salt HEPES buffer (10 mM HEPES, 50 mM NaCl, 5 mM EDTA) or Pierce IP lysis buffer (25 mM Tris/HCl pH 7.4, 150 mM NaCl, 1 mM EDTA, 1% NP-40, 5% glycerol) with 1% Halt protein/phosphatase inhibitor (ThermoFisher Scientific; 78446). Samples were spun at 17,100xg for 15 minutes at 4˚C. Protein concentration were measured in the detergent soluble protein fraction by BCA assay (Pierce). Cell lysate was immunoprecipitated with Magstrep Type3 beads (IBA Lifesciences; 2-4090-002) overnight with end/end rocking at 4˚C following the protocol provided by the manufacturer. Bound material was eluted from beads in Buffer BXT (0.1

M Tris/HCL pH 8.0, 0.15 M NaCl, 1 mM EDTA, 0.05M Biotin)+β-Mercaptoethanol (BME) at 95˚C for 5 minutes. 10% Input, eluted material, and flow-through was then subjected to SDS/PAGE and Western blotting as described below.

3.3.10 Western Blot

Cell lysis and western blotting was performed as previously described with minor modifications (Johnson et al., 2020). In brief, cells were lysed on ice in either RIPA Buffer (50 mM tris pH = 8.0, 150 mM NaCl, 0.1% SDS, 1% trition-x-100, 0.5% sodium deoxycholate) or cytoplasmic lysis buffer (50 mM tris pH = 8.0, 150 mM NaCl, 0.5% trition-x-100) with 1% protein/phosphatase inhibitor (ThermoFisher; 78442). The RIPA lysate was sonicated and centrifuged for 15 min at 14,000 rpm at 4 °C. The cytoplasmic lysate was vortexed and centrifuged for 15 min at 14,000 rpm at 4 °C. The supernatant was saved as the detergent soluble protein fraction. Protein concentration were measured in the detergent soluble protein fraction by BCA assay (Pierce). Next, cell lysates were analyzed for relative protein expression using SDS/PAGE followed by two-channel infrared quantitative western blots as described previously (Deng et al., 2014b). The samples were denatured in 1X Laemmli loading buffer with 5% tris(2-carboxyethyl) phosphine (TCEP) at 70°C for 15 min. Equal amounts of protein were loaded into a 4–20% PROTEAN TGX Precast Gels (Bio-Rad). After transferring to 0.2 μm nitrocellulose membranes, some blots were stained with Revert 700 (LI-COR; 926–11,010) to measure total protein for normalization and signal was captured at 700 nm on an Odyssey Fc Imaging System (LI- COR), and then destained following the manufacture's protocol. Protein blots were then blocked in EveryBlot Blocking Buffer (Bio-Rad; 12010020) for 5 minutes at room temperature and incubated with primary antibodies (diluted in blocking buffer) overnight at 4 °C. Membranes were washed three times for five minutes

in TBST and then incubated with the appropriate secondary antibody diluted in blocking buffer for 60 min at room temperature. Lastly, membranes were washed three times with TBST for five minutes and visualized using the Odyssey Fc Imaging System (LI-COR). The following primary antibodies were used: Twin-Strep-tag® (IBA Lifesciences; 2-1517-001; 1:4000), FUS (1:2000; Bethyl Laboratories; A300-302A), UPF1 (Cell Signaling Technologies; 12040S; 1:1000), MOV10 (Proteintech; 10370-1-AP; 1:800), VPS35 (Cell Signaling Technologies; 81453S; 1:1000), eIF2α (Cell Signaling Technologies; 9722S; 1:500), G3BP1 (Proteintech; 13057-2-AP; 1:2000), PABP1 (Cell Signaling Technologies; 4992S; 1:1000), CLTA (Proteintech; 10852-1-AP; 1:1000), G3BP1 (Proteintech; 13057-2-AP; 1:2000), TAF-15 (Bethyl Laboratories; A300-308A); EWS (Epitomics; 3319-1; 1:1000), Anti-Puromycin (Sigma-Aldrich; MABE343; 1:5000), LC3A/B (Cell Signaling Technologies; 12741; 1:1000); SQSTM1/p62 (Cell Signaling Technologies; 5114; 1:1000), GAPDH (Cell Signaling Technologies; 2118; 1:10,000), and H3 (Millipore; 06-599; 1:5000).

3.3.11 Quantitative PCR (qPCR)

48 hours post transfection, cells were harvested for RNA using TRIzol™ Reagent (ThermoFisher Scientific; 15596026) following manufacturer guidelines. Equal amounts of RNA were used to create the cDNA library using the High-Capacity cDNA Reverse Transcription Kit with RNase Inhibitor (ThermoFisher Scientific; 4374966). qPCR was performed on a CFX96 Touch Real-Time PCR Detection System (Bio-Rad) using the PowerUp™ SYBR™ Green Master Mix (ThermoFisher; A25741). Results were quantified using the ΔΔCT method. Primers are listed in Supplemental Table 2.

3.3.12 SUnSet Assay

Puromycin was obtained from Gibco suspended in 20mM HEPES pH 6.7. Drug was aliquoted and stored at -20˚C (ThermoFisher Scientific; A1113803). 48 hours post transfection, cells were treated with 1 μM puromycin diluted in cell culture media for 30 minutes at 37˚C/5% CO_2. Control cells were treated with vehicle (20 mM HEPES pH 6.7) diluted in cell culture media for 30 minutes at 37˚C/5%CO_2. Following treatment, cells were lysed in RIPA lysis buffer+1% protein/phosphatase inhibitor and subjected to SDS/PAGE and Western blotting as described above.

3.3.13 Autophagosome assay

Bafilomycin A1 (Baf) was obtained from Tocris (#1334) and resuspended in DMSO dimethyl sulfoxide (DMSO) and aliquoted and stored at -20˚C. 48 hours post-transfection, cells were treated with 0.1 μM Baf diluted in cell culture media for 4 hours at 37˚C/5% CO_2. Control cells were treated with vehicle (DMSO) diluted in cell culture media for 4 hours at 37˚C/5%CO_2. Following treatment, cells were lysed in RIPA lysis buffer+1% protein/phosphatase inhibitor and subjected to SDS/PAGE and Western blotting as described above.

3.3.14 Statistical analysis

All statistical analysis was performed using GraphPad Prism 8 (San Diego, CA). Effect of variant on FUS localization was determined using an ordinary one-way analysis of variance (ANOVA) with Tukey's post-hoc test (**Figures 3.1C, D**). Effect of variant on UPF1 mRNA fold change expression was determined using an ordinary one-way ANOVA with Tukey's post-hoc test (**Figure 3.5A**). Effect of variant on mRNA fold change for other targets was determined using a two-way ANOVA with Tukey's post-hoc test (**Figure 3.5B**). Effect of variant on autophagosome markers was determined using a

two-way ANOVA with Tukey's post-hoc test (**Figures 3.5F, G**). Significance was reached at $p < 0.05$. Significance is designated as $p < 0.05$ (*), $p \leq 0.0021$ (**), $p \leq 0.0002$ (***), $p \leq 0.0001$ (****). All quantified blots either normalized to total protein (**Figures 3.1E, 5D, F, G**), GAPDH (**Figures 3.1D, E**), or H3 (**Figures 3.1D, E**).

3.4 Results

APEX2 tagged Phosphomimetic FUS (FUS PM) recapitulates p-FUS localization phenotype

FUS dysfunction is involved in FTD and ALS disease pathogenesis. However, many basic aspects of FUS function and regulation are unknown. For example, it is unclear how phosphorylation of FUS, or the presence of ALS-associated mutations, alters the function of FUS and associated pathways. To gain insight into these questions, we set out to define the protein binding network, or interactome, of FUS by performing proximity labeling mediated by ascorbate peroxidase 2 (APEX2). We genetically fused APEX2 to the N-terminus of three FUS protein variants via a $(GGGS)_3$ linker to generate three Twin-Strep-tagged® constructs: 1) wild-type human FUS (FUS WT), 2) phosphomimetic FUS (FUS PM), and 3) the ALS-linked P525L mutant FUS (FUS P525L) (**Figure 3.1A**). FUS PM was generated by substituting the 12 consensus S/T_Q residues, which are phosphorylated by DNA-PK following DSB, with the negatively charged amino acid aspartate (Deng et al., 2014b; Johnson et al., 2020). The FUS P525L mutation was first identified in 2012 and causes a severe form of juvenile ALS (Conte et al., 2012; Zhou et al., 2020). FUS P525L robustly increases cytoplasmic localization of FUS and alters the transcriptome, proteome, and the spliceosome in multiple model systems (De Santis et al., 2017; Garone et al., 2020; Humphrey et al., 2020). Therefore, the APEX2-FUS P525L mutant 1) served as a positive control for FUS cytoplasmic

localization, 2) provided insight into the pathogenic nature of ALS-linked mutations, and 3) was a useful comparison to determine if FUS PM resembles a pathogenic phenotype (Monahan et al., 2017; Rhoads et al., 2018a).

We first asked if fusion of APEX2 maintained the expected sub-cellular localization of the FUS variants. We expressed the three APEX2 fusion constructs in HEK293T cells and biochemically fractionated cells into a soluble cytoplasmic and nuclear fraction (**Figure 3.1B**). Endogenous FUS protein was enriched in the nuclear fraction and the ratio of cytoplasmic/nuclear FUS was unchanged regardless of APEX2-fusion protein expression (**Figure 3.1C**). Previously, we reported that the cytoplasmic localization of phosphorylated FUS induced by DSB can be mimicked by phosphomimetic substitution of the 12 consensus DNA-PK phosphorylation sites (serine or threonine followed by glutamine) with aspartate (D) (Deng et al., 2014b). As anticipated, a larger proportion of APEX2-FUS PM was found in the cytoplasm compared to the nucleus via western blot (**Figure 3.1D**). Western blot analysis also revealed a significant increase in APEX2-FUS WT and APEX2-FUS P525L localized to the soluble nuclear fraction (**Figure 3.1E**). FUS-ALS mutations such as P525L typically induce an accumulation of FUS into insoluble cytoplasmic inclusions (Neumann et al., 2009a; Nolan et al., 2016). As such, we examined the insoluble protein fraction and found that APEX2-FUS WT and APEX2-P525L FUS were both significantly increased in the insoluble fraction compared to APEX2-FUS PM. This suggested that a significant fraction of APEX2-FUS WT and APEX2-FUS P252L is detergent insoluble (**Figure 3.1E**). Insoluble APEX2-FUS WT/P525L protein could localize to either the nucleus or the cytoplasm.

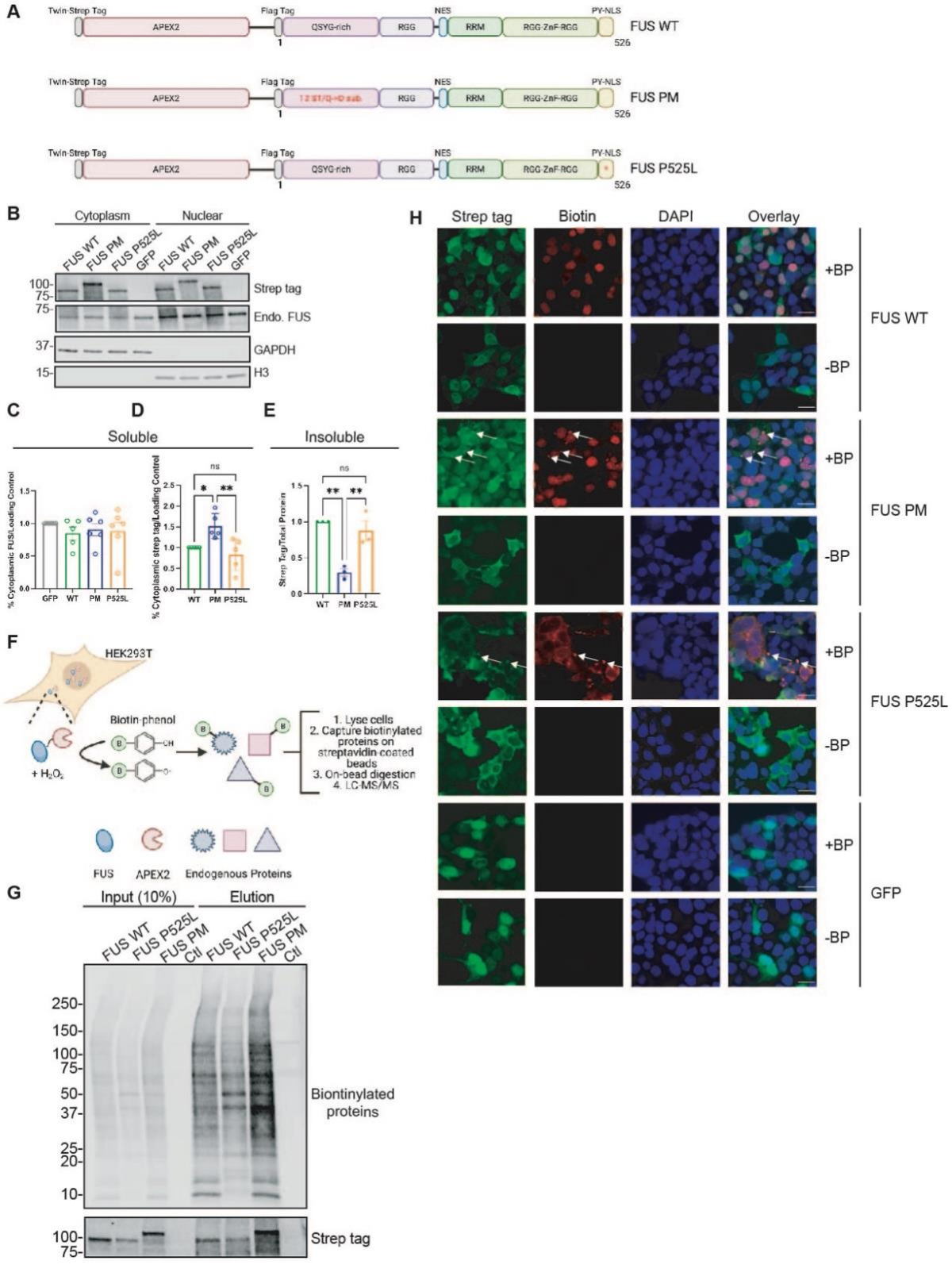
A
Twin-Strep Tag
APEX2
Flag Tag
QSYG-rich
RGG
NES
RRM
RGG-ZnF-RGG
PY-NLS
FUS WT
FUS PM
FUS P525L
1
526
B
Cytoplasm
Nuclear
FUS WT
FUS PM
FUS P525L
GFP
Strep tag
Endo. FUS
GAPDH
H3
C
D
E
Soluble
Insoluble
% Cytoplasmic FUS/Loading Control
% Cytoplasmic strep tag/Loading Control
Strep Tag/Total Protein
ns
GFP
WT
PM
P525L
F
HEK293T
Biotin-phenol
+ H2O2
1. Lyse cells
2. Capture biotinylated proteins on streptavidin-coated beads
3. On-bead digestion
4. LC-MS/MS
FUS
APEX2
Endogenous Proteins
G
Input (10%)
Elution
FUS WT
FUS P525L
FUS PM
Ctl
250-
150-
100-
75-
50-
37-
25-
20-
10-
Biontinylated proteins
Strep tag
H
Strep tag
Biotin
DAPI
Overlay
+BP
-BP
FUS WT
FUS PM
FUS P525L
GFP

Figure 3.1 Biotinylation pattern induced by APEX2 is dependent on FUS variant localization and solubilization

(A) Graphical representation of the domain structures within the three APEX2-FUS fusion constructs. Each construct contains a twin-strep tag for identification in downstream applications, APEX2, a linker sequence and a variant of human full-length FUS. The three FUS variants are: wildtype FUS (FUS WT), phosphomimetic FUS where either serine or threonine at the 12 DNA-PK consensus sites (S/T-Q) were mutated to aspartic acid (D), and pathogenic P525L mutant FUS. Created with BioRender.com. (B) HEK293T cells expressing the three APEX2-FUS fusion constructs were fractionated for cytoplasm and nuclear fractions. GAPDH and H3 were used as markers for cytoplasmic and nuclear fractions, respectively. (C) Quantification of (B) for the percentage of strep-tagged APEX2 fusion proteins found within the soluble cytoplasmic fraction and normalized to loading control. (D) Quantification of (B) for the percentage of endogenous FUS found within the soluble cytoplasmic fraction and normalized to loading control. (E) Quantification of the proportion of strep-tagged APEX2 fusion proteins within the detergent insoluble fraction and normalized to total protein (Immunoblot not shown). (F) Schematic representation of APEX2 proximity labeling and biotin enrichment in presence of H_2O_2 and biotin-phenol. Created with BioRender.com. (G) Enrichment of biotinylated proteins from HEK293T cells expressing various APEX2 constructs and treated with biotin-phenol and H_2O_2. Input is 1% of sample loaded onto magnetic beads coated with streptavidin; Elute is 10% of sample eluted off beads. Samples are wildtype FUS (FUS WT), P525L FUS (FUS P525L), Phosphomimetic FUS (FUS PM), and non-transfected control (CTL). Input and elution were analyzed for biotinylated proteins (streptavidin) and Twin-Strep-tag®

(strep tag). (H) Immunostaining of HEK293T cells expressing the three APEX2-FUS fusion constructs that have been given biotin-phenol (BP) and H_2O_2 for twin-strep tag (fusion protein) and streptavidin (biotin). Scale bar represents 20μm.

Therefore, we next utilized immunofluorescent staining to determine the sub-cellular localization of the APEX2 fusion proteins without relying on detergent-based fractionation. In line with western blot analysis, APEX2-FUS WT was found in the cytoplasm and nucleus. In contrast, both APEX2-FUS PM and APEX2-FUS P525L showed a more pronounced cytoplasmic localization (**Figure 3.1H**). Taken together, our data demonstrate that the APEX2 fusion FUS variants localize to expected cellular compartments.

APEX2-FUS variants exhibit unique biotinylation patterns

To further validate the proximity ligation system, we confirmed that the APEX2 fusion proteins are active and can biotinylate endogenous proteins. APEX2 requires the addition of biotin-phenol and H_2O_2 to catalyze the biotinylation of proximal endogenous proteins (**Figure 3.1F**). When we treated cells expressing the APEX2-FUS variants with biotin-phenol and H_2O_2, we observed robust and variant specific, biotin labeling of endogenous proteins as detected by immunofluorescence with streptavidin (**Figure 3.1H**). In contrast, we did not observe biotin labeling in cells that were not treated with biotin-phenol or H_2O_2 (**Appendix B Supplementary Figure 1**). While APEX2-FUS WT exhibited a mixed nuclear and cytoplasmic localization when immunostained for the Twin-Strep-tag® (**Figure 3.1H**), it induced a primarily nuclear biotinylation pattern as determined by colocalization with streptavidin (biotin) and DAPI immunofluorescence. APEX2-FUS PM exhibited a diffuse cytoplasmic localization pattern with biotinylated proteins primarily labeled in the nucleus with interspersed cytoplasmic punctate (white arrows). APEX2-FUS P525L was localized primarily to the cytoplasm and induced biotinylation in the cytoplasm. Negative control cells expressing GFP show no

biotinylation following biotin-phenol and H_2O_2 addition. These results demonstrate that APEX2-FUS variants exhibit unique and specific patterns of biotinylation.

To identity the variant specific binding partners of APEX2-FUS proteins, we transfected HEK293T cells with three APEX2 constructs (APEX2-FUS WT, APEX2-FUS PM, or APEX2-FUS P525L) for 24 hours. Untransfected HEK293T cells were grown in parallel for 24 hours and served as a control group. All biological groups contained technical replicates done in quadruplicate. We incubated each experimental group of cells with biotin-phenol for 30 minutes followed by H_2O_2 for 1 minute to induce biotinylation of proximal endogenous proteins. The reaction was quenched, and lysates were collected (**Figure 3.1G**). While control cells did not receive biotin-phenol, they did receive H_2O_2 and underwent all downstream processing. Biotinylated proteins were enriched from the cell lysates using streptavidin affinity purification. Western blot analysis of ~10% of the volume of streptavidin beads confirm enrichment of biotinylated proteins and revealed that each APEX2 FUS variant showed a distinct biotinylation pattern (**Figure 3.1G**). The remaining affinity-purified biotinylated proteins were used for unbiased proteomic analysis.

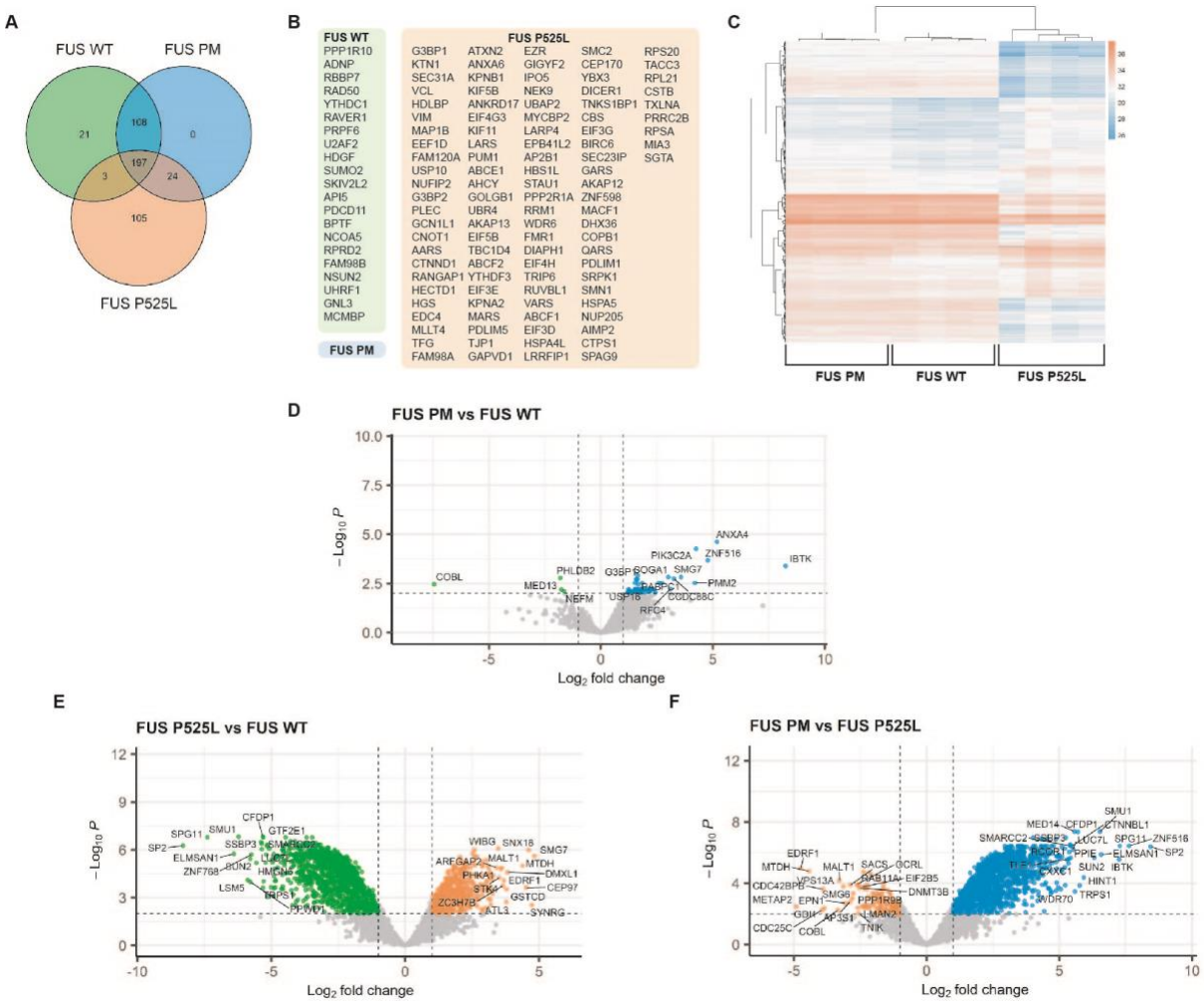

Figure 3.2 The FUS WT, FUS PM, and FUS P525L variants have unique interactome signatures.

(A) Venn diagram of overlap of proteins in the 10% of intensity for the three FUS variant groups. (B) Proteins identified uniquely in each group are highlighted in colored boxes for three FUS variants. (C) Hierarchical clustering of samples based on the intensity profiles of the 10% of protein hits. Missing values are colored gray. (D) Volcano plot showing statistically significant enriched proteins identified between FUS WT and FUS PM. (E) Volcano plot showing statistically significant enriched proteins identified between FUS PM and FUS P525L. (F) Volcano plot showing statistically significant enriched proteins identified between FUS P525L and FUS WT.

APEX2-induced biotinylation identities novel binding partners of FUS variants

To identify novel FUS interacting proteins across WT and mutant FUS proteins, we performed mass spectrometry-based proteomics using label-free quantitation (LFQ). A total of 4,954 unique proteins were identified and quantified across all 16 samples (4 replicates across 4 conditions). Significance Analysis of INTeractome (SAINT) analysis was performed to compute confidence scores to determine whether the putative interactions (prey) for each APEX2-FUS (bait) variant was real (Choi et al., 2012). Prey with spurious interactions across all APEX2-FUS baits (*sensu* SAINT analysis; probability < 0.95) were eliminated from further analysis. Finally, the mean intensity of control sample was subtracted from each sample intensity value for remaining prey proteins, leaving 3,349 proteins classified as putative interacting proteins in at least one sample.

Of the 3,349 proteins that met our filtering criteria, 3,229 (96.4%) were shared between all three groups suggesting substantial redundancy in binding partners between our three FUS variants (**Appendix B Supplementary Figure 2D**). However, analysis from unsupervised hierarchical clustering analysis, heatmap analysis, and principal component analysis of each variant suggested that the proteins from the APEX2-FUS PM variant were more similar to the APEX2-FUS WT variant than to the pathogenic APEX2-FUS P525L variant (**Figure 3.2C; Appendix B Supplementary Figure 2B/CE**). Given this, we reasoned that although the three variants enriched for many of the same proteins, the top proteins (i.e. the proteins most enriched for each variant) may be unique. As such, we specifically compared the top 10% most abundant proteins for each group (**Figure 3.2A**). We identified a total of 458 proteins in the top

10% of biotinylated proteins across the three variants. Unlike the full dataset of proteins (**Appendix B Supplementary 2D**), only 197 proteins (43.0%) were shared between the three groups suggesting that each variant preferentially bound a different subset of proteins (**Figure 3.2A**). Furthermore, APEX2-FUS PM had no unique proteins in the subset of enriched binding partner sharing 305 of its proteins (92.7%) with APEX2-FUS WT (**Figure 3.2A**). In contrast, we identified 21 unique proteins in the top 10% most abundantly labeled proteins for APEX2-FUS WT and 105 unique proteins for APEX2-FUS P525L (**Figure 3.2B**). Taken together, these data suggest that while FUS PM interacts with a majority of the FUS WT binding partners, among the top 10% of proteins that interact with FUS PM, a subset exclusively interacts with pathogenic FUS P525L and not FUS WT. These interactions may impart novel functional characteristics to FUS PM that differ from FUS WT.

Next, we compared the relative abundance of the interacting proteins between the FUS WT and FUS PM variants (**Figure 3.2D**), the FUS P525L and FUS WT variants (**Figure 3.2E**), and the FUS PM and FUS P525L variants (**Figure 3.2F**). For each comparison, we utilized a stringent cutoff of $p<0.01$ to produce a dataset of significantly enriched proteins for each variant. Each differentially expressed gene set was then compared to the core ontologies (e.g. gene ontology (GO), KEGG processes, Reactome gene sets, canonical pathways and CORUM complexes) using Metascape to define the set's involvement in biological processes, functional categories, or enzymatic pathways (Zhou et al., 2019) (**Table 3.1**). 53 proteins (1.6% of total identified proteins) differed between FUS WT and FUS PM, 181 proteins (5.4% of total identified proteins) differed between FUS PM and FUS P525L and 1590 proteins (47.5% of total identified proteins) differed between FUS WT and FUS P525L (**Figure 3.2D/E/F**). Of the 49 proteins

differentially expressed in APEX2-FUS PM over APEX2-FUS WT, the top ontology categories are “mRNA catabolic process”, “translational assembly”, “stress granule assembly”, and “clathrin-mediated endocytosis” (**Table 3.1**). These functional categories occur in the cytoplasm suggesting FUS PM participates in more cytoplasmic pathways compared to FUS WT. Outside of the functional designations, we also identified a subset of novel binding partners for FUS in our datasets. For the remaining 4 proteins enriched in FUS WT over FUS PM we were unable to determine a categorical designation. These proteins were COBL, PHLDB2, MED13, and NEFM, all novel binding partners for FUS WT. Furthermore, the top 4 enriched proteins for FUS PM compared to FUS WT were IBTK, PIK3C2A, ZNF516, ANXA4 and are also novel binding partners for FUS.

Table 1

Comparison of gene ontology (GO) and reactome pathways enriched in the FUS WT, FUS PM, and FUS P525L proteomes

	GO ID	Description	-Log10(q-value)
FUS PM vs FUS WT			
Up in FUS PM	GO:0006402	mRNA Catabolic Process	6.84
Up in FUS PM	GO:0006413	Translational Assembly	3.90
Up in FUS PM	GO:0034063	Stress Granule Assembly	2.29
Up in FUS PM	R-HSA-8856828	Clathrin-Mediated Endocytosis	2.16
FUS PM vs FUS P525L			
Up in FUS PM	CORUM:351	Splicesome	96.69
Up in FUS PM	GO:0022613	Ribonucleoprotein Complex Biogenesis	90.78
Up in FUS PM	GO:0016569	Covalent Chromatin Modification	87.14
Up in FUS PM	GO:0006281	DNA Repair	80.15
Down in FUS PM	R-HSA-199991	Membrane Trafficking	12.87
Down in FUS PM	GO:0048193	Golgi Vesicle Transport	4.84
Down in FUS PM	GO:0120031	Plasma Membrane Bounded Cell Projection Assembly	3.99
Down in FUS PM	GO:0016482	Cytosolic Transport	3.99
FUS P525L vs FUS WT			
Down in FUS P525L	CORUM:351	Splicesome	96.72
Down in FUS P525L	GO:0022613	Ribonucleoprotein Complex Biogenesis	90.74
Down in FUS P525L	GO:0016569	Covalent Chromatin Modification	88.25
Down in FUS P525L	GO:0006281	DNA Repair	77.70
Down in FUS P525L	GO:0050684	Regulation of mRNA Processing	74.98
Up in FUS P525L	R-HSA-199991	Membrane Trafficking	39.20
Up in FUS P525L	GO:0006412	Translation	37.71
Up in FUS P525L	GO:0048193	Golgi Vesicle Transport	17.97
Up in FUS P525L	GO:0030029	Actin Filament Based Process	17.72

Table 3.1 Comparison of gene ontology (GO) and reactome pathways enriched in the FUS WT, FUS PM, and FUS P525L interactomes

Table of statistically enriched gene ontology (GO) and reactome pathways generated using Metascape, a web-based platform designed to provide users a comprehensive annotation of provided gene list.

181 proteins were differentially enriched between APEX2-FUS PM and APEX2-FUS P525L (**Figure 3.2E**). Of these proteins, clustering analysis revealed FUS PM enriched for proteins associated with functions in the nucleus including “spliceosome”, “ribonucleoprotein complex biogenesis”, “covalent chromatin modification” and “DNA repair”. APEX2-FUS P525L variant enriched for pathways that occur in the cytoplasm including “membrane trafficking”, “Golgi vesicle transport”, “plasma membrane bounded cell projection” and “cytosolic transport” (**Table 3.1**). Lastly, we identified 1590 proteins differentially enriched between APEX2-FUS WT and APEX2- FUS P525L (**Figure 3.2F**). Of these proteins, clustering analysis revealed FUS WT enriched for proteins associated with the nuclear functions of “spliceosome”, “ribonucleoprotein complex biogenesis”, “covalent chromatin modification” and “DNA repair” while FUS P525L enriched for proteins associated with the cytoplasmic functions of “membrane trafficking”, “translation”, “Golgi vesicle transport” and “actin filament-based process” (**Table 3.1**).

Next, we constructed dot plots to clearly visualize the intensity and confidence of the protein interaction across each APEX2-FUS variant using the Prohits-viz software suite (Knight et al., 2017). We performed this comparative analysis for the binding partners identified in the top four significantly enriched ontology categories for FUS PM vs FUS WT (gene ontology or reactome) using Prohits-viz (**Figure 3.3A/B/C/D**). From these dot plots, we saw that the binding intensity of the target proteins to the FUS WT, FUS PM, and FUS P525L variants tended to fall as low, medium, and high, respectively. This observation compliments the original observation from the Venn diagram and the hierarchical cluster that FUS PM may exist in a middle state between FUS WT and FUS

P525L function. A full list of dot plots for each identified ontology can be found in **Appendix B Supplementary Figure 3**.

Given that these GO terms were generated from gene sets of enriched proteins, we wanted to visualize the known interactions between FUS and the target genes of each gene set. We utilized the STRING database (version 11) to create an interaction network from each functional term (Szklarczyk et al., 2019) (**Figure 3.3E/F/GH**). STRING uses an algorithm built from a curated list of known protein interactions to estimate how likely the interaction is true given the available evidence (termed confidence). The confidence for each interaction is shown by the thickness of the line between each protein. In these networks, we observed with high confidence that FUS interacts with some of the proteins in each network. Even so, there are few reports from previous studies indicating that FUS directly interacts with most of the proteins in each gene set. This may indicate that FUS WT interacts with more proteins in each interaction network than previously thought. Furthermore, if true, this would provide evidence that N-terminal phosphorylation shifts the interaction landscape allowing FUS to interact with more proteins central to these functional categories. Leading us to ask, does FUS directly interact with the proteins identified in the gene sets, or are the interactions we observe in our APEX2 datasets indirect? To answer this, we selected a subset of proteins (both previously identified as direct interactions and novel interactions) from the gene sets to validate using traditional biochemical approaches (immunoprecipitation and immunofluorescence): G3BP1, UPF1, MOV10, eIF2α, VPS35, PABPC1 (PABP1), and CLTA.

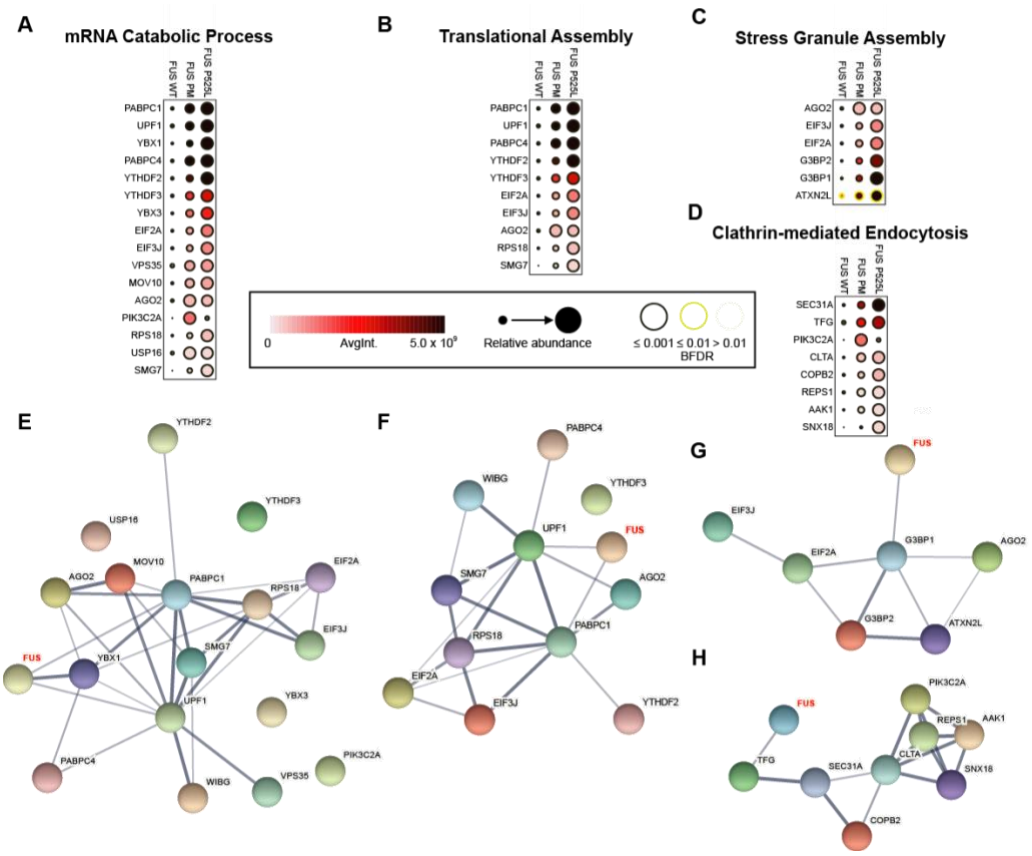

Figure 3.3 Visualization of protein hits for top gene ontology (GO) and reactome pathways reveals previously known and novel interaction partners of FUS variants

(A/B/C/D) Dot plot generated using ProHits-viz are a graphical representation of the relative binding intensity for the proteins mapped to (A) mRNA catabolic process, (B) translational assembly, (C) stress granule assembly, and (D) clathrin-mediated endocytosis GO term to the three FUS variants. (E/F/G/H) Protein interaction network for (E) mRNA catabolic process, (F) translational assembly, (G) stress granule assembly, and (H) clathrin-mediated endocytosis generated using String (version 11). Thickness of line between proteins indicates the strength of the empirical support for the interaction. FUS (in red) was added to network to demonstrate known binding partners.

Biochemical validation of FUS variant binding partners reveals novel interactions between FUS variants and APEX2 hits

We evaluated whether the FUS variants co-immunoprecipitated with the following selected endogenous targets: G3BP1, UPF1, MOV10, eIF2α, VPS35, PABPC1 (PABP1), and CLTA (**Figure 3.4A**). HEK293T cells were transfected with either Twin-Strep-tagged® FUS WT, FUS PM, or FUS P525L. All constructs were also GFP tagged at the N-terminus to allow visualization following transfection. We enriched for the strep-tagged FUS variants using Strep-Tactin®XT magnetic beads (IP) and western blotted for the potential endogenous binding partners (IB) (**Figure 3.4A**). As members of the FET family of proteins, EWS and TAF-15 are known binding partners of FUS and were used a positive control for interaction (**Figure 3.4A**, green bar) (dot plot for EWS and TAF15 in **Appendix B Supplementary Figure 3**) (Kovar, 2011). Next, we were able to replicate the direct binding reported in previous studies of UPF1, PABP1, G3BP1, and eIF2α to FUS WT and FUS P525L (**Figure 3.4A**, blue bar) (Di Salvio et al., 2015; Kamelgarn et al., 2018; Markmiller et al., 2018; Vance et al., 2013). In line with our APEX2 data, FUS PM also showed direct interaction with the above targets. We wanted to ensure that FUS PM bound proteins in a similar manner to biological relevant N-terminally phosphorylated FUS. Thus, we also confirmed that endogenous UPF1 binds preferentially to FUS treated with calicheamicin γ1 (CLM), a known inducer of N-terminal FUS phosphorylation (Deng et al., 2014b; Johnson et al., 2020; Rhoads et al., 2018a) (**Appendix B Supplementary Figure 4**). Lastly, we confirmed the interaction of three novel binding partners, VPS35, MOV10 and CLTA, to our three FUS variants (**Figure 3.4A**, red bar). This is the first report that FUS PM interacts with any of these proteins.

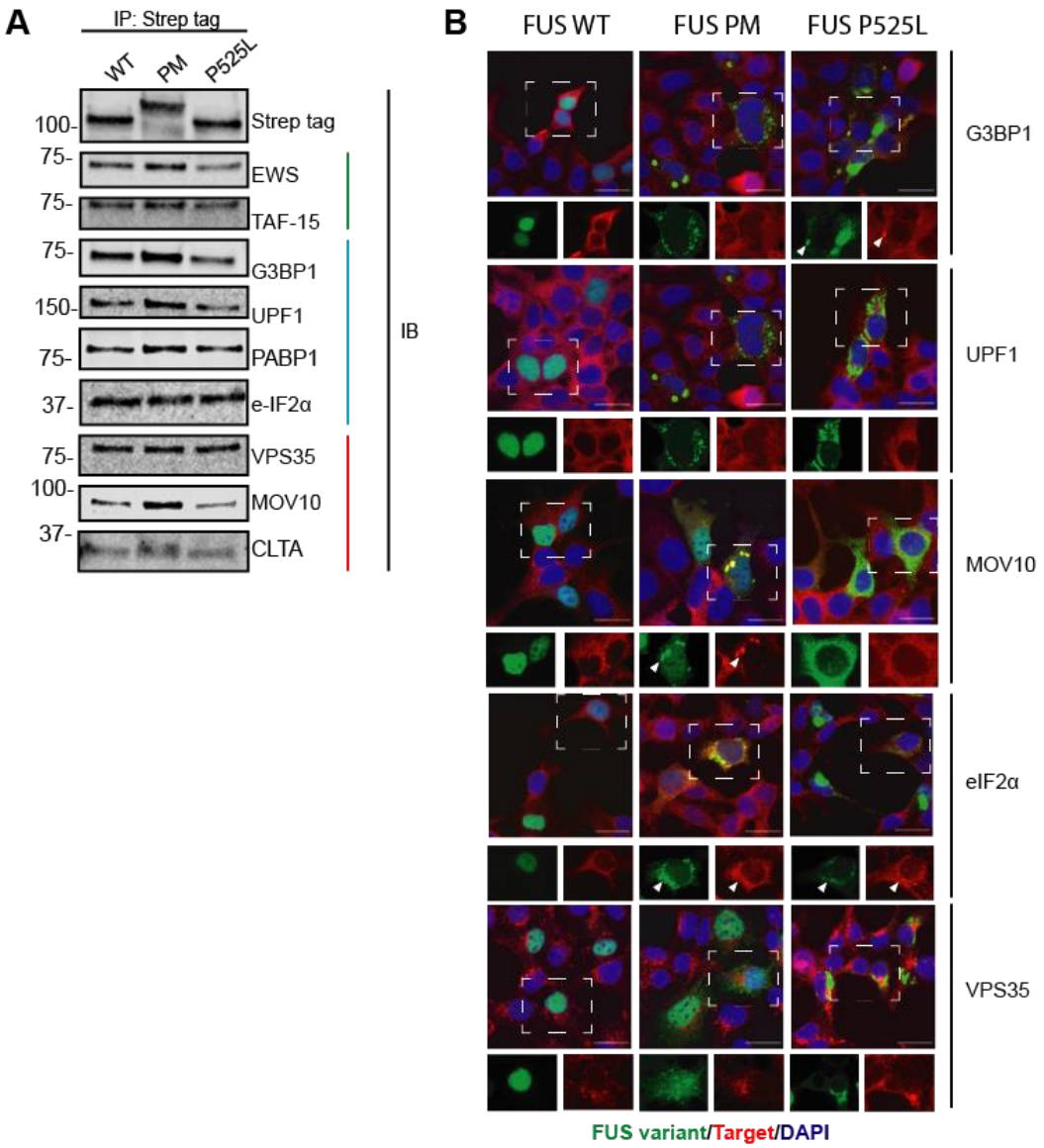

Figure 3.4 Verification of the interaction between select targets and FUS variants

(A) Immunoprecipitations (IP) for strep tag were performed on HEK293T cells expressing GFP-tagged FUS WT, FUS PM, and FUS P525L. Enriched lysate was western blotted (IB) for listed targets. (B) Immunofluorescence (IF) images show general localization patterns for a select number of targets. Co-localization of targets with FUS punctate is highlighted by white carrot. FUS variants are in green, targets are in red, DAPI is in blue. Scale bar represents 20μm.

Given that the three FUS variants are enriched in different cellular compartments (**Figure 3.1H**), we performed immunofluorescent staining for a subset of the top proteins to determine the spatial localization of the binding partners with the FUS variants (**Figure 3.4B**; PABP1, EWS and TAF15 not shown). We expressed the Twin-Strep-tagged® FUS variants in HEK293T and then co-stained for the endogenous target proteins. As expected, FUS WT was enriched in the nuclear compartment while FUS PM and FUS P525L localized to cytoplasm. The endogenous target proteins localized to cytoplasm. Given this, we saw spatial overlap of the endogenous target proteins with FUS PM and FUS P525L. For G3BP1 and MOV10, this overlap, at times, occurred in large puncta (**Figure 3.4B**, white arrow). Thus, our APEX2 generated dataset shows robust agreement with our biochemical validation.

The steady-state level of ATF3 mRNA is increased while global protein translation is enhanced in the presence of FUS PM

Based on the positive validation of our APEX2 protein targets, we set out to test whether the functional pathways suggested by our enrichment analysis were affected by the expression of a given FUS variant. We utilized four N-terminally GFP/Twin-Strep-tagged® FUS constructs: 1) wild-type human FUS (WT), 2) human FUS where the 12 serine/threonine's phosphorylated by DNA-PK are substituted with Alanine (Ala sub), 3) human FUS where the 12 serine/threonine's phosphorylated by DNA-PK has been substituted with the negatively charged aspartic acid (PM), 4) human FUS truncated at exon 15 (delta 15). We utilized the delta 15 truncation mutant as a proxy for P525L mutation. We used the pcDNA3.1 empty vector (EV) as a control.

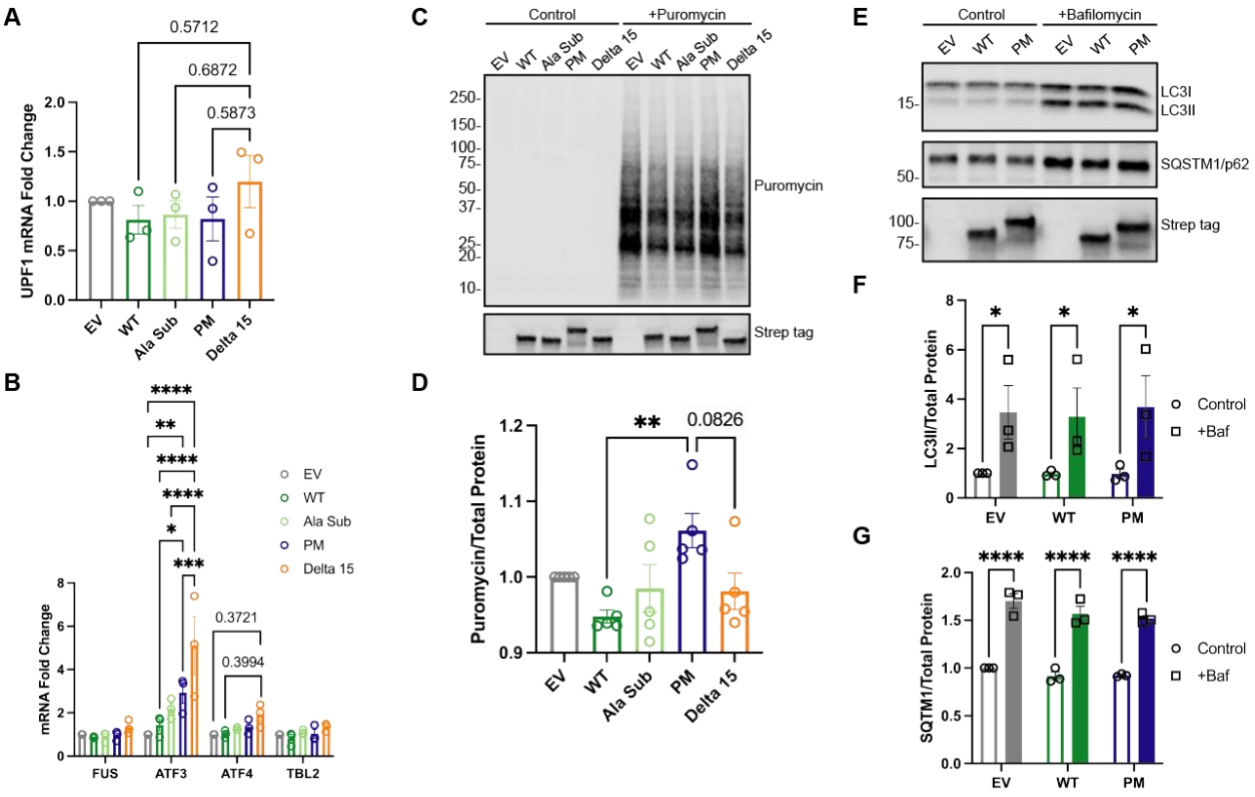

Figure 3.5 Biochemical validation of GO pathways show alternations in nonsense mediated decay and translation independent of clathrin-mediated endocytosis between the FUS variants

(A) Level of UPF1 mRNA was quantified by qPCR using the ΔΔ cycle threshold (ΔΔCT) method and then the fold change was calculated against the empty vector control (EV). (B) Level of various targets of nonsense-mediated decay were quantified by qPCR using the ΔΔ cycle threshold (ΔΔCT) method and then the fold change was calculated against the empty vector control (EV). (C) Representative immunoblot of SUnSET assay measuring the incorporation of puromycin into growing polypeptide chains during translation. Control cells received HEPES buffer without puromycin for 30 minutes. (D) Quantification of immunoblot in (C). Error bars indicates mean ± SEM (n=5). Statistical significance was calculated by one-way ANOVA. (E) Representative

immunoblot for markers of autophagosome flux, LC3I/II and SQSTM1/p62. (F) Quantification of immunoblot in (C). Error bars indicates mean ± SEM (n=3). Statistical significance was calculated by two-way ANOVA.

We specifically focused on the pathways enhanced by FUS PM expression. The highest enriched ontology category for FUS PM over FUS WT was “mRNA catabolic process”, defined as the reactions and pathways associated with the breakdown of mRNA (**Table 3.1**). As an RNA/DNA binding protein, FUS expression has been shown to regulate ~700 mRNA transcripts related to the regulation of transcription, RNA processing, and cellular stress response (Colombrita et al., 2012). Expression of ALS-linked mutations in FUS can shift the global transcriptome (De Santis et al., 2017; van Blitterswijk et al., 2013). Specifically, a previous study reported that degradation of certain mRNA transcripts is increased following expression of the ALS-linked mutant FUS P525L (Kamelgarn et al., 2018). Given this and that we observed a positive interaction between the FUS variants and UPF1 and PABP1, both major mediators of mRNA decay, we asked whether expression of FUS PM altered the steady state levels certain mRNA transcripts (Lavysh and Neu-Yilik, 2020). We designed a quantitative PCR (qPCR) protocol that measured the total levels of the stress-related mRNA targets ATF3, ATF4, and TBL2 (**Appendix B Supplementary Table 2**). While total mRNA level for UPF1 and FUS were not significantly different between FUS variants, we saw a significant increase in ATF3 mRNA levels in HEK293T cells expressing PM compared to EV, WT, and delta 15 ($p=0.0034$, $p=0.0357$, and $p=0.0008$, respectively) (**Figure 3.5A/B**). Further, we observed a trend for an increase in ATF4 mRNA in HEK293T cells expressing delta 15 but not PM (EV vs. delta 15, $p=0.3721$; WT vs. delta 15, $p=0.3994$). We saw no difference in TBL2 mRNA levels following expression of FUS variants. Taken together, this data suggests that the steady state expression of certain transcripts is enhanced by FUS PM expression.

Next, we set out to examine whether expression of FUS PM affected the closely linked functional process, mRNA translation. NMD is thought to be tightly coupled to translation because 1) translation requires multiple NMD factors, 2) phosphorylated UPF1 suppresses translational initiation, and 3) re-initiation of translation downstream of the premature termination codon can prevent NMD (Brogna and Wen, 2009). A previous report showed evidence that FUS P525L decreased global protein translation (Kamelgarn et al., 2018). Taken together, with the fact that the next highest enriched functional pathway was "translational assembly", we utilized the SUrface SEnsing of Translation (SUnSET) assay to measure the amount of global protein synthesis between the FUS variants (Goodman and Hornberger, 2013) (**Figure 3.5C**). We saw a significant increase in the amount of protein synthesis in HEK293T cells expressing FUS PM compared to FUS WT ($p=0.0074$) (**Figure 3.5D**). Furthermore, we saw a trend toward a decrease in protein synthesis between PM and delta 15 ($p=0.0826$) (**Figure 3.5D**). As such, protein translation is unchanged by delta 15 expression and enhanced by FUS PM expression compared to FUS WT.

Lastly, we examined the amount of autophagosome formation as a proxy for "clathrin-mediated endocytosis". Clathrin-coated vesicles form the precursor phagophores and blocking clathrin-dependent endocytosis leads to a decrease in autophagosomes (Longatti et al., 2010). Further, two of our protein hits, CLTA and VPS35, are important for autophagosome formation (Tang et al., 2020a). Autophagosomes are double membrane vesicles that are integral to macroautophagy as they sequester cellular components and eventually fuse with acidic lysosomes to form autolysosomes and degrade engulfed material (Berg et al., 1998; Gordon and Seglen, 1988). We utilized an autophagic assay where we treated cells with bafilomycin (Baf), an

inhibitor of the lysosomal V-ATPase in order to block the fusion of autophagosomes leading to a build-up autophagosomes (Orhon and Reggiori, 2017). There was no difference in the levels of the autophagosome markers, LC3II and SQSTM1/p62, following expression of FUS variants, before or after Baf treatment (**Figure 3.5E/F/G**). Overall, these data suggest that while FUS PM expression affects early mRNA translation and regulation, it does not affect the total amount of autophagosomes or autophagosome flux.

3.5 Discussion

Proteomic analysis is a powerful tool that has revealed how pathogenic ALS-linked mutations (e.g. FUS P525L and R495X) may shift the proteome toward pathology (Baron et al., 2019; Garone et al., 2020; Kamelgarn et al., 2016). While these past studies have informed the role that a genetic mutation can have on protein-protein interactions, pathogenic FUS mutations only account for 4% of ALS cases and a handful of FTD cases (Broustal et al., 2010; Renton et al., 2014; Rohrer et al., 2009b; Snowden et al., 2011). Thus, these previous models do not address how non-genetic mediators of FUS pathology, such as post-translational modifications, may shift FUS function. Previous non-genetic models demonstrate that cytoplasmic accumulation of FUS can be triggered by other, non-genetic mechanisms including loss of transportin-1/FUS interaction, cellular stressors, and/or altered post-translational modifications (Bowden and Dormann, 2016; Darovic et al., 2015; Dormann et al., 2012; Higelin et al., 2016; Johnson et al., 2020; Sama et al., 2013; Scaramuzzino et al., 2013; Singatulina et al., 2019). Although hypomethylated FUS accumulates in in FTLD-FUS inclusions, genetic mutations, or cellular stressors, have not been discovered that explain this phenomenon (Dormann et al., 2012; Ravenscroft et al., 2013). Unlike methylation, our lab has shown

that a biologically relevant stressor, double strand DNA breaks (DSBs), triggers the DNA dependent protein kinase (DNA-PK) to phosphorylate FUS at 12 key S/T_Q residues in the N-terminal SYGQ-low complexity domain (Deng et al., 2014b; Johnson et al., 2020; Monahan et al., 2017; Murray et al., 2017; Rhoads et al., 2018a). Phosphorylated FUS (p-FUS) then accumulates in the cytoplasm of the cell (Deng et al., 2014a; Johnson et al., 2020). While previous studies have examined how DNA-PK mediated N-terminal phosphorylation of FUS may shift the structure of the N-terminus of FUS towards a more disordered state, none have determined whether phosphorylation at these residues alters the function of FUS in cells (Monahan et al., 2017; Murray et al., 2017). In this study, we investigated whether N-terminal phosphorylation at these 12 key residues shifts the FUS protein interactome and its cellular functions. We utilized the APEX2 system in combination with label-free proteomic analysis to investigate the role of N-terminal phosphorylation in the SYGQ-rich low complexity domain on FUS function. Overall, this study is the first to map changes in the FUS protein interactome associated with a PTM.

The first question we aimed to address was whether the proximity-labeled protein hits of FUS PM overlap more with homeostatic FUS WT or pathogenic FUS P525L. From the 3,349 proteins we identified in our study, 96.4% were shared between all three FUS variants (**Figure 3.2A/C**). This suggests that the pathogenic FUS P525L and the DSB-associated FUS PM variants can interact with the majority of FUS WT targets (**Figure 3.2A**). This is surprising as pathogenic versions of another ALS/FTD linked protein, TDP-43, have been shown to interact with a large proportion of novel binding partners compared to wild-type TDP-43 (Chou et al., 2018; Feneberg et al., 2020). As such functional changes seen in pathogenic FUS P525L and the DSB-

associated FUS PM variants may not be due to the development of novel protein interactions but instead are related to changes in the strength of interaction partners. For instance, methylation of key C-terminal residues in the RGG3 domain greatly shifts the strength of the interaction between FUS and its major nuclear import protein, transportin-1 (TNPO1) (Dormann et al., 2012; Hofweber et al., 2018a). Our data supports the idea that FUS pathology is not due to a general loss of FUS function, because pathogenic FUS P525L was still able to interact with most FUS WT target proteins (Sama et al., 2017; Scekic-Zahirovic et al., 2016). The findings suggest that pathogenesis may be due to changes in the strength of FUS interactions with other proteins.

To examine whether the strength of interactions between the FUS variants and protein hits differed, we focused on the top 10% most enriched protein hits for each variant and looked at the overlap of each group (**Figure 3.2A**). Each sample clearly separated into three distinct groups, with FUS WT and FUS PM overlapping more than FUS P525L (**Figure 3.2A/C**). This distribution suggests that while a majority of the protein interaction network is shared between the three groups, the datasets from FUS WT and FUS PM share more in common with each other than FUS P525L. If the protein binding partners of FUS PM mirror FUS WT more than FUS P525L, does this indicate that expression of FUS PM is not disruptive to cellular function? To answer this question, we utilized differential expression analysis to directly examine the relative differences in abundance between our three groups. We saw that the comparison of FUS WT and FUS P525L exhibited the highest number of differentially expressed proteins followed by the comparison of FUS PM and FUS P525L (**Figures 3.2D/E/F**). Likewise,

FUS PM also enriched for a subset of proteins over FUS WT, suggesting that FUS PM may participate in biology processes in a manner divergent from that of FUS WT.

We took advantage of the list of differentially enriched genes between our groups to understand whether FUS function was affected by FUS PM expression. Past studies have demonstrated that expression of FUS P525L leads to functional changes in ontological pathways including altered translation, altered splicing, and dysregulated chromatin (Baron et al., 2019; Kamelgarn et al., 2018; Marrone et al., 2019; Reber et al., 2016; Tibshirani et al., 2017). In line with these past studies, our APEX2-FUS P525L dataset was enriched for both cytoplasmic functional terms ("translation") and structural terms ("actin filament-based process"), while depleted for nuclear terms related to mRNA ("spliceosome" and "regulation of mRNA processing") and DNA processes ("covalent chromatin modification" and "DNA repair"). As such, APEX2-FUS P525L proximity biotinylated proteins tended to be localized to the cytoplasm, suggesting cytoplasmic functional pathways may be altered by FUS P525L expression (**Figure 3.1H**) (Sharma et al., 2016). Our FUS WT vs FUS P525L dataset agrees with previous functional studies demonstrating that nucleocytoplasmic shuttling is an important mediator of FUS function.

The identified subgroup of enriched ontology terms for FUS PM over FUS WT were "mRNA catabolic process", "translational assembly", "stress granule assembly" and "clathrin-mediated endocytosis". These terms covered primarily cytoplasmic functions consistent with the observation that FUS PM accumulates in the cytoplasm over FUS WT (**Figure 3.1D**). Even so, the role of N-terminal phosphorylation in pathology is a debated topic. Other studies report N-terminal phosphorylation reduces the propensity of FUS to aggregate in vitro, thereby supporting a model where phosphorylation may be

protective against cytoplasmic FUS-mediated toxicity (Monahan et al., 2017; Rhoads et al., 2018a). Interestingly, we provide evidence that N-terminal phosphorylation instead promotes the formation of FUS aggregates, albeit these aggregates were smaller in size than the aggregates in cells expressing FUS P525L (**Appendix B Supplementary Figure 5**). Aggregation of FUS, independent of a pathogenic genetic mutation, may itself be sufficient to induce neurodegeneration (Nolan et al., 2016). As such, this may suggest that aggregates of N-terminally phosphorylated FUS may induce cellular toxicity. Future studies will need to investigate the role these aggregates have in cellular heath.

Next, we utilized Prohits-viz to directly compare the abundance of the binding hits identified for these four ontology terms between each FUS variants (**Figure 3.3**). From this, we were able to visualize a multitude of proteins that overlap between ontology categories. We used this data along with the STRING interaction database to identify a subset of proteins from each ontology term that were either 1) previously identified binding partners for FUS WT (G3BP1, UPF1, PABP1, eIF2α) or 2) novel binding partners (VPS35, MOV10, CLTA) (Di Salvio et al., 2015; Kamelgarn et al., 2016; Kamelgarn et al., 2018; Markmiller et al., 2018; Verbeeck et al., 2012). As anticipated by the APEX2 datasets, we were able to confirm the interaction between all three FUS variants and the above targets utilizing two different methods: immunoprecipitation and immunofluorescence (**Figure 3.4A/B**). FUS pathology is thought to occur when this highly regulated process is dysregulated, leading to an *over-accumulation* of FUS into cytoplasmic aggregates (Verbeeck et al., 2012). Overtime, cytoplasmic FUS aggregates are thought to induce a toxic gain of function in the cytoplasm leading to neuronal cell death (Mitchell et al., 2012; Scekic-Zahirovic et al., 2016). In line with this,

FUS PM and FUS P525L localized in the cytoplasm with target proteins (**Figure 3.4B**). Even though FUS WT did not form distinct puncta or aggregates with these target proteins, we did detect a positive interaction through immunoprecipitation. It should be noted that FUS is a nucleocytoplasmic protein that shuttles between these two cellular compartments (Zhang and Chook, 2012; Zinszner et al., 1997). Therefore, while FUS accumulation into in the nuclear compartment is easily visualized through immunofluorescent staining, a significant portion of the protein is cytoplasmic (**Figure 3.1C**). Thus, our APEX2 dataset is validated using secondary confirmation by immunoprecipitation and immunofluorescent analysis.

Using immunoprecipitation, we identified novel interactions between all three FUS variants and VPS35, MOV10, and CLTA. VPS35 is a key component of the retromer trafficking complex and is highly expressed in pyramidal neurons, a key cellular target in FTLD-mediated pathology (Tang et al., 2020a). MOV10 is a member of the SF-1 RNA helicase family related to UPF1 and a component of the RNA-induced silencing complex (RISC) (Goodier et al., 2012). Exogenous expression of MOV10 was shown to ameliorate cell death in a TDP-43 model of ALS pathology (Barmada et al., 2015). Decreased expression of the endocytic protein, CLTA, has been reported as a potential general marker of early endocytic dysfunction in neurodegeneration (Li et al., 2019). While all three of these proteins have been previously linked to FTD/ALS pathology, no study has directly linked FUS binding to these targets. The positive validation of these targets opens new avenues to explore the role of these FUS variants on protein-protein interactions.

We set out to determine the extent that FUS PM expression affected functional pathways suggested by APEX2 analysis. Alterations in mRNA catabolic processing have

been strongly linked to both ALS and FTD. One such process is nonsense mediated decay (NMD). Nonsense mediated decay is a major cellular mechanism responsible for mRNA quality control by surveilling mRNA for premature termination codons (Brogna and Wen, 2009; Mendell et al., 2004). UPF1 and PABP1, two proteins differentially enriched in FUS PM over FUS WT, act as opposing forces mediating the degradation/stabilization of NMD-sensitive mRNAs (Silva et al., 2008). A recent report found that NMD was inhibited in a C9orf72-model of FTD pathology, indicating that NMD dysfunction could be a common finding across the ALS/FTD spectrum (Sun et al., 2020). Overexpression of UPF1 in a model of FTD ameliorated toxicity in a model of ALS, suggesting enhancing NMD may be beneficial (Ortega et al., 2020). In contrast, another report found that an ALS-linked FUS mutant enhanced NMD decay of targeted transcripts (Kamelgarn et al., 2018). What might explain these discrepancies? One possibility is that past studies utilized model systems derived from different species. Studies that found diminished NMD were performed in human-derived models or using an in vivo mouse model of FUS pathology, while the study that shows enhanced NMD was done in an immortalized mouse cell line (Ho et al., 2021; Kamelgarn et al., 2018; Sun et al., 2020). Recently, we reported that mouse cells do not recapitulate DSB-mediated N-terminal phosphorylation of FUS (Johnson et al., 2020), raising the possibility that FUS-mediated regulation of NMD is also not accurately recapitulated in mouse cells. To avoid these species-specific differences, we measured the steady-state levels of known targets of NMD using a qPCR assay in human HEK293T cells. We found that mRNA transcript levels of ATF3, but not ATF4, are significantly increased following expression of FUS PM and truncated FUS delta 15 (**Figure 3.5B**). These data suggest

that expression of FUS PM may shift the total levels of certain mRNA transcripts. Future studies will need to explore if NMD processes are responsible for this shift.

What might be causing this divergence in steady state ATF3 transcript levels? Various cellular stressors such as the production of reactive oxygen species or ER stress leads to upregulation of ATF3 and ATF4 (Kurosaki et al., 2019). ATF3 is a stress-induced transcriptional activator associated with binding genomic sites related to cellular stress (Zhao et al., 2016). In parallel, expression of ATF4 leads to ATP depletion, oxidative stress, and cell death (Feneberg et al., 2020). Interestingly, upregulation of ATF4 occurs first, before directly inducing the expression of ATF3 and other downstream transcriptional regulators. Given that we only assayed one time point, it is possible that while the 48-hour time point captures the change in total transcripts levels for ATF3, it may be too late to detect appreciable changes in ATF4 transcript levels (Jiang et al., 2004; Kurosaki et al., 2019). Furthermore, we did not detect altered transcript levels for two other targets of NMD (**Figure 3.5A/B**) (Huang et al., 2011; Kurosaki et al., 2019). Thus, expression of FUS PM expression may regulate specific mRNA transcripts. Consistent with this idea, previous studies have shown that not all perturbations to the NMD pathway equally affect transcript expression. For instance, depletion of NMD factor UPF2 enhanced ATF3 but not TBL2 mRNA transcript levels (Huang et al., 2011). Alternatively, induction of ATF3 mRNA following expression of FUS PM and delta 15 may reflect the role of ATF3 as a stress-responsive transcription factor (Rohini et al., 2018). Future studies should investigate the role FUS phosphorylation on stress response pathways and the specificity of mRNA catabolic suppression on other transcripts.

FUS function is closely linked to regulation of mRNA translation (Baron et al., 2013; Baron et al., 2019; Kamelgarn et al., 2018; Sévigny et al., 2020; Yasuda et al., 2013). In line with this, we saw that expression of FUS PM enhanced protein translation compared to FUS WT (**Figure 3.5D**). Interestingly, while we saw a trend, we did not find a significant change in protein synthesis following FUS delta 15 expression (**Figure 3.5D**). Cytoplasmically localized ribonucleoprotein complexes (RNP) granules containing FUS, wild-type or an ALS mutant, have been reported to participate in active protein translation (Yasuda et al., 2013). Accordingly, FUS PM and FUS P525L in the cytoplasm may enhance protein translation through a similar mechanism. It should be noted that while the SUnSET is thought to reliably measure protein translation it does have some limitations: 1) it measures relative rates of synthesis and is unable to capture the absolute changes and 2) differences in the amount of free puromycin may alter puromycin uptake (Goodman and Hornberger, 2013). Therefore, future studies should compare multiple methods of quantifying protein synthesis.

Lastly, we examined how expression of FUS PM may impact autophagy through autophagosome formation. Lysosome-mediated autophagy is a multi-stage process involving multiple cellular components. In this process, autophagosomes are an integral part of the autophagy cascade where they begin as phagophores that expand into autophagosomes and fuse with endosomes and lysosomes to allow degradation of the compartment contents (Longatti et al., 2010). Dysfunctional autophagosome formation and other aspects of the autophagy-lysosome pathway has been widely reported in ALS and FTD (Root et al., 2021). In this study, we idented CLTA as a binding partner for FUS, which is involved autophagosome formation. However, we did not detect any difference in the levels of two markers of autophagosomes following FUS WT and FUS

PM expression, suggesting autophagosome formation is not affected (**Figures 3.5F/G**) (Ravikumar et al., 2010). Nonetheless, it remains possible that phosphorylation of FUS, or expression of pathogenic *FUS* mutations, affects autophagy and related pathways (e.g. autophagic flux, lysosome health, fusion, endocytosis) (Klionsky et al., 2021; Root et al., 2021). Future studies should examine whether other parts of the clathrin-mediated endocytic pathway are affected by expression of FUS PM leads to changes in function.

We report the first study examining whether a post-translational modification, N-terminal phosphorylation, affects the FUS proteome. Using the APEX2 system, we identified a robust dataset of novel protein partners for FUS WT, FUS P525L, and a mimetic of N-terminal phosphorylation of FUS. We provide evidence that expression of phosphorylated FUS may impact cellular function by enhancing translation and suppressing mRNA degradation. These findings also shed light on fruitful avenues for future investigation. Future studies should examine how post-translational modifications of FUS regulate protein function within the cell and how non-genetic factors influence processes underlying disease. The discovery that phosphorylated FUS plays a unique role in the cytoplasm provides valuable insights into what functions may be dysregulated in the pathological cascades of ALS and FTD.

3.6 Acknowledgments

We thank all the members of the Kukar lab and the Emory Center for Neurodegenerative Disease (CND) for their support and helpful comments during this research. This work was supported by the National Institutes of Health (NIH)/NINDS grants (R01 NS093362, R01 NS105971), a New Vision Research Investigator Award, the Alzheimer's Drug Discovery Foundation (ADDF), and the Association for

Frontotemporal Degeneration (AFTD), the Bluefield Project to Cure Frontotemporal Dementia, and the BrightFocus Foundation to Thomas Kukar.

Chapter 4: Conclusions and future directions

4.1 Outline

As discussed in **Chapter 1**, FUS is a ubiquitously expressed protein involved in multiple cellular functions. Many of these functions are facilitated through the N-terminal PLD. However, multiple variables can affect the functionality of the PLD including FUS/TNPO1 interaction, RNA concentration, C-terminal methylation and phosphorylation. FUS can be phosphorylated at >50 serine/threonine/tyrosine residues spread between the N- and C-terminus (**Figure 1.3**) but it is unclear whether N-terminal sites can mediate FUS function. At the start of this dissertation, my lab had recently discovered that DSBs induced by a chemical treatment, CLM, triggers DNA-PK to phosphorylate FUS at 12 N-terminal residues (Deng et al., 2014b). This new species of phosphorylated FUS then accumulates in the cytoplasm. However, the functional role of cytoplasmic, phosphorylated FUS was unknown. As such, the objective of this dissertation was to address whether N-terminal phosphorylation of FUS at 12 S/T_Q residues in the PLD was a novel regulator of FUS function. I begin this discussion with a summary of the findings presented in **Chapters 2** and **3.** I then integrate these findings into the existing literature and present my proposed model for the role N-terminal phosphorylation plays in cellular function. Finally, I identify the most relevant future directions that will build a more complete understanding of how N-terminal phosphorylation shifts FUS function.

4.2 Summary of findings

Our original discovery in 2014 showed that FUS is phosphorylated by the PIKK family member DNA-PK_{cs} following DSB (Deng et al., 2014b). We attempted to expand upon this finding by investigating what functional pathways are affected by the cytoplasmic accumulation of phosphorylated FUS in a neuronally relevant model.

Multiple models exist to study human neurons including immortalized cells, induced pluripotent stem cells (iPSC)-derived neurons, and neurons from donor tissue but each of these models have limitations including cost and time (Deng et al., 2014b; Dolmetsch and Geschwind, 2011; Valtcheva et al., 2016). Given that primary mouse neurons circumvent many of these issues, they are a widely used model of neuronal function. FUS and DNA-PK$_{cs}$ are also conserved across mice and humans (Boubnov and Weaver, 1995; Hicks et al., 2000; Kuroda et al., 2000). Consequently, it was surprising to discover that primary mouse neurons do not phosphorylate FUS following CLM (**Chapter 2**). I showed that mouse cells treated with CLM do not activate DNA-PK$_{cs}$ to the same extent as human cells. This suggests that CLM is unable to induce FUS phosphorylation because DNA-PK$_{cs}$ is not adequately activated, making mouse-derived cells an inadequate model for CLM-mediated FUS phosphorylation.

Following this finding, I switched to a human immortalized cell model, HEK293T, for the completion of my studies. I used a proximity labeling approach, APEX2 coupled with label free proteomics to identify the protein interaction partners of phosphorylated FUS (**Chapter 3**). I discovered that while phosphorylated FUS shares a majority of its binding partners with the general FUS proteome, phosphorylation enhances the interaction of FUS with a subset of proteins involved in mRNA translation and metabolism. As such, cells may promote the N-terminal phosphorylation of FUS as a novel method to regulate expression of specific mRNAs.

4.3 Inbred mice may be an insufficient model for DNA damage induced FUS pathology

Animal models allow biomedical researchers to explore complex scientific questions in manageable and scalable systems. Of these models, the inbred laboratory

mouse (*Mus Musculus*) has become the most commonly used experimental model to investigate human disease (Carbone, 2021). However, the frequent use of mouse models does not mean that mice accurately recapitulate all aspects of the diseases they are used to study. In this dissertation, I showed that mouse cells are incapable of phosphorylating FUS following chemical induction of DSBs (**Chapter 2**). What could cause this species-specific divergence? We can outline differences between mice and humans at various levels starting at the genome. The mouse genome is 14% smaller and only aligns to 40% of the human genome at the nucleotide level. While humans and mice share a comparable amount of protein coding genes, ~1% of mouse proteins also have no human ortholog suggesting appreciable differences in protein function between humans and mice (Breschi et al., 2017; Chinwalla et al., 2002). Furthermore, transcriptional regulation is significantly different for ~89% genomic targets and recent estimates consistently report that humans express a more complex assortment of regulatory, noncoding RNAs than mice (Breschi et al., 2017; Odom et al., 2007; Yue et al., 2014). Thus, these findings suggest that protein expression in humans and mice could vary considerably.

These differences further extend to the system level. As FTD and ALS pathology primarily targets neurons, it becomes important to establish the general differences in the mouse and human nervous system. While the cellular architecture of the nervous system is relatively conserved between mice and humans, gene expression of neurotransmitter receptors, ion channels and cell-adhesion molecules all significantly vary. This may account for the reported differences in cellular distribution and morphology of neurons between the two species (Hodge et al., 2019). Furthermore, the brain contains the second highest percentage of gene expression differences between

mice and humans (Lin et al., 2014a). Specifically, up to 30% of the proteins in the extracellular and post-synaptic density matrix differ between humans and mice (Bayés et al., 2012; Pokhilko et al., 2021). These differences at the protein level support the idea that mouse and human neurons may respond to their environments through divergent mechanisms. For example, mice are a much shorter-lived species than humans and thus their neurons need to deal with less damage over a lifetime. It is known that longer-lived species such as humans have higher expression of DNA repair genes and pathways (MacRae et al., 2015; Waterston et al., 2002). Furthermore, previous data has shown that human and mouse neurons show divergent DNA repair complex activation for the PIKK family member ATR (Martin and Chang, 2018). When activated, PIKK family kinases phosphorylate a wide variety of overlapping targets through the same S/T_Q consensus sequence (Blackford and Jackson, 2017). As such, there was already a precedent that PIKK kinase activation is divergent between humans and mice. This aligns with my finding that mouse cells exhibit insufficient activation of the PIKK family kinase, DNA-PK$_{cs}$ (**Chapter 2**).

Why might FUS-mediated DNA repair function differ between mouse and human cells? Mouse KO studies were the first to report that DNA repair is mediated by FUS expression (**Chapter 1**). Subsequent studies done in both humans and mice show that knockdown of FUS leads to diminished HR and NHEJ, suggesting FUS mediates efficient DNA repair in both species (Mastrocola et al., 2013; Wang et al., 2013). Interestingly, KO of FUS in outbred (CD1) but not inbred mouse lines (C57 BL/6) had no effect on mouse survival and tissue composition. This could be because outbred mice have increased genetic diversity than inbred mice. This suggests that genetic differences might mediate the impact the FUS loss in DNA repair (Hicks et al., 2000; Kuroda et al.,

2000). There is a precedent that different inbred mouse lines display varying predispositions towards neurodegeneration. For example, genetic KO of a tRNA, n-Tr20, in C57 BL/6J but not C57 BL/6N mice leads to neurodegeneration (Ishimura et al., 2014). Recent studies comparing individuals from inbred mouse lines such as C57 BL/6 have also shown that even within populations thought to be genetically homogenous, there is more genetic variability than previously anticipated (Tuttle et al., 2018). Therefore, different mouse lines or even individual mice may utilize FUS in DNA repair to different extents. The variability of this response to DSBs could indicate that mice may not be the optimal model to investigate FUS function. As such, in my next study, I exclusively used a human-derived cell line, HEK293T cells.

4.4 N-terminal phosphorylation in phase separation

How might phosphorylation of these 12 N-terminal residues trigger cytoplasmic accumulation in human cells? FUS self-assembles through the PLD to mediate its various functions (Yang et al., 2014). The initial hypothesis was that addition of these 12 negatively charged amino acids would bring order to the traditionally disordered N-terminal PLD (Monahan et al., 2017). Through this ordering, FUS would be prevented from associating with other FUS proteins as the negative charges would repel self-assembly and inhibit the protein's ability to phase separate. From here, unassembled FUS would be more available for nuclear export leading to the observed cytoplasmic accumulation. This hypothesis then speculates that FUS would diffusely localize to the cytoplasm. However, in **Chapter 3** I provide compelling evidence that N-terminal phosphorylation can cause the accumulation of FUS into cytoplasmic aggregates. The cause of this discrepancy is currently unknown.

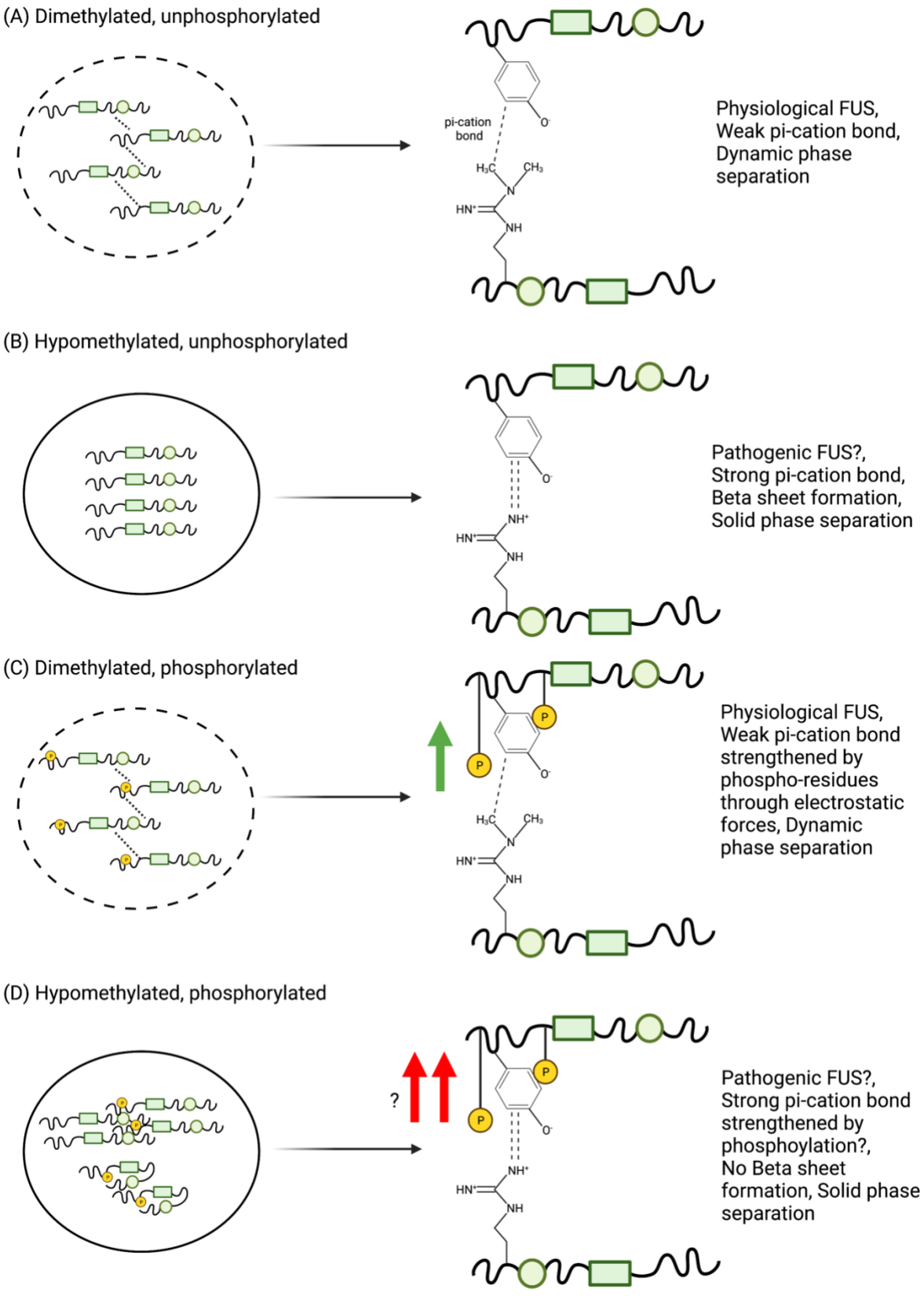
(A) Dimethylated, unphosphorylated
pi-cation bond
Physiological FUS, Weak pi-cation bond, Dynamic phase separation
(B) Hypomethylated, unphosphorylated
Pathogenic FUS?, Strong pi-cation bond, Beta sheet formation, Solid phase separation
(C) Dimethylated, phosphorylated
Physiological FUS, Weak pi-cation bond strengthened by phospho-residues through electrostatic forces, Dynamic phase separation
(D) Hypomethylated, phosphorylated
?
Pathogenic FUS?, Strong pi-cation bond strengthened by phosphoylation?, No Beta sheet formation, Solid phase separation

Figure 4.1 Effect of N-terminal phosphorylation on phase separation

(A) Dimethylated, unphosphorylated FUS forms pi-cation bonds between its' N-terminal tyrosine and C-terminal methylated arginine. Pi-cation bonds are noncovalent interactions between a benzene ring and a positively charged ion. These weak pi-cation bonds allow dynamic phase separation. (B) Hypomethylated, unphosphorylated FUS forms strong pi-cation bonds may encourage beta-sheet formation. This leads to stacking of FUS protein into solid aggregates. (C) Dimethylated, phosphorylated FUS forms weak pi-cation bonds. The 12 S/T_Q residues that are phosphorylated adds additional negative charge that strengthens the pi-cation bonds. These interactions allow dynamic phase separation. (D) Hypomethylated, phosphorylated FUS forms strong pi-cation that cause FUS to form strong inter- and intramolecular interactions between the N- and C- terminus. This causes stacking of FUS protein into solid aggregates. Created in Biorender.com.

The ability of FUS to phase separate is largely mediated through the pi-cation interactions of the tyrosine rich N-terminal PLD domain and the C-terminal arginine rich RGG domains (**Chapter 1**). Before it was widely understood that the C-terminus is essential for proper phase separation of FUS, early work focused on studying the PLD/LC domain. Truncation mutants containing only the FUS PLD/LC domain were found to readily phase separate *in vitro*. Further, induction of N-terminal phosphorylation reduced phase separation of the PLD/LC domain (Ding et al., 2020; Luo et al., 2018; Monahan et al., 2017; Murray et al., 2017). However, when the authors induced phosphorylation of either some or all 12 S/T_Q sites in full length FUS, they observed comparable phase separation to the unphosphorylated variant (Monahan et al., 2017). Phosphorylated FUS even showed a decreased propensity to enter into the solid-phase aggregates associated with disease (Monahan et al., 2017; Owen et al., 2020). Furthermore, a computational model of FUS phase separation supports the idea that phosphorylation can increase the protein's propensity to phase separate (Vernon et al., 2018). There is even evidence that this effect is not specific to only the 12 S/T_Q sites as phosphorylation of FUS at three other non-DNA-PK_{cs} sites can also disrupts the phase transition from dynamic to solid-phase aggregates. It should be noted though that there is one report that insertion of a negatively charged amino acid in the PLD at a site other than a serine or threonine does promote solid-phase aggregation. This suggests the negative charges must occur at the established phosphorylation sites for FUS to retain its dynamic characteristics (Owen et al., 2020; Patel et al., 2015).

There is compelling evidence that N-terminal phosphorylation can strengthen phase separation of FUS particles but it remains unclear whether N-terminal phosphorylation mediates toxic aggregation. Certain proteins structures are more prone

to form toxic aggregates. One of the most studied structures that induce toxic aggregation are amyloid fibrils. Amyloid fibrils form when a soluble protein assembles into stable fibers. These stable fibers contain multiple β-sheets that stack through hydrogen bounding and wound around an amyloid core structure (Rambaran and Serpell, 2008). The classic example of amyloid formation is in Alzheimer's disease pathology, where the aggregation of amyloid-β peptides is derived from the improper cleavage of soluble amyloid precursor protein (APP) (van der Kant et al., 2020). While amyloid deposition is a common feature of many protein misfolding disorders including FTLD-TDP and sporadic ALS, aggregates in FTLD with FUS pathology are not immunoreactive for *pathogenic* amyloid structures (Bigio et al., 2013; Knowles et al., 2014). This could be due to the structure of the FUS amyloid-like core. As discussed in **Chapter 1**, there is strong evidence that FUS contains an amyloid core but that this core does not contain the necessary side chains to promote β-sheet packing (Luo et al., 2018; Murray et al., 2017). It is currently unknown how the FUS core could transition to promoting aggregation. Past studies have shown that FUS aggregates are hypomethylated at the C-terminus and that this promotes aggregations (**Chapter 1**). Could another set of PTMs at the N-terminus work in tandem with C-terminal hypomethylation to shift the core structure towards aggregation?

It is unknown whether FTLD-FUS aggregates contain N-terminally phosphorylated FUS. Even so, past studies have shown that hypomethylated FUS is present in FTLD-FUS aggregates (**Chapter 1**). Thus, we might gain some hints from the structure of hypomethylated FUS aggregates. While hypomethylated FUS inclusions are not immunoreactive for amyloid using the traditional thioflavin T dye, Qamar et al. showed that they are immunoreactive for β-sheet aggregates commonly seen in tau

pathology using the fluorescent dye, formyl thiophene acetic acid (pFTAA) (Qamar et al., 2018). Furthermore, aggregates of hypomethylated FUS are heterogenous assemblies, containing regions of solid and diffuse FUS aggregation. These solid regions have increased antiparallel cross-β sheet content and intermolecular hydrogen bonding making the aggregates more stable and potentially toxic to a cell (Qamar et al., 2018). Could a subset of hypomethylated FUS also be phosphorylated at N-terminal residues? This would suggest that methylation and phosphorylation may be working together to mediate solid-phase separation. As such, I propose a model of FUS aggregation in **Figure 4.1** that combines methylation and phosphorylation.

Altogether, current evidence suggests that S/T_Q phosphorylation does not disrupt phase separation in cells. Instead, it may induce phase separation by increasing the strength of the tyrosine-arginine interactions through electrostatic forces. Pathology may arise when FUS shifts from a dimethylated to a hypomethylated state, increasing the strength of the intramolecular pi-cation interactions and causing the formation of stabilizing hydrogen bonding (**Figure 4.1**).

4.5 Proposed role of N-terminal phosphorylation in cellular function

At the beginning of my studies in **Chapter 3,** I hypothesized that the interaction between FUS and its binding partners would be shifted by N-terminal phosphorylation, thereby modulating the role FUS has in various functional pathways. My data show that by mimicking FUS phosphorylation using a phosphomimetic (FUS PM), the FUS proteome shifts towards enhanced interaction with cytoplasmic proteins involved in translation, mRNA metabolism, SG formation, and clathrin-mediated endocytosis. My data further suggests that cells expressing FUS PM exhibit enhanced translation coupled with diminished NMD.

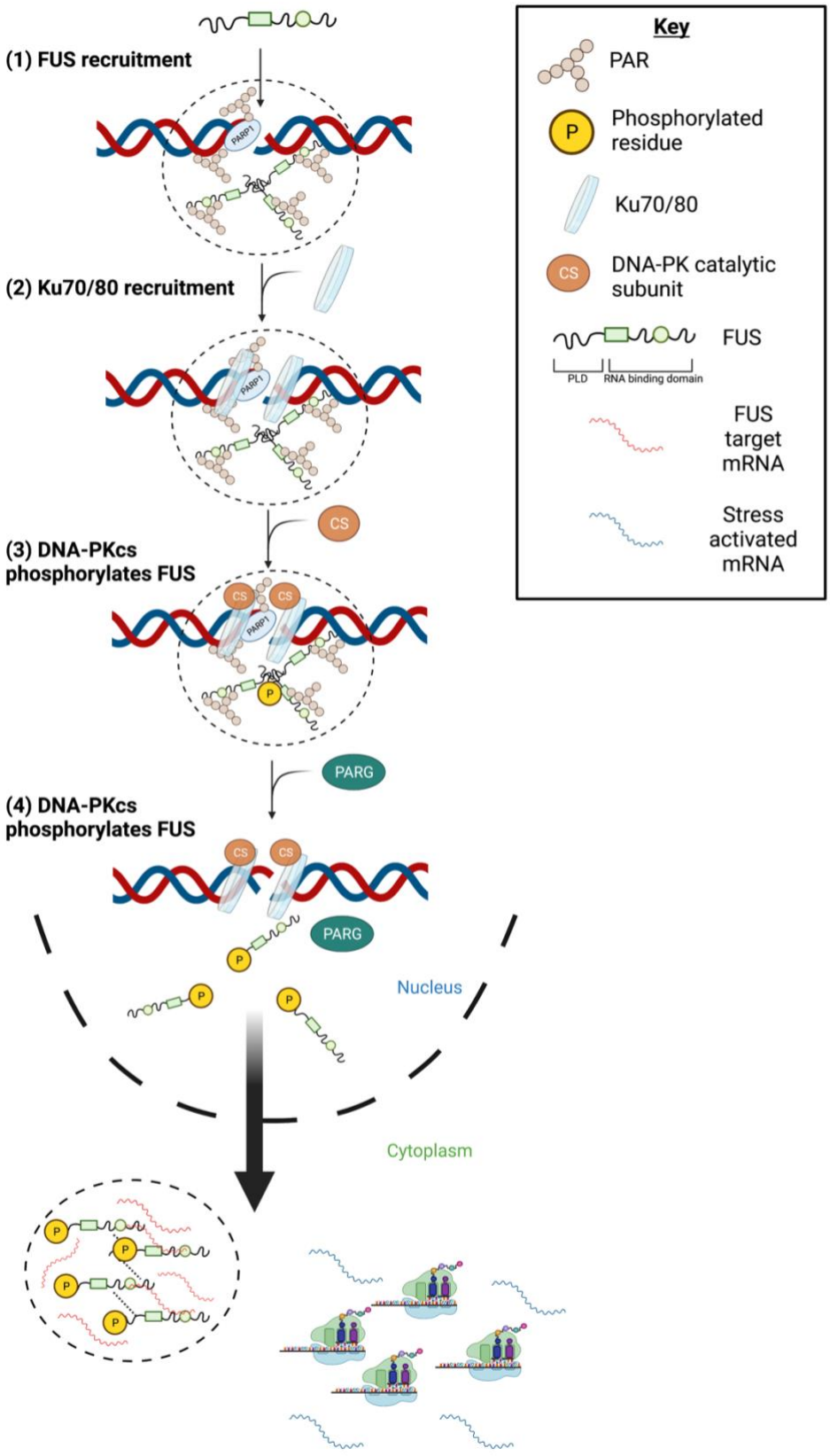
(1) FUS recruitment
PARP1
(2) Ku70/80 recruitment
PARP1
CS
(3) DNA-PKcs phosphorylates FUS
CS
CS
PARP1
P
PARG
(4) DNA-PKcs phosphorylates FUS
CS
CS
PARG
P
Nucleus
P
P
Cytoplasm
P
P
P
P
Key
PAR
P
Phosphorylated residue
Ku70/80
CS
DNA-PK catalytic subunit
FUS
PLD
RNA binding domain
FUS target mRNA
Stress activated mRNA

Figure 4.2 Effect of N-terminal phosphorylation on cellular function

(1) FUS is recruited by PARP1 to the site of DNA damage undergoing alternative NHEJ. FUS triggers phase separation, creating a compartment of damaged DNA and DNA repair proteins. (2) This recruits Ku70/80 to DSB site. (3) Ku70/80 recruits the DNA-PK catalytic subunit (cs). DNA-PK$_{cs}$ phosphorylates FUS (4) Phosphorylated FUS dissociates from site of DSB and exports either through an interaction between its nuclear export sequence (NES) and an exportin protein or through passive diffusion. (5) phosphorylated FUS triggers phase separation, sequestering mRNA and proteins into a ribonucleoprotein (RNP) granule. This allows stress-sensitive mRNAs to be preferentially translated.

The next question is what transcripts are targets of this mechanism? It would make sense that the transcripts that are typically targeted by FUS enter into the aggregates created by N-terminally phosphorylated FUS where they are silenced. As summarized in **Chapter 1**, FUS can interact with hundreds of cytoplasmic mRNA transcripts. Of these mRNAs, FUS activity is most important for regulating the gene expression in cell types affected by FTD and ALS (cortical neurons, motor neurons and glial cells) (Fujioka et al., 2013). GO analysis reveals that these genes are involved in various integral cellular processes including RNA metabolism, phospholipid metabolism, neuron projection, protein transport, synaptic transmission, and regulation of apoptosis (Colombrita et al., 2015; Fujioka et al., 2013). If these transcripts are repressed inside the ribonucleoprotein (RNP) granules containing N-terminally phosphorylated, what transcripts are responsible for the increased global protein synthesis? Typically RNP granule formation suppresses mRNA transcripts involved in homeostatic functions, thereby allowing the cell to favor translation of stress responsive transcripts (Buchan and Parker, 2009). In line with this idea, I found that expression of FUS PM causes an accumulation of the stress responsive mRNA transcript ATF3. Therefore, my data suggests that a major functional outcome of N-terminal phosphorylation is the modulation of mRNA metabolism towards a stress responsive state. This may promote expression of proteins involved in stress response such as chaperones, stress activated transcriptome factors, and proteolysis proteins.

Taken together, I propose the model outlined in **Figure 4.2** where DSBs are repaired through alterative NHEJ which triggers PARP1 recruitment to sites of DNA damage. PARP1 begins PARylation of proximal proteins, leading to FUS recruitment. FUS binds to the site of DNA damage through its PLD and initiates the formation phase

separation compartment containing the damaged DNA, PAR residues, and other RBPs capable of phase separating. This phase separation increases the local concentration DNA repair factors and allows the additional recruitment of other DNA repair factors such as Ku70/80. Ku70/80 then recruits the DNA-PK$_{cs}$ which begins to phosphorylate FUS as PARG1, the enzyme responsible for hydrolyzing PAR triggers FUS dissociation from DNA (Wang et al., 2013). It is during this time that DNA-PK$_{cs}$ then phosphorylates H2AX, allowing activation downstream repair processes (Stiff et al., 2004). This newly phosphorylated FUS then exports from the nucleus either through the NES or passive diffusion into the cytoplasm. In the cytoplasm, phosphorylated FUS then begins to phase separate, recruiting various mRNA species and proteins into aggregates. This would then allow the cell to shift its translational machinery towards prioritizing stress responsive proteins that can help with DNA repair. Therefore, N-terminal phosphorylation may be a stress response that, like methylation, can become dysregulated, leading to enhanced FUS aggregation and cellular toxicity. Therefore, in **section 4.6**, I propose future studies that can be carried out to test my proposed model.

4.6 Future Directions

Direction 1: Evaluating DNA repair pathways between mice and humans

As discussed in **section 4.3**, one of the reasons mouse models of FTD/ALS-FUS may be unable to recapitulate FUS pathology may be due to differences in the DSBs DNA repair response. Proper DNA-PK$_{cs}$ activation is an integral for recruitment of downstream proteins to sites undergoing NHEJ but I demonstrate that mouse cells fail to properly activate DNA-PK$_{cs}$ (**Chapter 2**). While there are multiple reports that humans have higher expression of DNA repair genes than mice (**section 4.3**), no study

has done a comprehensive review of the differences in 1) expression levels, 2) activation status and 3) level of protein recruitment to sites of DNA damage.

Past studies that have attempted to compare mouse and human tissues have encountered various technical issues including differences in the collection of the tissue and analysis of the tissue using different machines (Breschi et al., 2017). To circumvent these issues, I propose that iPSCs are generated from 1) control humans, 2) an inbred mouse line (e.g. C57 BL/6), and 3) an outbred mouse line (e.g. CD-1). iPSCs should then be differentiated into a long lived and FTLD-relevant cell type such as cortical neurons. Following this, transcriptomic and proteomic analysis can be undertaken following induction of varying types of DNA damage (e.g. UVA-microirradiation, chemical treatment). Lastly, imaging at different time points will reveal whether recruitment to sites of DNA damage is different between the mouse and human neurons. Completion of these studies will allow future studies to understand whether mice are a good model for the type of DNA damage they are studying.

Direction 2: Evaluating the FUS proteome's response to stress in mice and humans

Since mouse FUS is retained in the nucleus following CLM-induced DSB (**Chapter 2**), it continues to interact with nuclear proteins. In contrast, human FUS is phosphorylated and accumulates in the cytoplasm. As such, the population of proteins accessible to human FUS during DSB-mediated stress is different than the population for mouse FUS. A protein's function is dependent its interaction partners as proteins do not function independently. Therefore, comparing the interaction partners of mouse and human FUS during different stress events could inform why mouse cells responds differently to DSBs. This study could be completed in the iPSC derived neurons from **direction 1**. I propose that a future study engineers an APEX2 fusion to mouse and

human FUS and express these fusion proteins in their respectively host species. iPSC-derived neurons should then be treated with various triggers of DSBs to induce FUS-mediated DNA repair. Unlike the label free APEX2-proteomic strategy utilized in **Chapter 3**, I propose this study should be completed using the tandem mass tag (TMT) strategy that allows direct quantification between the samples from the two species. Completion of these studies will provide a comparative list of proteins binding partners for mouse and human FUS. This will inform how mouse cells utilize FUS differentially to handle stress.

Direction 3: Proteomic mapping of the PTM present in FUS inclusion

As discussed in **Chapter 1**, FUS contains multiple PTM sites outside of the N-terminal S/T_Q phosphorylation sites. Many of this sites impact the ability of FUS to undergo phase separation (Rhoads et al., 2018b). In **Figure 4.2**, I present a model whereby both N-terminal phosphorylation and C-terminal methylation may mediate the transition of FUS from phase separation to solid aggregate formation. One method to explore the validity of this model would be to map the PTMs associated with aggregating FUS in post-mortem patient brains. Previous studies have attempted to identify individual PTM sites using labor intensive biochemical techniques such as immunoprecipitation, antibody creation, and confirmation in cellular models (Dormann et al., 2012). Instead, there are techniques that allow the user to enrich for modified proteins and using liquid chromatography-tandem mass spectrometry (LC-MS/MS) paired with computational data analysis to identify the modified sites (Zhao and Jensen, 2009). I propose that the insoluble fraction is enriched in post-mortem brains from control, FTLD-FET, and ALS-FUS patients. Using LC-MS/MS, the PTM sites on FUS can be identified. Completion of these studies will determine whether the PTM signature

of FTLD-FET is influenced by N-terminal phosphorylation. Furthermore, by using an unbiased approach, researchers will be able to determine if other PTM's (e.g. additional phosphorylation, ubiquitination, and SUMOylation sites) are overrepresented in patient inclusions compared to controls.

Direction 4: In vitro *characterization of the influence various PTMs have on phase separation*

As discussed in **section 4.4**, past studies have examined the roles methylation or N-terminal phosphorylation play in phase separation individually (Murray et al., 2017; Qamar et al., 2018). Currently, no study has examined the role concurrent PTM's (such as N-terminal phosphorylation and C-terminal methylation) may have on phase separation. I propose that a future study can study this by using an *in vitro* phase separation assay where one can artificially induce the phase separation of purified FUS protein (Murakami et al., 2015). In this study, FUS would be genetically modified to mimic phosphorylation and methylation at the PTM sites identified in **direction 3** (Monahan et al., 2017; Murakami et al., 2015; Qamar et al., 2018). Through this study, the researchers can use these mimics to study if the PTMs affect phase separation to a greater extent individually or as a pair. Completion of this study will provide a more biologically relevant tool to study the role of PTMs in phase separation.

Direction 5: Role of N-terminal phosphorylation of FUS in RNA regulation

As discussed in the **Chapter 1** and **section 4.5**, FUS regulates the expression of hundreds of mRNAs. In **Chapter 3**, I present data that suggest N-terminal phosphorylation of FUS causes differential interaction of FUS with proteins involved in RNA metabolism. I hypothesize that expression of N-terminally phosphorylated FUS shifts the transcriptome of the cell, possibly through shifting the binding affinity of FUS

to its target mRNA species. The APEX2 system can be used to enrich for proximal mRNA instead of proteins (Kaewsapsak et al., 2017). The iPSC neurons generated in **direction 2** would express a APEX2-FUS protein that could be modified into a phosphomimetic variant of FUS (e.g. **Chapter 3**). I propose that proximity labeling is initiated in cells expressing either FUS WT or FUS PM. The RNA interacting with the FUS variants can then be pull downed and identified using RNA-Seq analysis. Through this, the RNA species that preferentially binds phosphomimetic FUS will be identified and a comparison can be done to determine if N-terminal phosphorylation shifts the population of RNAs interacting with FUS.

Direction 6: Determining the structure of N-terminally phosphorylated FUS aggregates

Qamar et al. observed that hypomethylated FUS aggregates are immunoreactive for pFTAA. Given the model I propose in **Figure 4.2,** I theorize that N-terminal phosphorylation and hypomethylation work in tandem to facilitate the formation of solid FUS aggregates. Given this, I hypothesize that N-terminally phosphorylated aggregates will be immunoreactive for pFTAA like hypomethylated FUS. I propose that a future study could induce aggregate formation of N-terminally phosphorylated FUS in both an *in vitro* liquid phase separation model (**direction 5**) and a cellular model (**Chapter 3**). Aggregates could then be stained using the amyloidophylic fluorescent dyes, thioflavin T and thioflavin S, and the tau aggregate fluorescence dye, pFTAA. Through using both *in vitro* and *in vivo* models, researchers will be able to determine whether the behavior of the aggregates is different in the test tube compared to the biological relevant cell. Following this, aggregate staining should be completed on FTLD-FUS, ALS-FUS and control brains to determine whether the aggregate formation

present in the above models (immunoreactive for either thioflavin positive or pFTAA positive) is similar to what is seen human disease.

4.7 Final Conclusions

Like all good explorations into human biology, this dissertation ends by asking more questions. I discovered that DSB-mediated FUS phosphorylation is a species-specific stress response that may assist cells in managing a two-pronged defense against DNA damage: First, FUS mediates recruitment of DNA repair proteins to the site of damage. Second, phosphorylated FUS directs formation of RNP granules to promote stress responsive protein activation (summarized in **Figure 4.2**). As such, the studies presented in this dissertation illustrate the importance of studying the role of PTMs in FUS function.

References

(1994). Clinical and neuropathological criteria for frontotemporal dementia. The Lund and Manchester Groups. J Neurol Neurosurg Psychiatry *57*, 416-418.

Abrahams, S., Leigh, P.N., Harvey, A., Vythelingum, G.N., Grisé, D., and Goldstein, L.H. (2000). Verbal fluency and executive dysfunction in amyotrophic lateral sclerosis (ALS). Neuropsychologia *38*, 734-747.

Abramzon, Y.A., Fratta, P., Traynor, B.J., and Chia, R. (2020). The Overlapping Genetics of Amyotrophic Lateral Sclerosis and Frontotemporal Dementia. Frontiers in neuroscience *14*, 42.

Ahmed, R.M., Devenney, E.M., Strikwerda-Brown, C., Hodges, J.R., Piguet, O., and Kiernan, M.C. (2020). Phenotypic variability in ALS-FTD and effect on survival. Neurology *94*, e2005-e2013.

Ahmed, R.M., Irish, M., van Eersel, J., Ittner, A., Ke, Y.D., Volkerling, A., van der Hoven, J., Tanaka, K., Karl, T., Kassiou, M.*, et al.* (2017). Mouse models of frontotemporal dementia: A comparison of phenotypes with clinical symptomatology. Neuroscience and biobehavioral reviews *74*, 126-138.

Al-Chalabi, A., and Hardiman, O. (2013). The epidemiology of ALS: a conspiracy of genes, environment and time. Nat Rev Neurol *9*, 617-628.

Alzheimer, A. (1911). Über eigenartige Krankheitsfälle des späteren Alters. Zeitschrift für die gesamte Neurologie und Psychiatrie *4*, 356.

Aman, P., Panagopoulos, I., Lassen, C., Fioretos, T., Mencinger, M., Toresson, H., Höglund, M., Forster, A., Rabbitts, T.H., Ron, D.*, et al.* (1996). Expression patterns of the human sarcoma-associated genes FUS and EWS and the genomic structure of FUS. Genomics *37*, 1-8.

Aman, P., Ron, D., Mandahl, N., Fioretos, T., Heim, S., Arheden, K., Willén, H., Rydholm, A., and Mitelman, F. (1992). Rearrangement of the transcription factor gene CHOP in myxoid liposarcomas with t(12;16)(q13;p11). Genes, chromosomes & cancer *5*, 278-285.

An, J., Huang, Y.-C., Xu, Q.-Z., Zhou, L.-J., Shang, Z.-F., Huang, B., Wang, Y., Liu, X.-D., Wu, D.-C., and Zhou, P.-K. (2010). DNA-PKcs plays a dominant role in the regulation of H2AX phosphorylation in response to DNA damage and cell cycle progression. BMC molecular biology *11*, 18.

Andersson, M.K., Ståhlberg, A., Arvidsson, Y., Olofsson, A., Semb, H., Stenman, G., Nilsson, O., and Åman, P. (2008). The multifunctional FUS, EWS and TAF15 proto-oncoproteins show cell type-specific expression patterns and involvement in cell spreading and stress response. BMC cell biology *9*, 37.

Arai, T., Hasegawa, M., Akiyama, H., Ikeda, K., Nonaka, T., Mori, H., Mann, D., Tsuchiya, K., Yoshida, M., Hashizume, Y.*, et al.* (2006). TDP-43 is a component of ubiquitin-positive tau-negative inclusions in frontotemporal lobar degeneration and amyotrophic lateral sclerosis. Biochem Biophys Res Commun *351*, 602-611.

Aran, F. (1850). Recherches sur une maladie non encore décrite du système musculaire (atrophie musculaire progressive). Arch Gen Med *24*, 5-35,172-214.

Arthur, K.C., Calvo, A., Price, T.R., Geiger, J.T., Chiò, A., and Traynor, B.J. (2016). Projected increase in amyotrophic lateral sclerosis from 2015 to 2040. Nature communications *7*, 12408-12408.

Audebert, M., Salles, B., and Calsou, P. (2004). Involvement of poly(ADP-ribose) polymerase-1 and XRCC1/DNA ligase III in an alternative route for DNA double-strand breaks rejoining. The Journal of biological chemistry *279*, 55117-55126.

Baechtold, H., Kuroda, M., Sok, J., Ron, D., Lopez, B.S., and Akhmedov, A.T. (1999). Human 75-kDa DNA-pairing protein is identical to the pro-oncoprotein TLS/FUS and is able to promote D-loop formation. The Journal of biological chemistry *274*, 34337-34342.

Bahia, V.S., Takada, L.T., and Deramecourt, V. (2013). Neuropathology of frontotemporal lobar degeneration: a review. Dement Neuropsychol *7*, 19-26.

Bang, J., Spina, S., and Miller, B.L. (2015). Frontotemporal dementia. Lancet (London, England) *386*, 1672-1682.

Barmada, S.J., Ju, S., Arjun, A., Batarse, A., Archbold, H.C., Peisach, D., Li, X., Zhang, Y., Tank, E.M.-H., Qiu, H., *et al.* (2015). Amelioration of toxicity in neuronal models of amyotrophic lateral sclerosis by hUPF1. Proceedings of the National Academy of Sciences of the United States of America *112*, 7821-7826.

Baron, D.M., Kaushansky, L.J., Ward, C.L., Sama, R.R.K., Chian, R.-J., Boggio, K.J., Quaresma, A.J.C., Nickerson, J.A., and Bosco, D.A. (2013). Amyotrophic lateral sclerosis-linked FUS/TLS alters stress granule assembly and dynamics. Molecular neurodegeneration *8*, 30.

Baron, D.M., Matheny, T., Lin, Y.-C., Leszyk, J.D., Kenna, K., Gall, K.V., Santos, D.P., Tischbein, M., Funes, S., Hayward, L.J., *et al.* (2019). Quantitative proteomics identifies proteins that resist translational repression and become dysregulated in ALS-FUS. Human molecular genetics *28*, 2143-2160.

Bäumer, D., Hilton, D., Paine, S.M., Turner, M.R., Lowe, J., Talbot, K., and Ansorge, O. (2010). Juvenile ALS with basophilic inclusions is a FUS proteinopathy with FUS mutations. Neurology *75*, 611-618.

Bayés, À., Collins, M.O., Croning, M.D.R., van de Lagemaat, L.N., Choudhary, J.S., and Grant, S.G.N. (2012). Comparative Study of Human and Mouse Postsynaptic Proteomes Finds High Compositional Conservation and Abundance Differences for Key Synaptic Proteins. PLOS ONE *7*, e46683.

Belzil, V.V., Daoud, H., St-Onge, J., Desjarlais, A., Bouchard, J.P., Dupre, N., Lacomblez, L., Salachas, F., Pradat, P.F., Meininger, V.*, et al.* (2011). Identification of novel FUS mutations in sporadic cases of amyotrophic lateral sclerosis. Amyotroph Lateral Scler *12*, 113-117.

Belzil, V.V., Valdmanis, P.N., Dion, P.A., Daoud, H., Kabashi, E., Noreau, A., Gauthier, J., Hince, P., Desjarlais, A., Bouchard, J.P.*, et al.* (2009). Mutations in FUS cause FALS and SALS in French and French Canadian populations. Neurology *73*, 1176-1179.

Bennetzen, M.V., Kosar, M., Bunkenborg, J., Payne, M.R., Bartkova, J., Lindström, M.S., Lukas, J., Andersen, J.S., Bartek, J., and Larsen, D.H. (2018). DNA damage-induced dynamic changes in abundance and cytosol-nuclear translocation of proteins involved in translational processes, metabolism, and autophagy. Cell cycle (Georgetown, Tex) *17*, 2146-2163.

Bensimon, G., Lacomblez, L., and Meininger, V. (1994). A controlled trial of riluzole in amyotrophic lateral sclerosis. ALS/Riluzole Study Group. N Engl J Med *330*, 585-591.

Berg, T.O., Fengsrud, M., Strømhaug, P.E., Berg, T., and Seglen, P.O. (1998). Isolation and characterization of rat liver amphisomes. Evidence for fusion of autophagosomes with both early and late endosomes. The Journal of biological chemistry *273*, 21883-21892.

Bigio, E.H., Wu, J.Y., Deng, H.-X., Bit-Ivan, E.N., Mao, Q., Ganti, R., Peterson, M., Siddique, N., Geula, C., Siddique, T., *et al.* (2013). Inclusions in frontotemporal lobar degeneration with TDP-43 proteinopathy (FTLD-TDP) and amyotrophic lateral sclerosis (ALS), but not FTLD with FUS proteinopathy (FTLD-FUS), have properties of amyloid. Acta neuropathologica *125*, 463-465.

Blackford, A.N., and Jackson, S.P. (2017). ATM, ATR, and DNA-PK: The Trinity at the Heart of the DNA Damage Response. Molecular Cell *66*, 801-817.

Blair, I.P., Williams, K.L., Warraich, S.T., Durnall, J.C., Thoeng, A.D., Manavis, J., Blumbergs, P.C., Vucic, S., Kiernan, M.C., and Nicholson, G.A. (2010). FUS mutations in amyotrophic lateral sclerosis: clinical, pathological, neurophysiological and genetic analysis. J Neurol Neurosurg Psychiatry *81*, 639-645.

Blighe, K., Rana, S., and Lewis, M. (2020). EnhancedVolcano: Publication-ready volcano plots with enhanced colouring and labeling. (R package).

Boehringer, A., Garcia-Mansfield, K., Singh, G., Bakkar, N., Pirrotte, P., and Bowser, R. (2017). ALS Associated Mutations in Matrin 3 Alter Protein-Protein Interactions and Impede mRNA Nuclear Export. Scientific reports *7*, 14529.

Bogaert, E., Boeynaems, S., Kato, M., Guo, L., Caulfield, T.R., Steyaert, J., Scheveneels, W., Wilmans, N., Haeck, W., Hersmus, N., *et al.* (2018). Molecular Dissection of FUS Points at Synergistic Effect of Low-Complexity Domains in Toxicity. Cell Rep *24*, 529-537.e524.

Bohgaki, T., Bohgaki, M., and Hakem, R. (2010). DNA double-strand break signaling and human disorders. Genome integrity *1*, 15.

Boillée, S., Yamanaka, K., Lobsiger, C.S., Copeland, N.G., Jenkins, N.A., Kassiotis, G., Kollias, G., and Cleveland, D.W. (2006). Onset and progression in inherited ALS determined by motor neurons and microglia. Science *312*, 1389-1392.

Bosco, D.A., Lemay, N., Ko, H.K., Zhou, H., Burke, C., Kwiatkowski Jr, T.J., Sapp, P., McKenna-Yasek, D., Brown Jr, R.H., and Hayward, L.J. (2010). Mutant FUS proteins that cause amyotrophic lateral sclerosis incorporate into stress granules. Human molecular genetics *19*, 4160-4175.

Boubnov, N.V., and Weaver, D.T. (1995). scid cells are deficient in Ku and replication protein A phosphorylation by the DNA-dependent protein kinase. Molecular and Cellular Biology *15*, 5700.

Bowden, H.A., and Dormann, D. (2016). Altered mRNP granule dynamics in FTLD pathogenesis. Journal of Neurochemistry *138 Suppl 1*, 112-133.

Boxer, A.L., Gold, M., Feldman, H., Boeve, B.F., Dickinson, S.L.-J., Fillit, H., Ho, C., Paul, R., Pearlman, R., Sutherland, M.*, et al.* (2020). New directions in clinical trials for frontotemporal lobar degeneration: Methods and outcome measures. Alzheimer's & dementia : the journal of the Alzheimer's Association *16*, 131-143.

Bradfield, N.I., McLean, C., Drago, J., Darby, D.G., and Ames, D. (2017). Rapidly progressive Fronto-temporal dementia (FTD) associated with Frontotemporal lobar degeneration (FTLD) in the presence of Fused in Sarcoma (FUS) protein: a rare, sporadic, and aggressive form of FTD. International psychogeriatrics *29*, 1743-1746.

Brain, R. (1956). Diseases of the nervous system. The Journal of Nervous and Mental Disease *123*, 304.

Brain, W. (1962). Diseases of the nervous system, 6th edn (Oxford: Oxford University Press).

Breschi, A., Gingeras, T.R., and Guigó, R. (2017). Comparative transcriptomics in human and mouse. Nat Rev Genet *18*, 425-440.

Brogna, S., and Wen, J. (2009). Nonsense-mediated mRNA decay (NMD) mechanisms. Nature structural & molecular biology *16*, 107-113.

Brooks, B.R., Miller, R.G., Swash, M., and Munsat, T.L. (2000). El Escorial revisited: revised criteria for the diagnosis of amyotrophic lateral sclerosis. Amyotroph Lateral Scler Other Motor Neuron Disord *1*, 293-299.

Broustal, O., Camuzat, A., Guillot-Noel, L., Guy, N., Millecamps, S., Deffond, D., Lacomblez, L., Golfier, V., Hannequin, D., Salachas, F.*, et al.* (2010). FUS mutations in frontotemporal lobar degeneration with amyotrophic lateral sclerosis. Journal of Alzheimer's disease : JAD *22*, 765-769.

Brown, J.A., Min, J., Staropoli, J.F., Collin, E., Bi, S., Feng, X., Barone, R., Cao, Y., O'Malley, L., Xin, W.*, et al.* (2012). SOD1, ANG, TARDBP and FUS mutations in amyotrophic lateral sclerosis: a United States clinical testing lab experience. Amyotroph Lateral Scler *13*, 217-222.

Brown, R.H., and Al-Chalabi, A. (2017). Amyotrophic Lateral Sclerosis. The New England journal of medicine *377*, 1602-1602.

Brunet, M.A., Jacques, J.-F., Nassari, S., Tyzack, G.E., McGoldrick, P., Zinman, L., Jean, S., Robertson, J., Patani, R., and Roucou, X. (2021). The FUS gene is dual-coding with both proteins contributing to FUS-mediated toxicity. EMBO reports *22*, e50640.

Bruun, M., Koikkalainen, J., Rhodius-Meester, H.F.M., Baroni, M., Gjerum, L., van Gils, M., Soininen, H., Remes, A.M., Hartikainen, P., Waldemar, G.*, et al.* (2019). Detecting frontotemporal dementia syndromes using MRI biomarkers. Neuroimage Clin *22*, 101711-101711.

Buchan, J.R., and Parker, R. (2009). Eukaryotic Stress Granules: The Ins and Outs of Translation. Molecular Cell *36*, 932-941.

Buée, L., and Delacourte, A. (1999). Comparative biochemistry of tau in progressive supranuclear palsy, corticobasal degeneration, FTDP-17 and Pick's disease. Brain Pathol *9*, 681-693.

Burma, S., and Chen, D.J. (2004). Role of DNA-PK in the cellular response to DNA double-strand breaks. DNA repair *3*, 909-918.

Burrell, J.R., Halliday, G.M., Kril, J.J., Ittner, L.M., Götz, J., Kiernan, M.C., and Hodges, J.R. (2016). The frontotemporal dementia-motor neuron disease continuum. Lancet *388*, 919-931.

Burrell, J.R., Kiernan, M.C., Vucic, S., and Hodges, J.R. (2011). Motor neuron dysfunction in frontotemporal dementia. Brain *134*, 2582-2594.

Cairns, N.J., Grossman, M., Arnold, S.E., Burn, D.J., Jaros, E., Perry, R.H., Duyckaerts, C., Stankoff, B., Pillon, B., Skullerud, K.*, et al.* (2004). Clinical and neuropathologic variation in neuronal intermediate filament inclusion disease. Neurology *63*, 1376-1384.

Calvio, C., Neubauer, G., Mann, M., and Lamond, A.I. (1995). Identification of hnRNP P2 as TLS/FUS using electrospray mass spectrometry. RNA (New York, NY) *1*, 724-733.

Carbone, L. (2021). Estimating mouse and rat use in American laboratories by extrapolation from Animal Welfare Act-regulated species. Scientific Reports *11*, 493.

Carter, R.L., Chen, Y., Kunkanjanawan, T., Xu, Y., Moran, S.P., Putkhao, K., Yang, J., Huang, A.H.C., Parnpai, R., and Chan, A.W.S. (2014). Reversal of cellular phenotypes in neural cells derived from Huntington's disease monkey-induced pluripotent stem cells. Stem cell reports *3*, 585-593.

Celeste, A., Difilippantonio, S., Difilippantonio, M.J., Fernandez-Capetillo, O., Pilch, D.R., Sedelnikova, O.A., Eckhaus, M., Ried, T., Bonner, W.M., and Nussenzweig, A. (2003). H2AX haploinsufficiency modifies genomic stability and tumor susceptibility. Cell *114*, 371-383.

Chakravarthy, B.R., Walker, T., Rasquinha, I., Hill, I.E., and MacManus, J.P. (1999). Activation of DNA-dependent protein kinase may play a role in apoptosis of human neuroblastoma cells. Journal of Neurochemistry *72*, 933-942.

Chan, D.W., Chen, B.P.-C., Prithivirajsingh, S., Kurimasa, A., Story, M.D., Qin, J., and Chen, D.J. (2002). Autophosphorylation of the DNA-dependent protein kinase catalytic subunit is required for rejoining of DNA double-strand breaks. Genes & Development *16*, 2333-2338.

Charcot, J. (1874). Amyotrophies spinales deuteropathiques sclérose latérale amyotrophique & sclérose latérale amyotrophique. Bureaux du Progrès Médical *2*, 234-266.

Chartier, L., Rankin, L.L., Allen, R.E., Kato, Y., Fusetani, N., Karaki, H., Watabe, S., and Hartshorne, D.J. (1991). Calyculin-A increases the level of protein phosphorylation and changes the shape of 3T3 fibroblasts. Cell motility and the cytoskeleton *18*, 26-40.

Chatterjee, N., and Walker, G.C. (2017). Mechanisms of DNA damage, repair, and mutagenesis. Environ Mol Mutagen *58*, 235-263.

Chen, B.P.C., Chan, D.W., Kobayashi, J., Burma, S., Asaithamby, A., Morotomi-Yano, K., Botvinick, E., Qin, J., and Chen, D.J. (2005). Cell cycle dependence of DNA-dependent protein kinase phosphorylation in response to DNA double strand breaks. The Journal of biological chemistry *280*, 14709-14715.

Chen, J.J. (2020). Overview of current and emerging therapies for amytrophic lateral sclerosis.

Chen, L., Yun, S.W., Seto, J., Liu, W., and Toth, M. (2003). The fragile x mental retardation protein binds and regulates a novel class of mRNAs containing u rich target sequences. Neuroscience *120*, 1005-1017.

Chinwalla, A.T., Cook, L.L., Delehaunty, K.D., Fewell, G.A., Fulton, L.A., Fulton, R.S., Graves, T.A., Hillier, L.W., Mardis, E.R., McPherson, J.D.*, et al.* (2002). Initial sequencing and comparative analysis of the mouse genome. Nature *420*, 520-562.

Chiò, A., Calvo, A., Moglia, C., Ossola, I., Brunetti, M., Sbaiz, L., Lai, S.L., Abramzon, Y., Traynor, B.J., and Restagno, G. (2011). A de novo missense mutation of the FUS gene in a "true" sporadic ALS case. Neurobiol Aging *32*, 553.e523-556.

Chiò, A., Logroscino, G., Hardiman, O., Swingler, R., Mitchell, D., Beghi, E., Traynor, B.G., and Eurals, C. (2009a). Prognostic factors in ALS: A critical review. Amyotroph Lateral Scler *10*, 310-323.

Chiò, A., Moglia, C., Canosa, A., Manera, U., Vasta, R., Brunetti, M., Barberis, M., Corrado, L., D'Alfonso, S., Bersano, E.*, et al.* (2019). Cognitive impairment across ALS clinical stages in a population-based cohort. Neurology *93*, e984-e994.

Chiò, A., Mora, G., Leone, M., Mazzini, L., Cocito, D., Giordana, M.T., Bottacchi, E., and Mutani, R. (2002). Early symptom progression rate is related to ALS outcome: a prospective population-based study. Neurology *59*, 99-103.

Chiò, A., Restagno, G., Brunetti, M., Ossola, I., Calvo, A., Mora, G., Sabatelli, M., Monsurrò, M.R., Battistini, S., Mandrioli, J.*, et al.* (2009b). Two Italian kindreds with familial amyotrophic lateral sclerosis due to FUS mutation. Neurobiol Aging *30*, 1272-1275.

Cho, I.K., Hunter, C.E., Ye, S., Pongos, A.L., and Chan, A.W.S. (2019a). Combination of stem cell and gene therapy ameliorates symptoms in Huntington's disease mice. NPJ Regenerative medicine *4*, 7.

Cho, I.K., Yang, B., Forest, C., Qian, L., and Chan, A.W.S. (2019b). Amelioration of Huntington's disease phenotype in astrocytes derived from iPSC-derived neural progenitor cells of Huntington's disease monkeys. PloS one *14*, e0214156.

Choi, H., Liu, G., Mellacheruvu, D., Tyers, M., Gingras, A.C., and Nesvizhskii, A.I. (2012). Analyzing protein-protein interactions from affinity purification-mass spectrometry data with SAINT. Curr Protoc Bioinformatics *Chapter 8*, Unit8.15.

Chou, C.-C., Zhang, Y., Umoh, M.E., Vaughan, S.W., Lorenzini, I., Liu, F., Sayegh, M., Donlin-Asp, P.G., Chen, Y.H., Duong, D.M.*, et al.* (2018). TDP-43 pathology disrupts nuclear pore complexes and nucleocytoplasmic transport in ALS/FTD. Nature neuroscience *21*, 228-239.

Colombrita, C., Onesto, E., Buratti, E., de la Grange, P., Gumina, V., Baralle, F.E., Silani, V., and Ratti, A. (2015). From transcriptomic to protein level changes in TDP-43 and FUS loss-of-function cell models. Biochimica et biophysica acta *1849*, 1398-1410.

Colombrita, C., Onesto, E., Megiorni, F., Pizzuti, A., Baralle, F.E., Buratti, E., Silani, V., and Ratti, A. (2012). TDP-43 and FUS RNA-binding proteins bind distinct sets of cytoplasmic messenger RNAs and differently regulate their post-transcriptional fate in motoneuron-like cells. The Journal of biological chemistry *287*, 15635-15647.

Conte, A., Lattante, S., Zollino, M., Marangi, G., Luigetti, M., Del Grande, A., Servidei, S., Trombetta, F., and Sabatelli, M. (2012). P525L FUS mutation is consistently associated with a severe form of juvenile amyotrophic lateral sclerosis. Neuromuscular disorders : NMD *22*, 73-75.

Corrado, L., Del Bo, R., Castellotti, B., Ratti, A., Cereda, C., Penco, S., Sorarù, G., Carlomagno, Y., Ghezzi, S., Pensato, V.*, et al.* (2010). Mutations of FUS gene in sporadic amyotrophic lateral sclerosis. J Med Genet *47*, 190-194.

Coyle-Gilchrist, I.T., Dick, K.M., Patterson, K., Vázquez Rodríquez, P., Wehmann, E., Wilcox, A., Lansdall, C.J., Dawson, K.E., Wiggins, J., Mead, S.*, et al.* (2016). Prevalence, characteristics, and survival of frontotemporal lobar degeneration syndromes. Neurology *86*, 1736-1743.

Crozat, A., Aman, P., Mandahl, N., and Ron, D. (1993). Fusion of CHOP to a novel RNA-binding protein in human myxoid liposarcoma. Nature *363*, 640-644.

Cruz, M.P. (2018). Edaravone (Radicava): A Novel Neuroprotective Agent for the Treatment of Amyotrophic Lateral Sclerosis. P T *43*, 25-28.

Darovic, S., Prpar Mihevc, S., Župunski, V., Gunčar, G., Štalekar, M., Lee, Y.-B., Shaw, C.E., and Rogelj, B. (2015). Phosphorylation of C-terminal tyrosine residue 526 in FUS impairs its nuclear import. Journal of cell science *128*, 4151-4159.

Dawson, T.M., Golde, T.E., and Lagier-Tourenne, C. (2018). Animal models of neurodegenerative diseases. Nature neuroscience *21*, 1370-1379.

de Boer, E.M.J., Orie, V.K., Williams, T., Baker, M.R., De Oliveira, H.M., Polvikoski, T., Silsby, M., Menon, P., van den Bos, M., Halliday, G.M.*, et al.* (2020). TDP-43 proteinopathies: a new wave of neurodegenerative diseases. J Neurol Neurosurg Psychiatry *92*, 86-95.

De Santis, R., Santini, L., Colantoni, A., Peruzzi, G., de Turris, V., Alfano, V., Bozzoni, I., and Rosa, A. (2017). FUS Mutant Human Motoneurons Display Altered Transcriptome and microRNA Pathways with Implications for ALS Pathogenesis. Stem cell reports.

Dedon, P.C., Salzberg, A.A., and Xu, J. (1993). Exclusive production of bistranded DNA damage by calicheamicin. Biochemistry *32*, 3617-3622.

DeJesus-Hernandez, M., Kocerha, J., Finch, N., Crook, R., Baker, M., Desaro, P., Johnston, A., Rutherford, N., Wojtas, A., Kennelly, K.*, et al.* (2010). De novo truncating FUS gene mutation as a cause of sporadic amyotrophic lateral sclerosis. Hum Mutat *31*, E1377-1389.

DeJesus-Hernandez, M., Mackenzie, I.R., Boeve, B.F., Boxer, A.L., Baker, M., Rutherford, N.J., Nicholson, A.M., Finch, N.A., Flynn, H., Adamson, J.*, et al.* (2011). Expanded GGGGCC hexanucleotide repeat in noncoding region of C9ORF72 causes chromosome 9p-linked FTD and ALS. Neuron *72*, 245-256.

Deng, H., Gao, K., and Jankovic, J. (2014a). The role of FUS gene variants in neurodegenerative diseases. Nature reviews Neurology *10*, 337-348.

Deng, Q., Holler, C.J., Taylor, G., Hudson, K.F., Watkins, W., Gearing, M., Ito, D., Murray, M.E., Dickson, D.W., Seyfried, N.T.*, et al.* (2014b). FUS is phosphorylated by DNA-PK and accumulates in the cytoplasm after DNA damage. The Journal of neuroscience : the official journal of the Society for Neuroscience *34*, 7802-7813.

Di Salvio, M., Piccinni, V., Gerbino, V., Mantoni, F., Camerini, S., Lenzi, J., Rosa, A., Chellini, L., Loreni, F., Carrì, M.T.*, et al.* (2015). Pur-alpha functionally interacts with FUS carrying ALS-associated mutations. Cell death & disease *6*, e1943-e1943.

Ding, X., Sun, F., Chen, J., Chen, L., Tobin-Miyaji, Y., Xue, S., Qiang, W., and Luo, S.-Z. (2020). Amyloid-Forming Segment Induces Aggregation of FUS-LC Domain from Phase Separation Modulated by Site-Specific Phosphorylation. Journal of Molecular Biology *432*, 467-483.

Doi, H., Okamura, K., Bauer, P.O., Furukawa, Y., Shimizu, H., Kurosawa, M., Machida, Y., Miyazaki, H., Mitsui, K., Kuroiwa, Y.*, et al.* (2008). RNA-binding protein TLS is a major nuclear aggregate-interacting protein in huntingtin exon 1 with expanded polyglutamine-expressing cells. The Journal of biological chemistry *283*, 6489-6500.

Dolmetsch, R., and Geschwind, D.H. (2011). The human brain in a dish: the promise of iPSC-derived neurons. Cell *145*, 831-834.

Dormann, D., and Haass, C. (2011). TDP-43 and FUS: a nuclear affair. Trends Neurosci *34*, 339-348.

Dormann, D., Madl, T., Valori, C.F., Bentmann, E., Tahirovic, S., Abou-Ajram, C., Kremmer, E., Ansorge, O., Mackenzie, I.R.A., Neumann, M.*, et al.* (2012). Arginine methylation next to the PY-NLS modulates Transportin binding and nuclear import of FUS. The EMBO journal *31*, 4258-4275.

Dormann, D., Rodde, R., Edbauer, D., Bentmann, E., Fischer, I., Hruscha, A., Than, M.E., Mackenzie, I.R.A., Capell, A., Schmid, B.*, et al.* (2010). ALS-associated fused in sarcoma (FUS) mutations disrupt Transportin-mediated nuclear import. The EMBO journal *29*, 2841-2857.

Droppelmann, C.A., Campos-Melo, D., Ishtiaq, M., Volkening, K., and Strong, M.J. (2014). RNA metabolism in ALS: when normal processes become pathological. Amyotroph Lateral Scler Frontotemporal Degener *15*, 321-336.

Ederle, H., Funk, C., Abou-Ajram, C., Hutten, S., Funk, E.B.E., Kehlenbach, R.H., Bailer, S.M., and Dormann, D. (2018). Nuclear egress of TDP-43 and FUS occurs independently of Exportin-1/CRM1. Scientific reports *8*, 451.

Elmroth, K., Nygren, J., Mårtensson, S., Ismail, I.H., and Hammarsten, O. (2003). Cleavage of cellular DNA by calicheamicin gamma1. DNA repair *2*, 363-374.

Erkkinen, M.G., Kim, M.-O., and Geschwind, M.D. (2018). Clinical Neurology and Epidemiology of the Major Neurodegenerative Diseases. Cold Spring Harbor perspectives in biology *10*.

Feneberg, E., Gordon, D., Thompson, A.G., Finelli, M.J., Dafinca, R., Candalija, A., Charles, P.D., Mäger, I., Wood, M.J., Fischer, R.*, et al.* (2020). An ALS-linked mutation in TDP-43 disrupts normal protein interactions in the motor neuron response to oxidative stress. Neurobiology of disease *144*, 105050.

Ferrari, R., Kapogiannis, D., Huey, E.D., and Momeni, P. (2011). FTD and ALS: a tale of two diseases. Curr Alzheimer Res *8*, 273-294.

Finnie, N.J., Gottlieb, T.M., Blunt, T., Jeggo, P.A., and Jackson, S.P. (1995). DNA-dependent protein kinase activity is absent in xrs-6 cells: implications for site-specific recombination and DNA double-strand break repair. Proceedings of the National Academy of Sciences *92*, 320-324.

Foster, L.A., and Salajegheh, M.K. (2019). Motor Neuron Disease: Pathophysiology, Diagnosis, and Management. Am J Med *132*, 32-37.

Fujii, R., Okabe, S., Urushido, T., Inoue, K., Yoshimura, A., Tachibana, T., Nishikawa, T., Hicks, G.G., and Takumi, T. (2005). The RNA binding protein TLS is translocated to dendritic spines by mGluR5 activation and regulates spine morphology. Current biology : CB *15*, 587-593.

Fujii, R., and Takumi, T. (2005). TLS facilitates transport of mRNA encoding an actin-stabilizing protein to dendritic spines. Journal of Cell Science *118*, 5755-5765.

Fujioka, Y., Ishigaki, S., Masuda, A., Iguchi, Y., Udagawa, T., Watanabe, H., Katsuno, M., Ohno, K., and Sobue, G. (2013). FUS-regulated region- and cell-type-specific transcriptome is associated with cell selectivity in ALS/FTLD. Scientific reports *3*, 2388-2388.

Gami-Patel, P., Bandopadhyay, R., Brelstaff, J., Revesz, T., and Lashley, T. (2016). The presence of heterogeneous nuclear ribonucleoproteins in frontotemporal lobar degeneration with FUS-positive inclusions. Neurobiology of aging *46*, 192-203.

Gans, A. (1923). Zwei Fälle von Pickscher Atrophie des Stirnhirns. Zbl Neur *33*, 516.

Gao, C.-H. (2021). ggVennDiagram: A 'ggplot2' Implement of Venn Diagram (R package).

Gardiner, M., Toth, R., Vandermoere, F., Morrice, N.A., and Rouse, J. (2008). Identification and characterization of FUS/TLS as a new target of ATM. The Biochemical journal *415*, 297-307.

Garone, M.G., Alfano, V., Salvatori, B., Braccia, C., Peruzzi, G., Colantoni, A., Bozzoni, I., Armirotti, A., and Rosa, A. (2020). Proteomics analysis of FUS mutant human motoneurons reveals altered regulation of cytoskeleton and other ALS-linked proteins via 3'UTR binding. Scientific reports *10*, 11827-11828.

Gierlinski, M., Gastaldello, F., Cole, C., and Barton, G.J. (2018). Proteus: an R package for downstream analysis of MaxQuant output. bioRxiv.

Gittings, L.M., Foti, S.C., Benson, B.C., Gami-Patel, P., Isaacs, A.M., and Lashley, T. (2019). Heterogeneous nuclear ribonucleoproteins R and Q accumulate in pathological inclusions in FTLD-FUS. Acta Neuropathologica Communications *7*, 18-13.

Gong, J., Huang, M., Wang, F., Ma, X., Liu, H., Tu, Y., Xing, L., Zhu, X., Zheng, H., Fang, J.*, et al.* (2017). RBM45 competes with HDAC1 for binding to FUS in response to DNA damage. Nucleic acids research *45*, 12862-12876.

Goodier, J.L., Cheung, L.E., and Kazazian, H.H. (2012). MOV10 RNA helicase is a potent inhibitor of retrotransposition in cells. PLoS genetics *8*, e1002941.

Goodman, C.A., and Hornberger, T.A. (2013). Measuring protein synthesis with SUnSET: a valid alternative to traditional techniques? Exercise and sport sciences reviews *41*, 107-115.

Gordon, P.B., and Seglen, P.O. (1988). Prelysosomal convergence of autophagic and endocytic pathways. Biochemical and Biophysical Research Communications *151*, 40-47.

Gorno-Tempini, M.L., Dronkers, N.F., Rankin, K.P., Ogar, J.M., Phengrasamy, L., Rosen, H.J., Johnson, J.K., Weiner, M.W., and Miller, B.L. (2004). Cognition and anatomy in three variants of primary progressive aphasia. Ann Neurol *55*, 335-346.

Gowell, M., Baker, I., Ansorge, O., and Husain, M. (2021). Young-onset frontotemporal dementia with FUS pathology. Practical Neurology *21*, 149-152.

Greaves, C.V., and Rohrer, J.D. (2019). An update on genetic frontotemporal dementia. Journal of Neurology *266*, 2075-2086.

Groen, E.J., van Es, M.A., van Vught, P.W., Spliet, W.G., van Engelen-Lee, J., de Visser, M., Wokke, J.H., Schelhaas, H.J., Ophoff, R.A., Fumoto, K.*, et al.* (2010). FUS mutations in familial amyotrophic lateral sclerosis in the Netherlands. Arch Neurol *67*, 224-230.

Gromicho, M., Oliveira Santos, M., Pinto, A., Pronto-Laborinho, A., and De Carvalho, M. (2017). Young-onset rapidly progressive ALS associated with heterozygous FUS mutation. Amyotrophic Lateral Sclerosis and Frontotemporal Degeneration *18*, 451-453.

Grossman, A.B., Woolley-Levine, S., Bradley, W.G., and Miller, R.G. (2007). Detecting neurobehavioral changes in amyotrophic lateral sclerosis. Amyotroph Lateral Scler *8*, 56-61.

Güttinger, S., Mühlhäusser, P., Koller-Eichhorn, R., Brennecke, J., and Kutay, U. (2004). Transportin2 functions as importin and mediates nuclear import of HuR. Proceedings of the National Academy of Sciences *101*, 2918-2923.

Hallier, M., Lerga, A., Barnache, S., Tavitian, A., and Moreau-Gachelin, F. (1998). The transcription factor Spi-1/PU.1 interacts with the potential splicing factor TLS. The Journal of biological chemistry *273*, 4838-4842.

Hennig, S., Kong, G., Mannen, T., Sadowska, A., Kobelke, S., Blythe, A., Knott, G.J., Iyer, K.S., Ho, D., Newcombe, E.A.*, et al.* (2015). Prion-like domains in RNA binding proteins are essential for building subnuclear paraspeckles. The Journal of cell biology *210*, 529-539.

Hewitt, C., Kirby, J., Highley, J.R., Hartley, J.A., Hibberd, R., Hollinger, H.C., Williams, T.L., Ince, P.G., McDermott, C.J., and Shaw, P.J. (2010). Novel FUS/TLS

mutations and pathology in familial and sporadic amyotrophic lateral sclerosis. Arch Neurol *67*, 455-461.

Hicks, G.G., Singh, N., Nashabi, A., Mai, S., Bozek, G., Klewes, L., Arapovic, D., White, E.K., Koury, M.J., Oltz, E.M., *et al.* (2000). Fus deficiency in mice results in defective B-lymphocyte development and activation, high levels of chromosomal instability and perinatal death. Nature genetics *24*, 175-179.

Higelin, J., Demestre, M., Putz, S., Delling, J.P., Jacob, C., Lutz, A.-K., Bausinger, J., Huber, A.-K., Klingenstein, M., Barbi, G., *et al.* (2016). FUS Mislocalization and Vulnerability to DNA Damage in ALS Patients Derived hiPSCs and Aging Motoneurons. Frontiers in cellular neuroscience *10*, 290.

Ho, W.Y., Agrawal, I., Tyan, S.-H., Sanford, E., Chang, W.-T., Lim, K., Ong, J., Tan, B.S.Y., Moe, A.A.K., Yu, R., *et al.* (2021). Dysfunction in nonsense-mediated decay, protein homeostasis, mitochondrial function, and brain connectivity in ALS-FUS mice with cognitive deficits. Acta Neuropathologica Communications *9*, 9-24.

Hodge, R.D., Bakken, T.E., Miller, J.A., Smith, K.A., Barkan, E.R., Graybuck, L.T., Close, J.L., Long, B., Johansen, N., Penn, O., *et al.* (2019). Conserved cell types with divergent features in human versus mouse cortex. Nature *573*, 61-68.

Hodges, J.R., Davies, R., Xuereb, J., Kril, J., and Halliday, G. (2003). Survival in frontotemporal dementia. Neurology *61*, 349-354.

Hofweber, M., Hutten, S., Bourgeois, B., Spreitzer, E., Niedner-Boblenz, A., Schifferer, M., Ruepp, M.-D., Simons, M., Niessing, D., Madl, T., *et al.* (2018a). Phase Separation of FUS Is Suppressed by Its Nuclear Import Receptor and Arginine Methylation. Cell *173*, 706-719.e713.

Hofweber, M., Hutten, S., Bourgeois, B., Spreitzer, E., Niedner-Boblenz, A., Schifferer, M., Ruepp, M.D., Simons, M., Niessing, D., Madl, T.*, et al.* (2018b). Phase Separation of FUS Is Suppressed by Its Nuclear Import Receptor and Arginine Methylation. Cell *173*, 706-719.e713.

Hogan, D.B., Jette, N., Fiest, K.M., Roberts, J.I., Pearson, D., Smith, E.E., Roach, P., Kirk, A., Pringsheim, T., and Maxwell, C.J. (2016). The Prevalence and Incidence of Frontotemporal Dementia: a Systematic Review. The Canadian journal of neurological sciences Le journal canadien des sciences neurologiques *43 Suppl 1*, S96-S109.

Holler, C.J., Taylor, G., Deng, Q., and Kukar, T. (2017). Intracellular Proteolysis of Progranulin Generates Stable, Lysosomal Granulins that Are Haploinsufficient in Patients with Frontotemporal Dementia Caused by GRN Mutations. eNeuro *4*.

Huang, L., Lou, C.-H., Chan, W., Shum, E.Y., Shao, A., Stone, E., Karam, R., Song, H.-W., and Wilkinson, M.F. (2011). RNA homeostasis governed by cell type-specific and branched feedback loops acting on NMD. Molecular cell *43*, 950-961.

Hübers, A., Just, W., Rosenbohm, A., Müller, K., Marroquin, N., Goebel, I., Högel, J., Thiele, H., Altmüller, J., and Nürnberg, P. (2015). De novo FUS mutations are the most frequent genetic cause in early-onset German ALS patients. Neurobiology of aging *36*, 3117. e3111-3117. e3116.

Huey, E.D., Ferrari, R., Moreno, J.H., Jensen, C., Morris, C.M., Potocnik, F., Kalaria, R.N., Tierney, M., Wassermann, E.M., Hardy, J.*, et al.* (2012). FUS and TDP43 genetic variability in FTD and CBS. Neurobiol Aging *33*, 1016.e1019-1017.

Humphrey, J., Birsa, N., Milioto, C., McLaughlin, M., Ule, A.M., Robaldo, D., Eberle, A.B., Kräuchi, R., Bentham, M., Brown, A.-L.*, et al.* (2020). FUS ALS-causative

mutations impair FUS autoregulation and splicing factor networks through intron retention. Nucleic acids research *48*, 6889-6905.

Husi, H., Ward, M.A., Choudhary, J.S., Blackstock, W.P., and Grant, S.G.N. (2000). Proteomic analysis of NMDA receptor–adhesion protein signaling complexes. Nature Neuroscience *3*, 661-669.

Ishihara, H., Martin, B.L., Brautigan, D.L., Karaki, H., Ozaki, H., Kato, Y., Fusetani, N., Watabe, S., Hashimoto, K., and Uemura, D. (1989). Calyculin A and okadaic acid: inhibitors of protein phosphatase activity. Biochemical and Biophysical Research Communications *159*, 871-877.

Ishimura, R., Nagy, G., Dotu, I., Zhou, H., Yang, X.-L., Schimmel, P., Senju, S., Nishimura, Y., Chuang, J.H., and Ackerman, S.L. (2014). Ribosome stalling induced by mutation of a CNS-specific tRNA causes neurodegeneration. Science *345*, 455-459.

Jiang, H.-Y., Wek, S.A., McGrath, B.C., Lu, D., Hai, T., Harding, H.P., Wang, X., Ron, D., Cavener, D.R., and Wek, R.C. (2004). Activating Transcription Factor 3 Is Integral to the Eukaryotic Initiation Factor 2 Kinase Stress Response. Molecular and Cellular Biology *24*, 1365-1377.

Jiang, W., Estes, V.M., Wang, X.S., Shao, Z., Lee, B.J., Lin, X., Crowe, J.L., and Zha, S. (2019). Phosphorylation at S2053 in Murine (S2056 in Human) DNA-PKcs Is Dispensable for Lymphocyte Development and Class Switch Recombination. The Journal of Immunology *203*, 178-187.

Johnson, M.A., Deng, Q., Taylor, G., McEachin, Z.T., Chan, A.W.S., Root, J., Bassell, G.J., and Kukar, T. (2020). Divergent FUS phosphorylation in primate and mouse cells following double-strand DNA damage. Neurobiol Dis *146*, 105085.

Josephs, K.A., Holton, J.L., Rossor, M.N., Godbolt, A.K., Ozawa, T., Strand, K., Khan, N., Al-Sarraj, S., and Revesz, T. (2004). Frontotemporal lobar degeneration and ubiquitin immunohistochemistry. Neuropathol Appl Neurobiol *30*, 369-373.

Kaewsapsak, P., Shechner, D., Mallard, W., Rinn, J., and Ting, A.Y. (2017). Live-cell mapping of organelle-associated RNAs via proximity biotinylation combined with protein-RNA crosslinking. elife.

Kamelgarn, M., Chen, J., Kuang, L., Arenas, A., Zhai, J., Zhu, H., and Gal, J. (2016). Proteomic analysis of FUS interacting proteins provides insights into FUS function and its role in ALS. Biochimica et biophysica acta *1862*, 2004-2014.

Kamelgarn, M., Chen, J., Kuang, L., Jin, H., Kasarskis, E.J., and Zhu, H. (2018). ALS mutations of FUS suppress protein translation and disrupt the regulation of nonsense-mediated decay. Proceedings of the National Academy of Sciences of the United States of America *16*, 201810413.

Kansal, K., Mareddy, M., Sloane, K.L., Minc, A.A., Rabins, P.V., McGready, J.B., and Onyike, C.U. (2016). Survival in Frontotemporal Dementia Phenotypes: A Meta-Analysis. Dement Geriatr Cogn Disord *41*, 109-122.

Karaman, M.W., Herrgard, S., Treiber, D.K., Gallant, P., Atteridge, C.E., Campbell, B.T., Chan, K.W., Ciceri, P., Davis, M.I., Edeen, P.T., *et al.* (2008). A quantitative analysis of kinase inhibitor selectivity. Nature biotechnology *26*, 127-132.

Kassubek, J., Unrath A Fau - Huppertz, H.-J., Huppertz Hj Fau - Lulé, D., Lulé D Fau - Ethofer, T., Ethofer T Fau - Sperfeld, A.-D., Sperfeld Ad Fau - Ludolph, A.C., and Ludolph, A.C. (2005). Global brain atrophy and corticospinal tract alterations in ALS, as investigated by voxel-based morphometry of 3-D MRI.

Kato, M., Han, T.W., Xie, S., Shi, K., Du, X., Wu, L.C., Mirzaei, H., Goldsmith, E.J., Longgood, J., Pei, J.*, et al.* (2012). Cell-free Formation of RNA Granules: Low Complexity Sequence Domains Form Dynamic Fibers within Hydrogels. Cell *149*, 753-767.

Kato, S., Takikawa M Fau - Nakashima, K., Nakashima K Fau - Hirano, A., Hirano A Fau - Cleveland, D.W., Cleveland Dw Fau - Kusaka, H., Kusaka H Fau - Shibata, N., Shibata N Fau - Kato, M., Kato M Fau - Nakano, I., Nakano I Fau - Ohama, E., and Ohama, E. (2000). New consensus research on neuropathological aspects of familial amyotrophic lateral sclerosis with superoxide dismutase 1 (SOD1) gene mutations: inclusions containing SOD1 in neurons and astrocytes.

Kiernan, M.C., Vucic, S., Cheah, B.C., Turner, M.R., Eisen, A., Hardiman, O., Burrell, J.R., and Zoing, M.C. (2011). Amyotrophic lateral sclerosis. Lancet *377*, 942-955.

Kim, G., Gautier, O., Tassoni-Tsuchida, E., Ma, X.R., and Gitler, A.D. (2020). ALS Genetics: Gains, Losses, and Implications for Future Therapies. Neuron *108*, 822-842.

Kim, S.T., Lim, D.S., Canman, C.E., and Kastan, M.B. (1999). Substrate specificities and identification of putative substrates of ATM kinase family members. The Journal of biological chemistry *274*, 37538-37543.

Kim, Y.E., Oh, K.W., Kwon, M.J., Choi, W.J., Oh, S.I., Ki, C.S., and Kim, S.H. (2015). De novo FUS mutations in 2 Korean patients with sporadic amyotrophic lateral sclerosis. Neurobiol Aging *36*, 1604.e1617-1609.

Kırlı, K., Karaca, S., Dehne, H.J., Samwer, M., Pan, K.T., Lenz, C., Urlaub, H., and Görlich, D. (2015). A deep proteomics perspective on CRM1-mediated nuclear export and nucleocytoplasmic partitioning. eLife *4*, 1195.

Klionsky, D.J., Abdel-Aziz, A.K., Abdelfatah, S., Abdellatif, M., Abdoli, A., Abel, S., Abeliovich, H., Abildgaard, M.H., Abudu, Y.P., Acevedo-Arozena, A.*, et al.* (2021). Guidelines for the use and interpretation of assays for monitoring autophagy (4th edition)(1). Autophagy *17*, 1-382.

Knibb, J.A., Xuereb, J.H., Patterson, K., and Hodges, J.R. (2006). Clinical and pathological characterization of progressive aphasia. Ann Neurol *59*, 156-165.

Knight, J.D.R., Choi, H., Gupta, G.D., Pelletier, L., Raught, B., Nesvizhskii, A.I., and Gingras, A.-C. (2017). ProHits-viz: a suite of web tools for visualizing interaction proteomics data. Nature methods *14*, 645-646.

Knopman, D.S., and Roberts, R.O. (2011). Estimating the number of persons with frontotemporal lobar degeneration in the US population. Journal of molecular neuroscience : MN *45*, 330-335.

Knowles, T.P.J., Vendruscolo, M., and Dobson, C.M. (2014). The amyloid state and its association with protein misfolding diseases. Nature Reviews Molecular Cell Biology *15*, 384-396.

Kovalevich, J., and Langford, D. (2013). Considerations for the use of SH-SY5Y neuroblastoma cells in neurobiology. Methods in molecular biology (Clifton, NJ) *1078*, 9-21.

Kovar, H. (2011). Dr. Jekyll and Mr. Hyde: The Two Faces of the FUS/EWS/TAF15 Protein Family. Sarcoma *2011*, 837474.

Kril, J.J., and Halliday, G.M. (2011). Pathological staging of frontotemporal lobar degeneration. J Mol Neurosci *45*, 379-383.

Kuroda, M., Sok, J., Webb, L., Baechtold, H., Urano, F., Yin, Y., Chung, P., de Rooij, D.G., Akhmedov, A., Ashley, T.*, et al.* (2000). Male sterility and enhanced radiation sensitivity in TLS(-/-) mice. The EMBO journal *19*, 453-462.

Kurosaki, T., Popp, M.W., and Maquat, L.E. (2019). Quality and quantity control of gene expression by nonsense-mediated mRNA decay. Nature reviews Molecular cell biology *20*, 406-420.

Kwiatkowski, T.J., Bosco, D.A., Leclerc, A.L., Tamrazian, E., Vanderburg, C.R., Russ, C., Davis, A., Gilchrist, J., Kasarskis, E.J., Munsat, T.*, et al.* (2009). Mutations in the FUS/TLS gene on chromosome 16 cause familial amyotrophic lateral sclerosis. Science (New York, NY) *323*, 1205-1208.

Kwon, I., Kato, M., Xiang, S., Wu, L., Theodoropoulos, P., Mirzaei, H., Han, T., Xie, S., Corden, J.L., and McKnight, S.L. (2013). Phosphorylation-Regulated Binding of RNA Polymerase II to Fibrous Polymers of Low-Complexity Domains. Cell *155*, 1049-1060.

Kwon, M.J., Baek, W., Ki, C.S., Kim, H.Y., Koh, S.H., Kim, J.W., and Kim, S.H. (2012). Screening of the SOD1, FUS, TARDBP, ANG, and OPTN mutations in Korean patients with familial and sporadic ALS. Neurobiol Aging *33*, 1017.e1017-1023.

Lagier-Tourenne, C., Polymenidou, M., and Cleveland, D.W. (2010). TDP-43 and FUS/TLS: emerging roles in RNA processing and neurodegeneration. Human molecular genetics *19*, R46-R64.

Lagier-Tourenne, C., Polymenidou, M., Hutt, K.R., Vu, A.Q., Baughn, M., Huelga, S.C., Clutario, K.M., Ling, S.-C., Liang, T.Y., Mazur, C.*, et al.* (2012). Divergent roles of

ALS-linked proteins FUS/TLS and TDP-43 intersect in processing long pre-mRNAs. Nature neuroscience *15*, 1488-1497.

Lai, S.L., Abramzon, Y., Schymick, J.C., Stephan, D.A., Dunckley, T., Dillman, A., Cookson, M., Calvo, A., Battistini, S., Giannini, F.*, et al.* (2011). FUS mutations in sporadic amyotrophic lateral sclerosis. Neurobiol Aging *32*, 550.e551-554.

Lam, S.S., Martell, J.D., Kamer, K.J., Deerinck, T.J., Ellisman, M.H., Mootha, V.K., and Ting, A.Y. (2015). Directed evolution of APEX2 for electron microscopy and proximity labeling. Nature methods *12*, 51-54.

Lattante, S., Conte, A., Zollino, M., Luigetti, M., Del Grande, A., Marangi, G., Romano, A., Marcaccio, A., Meleo, E., Bisogni, G.*, et al.* (2012). Contribution of major amyotrophic lateral sclerosis genes to the etiology of sporadic disease. Neurology *79*, 66-72.

Lavysh, D., and Neu-Yilik, G. (2020). UPF1-Mediated RNA Decay-Danse Macabre in a Cloud. Biomolecules *10*, 999.

Lee, S.E., Seeley, W.W., Poorzand, P., Rademakers, R., Karydas, A., Stanley, C.M., Miller, B.L., and Rankin, K.P. (2012). Clinical characterization of bvFTD due to FUS neuropathology. Neurocase *18*, 305-317.

Lees-Miller, S.P., Sakaguchi, K., Ullrich, S.J., Appella, E., and Anderson, C.W. (1992). Human DNA-activated protein kinase phosphorylates serines 15 and 37 in the amino-terminal transactivation domain of human p53. Molecular and Cellular Biology *12*, 5041-5049.

Leighton, D.J., Newton, J., Stephenson, L.J., Colville, S., Davenport, R., Gorrie, G., Morrison, I., Swingler, R., Chandran, S., and Pal, S. (2019). Changing epidemiology of motor neurone disease in Scotland. J Neurol *266*, 817-825.

Lendahl, U., and McKay, R.D. (1990). The use of cell lines in neurobiology. Trends in neurosciences *13*, 132-137.

Lenzi, J., De Santis, R., de Turris, V., Morlando, M., Laneve, P., Calvo, A., Caliendo, V., Chiò, A., Rosa, A., and Bozzoni, I. (2015). ALS mutant FUS proteins are recruited into stress granules in induced pluripotent stem cell-derived motoneurons. Disease models & mechanisms *8*, 755-766.

Lerga, A., Hallier, M., Delva, L., Orvain, C., Gallais, I., Marie, J., and Moreau-Gachelin, F. (2001). Identification of an RNA Binding Specificity for the Potential Splicing Factor TLS*. Journal of Biological Chemistry *276*, 6807-6816.

Levone, B.R., Lenzken, S.C., Antonaci, M., Maiser, A., Rapp, A., Conte, F., Reber, S., Mechtersheimer, J., Ronchi, A.E., Mühlemann, O.*, et al.* (2021). FUS-dependent liquid–liquid phase separation is important for DNA repair initiation. Journal of Cell Biology *220*.

Li, K.W., Ganz, A.B., and Smit, A.B. (2019). Proteomics of neurodegenerative diseases: analysis of human post-mortem brain. Journal of Neurochemistry *151*, 435-445.

Lillo, P., Garcin, B., Hornberger, M., Bak, T.H., and Hodges, J.R. (2010). Neurobehavioral Features in Frontotemporal Dementia With Amyotrophic Lateral Sclerosis. Archives of Neurology *67*, 826-830.

Lin, S., Lin, Y., Nery, J.R., Urich, M.A., Breschi, A., Davis, C.A., Dobin, A., Zaleski, C., Beer, M.A., Chapman, W.C.*, et al.* (2014a). Comparison of the transcriptional landscapes between human and mouse tissues. Proceedings of the National Academy of Sciences *111*, 17224-17229.

Lin, Y.-C., Boone, M., Meuris, L., Lemmens, I., Van Roy, N., Soete, A., Reumers, J., Moisse, M., Plaisance, S., Drmanac, R.*, et al.* (2014b). Genome dynamics of the human embryonic kidney 293 lineage in response to cell biology manipulations. Nature communications *5*, 4767.

Ling, S.-C., Polymenidou, M., and Cleveland, D.W. (2013). Converging mechanisms in ALS and FTD: disrupted RNA and protein homeostasis. Neuron *79*, 416-438.

Liu, X., Niu, C., Ren, J., Zhang, J., Xie, X., Zhu, H., Feng, W., and Gong, W. (2013). The RRM domain of human fused in sarcoma protein reveals a non-canonical nucleic acid binding site. Biochimica et Biophysica Acta (BBA) - Molecular Basis of Disease *1832*, 375-385.

Lo Bello, M., Di Fini, F., Notaro, A., Spataro, R., Conforti, F.L., and La Bella, V. (2017). ALS-Related Mutant FUS Protein Is Mislocalized to Cytoplasm and Is Recruited into Stress Granules of Fibroblasts from Asymptomatic FUS P525L Mutation Carriers. Neuro-degenerative diseases *17*, 292-303.

Lomen-Hoerth, C., Murphy, J., Langmore, S., Kramer, J.H., Olney, R.K., and Miller, B. (2003). Are amyotrophic lateral sclerosis patients cognitively normal? Neurology *60*, 1094-1097.

Long, Z., Irish, M., Foxe, D., Hodges, J.R., Piguet, O., and Burrell, J.R. (2021). Heterogeneity of behavioural and language deficits in FTD–MND. Journal of Neurology.

Longatti, A., Orsi, A., and Tooze, S.A. (2010). Autophagosome formation: not necessarily an inside job. Cell research *20*, 1181-1184.

Longinetti, E., neurology, F.F.C.o.i., and 2019 (2019). Epidemiology of amyotrophic lateral sclerosis: an update of recent literature. ncbinlmnihgov *32*, 771-776.

López-Erauskin, J., Tadokoro, T., Baughn, M.W., Myers, B., McAlonis-Downes, M., Chillon-Marinas, C., Asiaban, J.N., Artates, J., Bui, A.T., Vetto, A.P.*, et al.* (2018). ALS/FTD-Linked Mutation in FUS Suppresses Intra-axonal Protein Synthesis and Drives Disease Without Nuclear Loss-of-Function of FUS. Neuron *100*, 816-830.e817.

Loughlin, F.E., Lukavsky, P.J., Kazeeva, T., Reber, S., Hock, E.M., Colombo, M., Von Schroetter, C., Pauli, P., Cléry, A., Mühlemann, O.*, et al.* (2019). The Solution Structure of FUS Bound to RNA Reveals a Bipartite Mode of RNA Recognition with Both Sequence and Shape Specificity. Mol Cell *73*, 490-504.e496.

Luo, F., Gui, X., Zhou, H., Gu, J., Li, Y., Liu, X., Zhao, M., Li, D., Li, X., and Liu, C. (2018). Atomic structures of FUS LC domain segments reveal bases for reversible amyloid fibril formation. Nat Struct Mol Biol *25*, 341-346.

Mackenzie, I.R., Foti, D., Woulfe, J., and Hurwitz, T.A. (2008). Atypical frontotemporal lobar degeneration with ubiquitin-positive, TDP-43-negative neuronal inclusions. Brain *131*, 1282-1293.

Mackenzie, I.R., Munoz, D.G., Kusaka, H., Yokota, O., Ishihara, K., Roeber, S., Kretzschmar, H.A., Cairns, N.J., and Neumann, M. (2011). Distinct pathological subtypes of FTLD-FUS. Acta Neuropathol *121*, 207-218.

Mackenzie, I.R.A., and Neumann, M. (2017). Fused in Sarcoma Neuropathology in Neurodegenerative Disease. Cold Spring Harbor perspectives in medicine, a024299.

Mackenzie, I.R.A., Neumann, M., Bigio, E.H., Cairns, N.J., Alafuzoff, I., Kril, J., Kovacs, G.G., Ghetti, B., Halliday, G., Holm, I.E.*, et al.* (2009). Nomenclature for neuropathologic subtypes of frontotemporal lobar degeneration: consensus recommendations. Acta neuropathologica *117*, 15-18.

Mackenzie, I.R.A., Neumann, M., Bigio, E.H., Cairns, N.J., Alafuzoff, I., Kril, J., Kovacs, G.G., Ghetti, B., Halliday, G., Holm, I.E.*, et al.* (2010). Nomenclature and nosology for neuropathologic subtypes of frontotemporal lobar degeneration: an update. Acta neuropathologica *119*, 1-4.

MacRae, S.L., Croken, M.M., Calder, R.B., Aliper, A., Milholland, B., White, R.R., Zhavoronkov, A., Gladyshev, V.N., Seluanov, A., Gorbunova, V.*, et al.* (2015). DNA repair in species with extreme lifespan differences. Aging *7*, 1171-1184.

Magnussen, M.J., and Glass, J.D. (2017). Chapter 2 - Natural History of Amyotrophic Lateral Sclerosis. In Molecular and Cellular Therapies for Motor Neuron Diseases, N. Boulis, D. O'Connor, and A. Donsante, eds. (Academic Press), pp. 25-41.

Maharana, S., Wang, J., Papadopoulos, D.K., Richter, D., Pozniakovsky, A., Poser, I., Bickle, M., Rizk, S., Guillén-Boixet, J., Franzmann, T.M.*, et al.* (2018). RNA buffers the phase separation behavior of prion-like RNA binding proteins. Science *360*, 918-921.

Mahboubi, H., Seganathy, E., Kong, D., and Stochaj, U. (2013). Identification of Novel Stress Granule Components That Are Involved in Nuclear Transport. PloS one *8*, e68356.

Mann, D.M.A., and Snowden, J.S. (2017). Frontotemporal lobar degeneration: Pathogenesis, pathology and pathways to phenotype. Brain pathology (Zurich, Switzerland) *27*, 723-736.

Marin, B., Boumédiene, F., Logroscino, G., Couratier, P., Babron, M.C., Leutenegger, A.L., Copetti, M., Preux, P.M., and Beghi, E. (2017). Variation in worldwide incidence of amyotrophic lateral sclerosis: a meta-analysis. Int J Epidemiol *46*, 57-74.

Markmiller, S., Soltanieh, S., Server, K.L., Mak, R., Jin, W., Fang, M.Y., Luo, E.-C., Krach, F., Yang, D., Sen, A.*, et al.* (2018). Context-Dependent and Disease-Specific Diversity in Protein Interactions within Stress Granules. Cell *172*, 590-604.e513.

Marrone, L., Drexler, H.C.A., Wang, J., Tripathi, P., Distler, T., Heisterkamp, P., Anderson, E.N., Kour, S., Moraiti, A., Maharana, S.*, et al.* (2019). FUS pathology in ALS is linked to alterations in multiple ALS-associated proteins and rescued by drugs stimulating autophagy. Acta neuropathologica *138*, 67-84.

Martin, D., Thompson, M.A., and Nadler, J.V. (1993). The neuroprotective agent riluzole inhibits release of glutamate and aspartate from slices of hippocampal area CA1. Eur J Pharmacol *250*, 473-476.

Martin, L.J., and Chang, Q. (2018). DNA Damage Response and Repair, DNA Methylation, and Cell Death in Human Neurons and Experimental Animal Neurons Are Different. Journal of neuropathology and experimental neurology *77*, 636-655.

Mastrocola, A.S., Kim, S.H., Trinh, A.T., Rodenkirch, L.A., and Tibbetts, R.S. (2013). The RNA-binding Protein Fused in Sarcoma (FUS) Functions Downstream of Poly(ADP-ribose) Polymerase (PARP) in Response to DNA Damage. The Journal of biological chemistry *288*, 24731-24741.

Matsumoto, T., Matsukawa, K., Watanabe, N., Kishino, Y., Kunugi, H., Ihara, R., Wakabayashi, T., Hashimoto, T., and Iwatsubo, T. (2018). Self-assembly of FUS through its low-complexity domain contributes to neurodegeneration. Human Molecular Genetics *27*, 1353-1365.

McCombe, P.A., and Henderson, R.D. (2010). Effects of gender in amyotrophic lateral sclerosis. Gend Med *7*, 557-570.

Meissner, M., Lopato, S., Gotzmann, J., Sauermann, G., and Barta, A. (2003). Proto-oncoprotein TLS/FUS is associated to the nuclear matrix and complexed with splicing factors PTB, SRm160, and SR proteins. Exp Cell Res *283*, 184-195.

Mejzini, R., Flynn, L.L., Pitout, I.L., Fletcher, S., Wilton, S.D., and Akkari, P.A. (2019). ALS Genetics, Mechanisms, and Therapeutics: Where Are We Now? Frontiers in neuroscience *13*, 1310.

Mendell, J.T., Sharifi, N.A., Meyers, J.L., Martinez-Murillo, F., and Dietz, H.C. (2004). Nonsense surveillance regulates expression of diverse classes of mammalian transcripts and mutes genomic noise. Nature genetics *36*, 1073-1078.

Mercy, L., Hodges, J.R., Dawson, K., Barker, R.A., and Brayne, C. (2008). Incidence of early-onset dementias in Cambridgeshire, United Kingdom. Neurology *71*, 1496-1499.

Merkle, D., Douglas, P., Moorhead, G.B.G., Leonenko, Z., Yu, Y., Cramb, D., Bazett-Jones, D.P., and Lees-Miller, S.P. (2002). The DNA-dependent protein kinase interacts with DNA to form a protein-DNA complex that is disrupted by phosphorylation. Biochemistry *41*, 12706-12714.

Millecamps, S., Salachas, F., Cazeneuve, C., Gordon, P., Bricka, B., Camuzat, A., Guillot-Noël, L., Russaouen, O., Bruneteau, G., Pradat, P.F.*, et al.* (2010). SOD1, ANG, VAPB, TARDBP, and FUS mutations in familial amyotrophic lateral sclerosis: genotype-phenotype correlations. J Med Genet *47*, 554-560.

Miller, R.G., Mitchell, J.D., and Moore, D.H. (2012). Riluzole for amyotrophic lateral sclerosis (ALS)/motor neuron disease (MND). Cochrane Database Syst Rev *2012*, Cd001447.

Mioshi, E., Hsieh, S., Savage, S., Hornberger, M., and Hodges, J.R. (2010). Clinical staging and disease progression in frontotemporal dementia. Neurology *74*, 1591-1597.

Mitchell, J.C., McGoldrick, P., Vance, C., Hortobagyi, T., Sreedharan, J., Rogelj, B., Tudor, E.L., Smith, B.N., Klasen, C., Miller, C.C.J.*, et al.* (2012). Overexpression of human wild-type FUS causes progressive motor neuron degeneration in an age- and dose-dependent fashion. Acta neuropathologica *125*, 273-288.

Mochizuki, Y., Isozaki, E., Takao, M., Hashimoto, T., Shibuya, M., Arai, M., Hosokawa, M., Kawata, A., Oyanagi, K., Mihara, B.*, et al.* (2012). Familial ALS with FUS P525L mutation: two Japanese sisters with multiple systems involvement. J Neurol Sci *323*, 85-92.

Molliex, A., Temirov, J., Lee, J., Coughlin, M., Kanagaraj, A.P., Kim, H.J., Mittag, T., and Taylor, J.P. (2015). Phase Separation by Low Complexity Domains Promotes Stress Granule Assembly and Drives Pathological Fibrillization. Cell *163*, 123-133.

Monahan, Z., Ryan, V.H., Janke, A.M., Burke, K.A., Rhoads, S.N., Zerze, G.H., O'Meally, R., Dignon, G.L., Conicella, A.E., Zheng, W.*, et al.* (2017). Phosphorylation of the FUS low-complexity domain disrupts phase separation, aggregation, and toxicity. The EMBO journal, e201696394.

Moore, K.M., Nicholas, J., Grossman, M., McMillan, C.T., Irwin, D.J., Massimo, L., Van Deerlin, V.M., Warren, J.D., Fox, N.C., Rossor, M.N.*, et al.* (2020). Age at symptom onset and death and disease duration in genetic frontotemporal dementia: an international retrospective cohort study. Lancet Neurol *19*, 145-156.

Munoz, D.G., Neumann, M., Kusaka, H., Acta, O.Y., and 2009 (2009). FUS pathology in basophilic inclusion body disease. Springer *118*, 617-627.

Murakami, T., Qamar, S., Lin, J.Q., Schierle, G.S.K., Rees, E., Miyashita, A., Costa, A.R., Dodd, R.B., Chan, F.T.S., Michel, C.H., *et al.* (2015). ALS/FTD Mutation-Induced Phase Transition of FUS Liquid Droplets and Reversible Hydrogels into Irreversible Hydrogels Impairs RNP Granule Function. Neuron *88*, 678-690.

Murray, D.T., Kato, M., Lin, Y., Thurber, K.R., Hung, I., McKnight, S.L., and Tycko, R. (2017). Structure of FUS Protein Fibrils and Its Relevance to Self-Assembly and Phase Separation of Low-Complexity Domains. Cell.

Muster, B., Rapp, A., and Cardoso, M.C. (2017). Systematic analysis of DNA damage induction and DNA repair pathway activation by continuous wave visible light laser micro-irradiation. AIMS Genet *4*, 47-68.

Nagayama, S., Minato-Hashiba, N., Nakata, M., Kaito, M., Nakanishi, M., Tanaka, K., Arai, M., Akiyama, H., and Matsui, M. (2012). Novel FUS mutation in patients with sporadic amyotrophic lateral sclerosis and corticobasal degeneration. J Clin Neurosci *19*, 1738-1739.

Naumann, M., Pal, A., Goswami, A., Lojewski, X., Japtok, J., Vehlow, A., Naujock, M., Günther, R., Jin, M., Stanslowsky, N., *et al.* (2018). Impaired DNA damage response signaling by FUS-NLS mutations leads to neurodegeneration and FUS aggregate formation. Nature communications *9*, 1208.

Neary, D., Snowden, J.S., and Mann, D.M. (2000). Cognitive change in motor neurone disease/amyotrophic lateral sclerosis (MND/ALS). J Neurol Sci *180*, 15-20.

Neumann, M., Bentmann, E., Dormann, D., Jawaid, A., DeJesus-Hernandez, M., Ansorge, O., Roeber, S., Kretzschmar, H.A., Munoz, D.G., Kusaka, H., *et al.* (2011). FET proteins TAF15 and EWS are selective markers that distinguish FTLD with FUS

pathology from amyotrophic lateral sclerosis with FUS mutations. Brain : a journal of neurology *134*, 2595-2609.

Neumann, M., Kwong, L.K., Truax, A.C., Vanmassenhove, B., Kretzschmar, H.A., Van Deerlin, V.M., Clark, C.M., Grossman, M., Miller, B.L., Trojanowski, J.Q.*, et al.* (2007). TDP-43-positive white matter pathology in frontotemporal lobar degeneration with ubiquitin-positive inclusions. Journal of neuropathology and experimental neurology *66*, 177-183.

Neumann, M., and Mackenzie, I.R.A. (2019). Review: Neuropathology of non-tau frontotemporal lobar degeneration. Neuropathol Appl Neurobiol *45*, 19-40.

Neumann, M., Rademakers, R., Roeber, S., Baker, M., Kretzschmar, H.A., and Mackenzie, I.R.A. (2009a). A new subtype of frontotemporal lobar degeneration with FUS pathology. Brain : a journal of neurology *132*, 2922-2931.

Neumann, M., Roeber, S., Kretzschmar, H.A., Rademakers, R., Baker, M., and Mackenzie, I.R.A. (2009b). Abundant FUS-immunoreactive pathology in neuronal intermediate filament inclusion disease. Acta neuropathologica *118*, 605-616.

Neumann, M., Sampathu, D.M., Kwong, L.K., Truax, A.C., Micsenyi, M.C., Chou, T.T., Bruce, J., Schuck, T., Grossman, M., Clark, C.M.*, et al.* (2006). Ubiquitinated TDP-43 in frontotemporal lobar degeneration and amyotrophic lateral sclerosis. Science *314*, 130-133.

Neumann, M., Valori, C.F., Ansorge, O., Kretzschmar, H.A., Munoz, D.G., Kusaka, H., Yokota, O., Ishihara, K., Ang, L.C., Bilbao, J.M.*, et al.* (2012). Transportin 1 accumulates specifically with FET proteins but no other transportin cargos in FTLD-FUS and is absent in FUS inclusions in ALS with FUS mutations. Acta Neuropathol *124*, 705-716.

Niu, C., Zhang, J., Gao, F., Yang, L., Jia, M., Zhu, H., and Gong, W. (2012). FUS-NLS/Transportin 1 complex structure provides insights into the nuclear targeting mechanism of FUS and the implications in ALS. PloS one *7*, e47056.

Nolan, M., Talbot, K., and Ansorge, O. (2016). Pathogenesis of FUS-associated ALS and FTD: insights from rodent models. Acta Neuropathol Commun *4*, 99.

O'Connor, C.M., Landin-Romero, R., Clemson, L., Kaizik, C., Daveson, N., Hodges, J.R., Hsieh, S., Piguet, O., and Mioshi, E. (2017). Behavioral-variant frontotemporal dementia: Distinct phenotypes with unique functional profiles. Neurology *89*, 570-577.

Odom, D.T., Dowell, R.D., Jacobsen, E.S., Gordon, W., Danford, T.W., MacIsaac, K.D., Rolfe, P.A., Conboy, C.M., Gifford, D.K., and Fraenkel, E. (2007). Tissue-specific transcriptional regulation has diverged significantly between human and mouse. Nature genetics *39*, 730-732.

Okayasu, R., Suetomi, K., Yu, Y., Silver, A., Bedford, J.S., Cox, R., and Ullrich, R.L. (2000). A deficiency in DNA repair and DNA-PKcs expression in the radiosensitive BALB/c mouse. Cancer research *60*, 4342-4345.

Olney, N.T., Spina, S., and Miller, B.L. (2017). Frontotemporal Dementia. Neurologic clinics *35*, 339-374.

Olszewska, D.A., Lonergan, R., Fallon, E.M., and Lynch, T. (2016). Genetics of Frontotemporal Dementia. Curr Neurol Neurosci Rep *16*, 107.

Onyike, C.U., and Diehl-Schmid, J. (2013). The epidemiology of frontotemporal dementia. Int Rev Psychiatry *25*, 130-137.

Orhon, I., and Reggiori, F. (2017). Assays to Monitor Autophagy Progression in Cell Cultures. Cells *6*, 20.

Ortega, J.A., Daley, E.L., Kour, S., Samani, M., Tellez, L., Smith, H.S., Hall, E.A., Esengul, Y.T., Tsai, Y.-H., Gendron, T.F.*, et al.* (2020). Nucleocytoplasmic Proteomic Analysis Uncovers eRF1 and Nonsense-Mediated Decay as Modifiers of ALS/FTD C9orf72 Toxicity. Neuron *106*, 90-107.e113.

Owen, I., Rhoads, S., Yee, D., Wyne, H., Gery, K., Hannula, I., Sundrum, M., and Shewmaker, F. (2020). The prion-like domain of Fused in Sarcoma is phosphorylated by multiple kinases affecting liquid- and solid-phase transitions. Mol Biol Cell *31*, 2522-2536.

Ozdilek, B.A., Thompson, V.F., Ahmed, N.S., White, C.I., Batey, R.T., and Schwartz, J.C. (2017). Intrinsically disordered RGG/RG domains mediate degenerate specificity in RNA binding. Nucleic Acids Research *45*, 7984-7996.

Patel, A., Lee, H.O., Jawerth, L., Maharana, S., Jahnel, M., Hein, M.Y., Stoynov, S., Mahamid, J., Saha, S., Franzmann, T.M.*, et al.* (2015). A Liquid-to-Solid Phase Transition of the ALS Protein FUS Accelerated by Disease Mutation. Cell *162*, 1066-1077.

Perrin, S. (2014). Preclinical research: Make mouse studies work. Nature *507*, 423-425.

Perrotti, D., Bonatti, S., Trotta, R., Martinez, R., Skorski, T., Salomoni, P., Grassilli, E., Lozzo, R.V., Cooper, D.R., and Calabretta, B. (1998). TLS/FUS, a pro-oncogene involved in multiple chromosomal translocations, is a novel regulator of BCR/ABL-mediated leukemogenesis. The EMBO journal *17*, 4442-4455.

Perrotti, D., Iervolino, A., Cesi, V., Cirinná, M., Lombardini, S., Grassilli, E., Bonatti, S., Claudio, P.P., and Calabretta, B. (2000). BCR-ABL Prevents c-Jun-Mediated

and Proteasome-Dependent FUS (TLS) Proteolysis through a Protein Kinase CβII-Dependent Pathway. Molecular and Cellular Biology *20*, 6159-6169.

Pick, A. (1892). Uber die Beziehungen der senilen Hirnatrophie zur Aphasie. Prag Med Wochenschr *17*, 165-167.

Podhorecka, M., Skladanowski, A., and Bozko, P. (2010). H2AX Phosphorylation: Its Role in DNA Damage Response and Cancer Therapy. Journal of nucleic acids *2010*.

Pokhilko, A., Brezzo, G., Handunnetthi, L., Heilig, R., Lennon, R., Smith, C., Allan, S.M., Granata, A., Sinha, S., Wang, T.*, et al.* (2021). Global proteomic analysis of extracellular matrix in mouse and human brain highlights relevance to cerebrovascular disease. J Cereb Blood Flow Metab, 271678x211004307.

Powers, C.A., Mathur, M., Raaka, B.M., Ron, D., and Samuels, H.H. (1998). TLS (translocated-in-liposarcoma) is a high-affinity interactor for steroid, thyroid hormone, and retinoid receptors. Molecular endocrinology (Baltimore, Md) *12*, 4-18.

Prasad, D.D., Ouchida, M., Lee, L., Rao, V.N., and Reddy, E.S. (1994). TLS/FUS fusion domain of TLS/FUS-erg chimeric protein resulting from the t(16;21) chromosomal translocation in human myeloid leukemia functions as a transcriptional activation domain. Oncogene *9*, 3717-3729.

Qamar, S., Wang, G., Randle, S.J., Ruggeri, F.S., Varela, J.A., Lin, J.Q., Phillips, E.C., Miyashita, A., Williams, D., Ströhl, F.*, et al.* (2018). FUS Phase Separation Is Modulated by a Molecular Chaperone and Methylation of Arginine Cation-π Interactions. Cell *173*, 720-734.e715.

Qiu, H., Lee, S., Shang, Y., Wang, W.-Y., Au, K.F., Kamiya, S., Barmada, S.J., Finkbeiner, S., Lui, H., Carlton, C.E.*, et al.* (2014). ALS-associated mutation FUS-R521C

causes DNA damage and RNA splicing defects. The Journal of clinical investigation *124*, 981-999.

Rabbitts, T.H., Forster, A., Larson, R., and Nathan, P. (1993). Fusion of the dominant negative transcription regulator CHOP with a novel gene FUS by translocation t(12;16) in malignant liposarcoma. Nature genetics *4*, 175-180.

Radcliffe, C., and Clarke, J.L. (1862). An important case of paralysis and muscular atrophy, with disease of the nervous centres. The British and foreign medico-chirurgical review *30*, 215.

Rademakers, R., Stewart, H., Dejesus-Hernandez, M., Krieger, C., Graff-Radford, N., Fabros, M., Briemberg, H., Cashman, N., Eisen, A., and Mackenzie, I.R. (2010). Fus gene mutations in familial and sporadic amyotrophic lateral sclerosis. Muscle Nerve *42*, 170-176.

Rambaran, R.N., and Serpell, L.C. (2008). Amyloid fibrils: abnormal protein assembly. Prion *2*, 112-117.

Ratnavalli, E., Brayne, C., Dawson, K., and Hodges, J.R. (2002). The prevalence of frontotemporal dementia. Neurology *58*, 1615-1621.

Ravenscroft, T.A., Baker, M.C., Rutherford, N.J., Neumann, M., Mackenzie, I.R., Josephs, K.A., Boeve, B.F., Petersen, R., Halliday, G.M., Kril, J.*, et al.* (2013). Mutations in protein N-arginine methyltransferases are not the cause of FTLD-FUS. Neurobiology of aging *34*, 2235.e2211-2233.

Ravikumar, B., Moreau, K., Jahreiss, L., Puri, C., and Rubinsztein, D.C. (2010). Plasma membrane contributes to the formation of pre-autophagosomal structures. Nature cell biology *12*, 747-757.

Reber, S., Jutzi, D., Lindsay, H., Devoy, A., Mechtersheimer, J., Levone, B.R., Domanski, M., Bentmann, E., Dormann, D., Mühlemann, O.*, et al.* (2021). The phase separation-dependent FUS interactome reveals nuclear and cytoplasmic function of liquid–liquid phase separation. Nucleic Acids Research *49*, 7713-7731.

Reber, S., Stettler, J., Filosa, G., Colombo, M., Jutzi, D., Lenzken, S.C., Schweingruber, C., Bruggmann, R., Bachi, A., Barabino, S.M.*, et al.* (2016). Minor intron splicing is regulated by FUS and affected by ALS-associated FUS mutants. The EMBO journal *35*, 1504-1521.

Renton, A.E., Chiò, A., and Traynor, B.J. (2014). State of play in amyotrophic lateral sclerosis genetics. Nature neuroscience *17*, 17-23.

Renton, A.E., Majounie, E., Waite, A., Simon-Sanchez, J., Rollinson, S., Gibbs, J.R., Schymick, J.C., Laaksovirta, H., van Swieten, J.C., Myllykangas, L.*, et al.* (2011). A hexanucleotide repeat expansion in C9ORF72 is the cause of chromosome 9p21-linked ALS-FTD. Neuron *72*, 257-268.

Revet, I., Feeney, L., Bruguera, S., Wilson, W., Dong, T.K., Oh, D.H., Dankort, D., and Cleaver, J.E. (2011). Functional relevance of the histone gammaH2Ax in the response to DNA damaging agents. Proceedings of the National Academy of Sciences of the United States of America *108*, 8663-8667.

Rhoads, S.N., Monahan, Z.T., Yee, D.S., Leung, A.Y., Newcombe, C.G., O'Meally, R.N., Cole, R.N., and Shewmaker, F.P. (2018a). The prionlike domain of FUS is multiphosphorylated following DNA damage without altering nuclear localization. Molecular biology of the cell *29*, 1786-1797.

Rhoads, S.N., Monahan, Z.T., Yee, D.S., and Shewmaker, F.P. (2018b). The Role of Post-Translational Modifications on Prion-Like Aggregation and Liquid-Phase Separation of FUS. International journal of molecular sciences *19*.

Ringholz, G.M., Appel, S.H., Bradshaw, M., Cooke, N.A., Mosnik, D.M., and Schulz, P.E. (2005). Prevalence and patterns of cognitive impairment in sporadic ALS. Neurology *65*, 586-590.

Ritchie, M.E., Phipson, B., Wu, D., Hu, Y., Law, C.W., Shi, W., and Smyth, G.K. (2015). limma powers differential expression analyses for RNA-sequencing and microarray studies. Nucleic Acids Res *43*, e47.

Robertson, J., Bilbao, J., Zinman, L., Hazrati, L.N., Tokuhiro, S., Sato, C., Moreno, D., Strome, R., Mackenzie, I.R., and Rogaeva, E. (2011). A novel double mutation in FUS gene causing sporadic ALS. Neurobiol Aging *32*, 553.e527-530.

Roch, B., Abramowski, V., Chaumeil, J., and de Villartay, J.-P. (2019). Cernunnos/Xlf Deficiency Results in Suboptimal V(D)J Recombination and Impaired Lymphoid Development in Mice. Frontiers in immunology *10*, 443.

Rohini, M., Haritha Menon, A., and Selvamurugan, N. (2018). Role of activating transcription factor 3 and its interacting proteins under physiological and pathological conditions. Int J Biol Macromol *120*, 310-317.

Rohrer, J.D. (2012). Structural brain imaging in frontotemporal dementia. Biochimica et Biophysica Acta (BBA) - Molecular Basis of Disease *1822*, 325-332.

Rohrer, J.D., Guerreiro, R., Vandrovcova, J., Uphill, J., Reiman, D., Beck, J., Isaacs, A.M., Authier, A., Ferrari, R., Fox, N.C., *et al.* (2009a). The heritability and genetics of frontotemporal lobar degeneration. Neurology *73*, 1451-1456.

Rohrer, J.D., Guerreiro, R., Vandrovcova, J., Uphill, J., Reiman, D., Beck, J., Isaacs, A.M., Authier, A., Ferrari, R., Fox, N.C., *et al.* (2009b). The heritability and genetics of frontotemporal lobar degeneration. Neurology *73*, 1451-1456.

Root, J., Merino, P., Nuckols, A., Johnson, M., and Kukar, T. (2021). Lysosome dysfunction as a cause of neurodegenerative diseases: Lessons from frontotemporal dementia and amyotrophic lateral sclerosis. Neurobiology of disease *154*, 105360.

Rosen, D.R., Siddique, T., Patterson, D., Figlewicz, D.A., Sapp, P., Hentati, A., Donaldson, D., Goto, J., O'Regan, J.P., and Deng, H.-X. (1993). Mutations in Cu/Zn superoxide dismutase gene are associated with familial amyotrophic lateral sclerosis. Nature *362*, 59-62.

Rulten, S.L., Rotheray, A., Green, R.L., Grundy, G.J., Moore, D.A., Gomez-Herreros, F., Hafezparast, M., and Caldecott, K.W. (2013). PARP-1 dependent recruitment of the amyotrophic lateral sclerosis-associated protein FUS/TLS to sites of oxidative DNA damage. Nucleic Acids Res.

Saberi, S., Stauffer, J.E., Schulte, D.J., and Ravits, J. (2015). Neuropathology of Amyotrophic Lateral Sclerosis and Its Variants. Neurologic clinics *33*, 855-876.

Sala, C., Rudolph-Correia, S., and Sheng, M. (2000). Developmentally regulated NMDA receptor-dependent dephosphorylation of cAMP response element-binding protein (CREB) in hippocampal neurons. J Neurosci *20*, 3529-3536.

Sama, R., Ward, C.L., cellular, L.K.J.o., and 2013 (2013). FUS/TLS assembles into stress granules and is a prosurvival factor during hyperosmolar stress. Wiley Online Library *228*, 2222-2231.

Sama, R.R., Ward, C.L., and Bosco, D.A. (2014). Functions of FUS/TLS From DNA Repair to Stress Response: Implications for ALS. ASN Neuro *6*.

Sama, R.R.K., Fallini, C., Gatto, R., McKeon, J.E., Song, Y., Rotunno, M.S., Penaranda, S., Abdurakhmanov, I., Landers, J.E., Morfini, G.*, et al.* (2017). ALS-linked FUS exerts a gain of toxic function involving aberrant p38 MAPK activation. Scientific reports *7*, 115.

Scaramuzzino, C., Monaghan, J., Milioto, C., Lanson, N.A.J., Maltare, A., Aggarwal, T., Casci, I., Fackelmayer, F.O., Pennuto, M., and Pandey, U.B. (2013). Protein arginine methyltransferase 1 and 8 interact with FUS to modify its sub-cellular distribution and toxicity in vitro and in vivo. PloS one *8*, e61576.

Scekic-Zahirovic, J., Sendscheid, O., El Oussini, H., Jambeau, M., Sun, Y., Mersmann, S., Wagner, M., Dieterlé, S., Sinniger, J., Dirrig-Grosch, S.*, et al.* (2016). Toxic gain of function from mutant FUS protein is crucial to trigger cell autonomous motor neuron loss. The EMBO journal *35*, 1077-1097.

Schindelin, J., Arganda-Carreras, I., Frise, E., Kaynig, V., Longair, M., Pietzsch, T., Preibisch, S., Rueden, C., Saalfeld, S., Schmid, B.*, et al.* (2012). Fiji: an open-source platform for biological-image analysis. Nature methods *9*, 676-682.

Schneider, C.A., Rasband, W.S., and Eliceiri, K.W. (2012). NIH Image to ImageJ: 25 years of image analysis. Nature methods *9*, 671-675.

Schwartz, J.C., Ebmeier, C.C., Podell, E.R., Heimiller, J., Taatjes, D.J., and Cech, T.R. (2012). FUS binds the CTD of RNA polymerase II and regulates its phosphorylation at Ser2. Genes & Development *26*, 2690-2695.

Schwartz, J.C., Wang, X., Podell, E.R., and Cech, T.R. (2013). RNA seeds higher-order assembly of FUS protein. Cell reports *5*, 918-925.

Senda, J., Kato S Fau - Kaga, T., Kaga T Fau - Ito, M., Ito M Fau - Atsuta, N., Atsuta N Fau - Nakamura, T., Nakamura T Fau - Watanabe, H., Watanabe H Fau -

Tanaka, F., Tanaka F Fau - Naganawa, S., Naganawa S Fau - Sobue, G., and Sobue, G. (2011). Progressive and widespread brain damage in ALS: MRI voxel-based morphometry and diffusion tensor imaging study.

Sévigny, M., Bourdeau Julien, I., Venkatasubramani, J.P., Hui, J.B., Dutchak, P.A., and Sephton, C.F. (2020). FUS contributes to mTOR-dependent inhibition of translation. The Journal of biological chemistry *295*, 18459-18473.

Seyfried, N.T., Dammer, E.B., Swarup, V., Nandakumar, D., Duong, D.M., Yin, L., Deng, Q., Nguyen, T., Hales, C.M., Wingo, T., *et al.* (2017). A Multi-network Approach Identifies Protein-Specific Co-expression in Asymptomatic and Symptomatic Alzheimer's Disease. Cell Syst *4*, 60-72.e64.

Sharma, A., Lyashchenko, A.K., Lu, L., Nasrabady, S.E., Elmaleh, M., Mendelsohn, M., Nemes, A., Tapia, J.C., Mentis, G.Z., and Shneider, N.A. (2016). ALS-associated mutant FUS induces selective motor neuron degeneration through toxic gain of function. Nature communications *7*, 10465.

Shelkovnikova, T.A., Robinson, H.K., Connor-Robson, N., and Buchman, V.L. (2013). Recruitment into stress granules prevents irreversible aggregation of FUS protein mislocalized to the cytoplasm. Cell cycle (Georgetown, Tex) *12*, 3194-3202.

Shelkovnikova, T.A., Robinson, H.K., Troakes, C., Ninkina, N., and Buchman, V.L. (2014). Compromised paraspeckle formation as a pathogenic factor in FUSopathies. Hum Mol Genet *23*, 2298-2312.

Shi, J., Shaw, C.L., Du Plessis, D., Richardson, A.M., Bailey, K.L., Julien, C., Stopford, C., Thompson, J., Varma, A., Craufurd, D., *et al.* (2005). Histopathological changes underlying frontotemporal lobar degeneration with clinicopathological correlation. Acta Neuropathol *110*, 501-512.

Shiihashi, G., Ito, D., Arai, I., Kobayashi, Y., Hayashi, K., Otsuka, S., Nakajima, K., Yuzaki, M., Itohara, S., and Suzuki, N. (2017). Dendritic Homeostasis Disruption in a Novel Frontotemporal Dementia Mouse Model Expressing Cytoplasmic Fused in Sarcoma. EBioMedicine.

Shiihashi, G., Ito, D., Yagi, T., Nihei, Y., Ebine, T., and Suzuki, N. (2016). Mislocated FUS is sufficient for gain-of-toxic-function amyotrophic lateral sclerosis phenotypes in mice. Brain : a journal of neurology *139*, 2380-2394.

Siddique, T., and Ajroud-Driss, S. (2011). Familial amyotrophic lateral sclerosis, a historical perspective. Acta Myol *30*, 117-120.

Silva, A.L., Ribeiro, P., Inácio, A., Liebhaber, S.A., and Romão, L. (2008). Proximity of the poly(A)-binding protein to a premature termination codon inhibits mammalian nonsense-mediated mRNA decay. RNA (New York, NY) *14*, 563-576.

Singatulina, A.S., Hamon, L., Sukhanova, M.V., Desforges, B., Joshi, V., Bouhss, A., Lavrik, O.I., and Pastre, D. (2019). PARP-1 Activation Directs FUS to DNA Damage Sites to Form PARG-Reversible Compartments Enriched in Damaged DNA. Cell reports *27*, 1809-1821.e1805.

Snowden, J.S., Hu, Q., Rollinson, S., Halliwell, N., Robinson, A., Davidson, Y.S., Momeni, P., Baborie, A., Griffiths, T.D., Jaros, E.*, et al.* (2011). The most common type of FTLD-FUS (aFTLD-U) is associated with a distinct clinical form of frontotemporal dementia but is not related to mutations in the FUS gene. Acta neuropathologica *122*, 99-110.

Solier, S., and Pommier, Y. (2009). The apoptotic ring: a novel entity with phosphorylated histones H2AX and H2B and activated DNA damage response kinases. Cell cycle (Georgetown, Tex) *8*, 1853-1859.

Spencer, K.R., Foster, Z.W., Rauf, N.A., Guilderson, L., Collins, D., Averill, J.G., Walker, S.E., Robey, I., Cherry, J.A.-O.X., Alvarez, V.E.*, et al.* (2020). Neuropathological profile of long-duration amyotrophic lateral sclerosis in military Veterans.

Sproviero, W., La Bella, V., Mazzei, R., Valentino, P., Rodolico, C., Simone, I.L., Logroscino, G., Ungaro, C., Magariello, A., Patitucci, A.*, et al.* (2012). FUS mutations in sporadic amyotrophic lateral sclerosis: clinical and genetic analysis. Neurobiol Aging *33*, 837.e831-835.

Stiff, T., O'Driscoll, M., Rief, N., Iwabuchi, K., Löbrich, M., and Jeggo, P.A. (2004). ATM and DNA-PK function redundantly to phosphorylate H2AX after exposure to ionizing radiation. Cancer Res *64*, 2390-2396.

Suárez-Calvet, M., Neumann, M., Arzberger, T., Abou-Ajram, C., Funk, E., Hartmann, H., Edbauer, D., Kremmer, E., Göbl, C., Resch, M.*, et al.* (2016). Monomethylated and unmethylated FUS exhibit increased binding to Transportin and distinguish FTLD-FUS from ALS-FUS. Acta neuropathologica *131*, 587-604.

Sukhanova, M.V., Singatulina, A.S., Pastré, D., and Lavrik, O.I. (2020). Fused in Sarcoma (FUS) in DNA Repair: Tango with Poly(ADP-ribose) Polymerase 1 and Compartmentalisation of Damaged DNA. International journal of molecular sciences *21*, 7020.

Sun, Y., Eshov, A., Zhou, J., Isiktas, A.U., and Guo, J.U. (2020). C9orf72 arginine-rich dipeptide repeats inhibit UPF1-mediated RNA decay via translational repression. Nature communications *11*, 3354-3359.

Suzuki, N., Aoki, M., Warita, H., Kato, M., Mizuno, H., Shimakura, N., Akiyama, T., Furuya, H., Hokonohara, T., Iwaki, A.*, et al.* (2010). FALS with FUS mutation in

Japan, with early onset, rapid progress and basophilic inclusion. J Hum Genet *55*, 252-254.

Svetoni, F., De Paola, E., La Rosa, P., Mercatelli, N., Caporossi, D., Sette, C., and Paronetto, M.P. (2017). Post-transcriptional regulation of FUS and EWS protein expression by miR-141 during neural differentiation. Human molecular genetics *26*, 2732-2746.

Svetoni, F., Frisone, P., and Paronetto, M.P. (2016). Role of FET proteins in neurodegenerative disorders. RNA biology *13*, 1089-1102.

Syriani, E., Morales, M., and Gamez, J. (2011). FUS/TLS gene mutations are the second most frequent cause of familial ALS in the Spanish population. Amyotroph Lateral Scler *12*, 118-123.

Szklarczyk, D., Gable, A.L., Lyon, D., Junge, A., Wyder, S., Huerta-Cepas, J., Simonovic, M., Doncheva, N.T., Morris, J.H., Bork, P., *et al.* (2019). STRING v11: protein-protein association networks with increased coverage, supporting functional discovery in genome-wide experimental datasets. Nucleic acids research *47*, D607-D613.

Takahama, K., Arai, S., Kurokawa, R., and Oyoshi, T. (2009). Identification of DNA binding specificity for TLS. Nucleic Acids Symp Ser (Oxf), 247-248.

Takahama, K., Kino, K., Arai, S., Kurokawa, R., and Oyoshi, T. (2008). Identification of RNA binding specificity for the TET-family proteins. Nucleic Acids Symp Ser (Oxf), 213-214.

Tan, A.Y., Riley, T.R., Coady, T., Bussemaker, H.J., and Manley, J.L. (2012). TLS/FUS (translocated in liposarcoma/fused in sarcoma) regulates target gene transcription via single-stranded DNA response elements. Proceedings of the National Academy of Sciences *109*, 6030-6035.

Tang, F.-L., Zhao, L., Zhao, Y., Sun, D., Zhu, X.-J., Mei, L., and Xiong, W.-C. (2020a). Coupling of terminal differentiation deficit with neurodegenerative pathology in Vps35-deficient pyramidal neurons. Cell death and differentiation *27*, 2099-2116.

Tang, X., Toro, A., T, G.S., Gao, J., Chalk, J., Oskarsson, B., and Zhang, K. (2020b). Divergence, Convergence, and Therapeutic Implications: A Cell Biology Perspective of C9ORF72-ALS/FTD. Mol Neurodegener *15*, 34.

Tenreiro, S., Eckermann, K., and Outeiro, T.F. (2014). Protein phosphorylation in neurodegeneration: friend or foe? Front Mol Neurosci *7*, 42.

Thibodeau, M.P., and Miller, B.L. (2013). 'Limits and current knowledge of Pick's disease: its differential diagnosis'. A translation of the 1957 Delay, Brion, Escourolle article. Neurocase *19*, 417-422.

Tibshirani, M., Zhao, B., Gentil, B.J.-C., Minotti, S., Marques, C., Keith, J., Rogaeva, E., Zinman, L., Rouaux, C., Robertson, J.*, et al.* (2017). Dysregulation of chromatin remodelling complexes in amyotrophic lateral sclerosis. Human molecular genetics.

Ticozzi, N., Silani, V., LeClerc, A.L., Keagle, P., Gellera, C., Ratti, A., Taroni, F., Kwiatkowski, T.J., Jr., McKenna-Yasek, D.M., Sapp, P.C.*, et al.* (2009). Analysis of FUS gene mutation in familial amyotrophic lateral sclerosis within an Italian cohort. Neurology *73*, 1180-1185.

Timney, B.L., Raveh, B., Mironska, R., Trivedi, J.M., Kim, S.J., Russel, D., Wente, S.R., Sali, A., and Rout, M.P. (2016). Simple rules for passive diffusion through the nuclear pore complex. Journal of Cell Biology *215*, 57-76.

Tradewell, M.L., Yu, Z., Tibshirani, M., Boulanger, M.-C., Durham, H.D., and Richard, S. (2012). Arginine methylation by PRMT1 regulates nuclear-cytoplasmic

localization and toxicity of FUS/TLS harbouring ALS-linked mutations. Human molecular genetics *21*, 136-149.

Traynor, B.J., Codd, M.B., Corr, B., Forde, C., Frost, E., and Hardiman, O.M. (2000). Clinical Features of Amyotrophic Lateral Sclerosis According to the El Escorial and Airlie House Diagnostic Criteria: A Population-Based Study. Archives of Neurology *57*, 1171-1176.

Troakes, C., Hortobágyi, T., Vance, C., Al-Sarraj, S., Rogelj, B., and Shaw, C.E. (2013). Transportin 1 colocalization with Fused in Sarcoma (FUS) inclusions is not characteristic for amyotrophic lateral sclerosis-FUS confirming disrupted nuclear import of mutant FUS and distinguishing it from frontotemporal lobar degeneration with FUS inclusions. Neuropathol Appl Neurobiol *39*, 553-561.

Tsai, C.P., Soong, B.W., Lin, K.P., Tu, P.H., Lin, J.L., and Lee, Y.C. (2011). FUS, TARDBP, and SOD1 mutations in a Taiwanese cohort with familial ALS. Neurobiol Aging *32*, 553.e513-521.

Tsai, R.M., and Boxer, A.L. (2014). Treatment of frontotemporal dementia. Curr Treat Options Neurol *16*, 319.

Turner, M.R., Swash, M., and Ebers, G.C. (2010). Lockhart Clarke's contribution to the description of amyotrophic lateral sclerosis. Brain *133*, 3470-3479.

Tuttle, A.H., Philip, V.M., Chesler, E.J., and Mogil, J.S. (2018). Comparing phenotypic variation between inbred and outbred mice. Nature methods *15*, 994-996.

Tyanova, S., Temu, T., and Cox, J. (2016). The MaxQuant computational platform for mass spectrometry-based shotgun proteomics. Nat Protoc *11*, 2301-2319.

Ubersax, J.A., and Ferrell, J.E., Jr. (2007). Mechanisms of specificity in protein phosphorylation. Nat Rev Mol Cell Biol *8*, 530-541.

Uranishi, H., Tetsuka, T., Yamashita, M., Asamitsu, K., Shimizu, M., Itoh, M., and Okamoto, T. (2001). Involvement of the pro-oncoprotein TLS (translocated in liposarcoma) in nuclear factor-kappa B p65-mediated transcription as a coactivator. J Biol Chem *276*, 13395-13401.

Urwin, H., Josephs, K.A., Rohrer, J.D., Mackenzie, I.R., Neumann, M., Authier, A., Seelaar, H., Van Swieten, J.C., Brown, J.M., Johannsen, P., *et al.* (2010). FUS pathology defines the majority of tau- and TDP-43-negative frontotemporal lobar degeneration. Acta Neuropathol *120*, 33-41.

Valtcheva, M.V., Copits, B.A., Davidson, S., Sheahan, T.D., Pullen, M.Y., McCall, J.G., Dikranian, K., and Gereau, R.W.t. (2016). Surgical extraction of human dorsal root ganglia from organ donors and preparation of primary sensory neuron cultures. Nature protocols *11*, 1877-1888.

van Blitterswijk, M., Vlam, L., van Es, M.A., van der Pol, W.L., Hennekam, E.A., Dooijes, D., Schelhaas, H.J., van der Kooi, A.J., de Visser, M., Veldink, J.H., *et al.* (2012). Genetic overlap between apparently sporadic motor neuron diseases. PLoS One *7*, e48983.

van Blitterswijk, M., Wang, E.T., Friedman, B.A., Keagle, P.J., Lowe, P., Leclerc, A.L., van den Berg, L.H., Housman, D.E., Veldink, J.H., and Landers, J.E. (2013). Characterization of FUS Mutations in Amyotrophic Lateral Sclerosis Using RNA-Seq. PLOS ONE *8*, e60788.

Van Damme, P., Robberecht, W., and Van Den Bosch, L. (2017). Modelling amyotrophic lateral sclerosis: progress and possibilities. Disease models & mechanisms *10*, 537-549.

van der Kant, R., Goldstein, L.S.B., and Ossenkoppele, R. (2020). Amyloid-β-independent regulators of tau pathology in Alzheimer disease. Nature Reviews Neuroscience *21*, 21-35.

Van Langenhove, T., van der Zee, J., Sleegers, K., Engelborghs, S., Vandenberghe, R., Gijselinck, I., Van den Broeck, M., Mattheijssens, M., Peeters, K., De Deyn, P.P.*, et al.* (2010). Genetic contribution of FUS to frontotemporal lobar degeneration. Neurology *74*, 366-371.

Van Mossevelde, S., Engelborghs, S., van der Zee, J., and Van Broeckhoven, C. (2018). Genotype-phenotype links in frontotemporal lobar degeneration. Nat Rev Neurol *14*, 363-378.

Vance, C., Rogelj, B., Hortobagyi, T., De Vos, K.J., Nishimura, A.L., Sreedharan, J., Hu, X., Smith, B., Ruddy, D., Wright, P.*, et al.* (2009a). Mutations in FUS, an RNA processing protein, cause familial amyotrophic lateral sclerosis type 6. Science (New York, NY) *323*, 1208-1211.

Vance, C., Rogelj, B., Hortobagyi, T., De Vos, K.J., Nishimura, A.L., Sreedharan, J., Hu, X., Smith, B., Ruddy, D., Wright, P.*, et al.* (2009b). Mutations in FUS, an RNA Processing Protein, Cause Familial Amyotrophic Lateral Sclerosis Type 6. Science (New York, NY) *323*, 1208-1211.

Vance, C., Scotter, E.L., Nishimura, A.L., Troakes, C., Mitchell, J.C., Kathe, C., Urwin, H., Manser, C., Miller, C.C., Hortobagyi, T.*, et al.* (2013). ALS mutant FUS disrupts nuclear localization and sequesters wild-type FUS within cytoplasmic stress granules. Human molecular genetics *22*, 2676-2688.

Verbeeck, C., Deng, Q., DeJesus-Hernandez, M., Taylor, G., Ceballos-Diaz, C., Kocerha, J., Golde, T., Das, P., Rademakers, R., Dickson, D.W.*, et al.* (2012). Expression

of Fused in sarcoma mutations in mice recapitulates the neuropathology of FUS proteinopathies and provides insight into disease pathogenesis. Molecular neurodegeneration *7*, 53.

Vernon, R.M., Chong, P.A., Tsang, B., Kim, T.H., Bah, A., Farber, P., Lin, H., and Forman-Kay, J.D. (2018). Pi-Pi contacts are an overlooked protein feature relevant to phase separation. Elife *7*.

Vieira, R.T., Caixeta, L., Machado, S., Silva, A.C., Nardi, A.E., Arias-Carrion, O., and Carta, M.G. (2013). Epidemiology of early-onset dementia: a review of the literature. Clinical practice and epidemiology in mental health : CP & EMH *9*, 88-95.

Virág, D., Dalmadi-Kiss, B., Vékey, K., Drahos, L., Klebovich, I., Antal, I., and Ludányi, K. (2020). Current Trends in the Analysis of Post-translational Modifications. Chromatographia *83*, 1-10.

Wang, W.-Y., Pan, L., Su, S.C., Quinn, E.J., Sasaki, M., Jimenez, J.C., Mackenzie, I.R.A., Huang, E.J., and Tsai, L.-H. (2013). Interaction of FUS and HDAC1 regulates DNA damage response and repair in neurons. Nature neuroscience *16*, 1383-1391.

Wang, X., Schwartz, J.C., and Cech, T.R. (2015). Nucleic acid-binding specificity of human FUS protein. Nucleic acids research *43*, 7535-7543.

Waterston, R.H., Lindblad-Toh, K., Birney, E., Rogers, J., Abril, J.F., Agarwal, P., Agarwala, R., Ainscough, R., Alexandersson, M., An, P.*, et al.* (2002). Initial sequencing and comparative analysis of the mouse genome. Nature *420*, 520-562.

Wimmer, T., Schreiber, F., Hensiek, N., Garz, C., Kaufmann, J., Machts, J., Vogt, S., Prudlo, J., Dengler, R., Petri, S.*, et al.* (2020). The upper cervical spinal cord in ALS assessed by cross-sectional and longitudinal 3T MRI. Scientific Reports *10*, 1783.

Woollacott, I.O., and Rohrer, J.D. (2016). The clinical spectrum of sporadic and familial forms of frontotemporal dementia. J Neurochem *138 Suppl 1*, 6-31.

Xicoy, H., Wieringa, B., and Martens, G.J.M. (2017). The SH-SY5Y cell line in Parkinson's disease research: a systematic review. Molecular neurodegeneration *12*, 10-11.

Yan, J., Deng, H.X., Siddique, N., Fecto, F., Chen, W., Yang, Y., Liu, E., Donkervoort, S., Zheng, J.G., Shi, Y.*, et al.* (2010). Frameshift and novel mutations in FUS in familial amyotrophic lateral sclerosis and ALS/dementia. Neurology *75*, 807-814.

Yan, L. (2021). ggvenn: Draw Venn Diagram by 'ggplot2' (R package).

Yang, L., Gal, J., Chen, J., and Zhu, H. (2014). Self-assembled FUS binds active chromatin and regulates gene transcription. Proceedings of the National Academy of Sciences of the United States of America *111*, 17809-17814.

Yasuda, K., Zhang, H., Loiselle, D., Haystead, T., Macara, I.G., and Mili, S. (2013). The RNA-binding protein Fus directs translation of localized mRNAs in APC-RNP granules. The Journal of Cell Biology *203*, 737-746.

Yoshizawa, T., Ali, R., Jiou, J., Fung, H.Y.J., Burke, K.A., Kim, S.J., Lin, Y., Peeples, W.B., Saltzberg, D., Soniat, M.*, et al.* (2018). Nuclear Import Receptor Inhibits Phase Separation of FUS through Binding to Multiple Sites. Cell *173*, 693-705.e622.

Younes, K., and Miller, B.L. (2020). Frontotemporal Dementia: Neuropathology, Genetics, Neuroimaging, and Treatments. The Psychiatric clinics of North America *43*, 331-344.

Young, J.J., Lavakumar, M., Tampi, D., Balachandran, S., and Tampi, R.R. (2018). Frontotemporal dementia: latest evidence and clinical implications. Ther Adv Psychopharmacol *8*, 33-48.

Yue, F., Cheng, Y., Breschi, A., Vierstra, J., Wu, W., Ryba, T., Sandstrom, R., Ma, Z., Davis, C., Pope, B.D., *et al.* (2014). A comparative encyclopedia of DNA elements in the mouse genome. Nature *515*, 355-364.

Zhang, Z.C., and Chook, Y.M. (2012). Structural and energetic basis of ALS-causing mutations in the atypical proline-tyrosine nuclear localization signal of the Fused in Sarcoma protein (FUS). Proc Natl Acad Sci U S A *109*, 12017-12021.

Zhao, J., Li, X., Guo, M., Yu, J., and Yan, C. (2016). The common stress responsive transcription factor ATF3 binds genomic sites enriched with p300 and H3K27ac for transcriptional regulation. BMC genomics *17*, 335-314.

Zhao, Y., and Jensen, O.N. (2009). Modification-specific proteomics: strategies for characterization of post-translational modifications using enrichment techniques. Proteomics *9*, 4632-4641.

Zhou, B., Wang, H., Cai, Y., Wen, H., Wang, L., Zhu, M., Chen, Y., Yu, Y., Lu, X., Zhou, M., *et al.* (2020). FUS P525L mutation causing amyotrophic lateral sclerosis and movement disorders. Brain and behavior *10*, e01625.

Zhou, Y., Liu, S., Liu, G., Oztürk, A., and Hicks, G.G. (2013). ALS-associated FUS mutations result in compromised FUS alternative splicing and autoregulation. PLoS genetics *9*, e1003895.

Zhou, Y., Liu, S., Oztürk, A., and Hicks, G.G. (2014). FUS-regulated RNA metabolism and DNA damage repair: Implications for amyotrophic lateral sclerosis and frontotemporal dementia pathogenesis. Rare Dis *2*, e29515-e29515.

Zhou, Y., Zhou, B., Pache, L., Chang, M., Khodabakhshi, A.H., Tanaseichuk, O., Benner, C., and Chanda, S.K. (2019). Metascape provides a biologist-oriented resource for the analysis of systems-level datasets. Nature communications *10*, 1523.

Zinszner, H., Sok, J., Immanuel, D., Yin, Y., and Ron, D. (1997). TLS (FUS) binds RNA in vivo and engages in nucleo-cytoplasmic shuttling. Journal of cell science *110 (Pt 15)*, 1741-1750.

Zou, Z.Y., Cui Ly Fau - Sun, Q., Sun Q Fau - Li, X.-G., Li Xg Fau - Liu, M.-S., Liu Ms Fau - Xu, Y., Xu Y Fau - Zhou, Y., Zhou Y Fau - Yang, X.-Z., and Yang, X.Z. De novo FUS gene mutations are associated with juvenile-onset sporadic amyotrophic lateral sclerosis in China.

Zou, Z.Y., Peng, Y., Feng, X.H., Wang, X.N., Sun, Q., Liu, M.S., Li, X.G., and Cui, L.Y. (2012). Screening of the FUS gene in familial and sporadic amyotrophic lateral sclerosis patients of Chinese origin. Eur J Neurol *19*, 977-983.

Appendix A: Supplemental Figures for Chapter 2

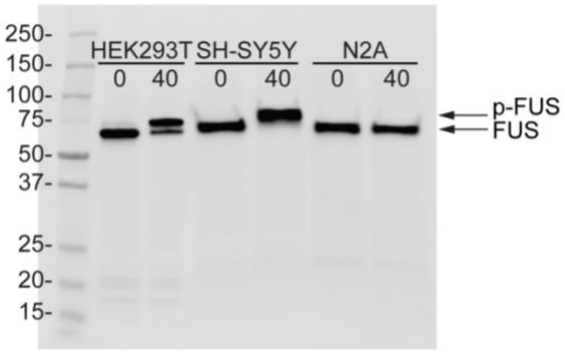

Supplemental Figure 1 Lack of lower-molecular weight FUS species in immortalized cell lines treated with CLM. *Human HEK293T cells, human SH-SY5Y cells, and mouse N2A cells were treated with CLM (0 or 40 nM) for 2 hours. Following treatment, cells were lysed using RIPA buffer and analyzed by SDS/PAGE and western blot using an antibody for total-FUS. No FUS immunoreactivity bands below 75 kDa were detected, suggesting CLM treatment does not generate smaller FUS fragments in HEK293T, SH-SY5Y cells, or N2A cells.*

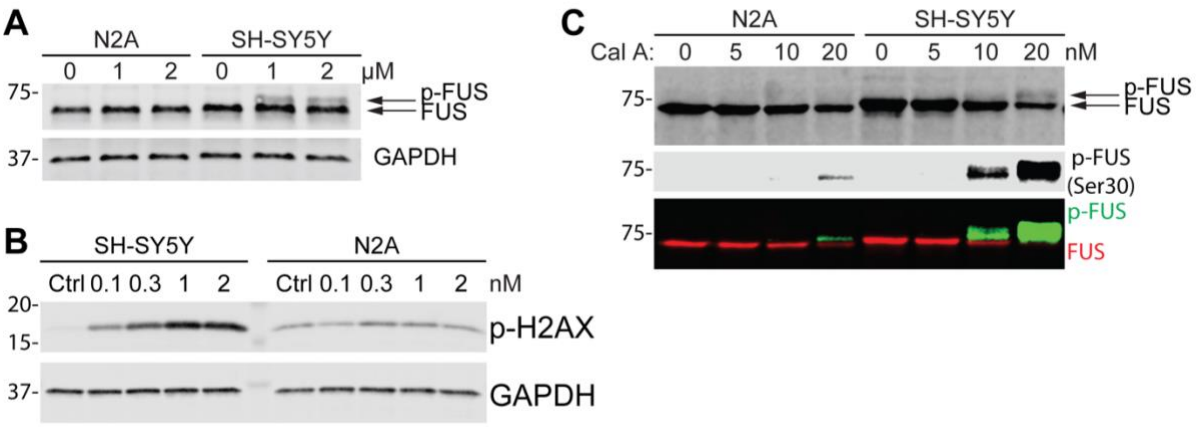

Supplemental Figure 2 Staurosporine and calyculin A treatment does not cause robust FUS phosphorylation in mouse N2A cells compared to human SH-SY5Y cells. *(A) SH-SY5Y and N2A cells were treated with 0, 1 μM, or 2 μM staurosporine. RIPA extracted whole cell lysates were analyzed using antibodies against: FUS and GAPDH. GAPDH was used as a loading control. (B) SH-SY5Y and N2A cells were treated with increasing doses of staurosporine (μM) or DMSO (vehicle control) for 3 hours. SH-SY5Y cells have a distinct dose-dependent increase in p-H2AX signal whereas N2A cells lack any noticeable change in p-H2AX signal. Following treatment, RIPA extracted whole cell lysate was analyzed with indicated antibodies. GAPDH was used as a loading control. (C) SH-SY5Y and N2A cells were treated with 0 (DMSO vehicle), 5 nM, 10 nM, or 20 nM Calyculin A. RIPA extracted whole cell lysate was analyzed using antibodies against: FUS and p-FUS (Ser30). Overlay reveals p-FUS is detected in both cells lines only at the highest dose tested, 20nM, but the p-FUS signal is greater in SH-SY5Y cells.*

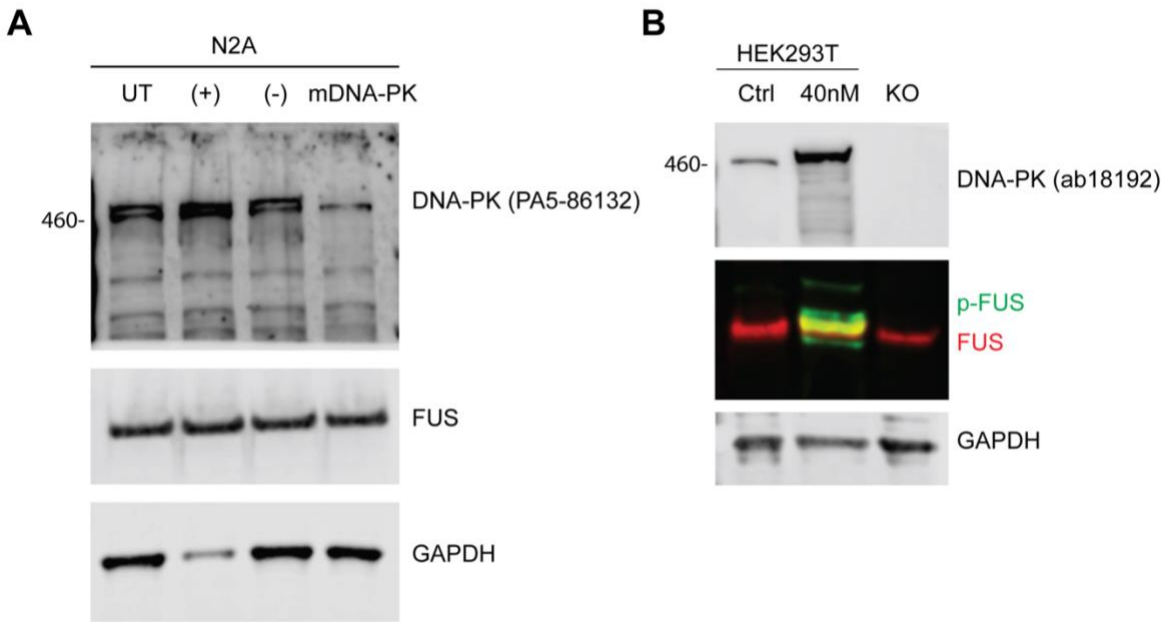

Supplemental Figure 3 Validation of antibody that recognizes mouse and human total and phosphorylated DNA-PK. *Targeted knockdown of mouse DNA-PK verifies specificity of antibody PA5-86134. (A) N2A cells were treated with ON-TargetPlus siRNA pool against GAPDH ((+); D-001830-20), nontargeting siRNA ((-);D-001810-0X) or Mouse PRKDC ((mDNA-PK); L-040958-00-0005) using DharmaFECT 1 transfection reagent. Cells were harvested after 72 hours and RIPA extracted whole cell lysate was probed for total DNA-PK using PA5-86134. Un-transfected (UT) cells act as negative control. (B) Antibody ab18192 detects phosphorylated, activated DNA-PK. HEK293T cells were treated either with DMSO (0) or 40 nM CLM (40 nM) for 2 hours. M059J cells are DNA-PK KO cells (KO). GAPDH is used as a loading control.*

Figure 3A/B/C

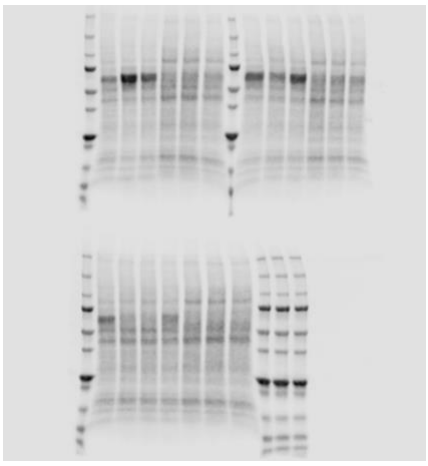

Figure 3D/F/G - Replicates 1 and 2

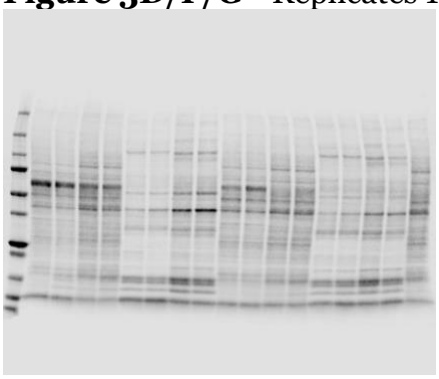

Figure 3D/F/G - Replicates 3 and 4

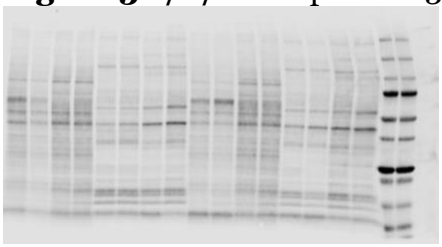

Figure 3D/F/G - Replicate 5

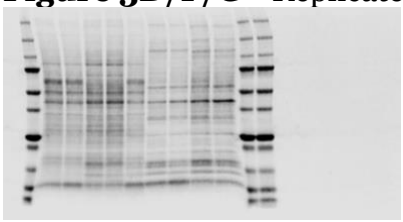

Figure 4B/C

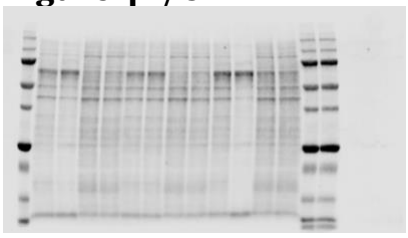

Figure 4E/F

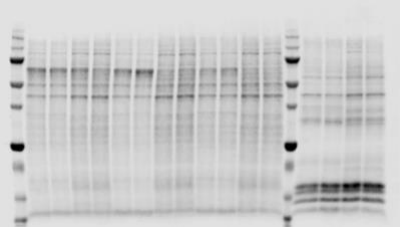

Supplemental Figure 4: Compilation of western blots stained for total protein prior to quantification. *In order to normalize protein levels for quantification, western blots were stained post-transfer (pre-block) for total protein using Revert 700 Total Protein Stain (LI-COR Biosciences). Total protein image (700 nM) of quantified bots for figures shown below.*

Appendix B: Supplemental Figures for Chapter 3

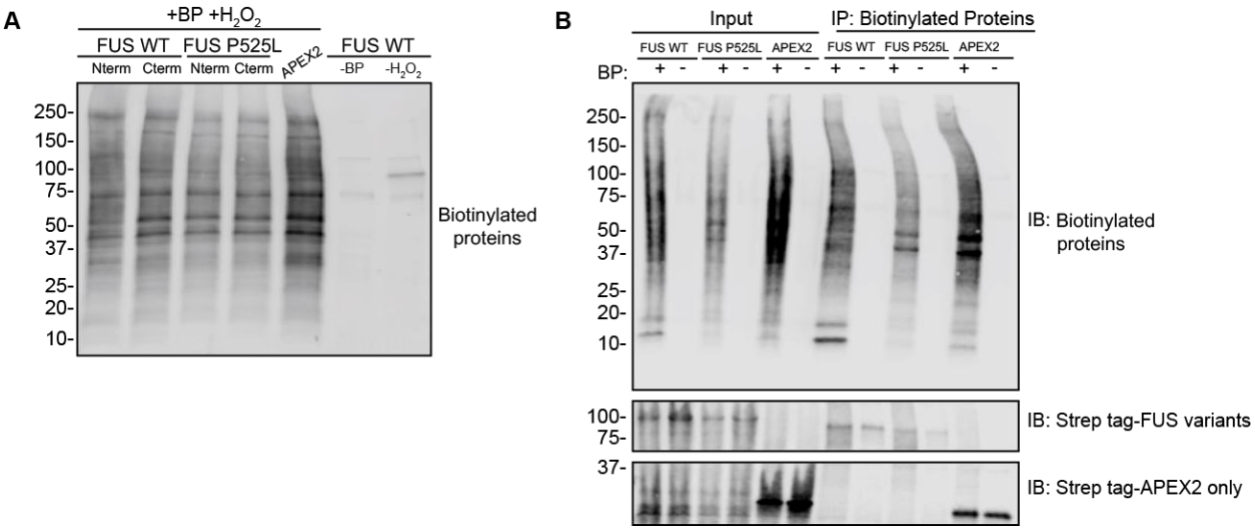

Supplemental Figure 1 Cells expressing APEX2-FUS fusion constructs must be given biotin-phenol (BP) and H2O2 to induce biotinylation

(A) Western blot of cell lysate from HEK293T cells expressing different APEX2-FUS fusion constructs. Constructs either had APEX2 fused to the N-terminus of the FUS variant (Nterm) or the C-terminus of the FUS variant (Cterm) or did not have FUS fused to APEX2 (APEX2). Following transfection, cells were 1) given biotin-phenol (BP) and H2O2 (+BP + H2O2), given only H2O2 (-BP) or given only BP (-H2O2). 24 hours post-transfection, biotinylation was induced, quenched and cells lysate was harvested and analyzed for biotinylated proteins (streptavidin).

(B) Immunoprecipitation of biotinylated proteins using magnetic beads coat in streptavidin showing biotinylated proteins can only be pulled down when cells were given biotin-phenol (BP). Input is 10% of sample loaded onto magnetic beads coated with streptavidin; Elute is 100% of sample eluted off beads. Samples are from cells expressing the following APEX2-FUS fusion proteins: wildtype FUS (FUS WT), P525L FUS (FUS P525L), and APEX2 without FUS fusion (APEX2). Input and elution were analyzed for biotinylated proteins (streptavidin) and Twin-Strep-tag® (strep tag).

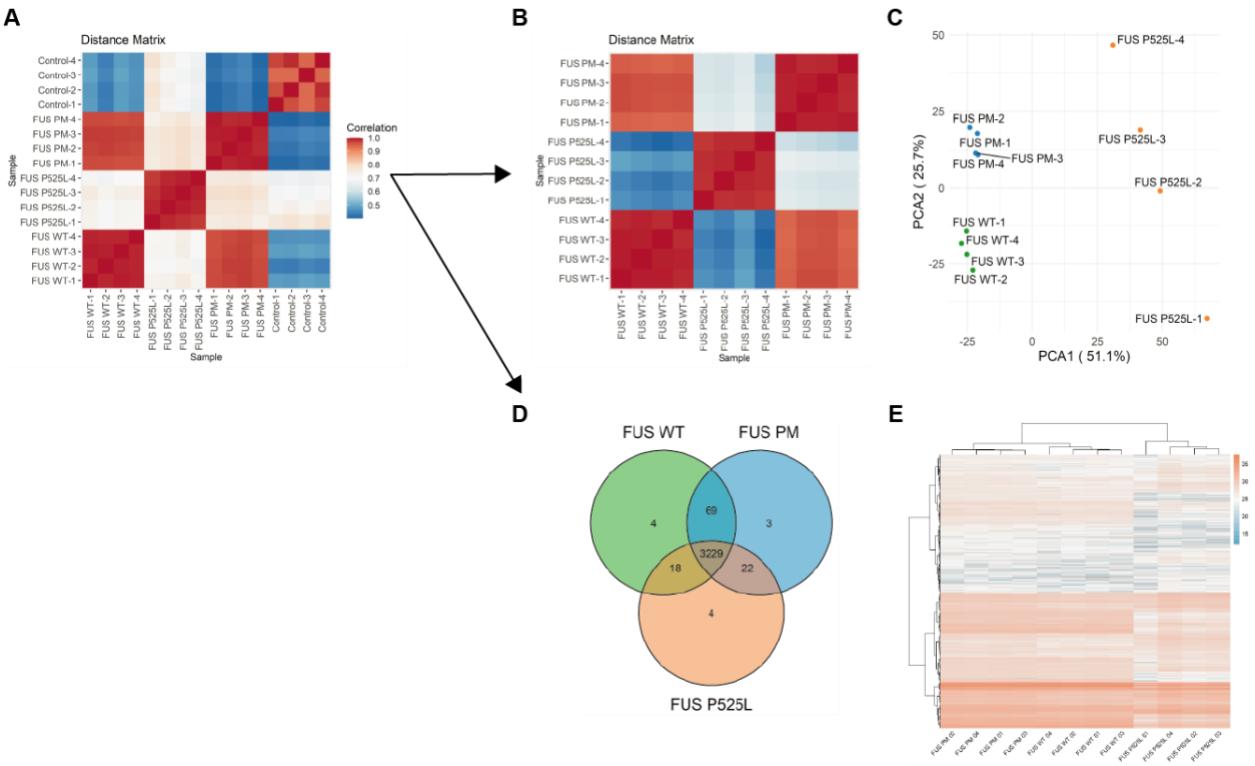

Supplemental Figure 2 Clustering of protein hits reveals specificity between FUS variant groups

(A) Distance matrix of all samples, including controls, showing the Pearson correlation between samples within and between groups with red indicating values closer to 1.0 and blue indicating values closer to 0.5. (B) Distance matrix of all samples, following normalization to control samples, showing the Pearson correlation between samples within and between groups with red indicating values closer to 1.0 and blue indicating values closer to 0.5. (C) Principal Component Analysis (PCA), excluding controls, showing reproducibility of data between biological replicates in three FUS variant groups. (D) Venn diagram of overlap of all protein hits for the three FUS variant groups. (E) Hierarchical clustering of samples based on the intensity profiles of all proteins identified. Missing values are colored gray.

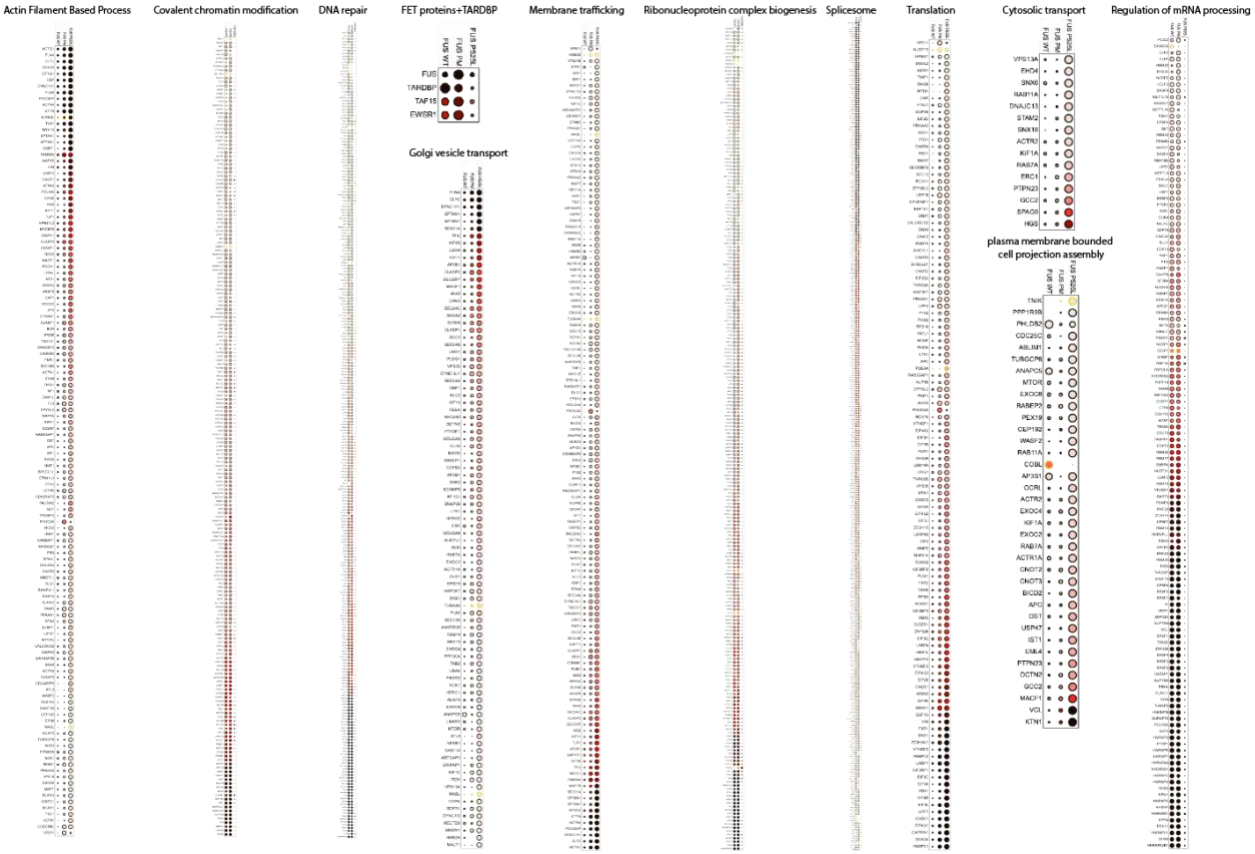

Supplemental Figure 3 Relative intensity of proteins hits that are relevant for identified ontologies. *Dot plots were generated using Prohits-viz are a graphical representation of the relative binding intensity of each protein against the three FUS variant groups.*

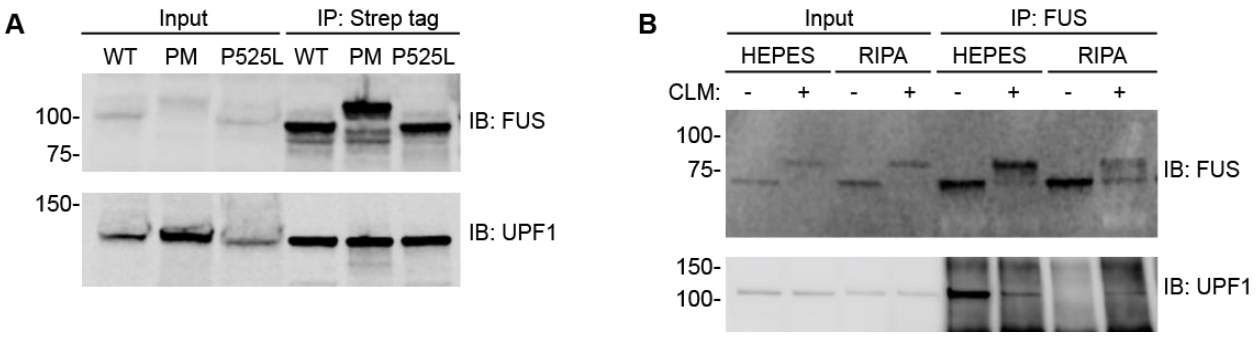

Supplemental Figure 4 Representative immunoprecipitation of FUS variants.

(A) Representative western blot (IB) showing clear enrichment of FUS variants following immunoprecipitation of Twin-Strep-tag® compared to input lysate. Input lysate is 10% of sample loaded Magstrep Type3 beads. (B) Immunoprecipitation for FUS in cells treated with either calicheamicin γ1 (CLM) (+) or vehicle (DMSO; (-)). HEK293T cells were treated with 40 nM of CLM for 3 hours at 37˚C/5% CO2. Cells were lysed either in HEPES (120 mM NaCl, 40 mM HEPES pH 7.4, 0.3% (w/v) CHAPS) or RIPA (150 mM NaCl, 1% NP-40, 0.5% sodium deoxycholate, 0.1% SDS, 50 mM Tris/HCl pH 8.0) based lysis buffer + protein/phosphatase inhibitor. Following lysis, equal amounts of protein were loaded onto Protein G Dynabeads (Thermofisher Scientific, 10003D) coated in FUS antibody (Bethyl Laboratories; A300-302A) for overnight capture and bound material was eluted off following manufacturer instructions. Input and elution was western blotted for listed targets.

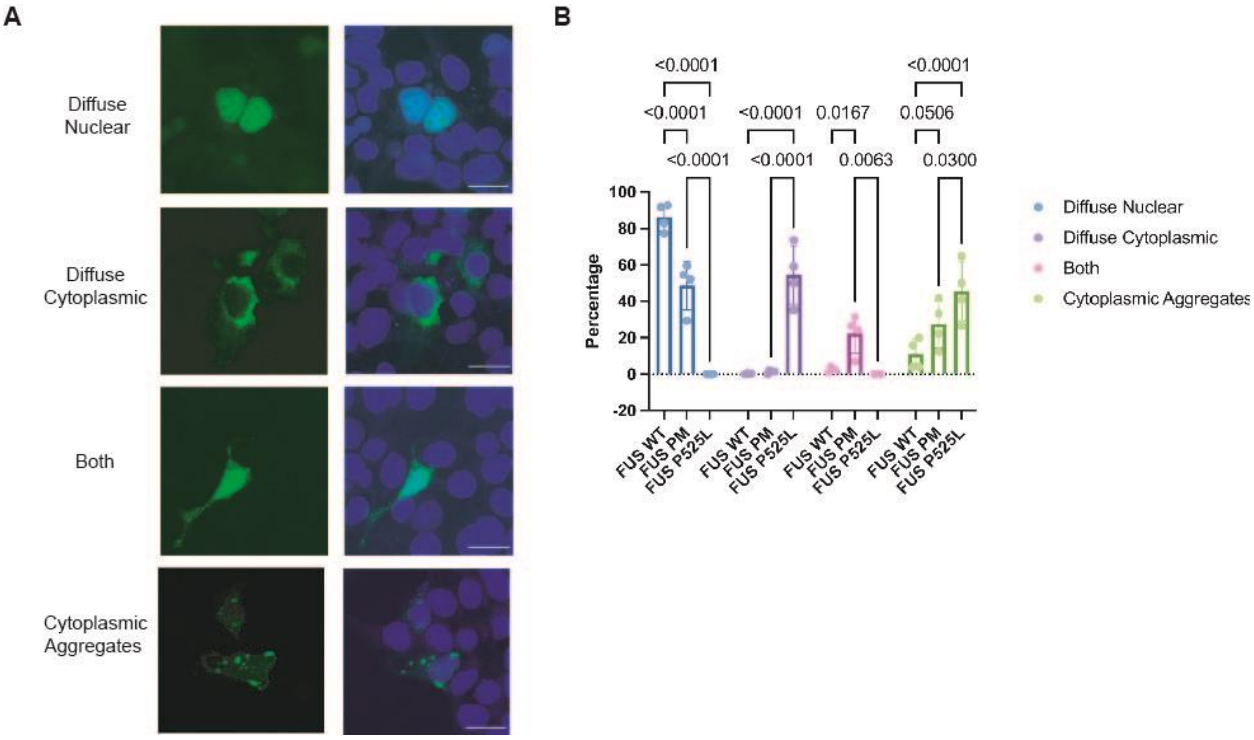

Supplemental Figure 5 FUS PM forms more cytoplasmic aggregates than FUS WT.

Cells were transfected with a GFP-tagged FUS variant (FUS WT, FUS PM, and FUS P525L). These are the variants used in Figures 3.4 and 3.5. On average 165 cells were then classified into one of four categories based on the localization of FUS: Diffuse Nuclear (signal was spread diffusely throughout the nucleus), Diffuse Cytoplasmic (signal was spread diffusely throughout the cytoplasm), Both (signal was spread diffusely throughout the nucleus and cytoplasm) and Cytoplasmic Aggregates (signal was present in cytoplasmic punctate). The boundaries of nucleus was determined using the DAPI signal. (A) Representative images of the four classifications schemes for FUS localization. (B) The percentage of cells in each category was calculated for each group and a two-way ANOVA was performed to determined significance (n=4). Error bars indicate mean ± SEM.